FINAL REPORT

FINAL REPORT

Evaluation of Chemical Dispersion Models using Atmospheric Plume Measurements from Field Experiments

EPA Contract No: EP-D-07-102
Work Assignment No: 4-06 and 5-08

Prepared for:

Office of Air Quality Planning and Standards
U.S. Environmental Protection Agency
109 T.W. Alexander Drive
Mail Code: C439-1
Research Triangle Park, NC 27709

Prepared by:
ENVIRON International Corporation
773 San Marin Drive, Suite 2115
Novato, California, 94998
Under Subcontract to the University of
North Carolina at Chapel Hill

September 2012
06-20443M6

ENVIRON

ENVIRON

Contents

TABLES

FIGURES

1.0   INTRODUCTION

1.1   BACKGROUND

Dispersion models, such as the Industrial Source Complex Short Term (ISCST; EPA, 1995) or American Meteorological Society/Environmental Protection Agency Regulatory Model (AERMOD; EPA, 2004; 2009c), typically assume steady, horizontally homogeneous wind fields instantaneously over the entire modeling domain and are usually limited to chemically inert pollutants and distances of less than 50 kilometers from a source. Therefore, dispersion model applications of distances of hundreds of kilometers from a source require other models or modeling systems. At these distances, the transport times are sufficiently long that the mean wind fields cannot be considered steady-state or homogeneous.

As part of the Prevention of Significant Deterioration (PSD) and New Source Review (NSR) programs, new sources or proposed modifications to existing sources may be required to assess the air quality and Air Quality Related Values (AQRVs) impacts at Class I and sensitive Class II areas that may be far away from the source. AQRVs include visibility and acid (sulfur and nitrogen) deposition. At these longer transport times, chemical conversion of pollutants is of increasing importance. In addition, visibility degradation at these distances tends to be dominated by sulfate and nitrate, which are not directly emitted but formed in the atmosphere from emitted gaseous SO_2 and NO_X through many complex chemical reactions. Thus, non-steady-state chemical dispersion models are needed to address air quality and AQRVs issues at distances beyond 50 km from a source.

The CALPUFF modeling system (Scire et al., 2000a,b) has been used in the past to address far-field air quality and AQRV issues. The current regulatory version of CALPUFF is Version 5.8 (V5.8). EPA has evaluated the CALPUFF, and other long range transport (LRT) dispersion models, against atmospheric field study tracer data (EPA, 2012). This evaluation assessed the ability of CALPUFF, and other LRT dispersion models, to predict the transport and dispersion of a chemically inert tracer at distances of 10s to 1000s km downwind. However, to address AQRVs not only requires the correct depiction of transport and dispersion, but also the chemical transformation of SO_2 and NO_X emissions to secondary $PM_{2.5}$ SO_4 and NO_3. The CALPUFF SO_4 and NO_3 formation algorithms are highly simplified and are not consistent with the current understanding of atmospheric chemistry (Morris et al., 2003; 2005; 2006). The EPA-recommended CALPUFF SO_4 and NO_3 formation algorithm (MESOPUFF II) was developed almost three decades ago (Scire et al., 1983). Recent efforts have been made to improve the CALPUFF formation algorithms (Karamchandani et al., 2008) that have been implemented in CALPUFF V6.4, but because it does not have sufficient information to properly simulate SO_4 and NO_3 formation rates (e.g., VOCs and the simulation of ozone and the radical cycle), it is incapable of correctly simulating atmospheric chemistry.

Ozone is a pollutant of increasing interest as new lower ozone standards are considered so there is a need to evaluate a new source's ozone impacts. To treat ozone requires a photochemical model with complete atmospheric chemistry. CALPUFF does not treat ozone.

1.2 PURPOSE

The purpose of this study is to evaluate chemistry dispersion models using atmospheric plume chemistry measurements. Three different dispersion models were evaluated using chemical plume concentration measurements from two field experiments.

1.3 OVERVIEW OF APPROACH

1.3.1 Field Experiments used in the Evaluation

Data from two field experiments that included aircraft or helicopter measurements of power plant plumes were used to evaluate the models. The first field experiment is the Nashville Field Intensive component of the Southern Oxidant Study in 1999 (SOS 99). As part of this study, daytime plumes from the Tennessee Valley Authority (TVA) Cumberland Power Plant, located in north-central Tennessee, were sampled by the TVA Bell 205 helicopter for selected days in July 2009. The other field experiment is the second Texas Air Quality Study (TexAQS II) in 2006. As part of this study, the National Oceanic and Atmospheric Administration's (NOAA) P-3 aircraft measured a wide suite of atmospheric species at high temporal resolution during a series of flights, including a nighttime flight downwind of the Oklaunion power plant in north Texas, near the Oklahoma border and the city of Wichita Falls, TX.

1.3.2 Models Evaluated

Three models were evaluated using the aircraft plume measurements from the two field experiments. Two of these models (CALPUFF v5.8 and SCICHEM) are puff models, while the third model, CAMx, is a photochemical grid model.

1.4 ORGANIZATION OF THE REPORT

Section 2 describes the technical approach to the model evaluations, including brief descriptions of the models and the field measurements used to evaluate the models, and the model evaluation approach. Sections 3 and 4 describe the model evaluation results using the, respectively, SOS 1999 Cumberland and TEXAQS II 2006 Oklaunion plume measurements. Section 5 provides the conclusions of the study and Section 6 provides the references.

2.0   Technical Approach

The three models evaluated in this study have different formulations and input requirements. Thus, there are some differences in the approaches used to apply and evaluate the models. For example, CAMx is a three-dimensional Eulerian photochemical grid model that requires gridded inputs (meteorology, land use, surface emissions, initial conditions, boundary conditions) as well as discrete point source emissions. The emissions, initial conditions and boundary conditions are required for a large number of species that are consistent with the gas-phase chemistry mechanism (e.g., CB05) and aerosol algorithm selected for the model application. CAMx can resolve sub-grid scale plumes using plume-in-grid (PiG) or by using a high-resolution grid.

Both CALPUFF and SCICHEM are Lagrangian puff models with SCICHEM using a more detailed treatment of chemistry than CALPUFF that is comparable to the chemical algorithms used in photochemical grid models (e.g., CAMx and CMAQ). SCICHEM can operate with routine and special meteorological observations as well as gridded meteorological fields, while CALPUFF is typically applied with gridded meteorology.

In the following sections, we briefly describe the aircraft data used to evaluate the models, followed by brief descriptions of the three models, and the approach used to apply and evaluate the models.

2.1   AIRCRAFT PLUME MEASUREMENTS

The models were evaluated using airborne measurements of power plant plumes from two separate studies in different regions of the country. The first set of measurements was conducted in July 1999 downwind of the TVA Cumberland power plant in central Tennessee by the TVA Bell 205 helicopter (Imhoff et al., 2000; Tanner et al., 2002) as part of the Nashville Field Intensive component of the Southern Oxidant Study in 1999 (SOS 99). The database includes high time resolution measurements of gaseous species across the plume and plume-integrated measurements of particulate species for selected plume traverses. The power plant is located approximately 80 km to the west-northwest of downtown Nashville and is the largest single source of NO_x emissions (~20 tons of NO_x/hour) in the region. The gas analyzers included an O_3 monitor, an SO_2 monitor and NO, NO_2, NO_x, and NO_y monitors.

The second set of airborne plume measurements was conducted during October 2006 as part of the second Texas Air Quality Study (TexAQS II). The plume measurements were taken by NOAA's P-3 aircraft, which measured a wide suite of atmospheric species at high temporal resolution during a series of nighttime flights, including flights downwind of several Texas power plants, such as the Oklaunion power plant in north Texas, near the Oklahoma border and the city of Wichita Falls, TX. At the time of TexAQS II, the Oklaunion power plant consisted of a single stack at 140 m above ground level that was operated with low NO_x burner technology, but without SCR. The NO_x emissions rate was approximately 31 tons/day, which is approximately 6.5% of (or 15 times less than) the NO_x emissions rate of the TVA Cumberland power plant. The measurements by the NOAA P-3 aircraft included nitrogen oxides and ozone (NO, NO_2, NO_y = total reactive nitrogen, O_3) by chemiluminescence, NO_2, NO_3 and N_2O_5 by cavity ring-down spectroscopy, HNO_3 by chemical ionization mass spectrometry, SO_2 by pulsed UV fluorescence and particulate surface area by a series of optical particle counters (Parrish et

al., 2009; Brown et al., 2009). The aircraft measurements also included meteorological data such as wind speed, wind direction, and temperature.

These two sets of measurements provide contrasting databases to evaluate reactive plume models, such as SCICHEM and CALPUFF, and grid models with sub-grid scale resolution, such as CAMx. The Cumberland measurements were made during the day, while the Oklaunion measurements were conducted during the night. The NO_x emissions from Cumberland were approximately 15 times the NO_x emissions from Oklaunion during their respective plume measurement periods. In the daytime Cumberland plume, the measured plume widths increased with downwind distance, while the Oklaunion measurements suggest that the plume width did not vary substantially at all downwind distances, ranging from 15 km to 60 km. The plume chemistries of the Cumberland and Oklaunion plumes were also significantly different, as will be shown later during the discussion of the results in Sections 3 and 4.

2.2   MODELS EVALUATED

2.2.1   CALPUFF

CALPUFF is a multi-layer, multi-species non-steady-state puff dispersion model that can simulate the effects of time- and space-varying meteorological conditions on pollutant transport, transformation, and removal (Scire et al., 2000a). It can accommodate arbitrarily varying point source, area source, volume source, and line source emissions. It is intended for use on scales from tens of meters to hundreds of kilometers from a source. However, the use of CALPUFF for transport distances larger than 200 to 300 km is not recommended (EPA, 1998). CALPUFF is currently the U.S. Environmental Protection Agency's (U.S. EPA) preferred model for assessing single-source long range (50-200 km) transport of chemically inert pollutants and their impacts on Federal Class I areas and on a case-by-case basis for certain near-field applications involving complex meteorological conditions (EPA, 2003). However, EPA has re-emphasized that AERMOD is the recommended model for near-field (<50 km) applications and has severely restricted the use of CALPUFF for regulatory near-field modeling (EPA, 2008).

The recommended meteorological inputs for applying CALPUFF are the time-dependent outputs of CALMET, a meteorological model that contains a diagnostic wind field module and overwater and overland boundary layer modules (Scire et al., 2000b). Although the CALMET/CALPUFF combination is the preferred approach for applying CALPUFF, CALPUFF can optionally use single station meteorological data for flexibility and consistency with regulatory models such as CTDMPLUS or ISCST3. The outputs of CALMET are hourly gridded fields of micro-meteorological parameters and three-dimensional wind and temperature fields. The wind field module in CALMET combines an objective analysis procedure using wind observations with diagnostic effects that include parameterized treatments of slope flows, valley flows, terrain kinematic effects, terrain blocking effects, and sea/lake breeze circulations. The boundary layer modules of CALMET produce gridded fields of micrometeorological parameters, such as friction velocity, convective velocity scale, and Monin-Obukhov lengths, as well as mixing heights and PGT stability classes. Inputs to CALMET include surface and upper air meteorological data. Optionally, CALMET can also use the outputs of prognostic meteorological models, such as MM5 or WRF, to create the meteorological fields required by CALPUFF.

EPA has developed a new Mesoscale Model InterFace (MMIF; Brashers and Emery, 2009; 2011) tool that performs a direct "pass through" of MM5 or WRF meteorological output to generate meteorological inputs for CALPUFF and other dispersion models. MMIF bypasses CALMET, which EPA has shown modifies and can degrade the MM5/WRF wind fields (EPA, 2009a).

2.2.1.1 CALPUFF V5.8

CALPUFF includes algorithms for near-source effects such as building downwash, transitional plume rise, partial plume penetration, subgrid scale terrain interactions as well as longer range effects such as pollutant removal due to wet scavenging and dry deposition, chemical transformation, vertical wind shear, overwater transport and coastal interaction effects.

CALPUFF provides a number of options to calculate dispersion coefficients, including turbulence-based dispersion coefficients (based on the standard deviations of the vertical and crosswind horizontal components of the wind), and the use of stability-based empirical relationships such as the Pasquill-Gifford or McElroy-Pooler dispersion coefficients. The most desirable approach is to use turbulence-based dispersion coefficients using measured turbulent velocity variances or intensity components, if such data are readily available and they are of good quality. Since reliable turbulent measurements are generally not available, the recommended approach is to use similarity theory to estimate the turbulent quantities using the micrometeorological variables calculated by CALMET. This approach is also referred to as first-order closure.

CALPUFF also has the capability to model the effects of vertical wind shear by explicitly allowing different puffs to be independently advected by their local average wind speed and direction, as well as by optionally allowing well-mixed puffs to split into two or more puffs when across-puff shear becomes important. Another refinement is an option to use a probability density function (pdf) model to simulate vertical dispersion during convective conditions.

CALPUFF includes parameterized chemistry modules for the formation of secondary sulfate and nitrate from the oxidation of the emitted primary pollutants, SO_2 and NO_x. The conversion processes are assumed to be linearly dependent on the relevant primary species concentrations, i.e., they are treated as first-order processes.

Various options are available to calculate the conversion rates. The simplest option is for the user to specify diurnally varying transformation rates. Additionally, there are two options in which the rates are internally calculated by CALPUFF. The first option is based on the MESOPUFF II scheme (Scire et al., 1983), in which the pseudo-first-order constants for the daytime gas-phase conversions of SO_2 to sulfate and NO_x to nitric acid and other (organic) nitrates are parameterized as functions of the background ozone concentration (provided as input to CALPUFF), the total solar radiation intensity, the stability index, and the plume NO_x concentrations. Constant nighttime gas-phase SO_2 and NO_x conversion rates are specified as default values in the model. Aqueous-phase conversion of SO_2 to sulfate is parameterized as a function of the relative humidity.

The second option is to use the RIVAD/ARM3 scheme which treats the NO and NO_2 conversion process in addition to the NO_2 to inorganic nitrate and SO_2 to sulfate conversions. This scheme assumes low background VOC concentrations and is not suitable for urban regions. The NO-NO_2-O_3 chemical system is first solved to get pseudo-steady-state concentrations of NO, NO_2,

and O_3. During the day, this system consists of the NO_2 photolysis reaction to yield NO and O_3 and the NO-O_3 titration reaction to yield NO_2. During the night, only the NO-O_3 titration reaction is considered. The steady-state daytime concentration of the hydroxyl radical, OH, is calculated from the final O_3 concentration after the solution of the NO-NO_2-O_3 system, and is used to estimate the rates of oxidation of SO_2 and NO_2 to H_2SO_4 and HNO_3, respectively. The RIVAD/ARM3 scheme does not explicitly calculate the aqueous-phase oxidation of SO_2 to sulfate. Instead, a constant heterogeneous SO_2 oxidation rate (0.2% per hour) is added to the homogeneous rate.

With both the MESOPUFF II and RIVAD/ARM3 chemistry options, a simple stoichiometric thermodynamic model is used to estimate the partitioning of total inorganic nitrate between gas-phase nitric acid and particle-phase ammonium nitrate. Total ammonia concentrations are provided as background values to the model, and the available ammonia for creating ammonium nitrate is computed as total ammonia minus sulfate to account for the preferential scavenging of ammonia by sulfate. Then, the gas-particle partitioning of total nitrate is estimated using the available ammonia concentration, the total nitrate concentration, and the equilibrium constant for the HNO_3-NH_3-NH_4NO_3 system (calculated as a function of the temperature and relative humidity).

CALPUFF uses dry deposition velocities to calculate the dry deposition of gaseous and particulate pollutants to the surface. These dry deposition velocities can either be user-specified or calculated internally in CALPUFF. A resistance-based model is used for the latter option. For gaseous pollutants, the resistances that are considered are the atmospheric resistance, the deposition layer resistance, and the canopy resistance. For particles, a gravitational settling term is included and the canopy resistance is assumed to be negligible.

The various resistances and particle settling rates are calculated as functions of atmospheric variables (e.g., stability and wind speed), surface characteristics (e.g., surface roughness, vegetation type, physiological state), and the properties of the depositing material (gas diffusivity, solubility, and reactivity; particle size, shape, and density).

CALPUFF uses the scavenging coefficient approach to parameterize wet deposition of gases and particles. The scavenging coefficient depends on pollutant characteristics (e.g., solubility and reactivity), as well as the precipitation rate and type of precipitation. The model provides default values for the scavenging coefficient for various species and two types of precipitation (liquid and frozen). These values may be overridden by the user.

2.2.2   SCICHEM

SCICHEM is a non-steady-state multi-species puff model, and is the reactive extension of the Second-order Closure Integrated PUFF model (SCIPUFF), incorporating a comprehensive treatment of gas and aqueous phase chemistry and aerosol thermodynamics (Karamchandani et al., 2000; EPRI, 2000). SCIPUFF simulates plume transport and dispersion using a second-order closure approach to solve the turbulent diffusion equations (EPRI, 1988; Sykes et al., 1993; Sykes and Henn, 1995; Sykes and Gabruk, 1997).

SCICHEM's meteorological input requirements are flexible. The model can assimilate observational data ranging from a single wind measurement to multiple profiles that include turbulence measurements and/or boundary layer parameters such as mixing layer height and

Pasquill-Gifford-Turner stability class. Alternatively, three-dimensional gridded wind and temperature fields generated by a prognostic model or other analyses can be used as input to SCICHEM after appropriate reformatting. Internally, the model uses bilinear interpolation to transform the meteorological data to a three-dimensional grid. If terrain information is also specified in conjunction with observational wind input or certain kinds of gridded input, then the interpolated wind field is adjusted by minimizing the divergence to ensure mass conservation.

SCICHEM represents a plume by a collection of three-dimensional puffs that are advected and dispersed according to the local meteorological and micrometeorological characteristics. Each puff has a Gaussian representation of the concentrations of emitted inert species. The overall plume, however, can have any spatial distribution of these concentrations, since it consists of a multitude of puffs that are independently affected by the transport and dispersion characteristics of the atmosphere.

The turbulent diffusion parameterization used in SCICHEM is based on second-order turbulence closure theories (Donaldson, 1973; Lewellen, 1977) providing a direct connection between measurable velocity statistics and predicted dispersion rates. The generality of the turbulence closure relations provides a dispersion representation for arbitrary conditions. Empirical models based on specific dispersion data are limited in their range of application, but the fundamental relationship between the turbulent diffusion and the velocity fluctuation statistics is applicable for a much wider range. The closure model has been applied on local scales up to 50 km range (EPRI, 1988) and also on continental scales up to 3000 km range (Sykes et al., 1993). The second-order closure algorithm has been shown to provide better model performance than both empirical algorithms, such as the Pasquill-Gifford-Turner (PGT) method and first-order closure algorithms that use similarity theory to relate the dispersion coefficients to micrometeorological variables (Gabruk et al., 1999).

SCICHEM can simulate the effect of wind shear since individual puffs will evolve according to their respective locations in an inhomogeneous velocity field. As puffs grow larger, they may encompass a volume that cannot be considered homogenous in terms of the meteorological variables. A puff splitting algorithm accounts for such conditions by dividing puffs that have become too large into a number of smaller puffs. Conversely, puffs may overlap significantly, thereby leading to an excessive computational burden. A puff merging algorithm allows individual puffs that are affected by the same (or very similar) micro-scale meteorology to combine into a single puff. Also, the effects of buoyancy on plume rise and initial dispersion are simulated by solving the conservation equations for mass, heat, and momentum.

SCICHEM can optionally calculate the effects of building downwash on plume rise and dispersion of stack emissions using the Plume Rise Model Enhancements (PRIME) model of Schulman et al. (2000).

The gas-phase chemical reactions within the puffs are simulated using a general framework that allows any chemical kinetic mechanism (e.g., CB-IV, CB05, SAPRC) to be treated. The user enters the chemical reactions and their associated rate parameters, and SCICHEM sets the corresponding system of ordinary differential equations (ODEs) to be solved. The resulting system of stiff ODEs is solved numerically using either the Livermore Solver for Ordinary

Differential Equations (LSODE) package (Hindmarsh, 1983) or a predictor-corrector solver (Young and Boris, 1977). While changing the gas-phase chemistry mechanism itself is relatively straightforward and does not require code changes, other model chemistry components (aerosol module, aqueous-chemistry module) are also dependent on the mechanism selected, and the associated codes need to be modified to accommodate mechanism changes. For the work described here, the CB-IV mechanism was used.

Chemical species concentrations in the puffs are treated as perturbations from the background concentrations. Because the model calculates a quadratic overlap term for use in the concentration fluctuation variance, it can account for the effect of overlapping puffs on nonlinear chemical reactions. The formulation of nonlinear chemical kinetics within the puff framework is described elsewhere (Karamchandani et al., 2000; EPRI, 2000).

SCICHEM can optionally simulate the effect of turbulence on chemical kinetics explicitly for each nonlinear reaction that is designated "turbulent" by the user by carrying the concentration fluctuation correlation of the reacting species as an additional puff variable. This effect is more pronounced near the stack and requires additional computational time and storage (Karamchandani et al., 2000).

The aqueous-phase chemistry module in SCICHEM is based on that used in the U.S. EPA's regional chemical transport model, CMAQ. The module includes the major pathways for aqueous-phase conversion of SO_2 to sulfate. A pathway is also included for the heterogeneous production of nitrate from N_2O_5 hydrolysis in the presence of cloud or fog droplets.

For $PM_{2.5}$ calculations, SCICHEM includes modules to simulate the partitioning of species among the gas, aqueous, and solid phases. ISORROPIA (Nenes et al., 1998) is used to simulate the thermodynamic equilibrium of inorganic species. For secondary organic aerosols (SOA), an empirical approach based on the results of smog chamber experiments conducted at Caltech is used to partition the SOA between the gas and particle phases. Particle size distribution is simulated using a sectional representation with 2 size sections.

SCICHEM uses dry deposition velocities to calculate the dry deposition of gaseous and particulate species to the surface. Gaseous dry deposition velocities are specified as constant values by the user. For particles, a gravitational fall speed is added to the dry deposition velocity that is calculated by multiplying the collection efficiency by the momentum deposition velocity. A vegetative canopy model is used to determine the collection efficiency over vegetation and a rough surface model is used to determine the collection efficiency over water or bare soil or rock. The momentum deposition velocity is a function of the surface roughness, mixed layer depth, and micrometeorological variables such as the friction velocity and the convective velocity scale.

When the aqueous-phase chemistry option is selected, the wet deposition of pollutants is computed from the cloudwater concentrations of pollutants and the precipitation rate. Otherwise, scavenging coefficients are used to calculate wet deposition. For gases, the scavenging coefficients are specified by the user for a reference precipitation rate of 1 mm/hr. For particles, the scavenging coefficients are calculated from the precipitation rate, the average raindrop diameter, and collision efficiency. The average raindrop diameter is calculated from the precipitation rate assuming a Marshall and Palmer raindrop distribution. The collision

efficiency is a function of the particle diameter, the raindrop diameter, the particle fall velocity, the raindrop fall velocity, the viscosities of air and water, the particle diffusivity, and the particle relaxation time.

The development of chemistry modules in SCICHEM has been sponsored by the Electric Power Research Institute (EPRI). The version of SCICHEM (v2100) used in this study uses the Carbon Bond IV (CB-IV) gas-phase chemistry mechanism (Gery et al., 1989) and aerosol treatment based on the Model of Aerosol Dynamics, Reaction, Ionization and Dissolution (MADRID) (Zhang et al., 2004).

2.2.3   CAMx

The Comprehensive Air quality Model with extensions (CAMx; ENVIRON, 2011) is an Eulerian photochemical dispersion model that allows for an integrated "one-atmosphere" assessment of gaseous and particulate air pollution (ozone, $PM_{2.5}$, PM_{10}, air toxics, mercury) over many scales ranging from plume to continental. CAMx simulates the emission, dispersion, chemical reaction, and removal of pollutants in the troposphere by solving the pollutant continuity equation for each chemical species on a system of nested three-dimensional grids. The Eulerian continuity equation describes the time dependency of the average species concentration within each grid cell volume as a sum of all of the physical and chemical processes operating on that volume. Chemistry is treated by simultaneously solving a set of reaction equations defined from specific chemical mechanisms. Pollutant removal includes both dry surface uptake (deposition) and wet scavenging by precipitation.

CAMx employs a two-way nested grid structure that allows CAMx to be run with coarse grid spacing over a wide regional domain in which high spatial resolution is not particularly needed, while within the same run, applying fine grid nests in specific areas where high resolution is needed. CAMx offers the ability for users to arbitrarily introduce and/or remove various nested grids at any point during the course of a simulation (referred to as Flexi-Nesting). Upon model restart, CAMx automatically diagnoses any changes to the grid system. Users can supply complete information for new grids (emissions, landuse, meteorology) or allow CAMx to interpolate any or all of these inputs from parent grids. Example applications of flexi-nesting include running spin-up days with a single coarse master grid and introducing nests just for episode days, or evaluating sensitivity to grid configuration when designing a model application.

CAMx includes multiple photochemical and gas phase chemistry mechanisms. Users can select among two version of Carbon Bond chemistry (CB05 and CB6) or the 1999 version of the Statewide Air Pollution Research Center chemistry (SAPRC99; CAMx Mechanism 5). CAMx also features a "one-atmosphere" treatment for ozone and particulate matter (PM) with detailed algorithms for the relevant science processes, including aqueous chemistry (RADM-AQ), inorganic aerosol thermodynamics/partitioning (ISORROPIA), and secondary organic aerosol formation/partitioning (SOAP). Nitrate uptake by calcium on fine crustal PM is calculated external to ISORROPIA. The particulate chemistry mechanism utilizes products from the gas-phase photochemistry for production of sulfate, nitrate, condensable organic gases, and chloride. The one-atmosphere ozone/PM treatment is linked to CB05, CB6, and SAPRC99 gas-phase chemistry. CAMx provides two options for the representation of the particle size distribution: a static two-mode coarse/fine (CF) scheme and the multi-sectional CMU scheme,

which treats the size evolution of each aerosol constituent among a number of fixed size sections.

Three options are available to solve gas-phase chemistry. The Euler-Backward Iterative (EBI) solver has replaced the original Chemistry Mechanism Compiler (CMC) solver employed in past versions of CAMx. EBI provides improved accuracy with similar speed compared to CMC. Alternatively, users may select the Implicit-Explicit Hybrid (IEH) chemical solver with accuracy is comparable to reference methods such as LSODE but is several times slower than the EBI solver. The model also includes the fully explicit Gear-type LSODE solver. LSODE can be used to "benchmark" a simulation to evaluate the performance of EBI or IEH.

CAMx features a Plume-in-Grid (PiG) sub-model to treat the chemistry and dispersion of point source emission plumes at sub-grid scales; individual plume segments or "puffs" are tracked by the Lagrangian module while undergoing dispersion and chemical evolution, until such time as their pollutant mass should be represented within the grid model framework. Gas-phase chemistry in PiG is treated with CB05, CB6 or SAPRC99 mechanisms and solved using LSODE; PM chemistry can also be treated. PiG includes a "sampling grid" capability to passively sample plume surface concentrations at any resolution, which is particularly useful to visualize near-source sub-grid scale impacts.

The horizontal advection solver options in CAMx include the Area Preserving Flux-Form advection solver of Bott (1989) and the Piecewise Parabolic Method (PPM) of Colella and Woodward (1984). These schemes possess high-order accuracy, little numerical diffusion and are sufficiently quick for applications on very large grids. Either of these solvers may be selected via the CAMx run control file. By default, CAMx employs a standard "K-theory" approach for vertical diffusion to account for sub-grid scale mixing layer-to-layer. Version 2 of the Asymmetric Convective Model (ACM2; Pleim, 2007) is available as an alternative to the K-theory approach, which is a hybrid of local K-theory and non-local convective transport between the surface and layers aloft.

CAMx offers two dry deposition options: the original approach based on the models of Wesely (1989) and Slinn and Slinn (1980); and an updated state-of-the-science approach based on the algorithms of Zhang et al. (2001; 2003). The Zhang scheme incorporates vegetation density effects via leaf area index (LAI), possesses an updated representation of non-stomatal deposition pathways including a better snow cover treatment, and has been tested extensively through its use in daily air quality forecasting. The original Wesely/Slinn model is formulated for 11 landuse categories, while the Zhang model uses 26 landuse categories.

The TUV radiative transfer and photolysis model, developed and distributed by the National Center of Atmospheric Research (NCAR, 2011), is used as a CAMx preprocessor to provide the air quality model with a multi-dimensional lookup table of clear-sky photolysis rates. CAMx includes two options to internally adjust clear-sky rates for the presence of clouds. The default approach uses a fast in-line version of TUV, which can also account for aerosol opacity (haze), while the original approach is based on the parameterization developed for the Regional Acid Deposition Model (RADM).

The CAMx "extensions" include: Ozone Source Apportionment Technology (OSAT); Particulate Source Apportionment Technology (PSAT); Decoupled Direct Method (DDM) and Higher-Order

Decoupled Direct Method (HDDM) for Source Sensitivity of Ozone and Other Gas Species; Process Analysis (PA); and Reactive Tracers (RTRAC).

2.3   APPLICATION OF MODELS

The three models described above were used to simulate the Cumberland and Oklaunion power plant plumes on July 6, 1999 and the night of October 10, 2006, respectively.

2.3.1 SOS 99 Cumberland Plume Measurements

July 6, 1999 was a clear day with light winds from the west and north-west, so that the plume from the Cumberland power plant was traveling towards Nashville. The TVA Bell 205 helicopter conducted 12 traverses of the Cumberland plume at downwind distances ranging from 11 km to 90 km and an average altitude of 500 m AGL. The first five traverses were conducted at a downwind distance of about 11 km from 11:06 a.m. LST to 11:33 a.m. LST. For all these traverses, the measurements indicated background ozone of approximately 60 ppb that was reduced to 10 to 30 ppb within the plume due to titration by the Cumberland NO_x emissions, with no ozone formation anywhere in the plume. The next three traverses were conducted at a downwind distance of about 31 km from 11:53 a.m. LST to 12:22 p.m. LST. For these traverses, background ozone at the plume centerline was reduced to about 40 ppb (20 ppb below background), but formation of ozone, up to 10 ppb above background, was observed at the plume edges (wings). Traverses 9 through 11 were conducted at a downwind distance of about 65 km from 3:05 p.m. LST to 3:29 p.m. LST. At this downwind distance, there was significant formation of ozone in the plume, up to about 90 ppb (i.e., 30 ppb above background). The last traverse was conducted from 3:49 p.m. LST to 4:02 p.m. LST at a downwind distance of about 90 km, with a peak ozone concentration of about 100 ppb at the plume centerline.

2.3.2   TexAQS II Oklaunion Plume Measurements

The Oklaunion plume traverses were conducted during the night and early morning of October 10 and 11, 2006 (Brown et al., 2011). The NOAA P-3 night flight included multiple intercepts of the Oklaunion plume at varying distances downwind, from about 14 km to 58 km downwind of the power plant. The wind direction was approximately from the north, such that the plumes were encountered on a series of east-west running transects at varying distances south of the plant. Many of the plume intercepts had excess NO and zero O_3 at plume center, indicating complete titration of the background ozone by the NO_x emissions from the power plant. Locating plumes advected downwind of a large point source from an aircraft at night was difficult because of the narrow plume depth in a vertically stratified nighttime atmosphere. Many transects failed to locate the plume at all, and transects separated by as little as 150 m encountered either strong plume intercepts or background air, indicating a plume depth of no more than 300 m. The majority of the intercepts, especially later in the flight and longer after sunset, found the plume only at the lowest operational P-3 altitude of approximately 300 m (Brown et al., 2011). Because the plume was sampled during the night, there was no ozone formation in the plume, unlike the Cumberland plume traverses, which were conducted during the day. Instead, the nighttime chemistry of NO_3 and N_2O_5 in the Oklaunion plume is of more relevance.

For all three models evaluated in this study, hourly SO_2 and NO_x emissions for the Cumberland and Oklaunion power plants during the study period were obtained from CEMS data from the

EPA Clean Air Markets Division (CAMD) website[1]. However, as mentioned previously there are significant differences among the models in their other input requirements, so we provide a brief summary of the preparation of inputs for the three models below.

2.3.3   SCICHEM Simulations

SCICHEM V2100 was used in the simulations described here. For both the Cumberland and Oklaunion plume simulations, SCICHEM was run in two configurations: with observed meteorology and with gridded meteorology (referred to as the MEDOC format) created by the MMIF pre-processor using WRF outputs (for Cumberland) and MM5 outputs (for Oklaunion).

For the Cumberland simulation with observed meteorology, hourly-varying surface and upper air meteorological data from four sites (Dickson, Gallatin, Eagleville and Cumberland) were used in the analysis. The first three of these sites are about 29 km southeast, 113 km east and 120 km southeast, respectively, of the source location, while the fourth is located at the source itself. These data and terrain heights for the domain were directly input to SCICHEM, which internally calculated gridded meteorological fields and boundary layer variables. The horizontal domain for the Cumberland simulations with observed meteorology was 396 km x 472 km with the source location defined at the center of the domain. In both directions, the horizontal grid spacing for SCICHEM simulations was 1/10th (~ 40 km) of the domain length. In the vertical direction, the domain extended up to 2 km with a resolution ranging from 20 m at the surface to 400 m at the top.

For the Oklaunion plume simulations, a pseudo-upper air meteorology file was created using the P-3 aircraft observations of wind speed, wind direction, and temperature. This provides a more representative characterization of the meteorological conditions at plume height than the routine twice-daily upper air measurements.

For the Cumberland and Oklaunion plume simulations with gridded meteorology inputs, the MMIF pre-processor was used to convert WRF and MM5 outputs, respectively, to the SCICHEM MEDOC format. The SCICHEM-WRF modeling domain for Cumberland was the 4 km resolution domain shown in Figure 2-1. The domain for the Oklaunion SCICHEM-MM5 application is shown in Figure 2-2.

For both the Cumberland and Oklaunion plume simulations, SCICHEM background concentrations were specified by averaging the Bell 205 and NOAA P-3 measurements before and after the plume intercepts. As mentioned previously in the discussion of the field measurements, the P-3 measured a larger suite of chemical species than the TVA helicopter, including VOCs, PAN, and nighttime species such as NO_3 and N_2O_5. For the daytime Cumberland simulations, background VOC concentrations typical of semi-rural to semi-urban conditions were used. The region around Cumberland and Nashville is heavily forested, with significant levels of isoprene (ranging from 1.5 to 10 ppb near the surface and lower values at higher altitudes) during the day (e.g., Luria et al., 2000) and sometimes even at night (e.g., Stroud et al., 2002). We used a background concentration of 1 ppb of isoprene at the aircraft altitude of approximately 500 m. Background concentrations of the OH and HO_2 radicals are

---

critical for the daytime Cumberland simulations, and we used mixing ratios in the range of values reported by Martinez et al. (2003) for the study period.

In addition to these input values, SCICHEM includes a number of parameters that control horizontal and vertical plume growth, as well as the degree of puff splitting and merging. The default values of the splitting and merging parameters are biased towards minimizing the number of puffs to optimize computational performance. This is adequate for most practical applications of the model, but typically results in a Gaussian profile across the plume and does not capture plume-edge effects such as the formation of ozone wings during the day or N_2O_5 wings during the night. To capture these fine-scale features that were observed in both the Cumberland and Oklaunion plume measurements, we increased puff resolution by allowing more puffs to split and less puffs to merge. For the nighttime Oklaunion plume with narrow plume widths and shallow plume depths (Brown et al., 2011), we limited puff growth in both the horizontal and vertical directions. Furthermore, the height of the Oklaunion plume was specified at 400 m, approximately the height at which most of the aircraft measurements were conducted, and initial plume dimensions were specified.

Model simulations were started at midnight (local standard time) and carried out for 24 hours for the daytime Cumberland scenario. For the nighttime Oklaunion simulations, the SCICHEM run was started in the early evening and run for 6 hours. SCICHEM uses variable time intervals for the plume dynamics and chemistry calculations, and generates the instantaneous concentration output at user-specified intervals. We used a 2 minute time step to allow a better comparison between the model results and the high-resolution aircraft measurements. To compare the model results with the observations, we selected the model output for the time interval closest to the observed sampling time.
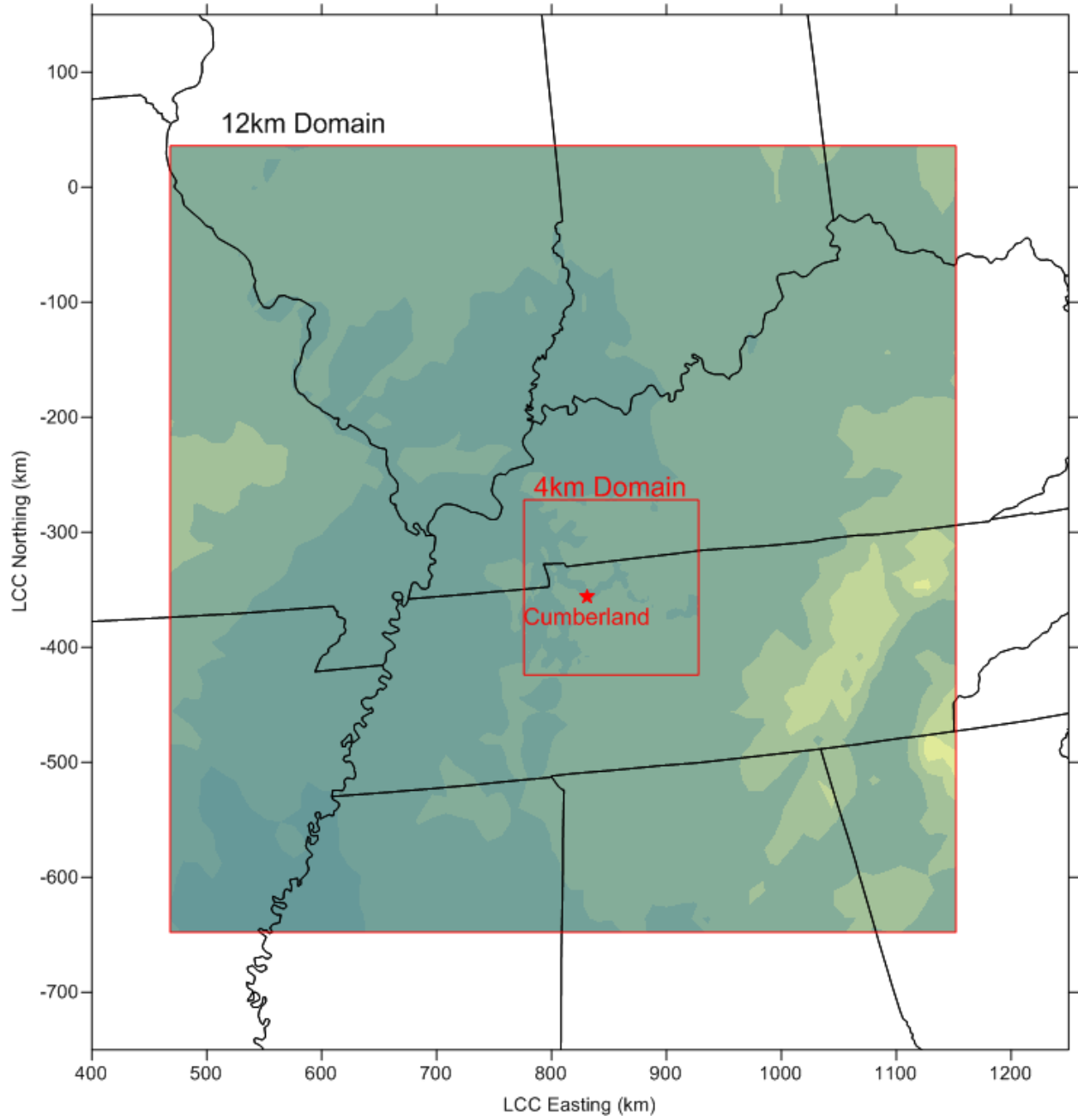
Figure 2-1. Modeling domain used for the SCICHEM SOS 99 Cumberland plume application with WRF meteorology.
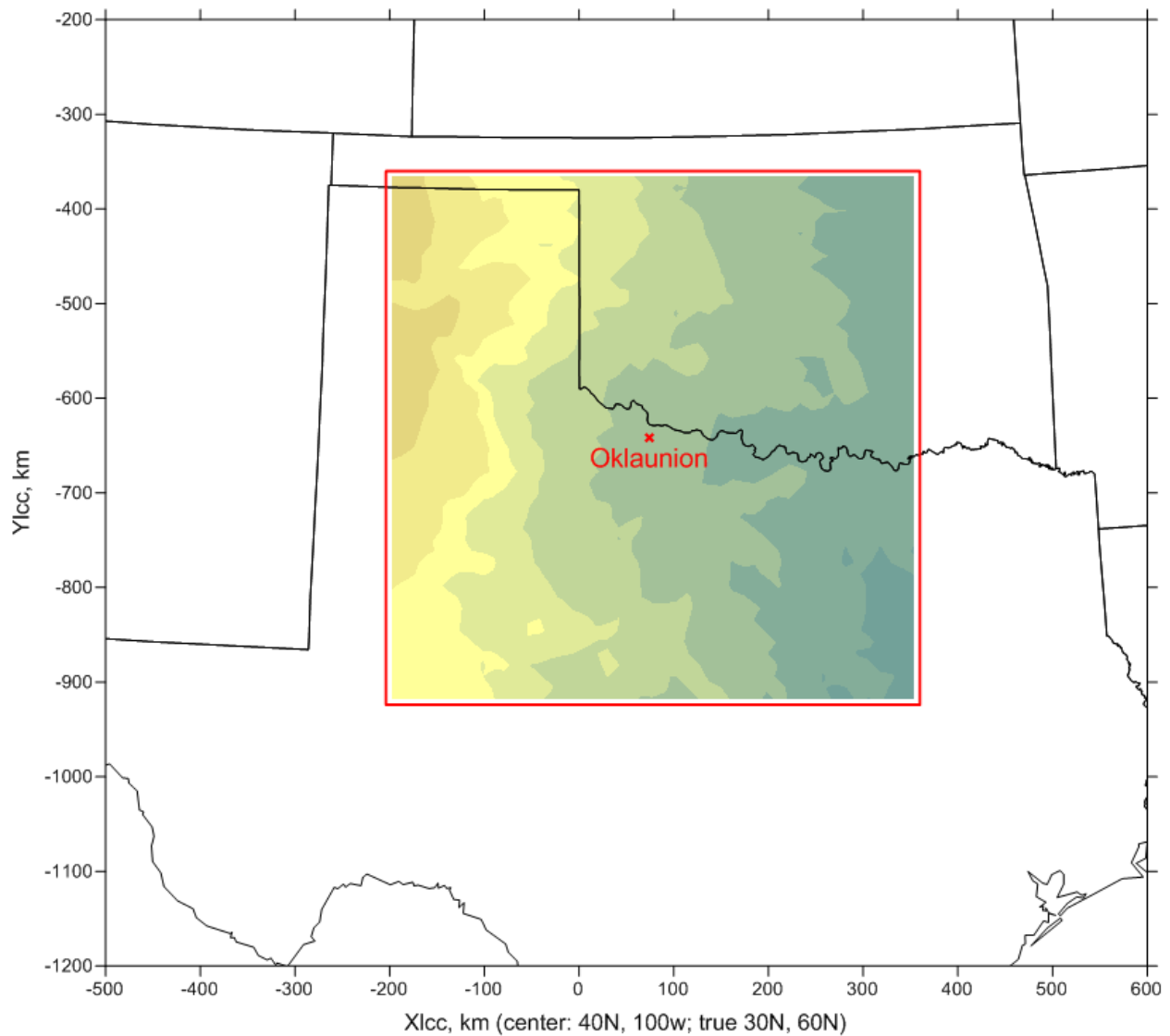
Figure 2-2. Modeling domain used for the SCICHEM TexAQS II Oklaunion plume application with MM5 meteorology. The colored box shows the 12 km model domain used for this assessment.

2.3.4 CAMx Simulations

The photochemical grid modeling was performed with the December 2010 version (version 5.4) of the Comprehensive Air quality Model with extensions (CAMx). To capture some of the fine scale behavior of the power plant plumes, the CAMx modeling was conducted with a flexi-nest option with fine resolution (500 m for the Cumberland simulations and 200 m for the Oklaunion simulations) downwind of the power plants, as well as with the Plume-in-Grid (PiG) option for Oklaunion.

The CAMx flexi-nesting capability allows for the introduction of a nested grid of arbitrary size and resolution, so long as its grid spacing is an integer division of its host grid resolution. Meteorological data are internally interpolated from the host grid to the flexi-nest. Although gridded emission inputs are evenly distributed across all flexi-nest grid cells that occupy each host grid cell (no resulting improvement in emission resolution), point sources are directly emitted into the specific flexi-nest grid column containing the stack (direct improvement in emissions resolution). Incoming boundary conditions for the flexi-nest are derived from the host grid as the model runs, and the evolution of mass distribution in the flexi-nest is transferred and averaged up to the host grid (this process is referred to as "2-way" interactive nesting). The PiG treatment in CAMx comprises a Lagrangian puff model, like SCICHEM, that operates in tandem with the host grid model to simulate the early dispersion and chemistry of point source plumes. Puff growth rates are determined from the grid-resolved meteorological fields and are based on SCICHEM equations, while plume chemistry is driven by point source emissions in combination with grid-scale background concentrations through an "incremental" plume chemistry concept. The PiG employs the full CB05 chemistry mechanism, which is integrated using the fully explicit Gear-type LSODE solver. Once puff horizontal dimensions are commensurate with the horizontal grid scale, the chemically aged puff mass increments are transferred to the grid column in which it resides according to the vertical extent of the puff. Additional details on PiG are provided in the CAMx User's Guide (ENVIRON, 2011).

For the July 1999 CAMx simulations of the Cumberland plume, the 12- and 4-km modeling domains shown in Figure 2-1 were used. The modeling vertical structure consists of 34 layers which match one-to-one with those used for the 1999 WRF meteorological model simulation. The 12- and 4-km simulations were conducted with one-way nesting, that is, the initial and boundary conditions for the 4-km grid were extracted from the 12-km simulation results. The initial and boundary conditions for the 12-km grid were extracted from the 3-dimensional outputs from a previous CAMx simulation for the year 1999 over the 36-km national RPO domain that was provided by EPA. The biogenic emissions were replaced with those estimated by the Model of Emissions of Gases and Aerosols from Nature (MEGAN; version 2.03a). A sensitivity simulation was also conducted with the original biogenic emissions which were generated from the SMOKE BEIS3 model. Figure 2-3 compares NO_x and non-methane volatile organic compounds (NMVOC) emissions from MEGAN and SMOKE BEIS3. MEGAN estimated significantly higher biogenic NMVOC emissions than SMOKE BEIS3 while estimating lower biogenic NO_x emissions.

Average altitudes of aircraft measurements range from 495 m to 511 m, which correspond approximately to the interface of the 8th and 9th model layers (Figure 2-4). For the model evaluation, we averaged concentrations of the 8th and 9th model layers and compared them

with the aircraft measurements. Figure 2-5 shows NO_x plumes originated from the Cumberland plant, predicted by the initial 4-km CAMx simulation. Although the 4-km grid resolution is not fine enough to capture details of the plume shape, it identifies directions of plume progress and helps to determine where to put a finer nested grid. The plume shapes and directions in the 8th and 9th model layers appear almost identical. Based on the results of this preliminary simulation, a 500-m fine grid was defined to track the Cumberland plume (shown as red rectangle in Figure 2-5) and modeled using the flexi-nesting technique in CAMx. As mentioned above, with flexi-nesting, the point-source emissions are modeled with finer resolution (500-m) while other model inputs (surface emissions, landuse, meteorology) are interpolated from the parent grid (4-km).

For the CAMx simulations of the dispersion and chemical evolution of the Oklaunion plume during October 10-11, 2006, two approaches were employed. In the first approach, CAMx was applied with the Plume-in-Grid (PiG) treatment for the Oklaunion power plant emissions. In the second approach, a super high-resolution nested grid (flexi-nest) sufficiently large was used so as to capture about 3 hours transport of the Oklaunion plume.

We used the October 2006 TCEQ Houston CAMx modeling database for the Oklaunion simulations. This dataset comprises meteorological, emissions, and other ancillary model inputs for TCEQ's standard 2-way nested grid system comprising a 36 km regional grid over the eastern US, a 12 km over the south-central US, and a 4 km grid over Houston. Only the 36 and 12 km grids were used in the simulations reported here. The model was run from 0000 LST October 10 through 2400 LST October 11, 2006 using preexisting CAMx results at 2400 LST October 9 as initial conditions.
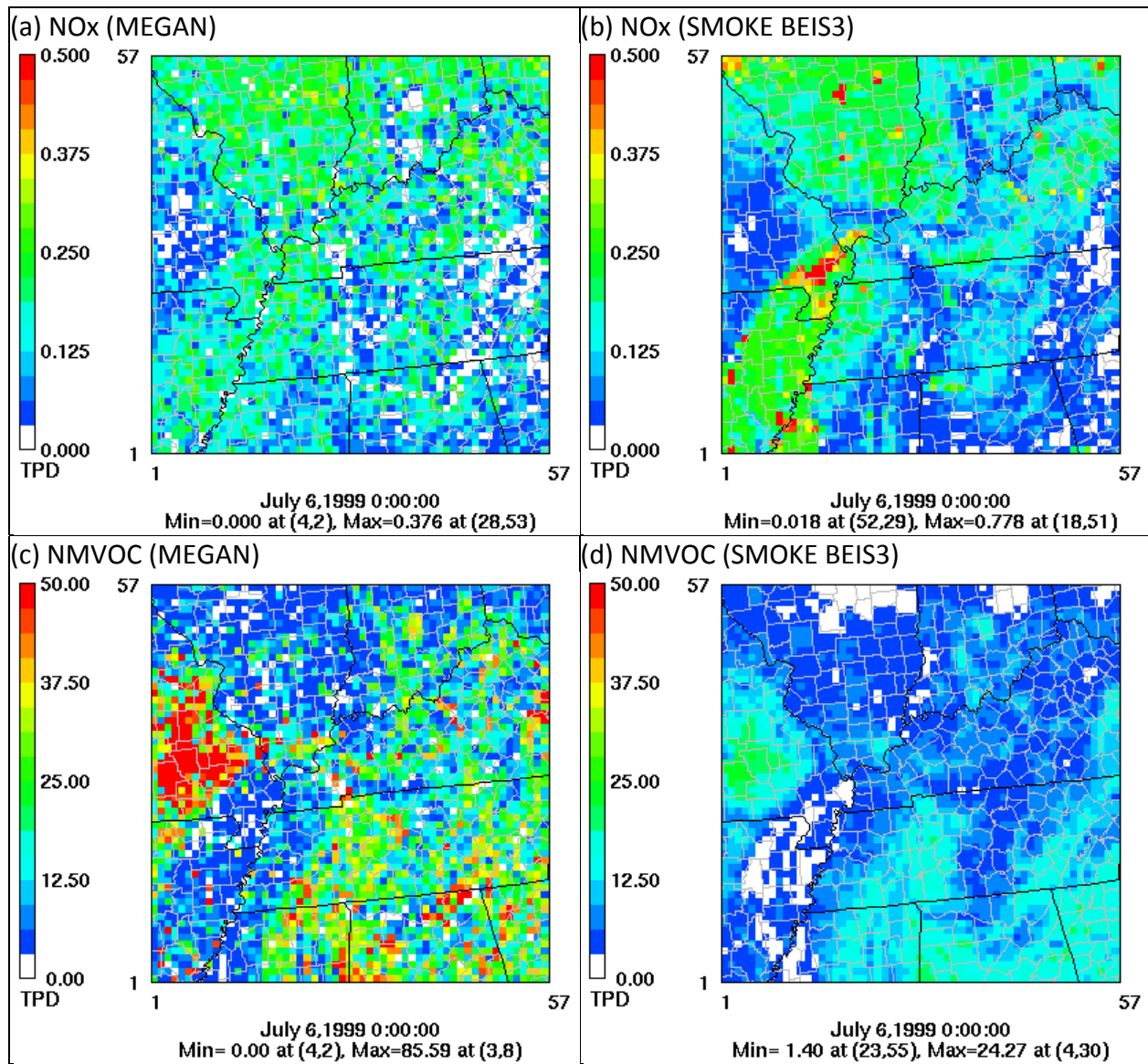
Figure 2-3. Daily total biogenic emissions (tons per day) of NO$_x$ (top) and NMVOC (bottom) estimated by MEGAN (left) and SMOKE BEIS3 (right) on July 6, 1999.
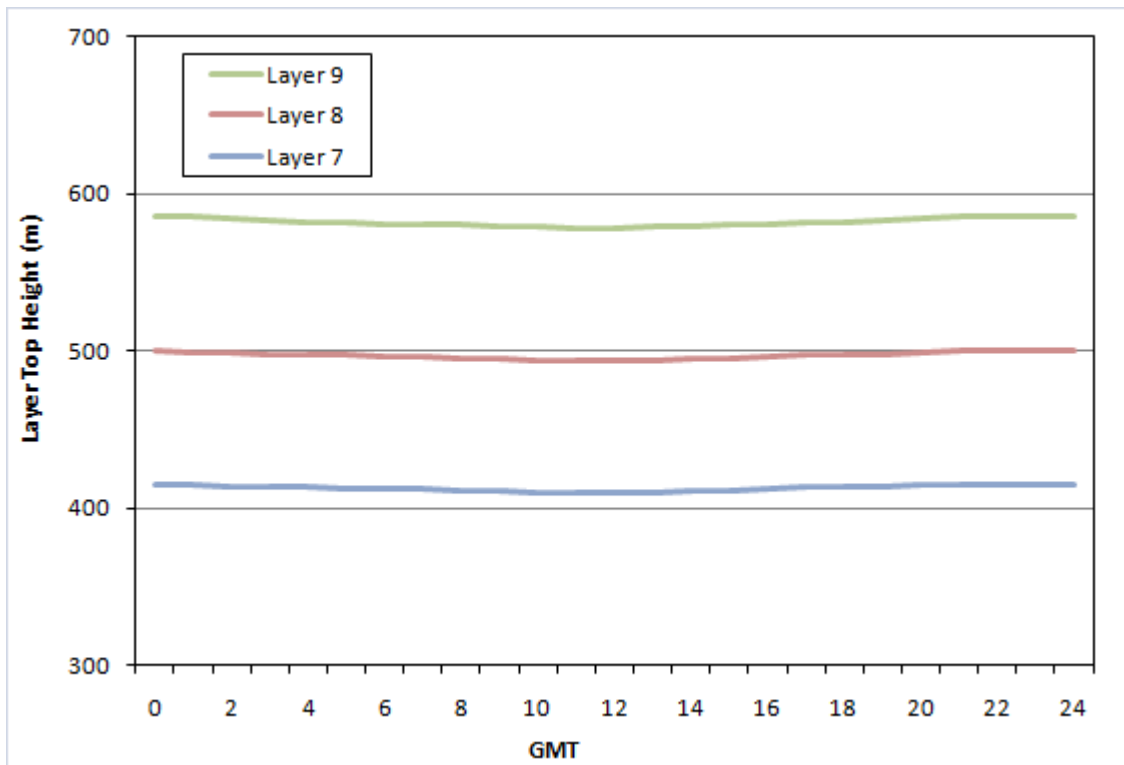
Figure 2-4. Model layer top heights averaged over the 4-km domain on July 6, 1999.
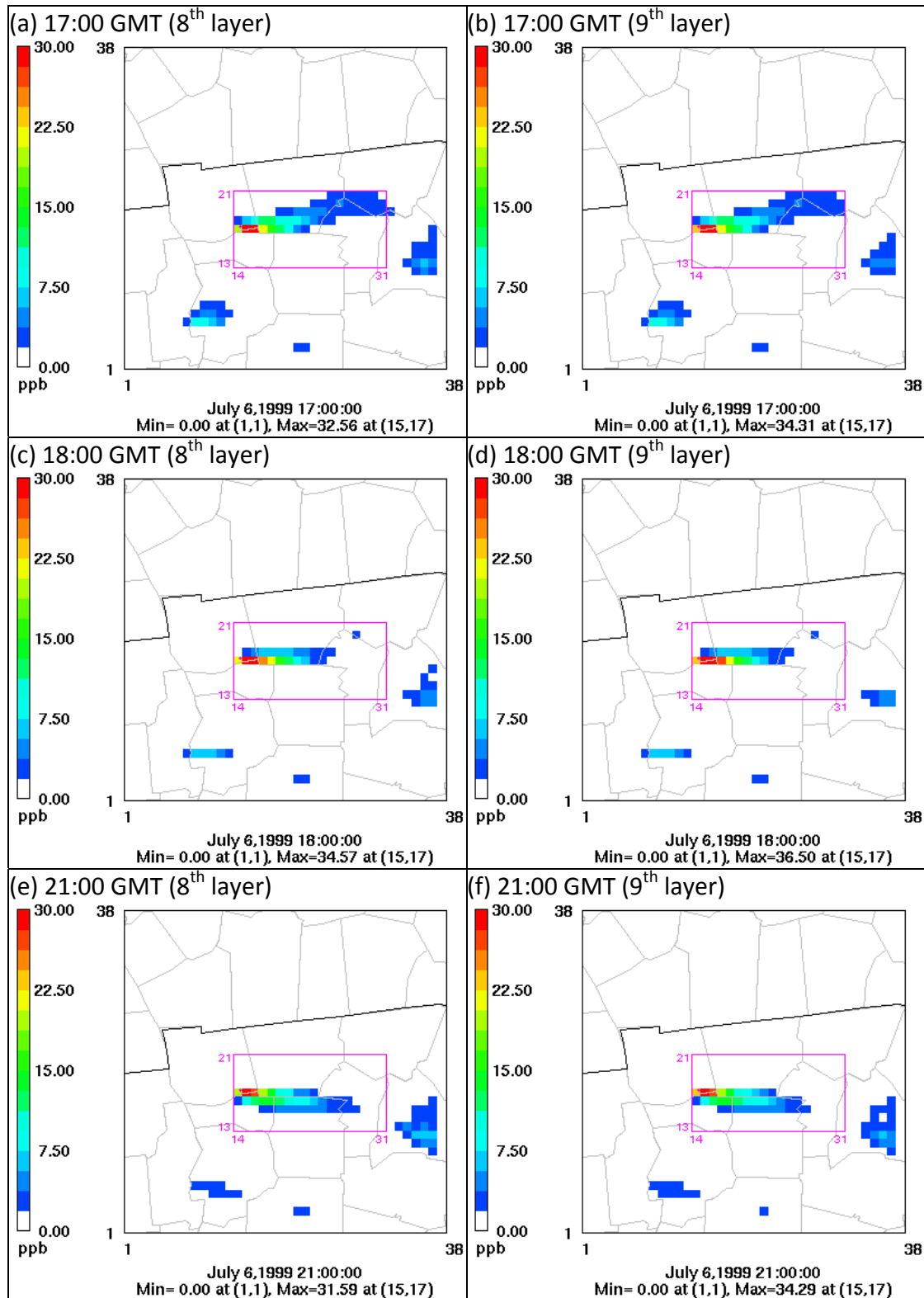
Figure 2-5. NO$_x$ concentrations on July 6 from the initial 4-km simulation. The purple rectangle shows the location of the high resolution (500 m) domain defined for tracking the Cumberland plume on July 6, 1999.

The PiG treatment was configured to simulate only the Oklaunion plume. By default, PiG is configured to treat each puff as a single "reactor" volume, which means that a puff-average concentration at any instant is determined by dividing total puff mass by its time-evolving volume. Of course, this underestimates concentrations in the plume core while overestimating concentrations near the plume edge. To investigate chemical evolution of the plume cross section in this study, each PiG puff was configured as a set of five reactors. In this case, total puff volume is divided into five equal sub-volumes that grow in proportion to the total puff, and emitted pollutant mass is initially distributed to each reactor according to a Gaussian distribution. As the puff moves and grows downstream, chemistry is calculated according to the conditions in each puff reactor, resulting in five plume regimes from the plume core to the plume edge.

A super high-resolution flexi-nest was also used to simulate the evolution of the Oklaunion plume in lieu of the PiG model. Results were compared against PiG results and observed conditions on the evening of October 10, 2010. We defined a flexi-nested grid spacing of 200 m occupying a set of 6x9 12 km grid cells (362x542 grid cells, 72x108 km) that includes the Oklaunion plant in the north with sufficient distance to the south to track about 3 hours of the downwind plume. CAMx was run with this flexi-nest for the hours of 1800-2400 LST, using initial conditions at 1800 LST from a previous CAMx run. This 6-hour 200 m resolution flexi-nest run took over 40 times longer (~14 hours) to run than a 24-hour PiG run using a 4 km grid resolution (20 minutes). This incremental runtime increase may not be as severe when starting from a finer resolution domain (e.g., 4 km) than the 12 km used in this analysis.

2.3.5   CALPUFF Simulations

Two CALPUFF runs were performed for each plume field experiment. CALPUFF v5.8 simulations were performed using meteorological inputs based on CALMET v5.8 and MMIF that does a direct reformatting of the WRF (SOS 1999) or MM5 (TexAQS II) prognostic meteorological model output.

For the CALPUFF v5.8 runs using with CALMET, the CALMET setting were chosen to match the FLM/EPA-required settings for long-range transport and the typical Air Quality Related Values (AQRV) analysis required in a Prevention of Significant Deterioration (PSD) application (FLAG, 2010; EPA, 2009b).

The MMIF version used in this study does not interpolate vertically to obtain CALPUFF meteorological inputs for a user-specific vertical layer structure as done by CALMET. Rather, the MMIF vertical layer structure must be defined based on the initial vertical layer structure in the MM5/WRF levels. Thus, the MMIF vertical levels where chosen to best match the EPA/FLM default levels. The final 10 vertical layers were reasonably close to the EPA/FLM-recommended vertical levels, but were thicker near the surface.

Background concentrations for HNO_3, O_3, and H_2O_2 were taken from the CAMx simulations, using daily domain-average conditions. Receptors were placed in a ring at the average down-wind distance, and average height above ground, as the observations. Receptor sets were specific to each hour of the observations, and a separate CALPUFF run was performed targeting each hour of the observations. This allowed for sufficient time to populate the grid with puffs, using hourly emissions (PTEMARB.DAT) translated from the CAMx emissions data for the two

point sources that were based on Continuous Emissions Monitoring Systems (CEMS) measurements.

2.3.6   Evaluation Approach

For all models, receptors were placed along an arc around the source located at the average downwind distance and at the height above ground for each plume traverse. This allows the determination of the plume centerline (as defined by the location of the maximum SO_2 or NO_y concentrations along a cross-wind traverse). In general, the predicted plume centerline positions from the models are expected to be displaced from the observed plume centerline position, and even from each other, due to small discrepancies in the wind fields used in the various models and the actual winds transporting the plumes during the study period. Thus, to facilitate the comparison of modeled cross-wind concentration profiles with observed profiles, we aligned the plume centerline locations between the predictions and observations.

3.0 Evaluation Using the 1999 SOS TVA Cumberland Measurements

This section describes the evaluation of the three models using the SOS 99 Cumberland plume measurement field experiment data.

3.1 SCICHEM EVALUATION

As discussed in Section 2.3.1, the July 6, 1999 Cumberland plume was sampled by the TVA helicopter along 12 plume traverses, at four downwind distances of 11, 31, 65 and 90 km. In this section, we compare the SCICHEM results for selected traverses at each downwind distance.

Before discussing the comparison of observed and modeled plume traverse concentration profiles, it is useful to determine the angular separation between the observed and modeled plume centerline locations, which results from discrepancies in the actual wind fields and the model wind fields, as discussed in Section 2.3.3.

Figure 3-1 shows the observed and modeled (using observed surface and upper air meteorology) plume transport directions and sampling arcs for each downwind distance. As seen in the figure, for the closest traverse at 11 km, the observed and simulated plume directions are in remarkably good agreement. For the traverses at the larger downwind distances, the plume directions are still in very good agreement, but there are some small differences in the locations of the plume centerlines. In contrast, when the MMIF-processed WRF meteorology is used, there are substantial deviations between the observed and simulated plume directions, as shown in Figure 3-2.

It is also useful to compare the observed and modeled plume widths, because a large part of the discrepancies between observed and predicted concentrations can be attributed to errors in the calculation of plume dispersion. The plume widths were calculated for each plume traverse as the extent of the plume that contains 95.5% of the SO_2 mass (representing 4 sigmas of a Gaussian distribution) in the traverse. Table 3-1 shows the observed and calculated plume widths for four traverses at the four downwind directions shown in Figure 3-1. The calculated plume widths are shown for the two different SCICHEM simulations (one with observed meteorology and the other with gridded meteorology based on WRF outputs).

Table 3-1. Selected TVA Bell 205 transects of the Cumberland power plant plume on July 6, 1999.

Transect	Downwind distance (km)	Measurement start time (LST)	Measurement end time (LST)	Plume width from measurements (km)	Plume width from SCICHEM (km)	
					Obs. Met.	WRF Met.
3	10.8	11:19:06 a.m.	11:24:51 a.m.	5.7	7.3	2.4
8	31.5	12:22:31 p.m.	12:28:21 p.m.	7.1	12.1	13.1
10	64.9	3:05:11 p.m.	3:16:16 p.m.	10.2	21.5	13.5
12	89.1	3:48:56 p.m.	4:02:46 p.m.	10.4	26.4	17.0

As shown in Table 3-1, when observed meteorology is used, SCICHEM always predicts wider plumes than the aircraft measurements. The best agreement between the observed and modeled (with observed meteorology) plume widths is for Traverse 3 at 11 km downwind. On

the other hand, when WRF meteorology is used, there is better agreement between observed and modeled plume widths and SCICHEM actually predicts a much narrower plume than inferred from measurements for Traverse 3. As shown below, this is partly due to the measured plume being asymmetric with a wider tail on one side than the other. Using WRF meteorology, the best agreement between modeled and observed plume widths is noted for Traverse 10 at 65 km downwind of Cumberland.

Figure 3-1. Observed and simulated (SCICHEM) plume transport directions and plume traverses at 11 km (top left), 31 km (top right), 65 km (bottom left) and 90 km (bottom right) downwind of the Cumberland power plant on July 6, 1999. SCICHEM results are based on measured surface and upper air meteorology.
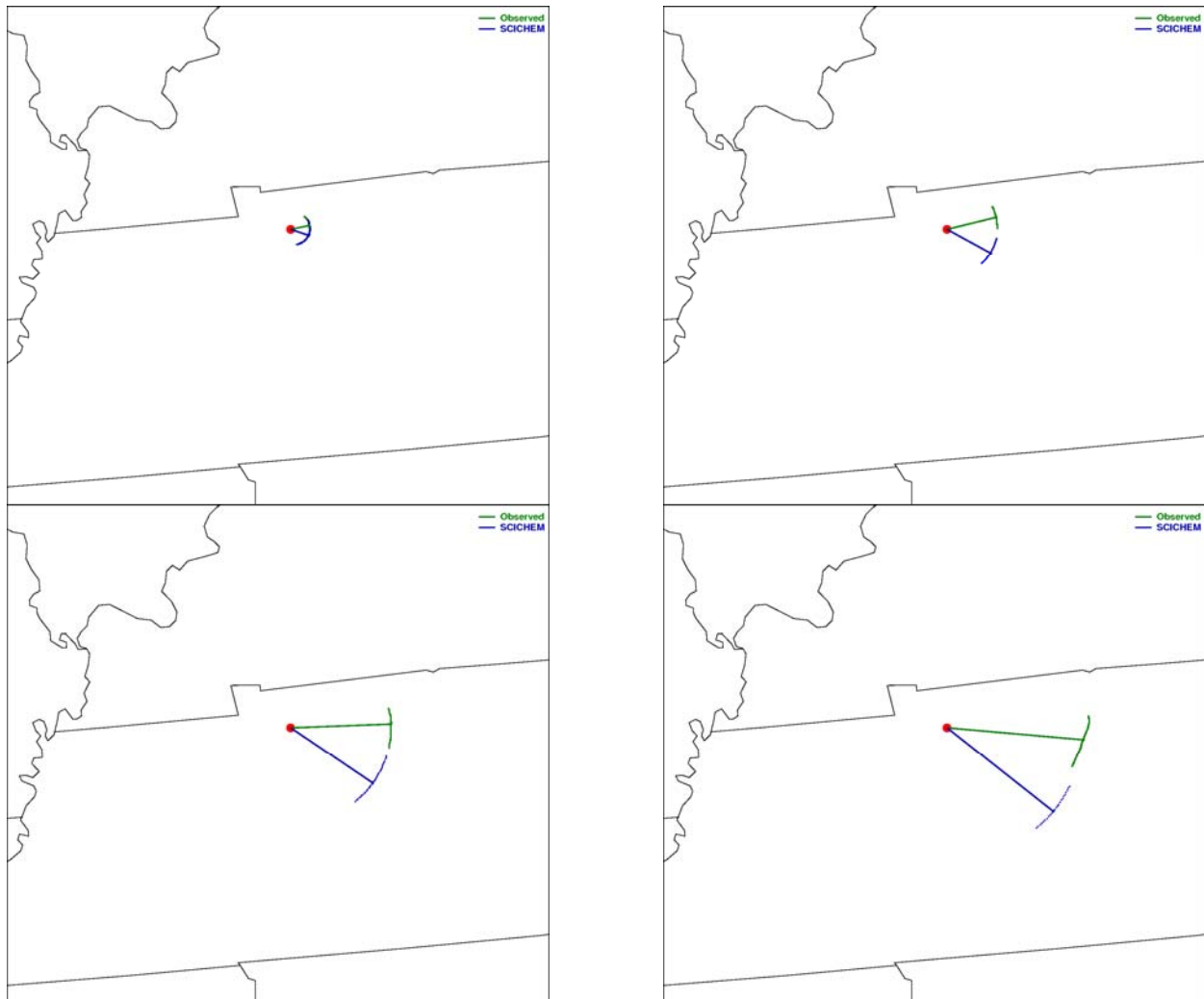
Figure 3-2. Observed and simulated (SCICHEM) plume transport directions and plume traverses at 11 km (top left), 31 km (top right), 65 km (bottom left) and 90 km (bottom right) downwind of the Cumberland power plant on July 6, 1999. SCICHEM results are based on WRF meteorology processed with MMIF.

Figures 3-3 compare observed concentrations of SO_2, NO_y, NO, NO_2, O_3 and NITR concentrations, for Traverse 3 of the Cumberland plume with SCICHEM predictions using observed meteorology. The SCICHEM predictions are extracted at 500 m, at about the sampling height of the helicopter measurements. NITR represents total inorganic nitrate (nitric acid + particulate nitrate). For the helicopter measurements, NITR is inferred as the difference between the NO_y and NO_y^* measurements, where NO_y^* is NO_y with an inlet nylon filter to remove nitric acid and particulate nitrate (Tanner et al., 2002). The observed peak SO_2 concentration is under-predicted by about 35% and the observed peak NO_y concentration is under-predicted by 50%, consistent with the wider plume predicted by SCICHEM (Table 3-1). The NO and NO_2 comparisons show that significantly more NO is converted to NO_2 in the modeled plume than in the observations – the peak NO_2/NO ratio in the measurements is about 0.75, while the corresponding ratio in the model is about 2. The background ozone is titrated to about 25 ppb at the plume centerline in the model compared to the 10 ppb in the observations. The measurements show significantly more formation of inorganic nitrate than predicted by the model at this relatively short downwind distance, which is surprising since nitrate and sulfate formation are expected to be slow during the early stages of the plume when oxidant levels are suppressed due to titration of ozone by the NO_x in the plume. The peak inorganic nitrate in the measurements is more than 5 times the peak inorganic nitrate predicted by SCICHEM.

Figure 3-4 shows the corresponding comparisons for SCICHEM predictions using WRF meteorology. In contrast to the results with observed meteorology, the narrower predicted plume with the WRF meteorology results in peak SO_2 and NO_y concentrations that are higher than the observed peaks by about 33% and 5% respectively. The NO and NO_2 comparisons show that the model still over-predicts the conversion of NO to NO_2 in the plume, though not as much as in the simulation with observed meteorology. The background ozone is completely titrated in the simulation with WRF meteorology. We also see that the inorganic nitrate produced with the WRF meteorology is almost twice the amount produced with observed meteorology – the peak inorganic nitrate in the measurements is now less than 3 times the SCICHEM prediction.

It should also be noted that, with the WRF meteorology, the simulated plume at the location and time of Traverse 3 is much higher (at 1600 m) than the observed plume or the simulated plume with observed meteorology. Possible explanations include higher plume rise with the WRF/MMIF meteorology and/or vertical updrafts transporting the plume to higher elevations. Additional analyses of the MMIF outputs will be required to understand this behavior.
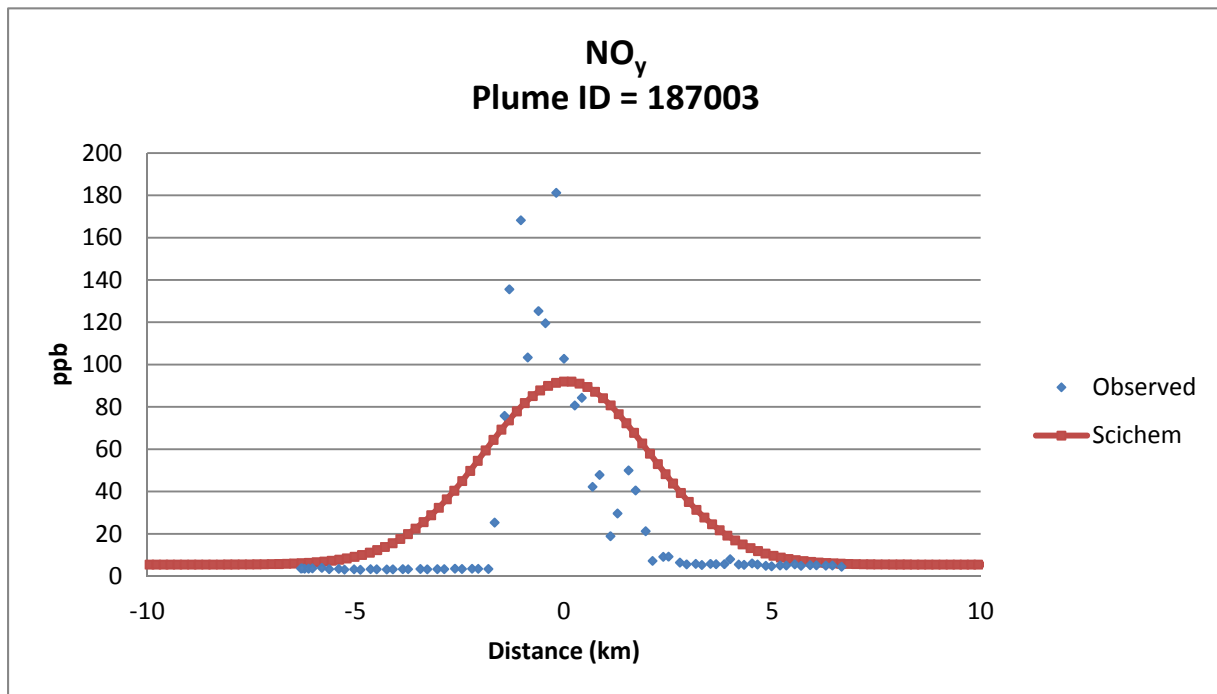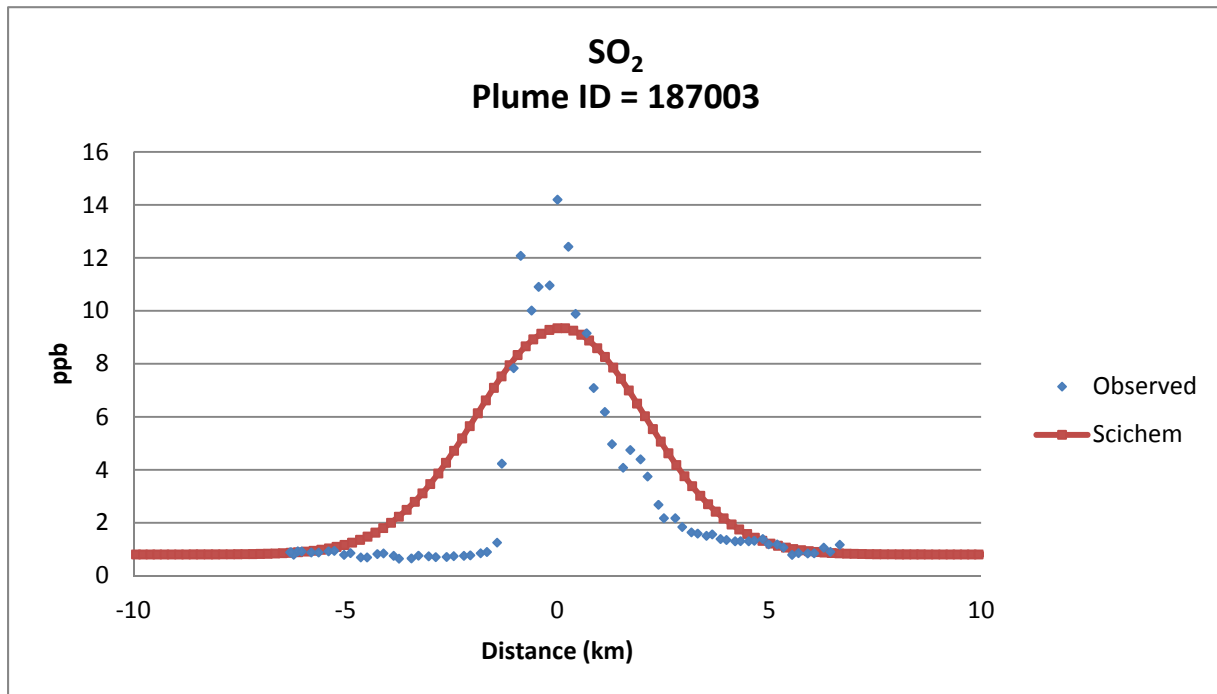
Figure 3-3a.   **Observed and simulated (SCICHEM) cross-wind plume concentrations of SO_2 and NO_y for Traverse 3 at 11 km downwind of the Cumberland power plant on July 6, 1999. SCICHEM results are based on measured surface and upper air meteorology.**
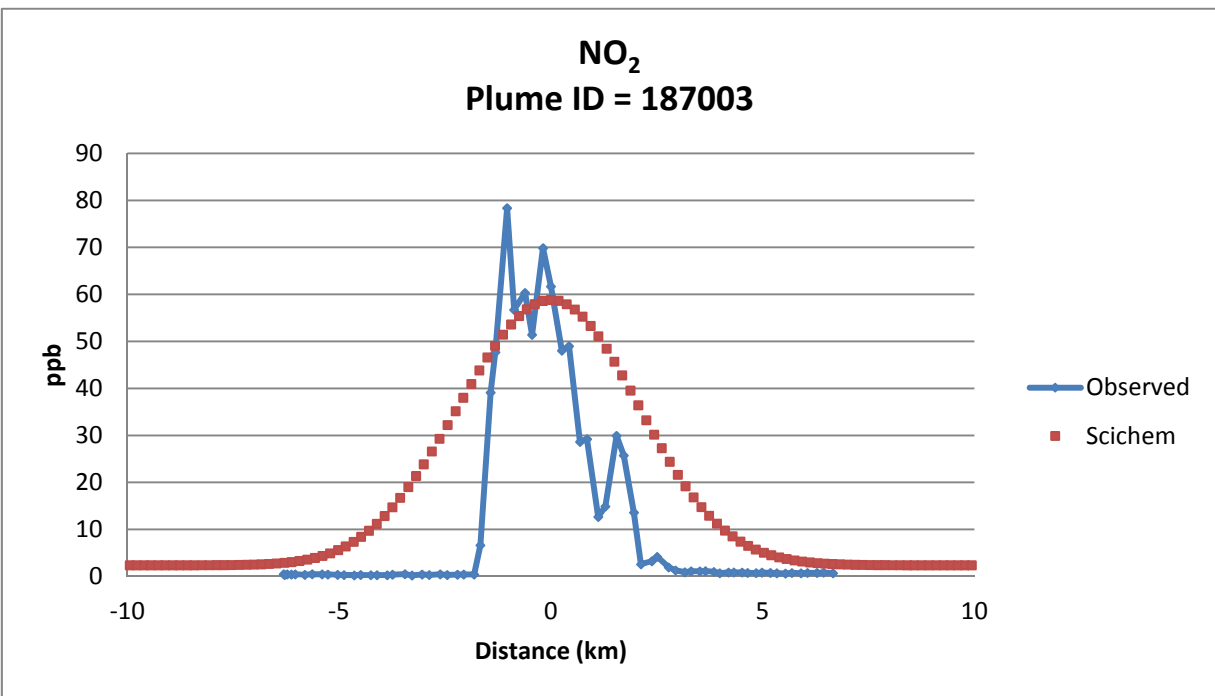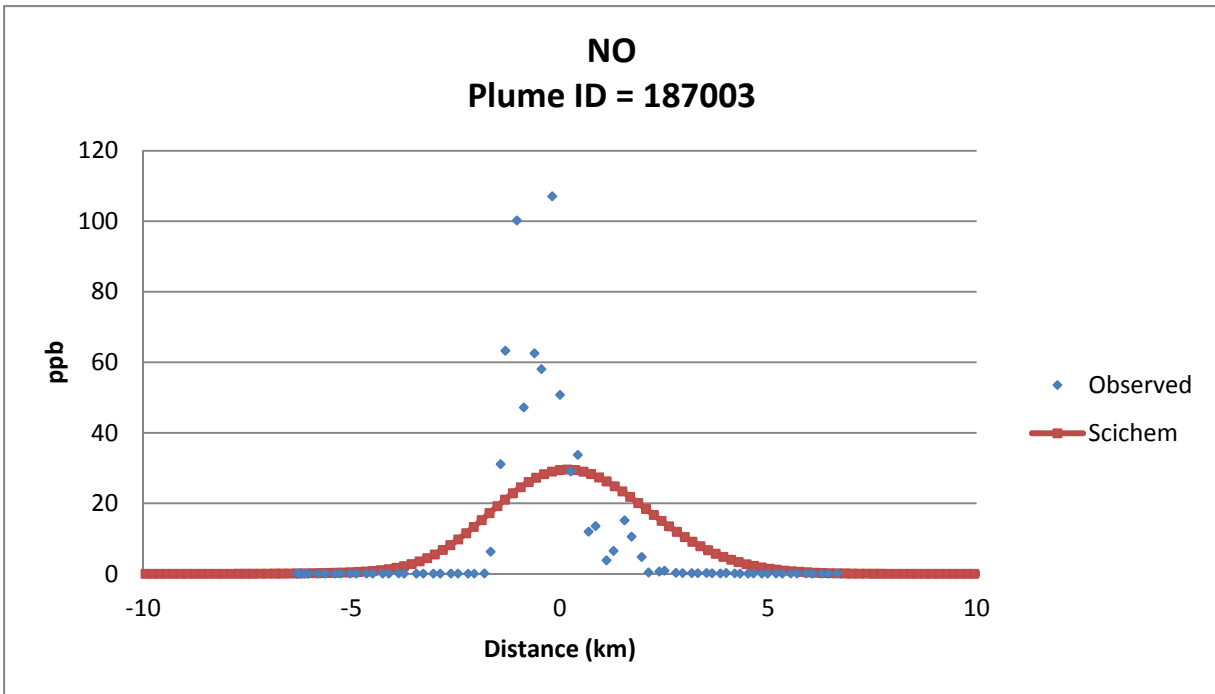
Figure 3-3b. **Observed and simulated (SCICHEM) cross-wind plume concentrations of NO and NO$_2$ for Traverse 3 at 11 km downwind of the Cumberland power plant on July 6, 1999. SCICHEM results are based on measured surface and upper air meteorology.**
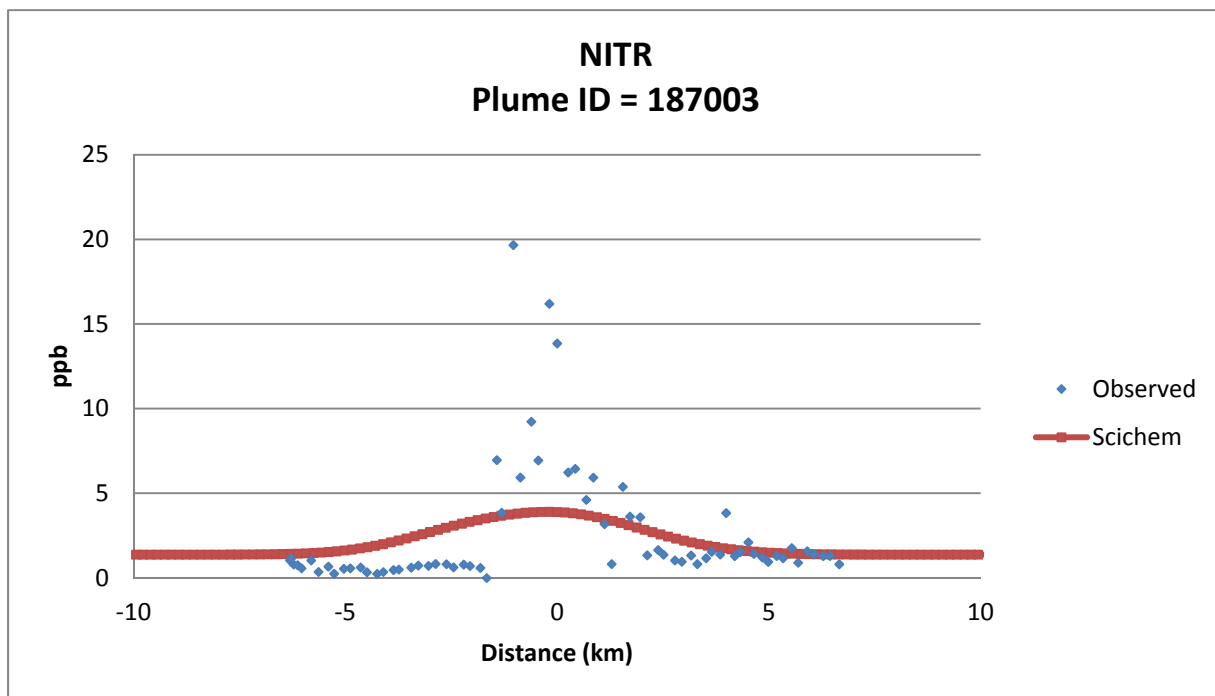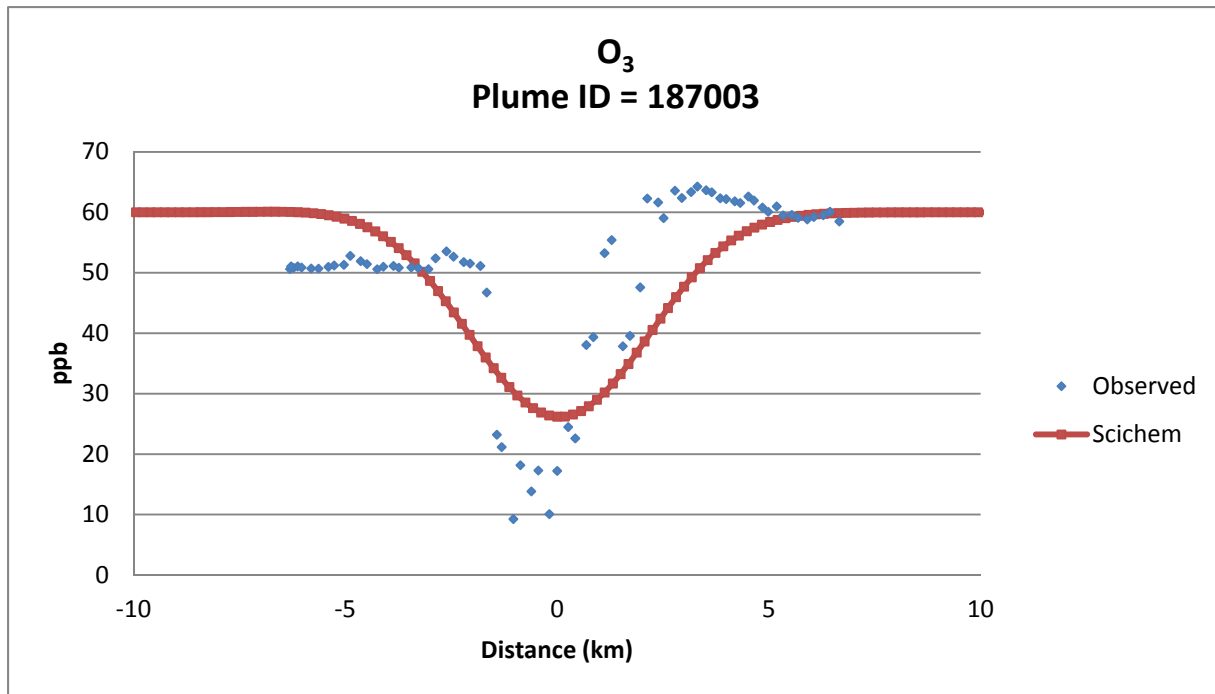
Figure 3-3c.   Observed and simulated (SCICHEM) cross-wind plume concentrations of O₃ and inorganic nitrate for Traverse 3 at 11 km downwind of the Cumberland power plant on July 6, 1999. SCICHEM results are based on measured surface and upper air meteorology.
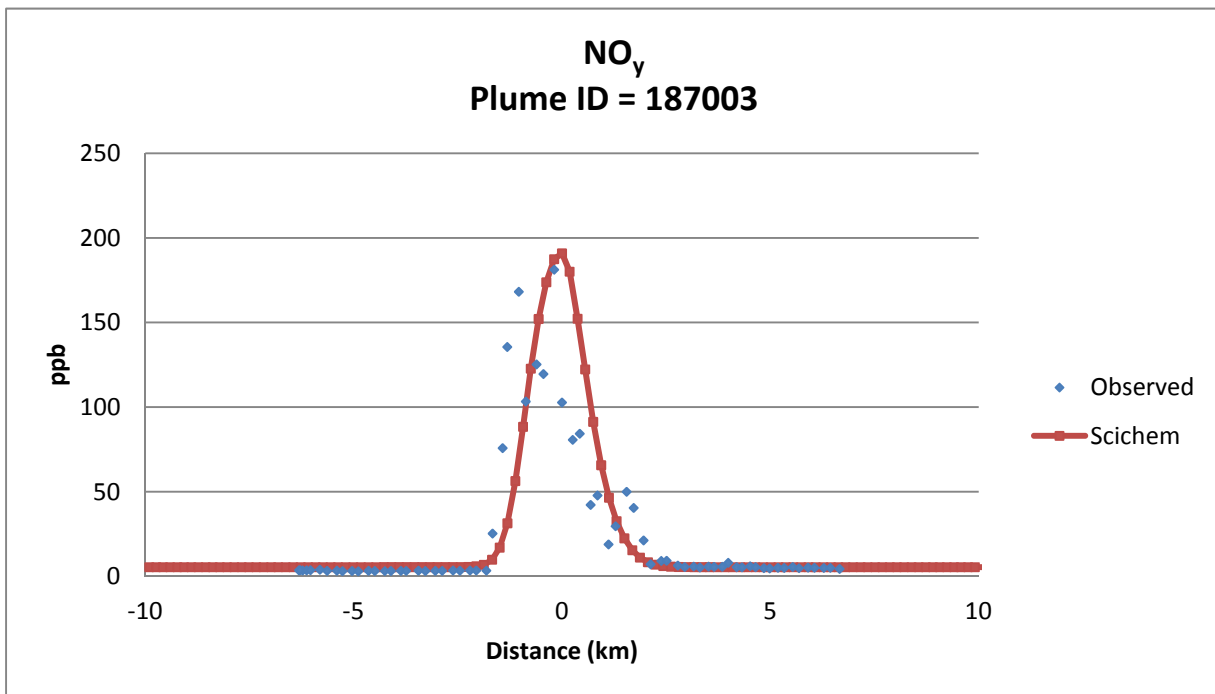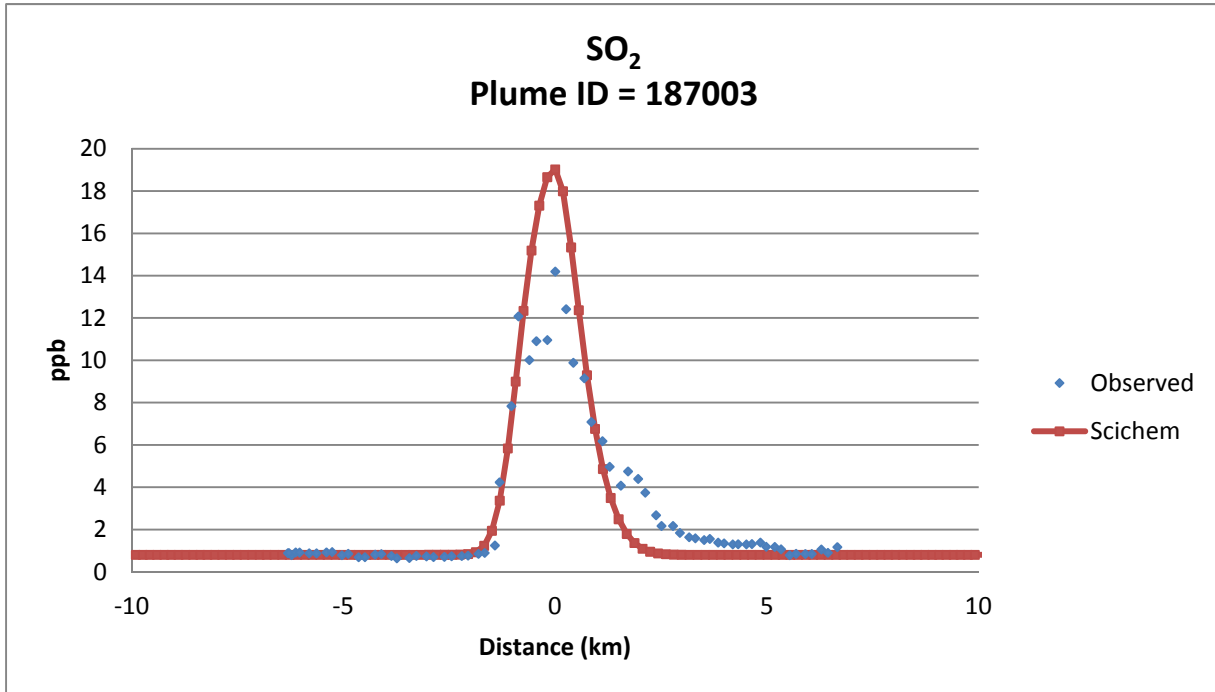
Figure 3-4a. **Observed and simulated (SCICHEM) cross-wind plume concentrations of SO$_2$ and NO$_y$ for Traverse 3 at 11 km downwind of the Cumberland power plant on July 6, 1999. SCICHEM results are based on WRF meteorology processed with MMIF.**
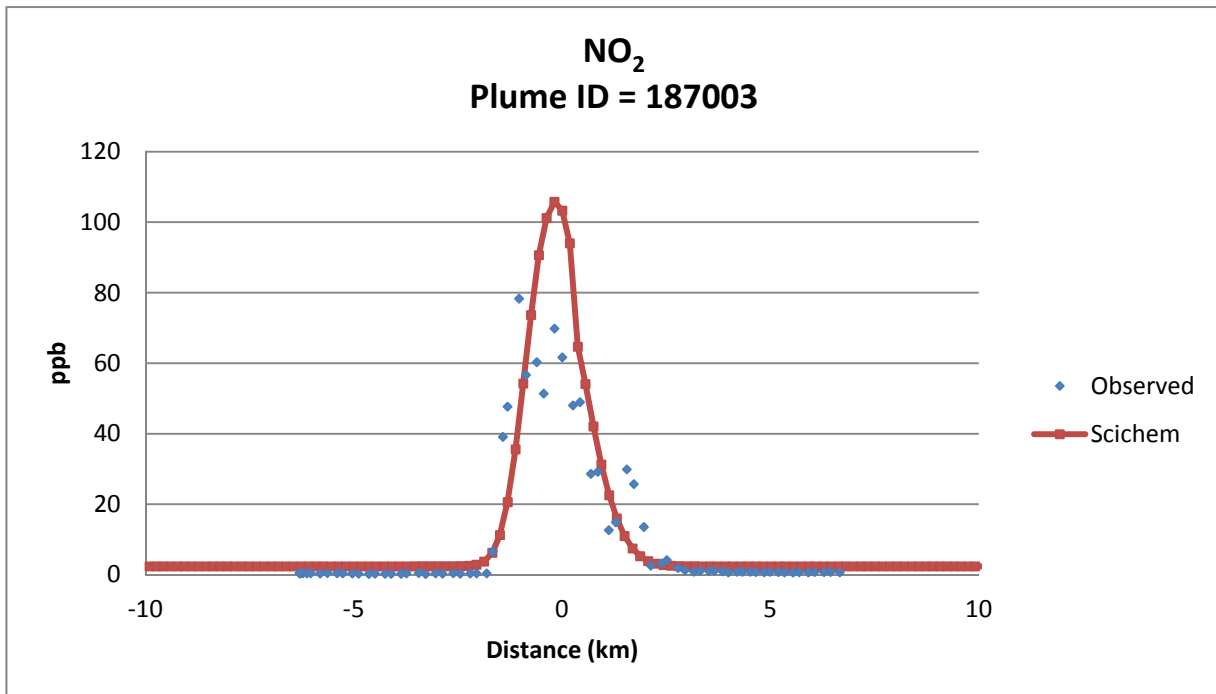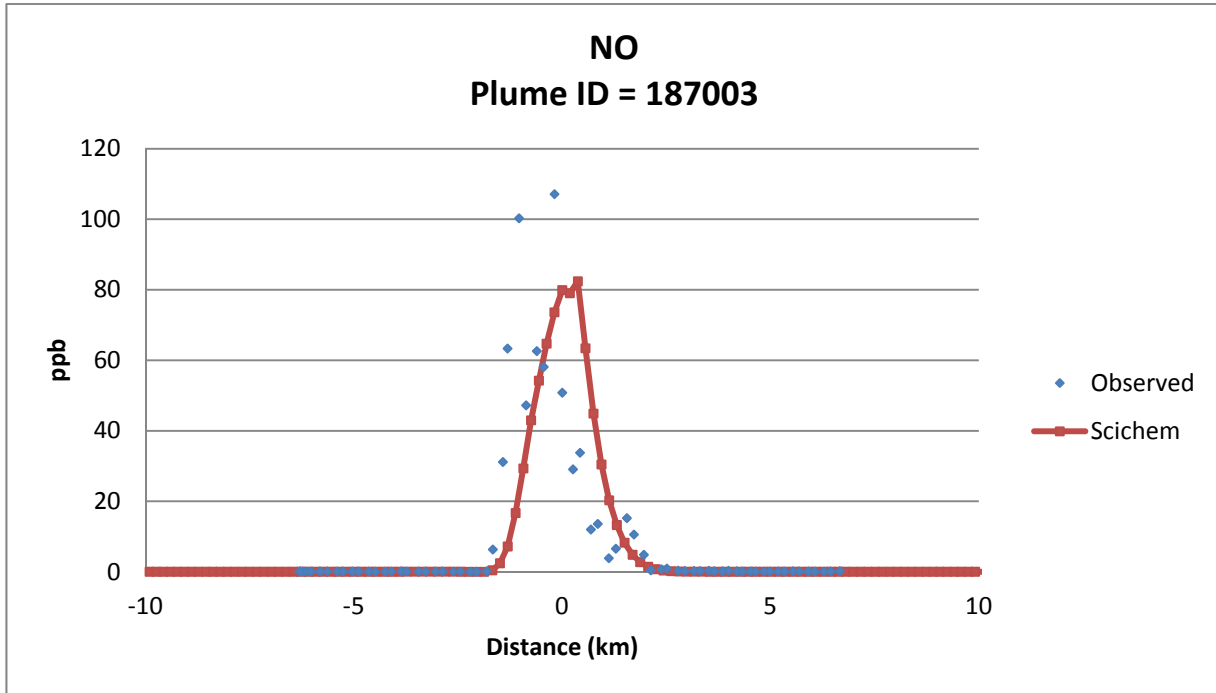
Figure 3-4b.   Observed and simulated (SCICHEM) cross-wind plume concentrations of NO and NO$_2$ for Traverse 3 at 11 km downwind of the Cumberland power plant on July 6, 1999. SCICHEM results are based on WRF meteorology processed with MMIF.
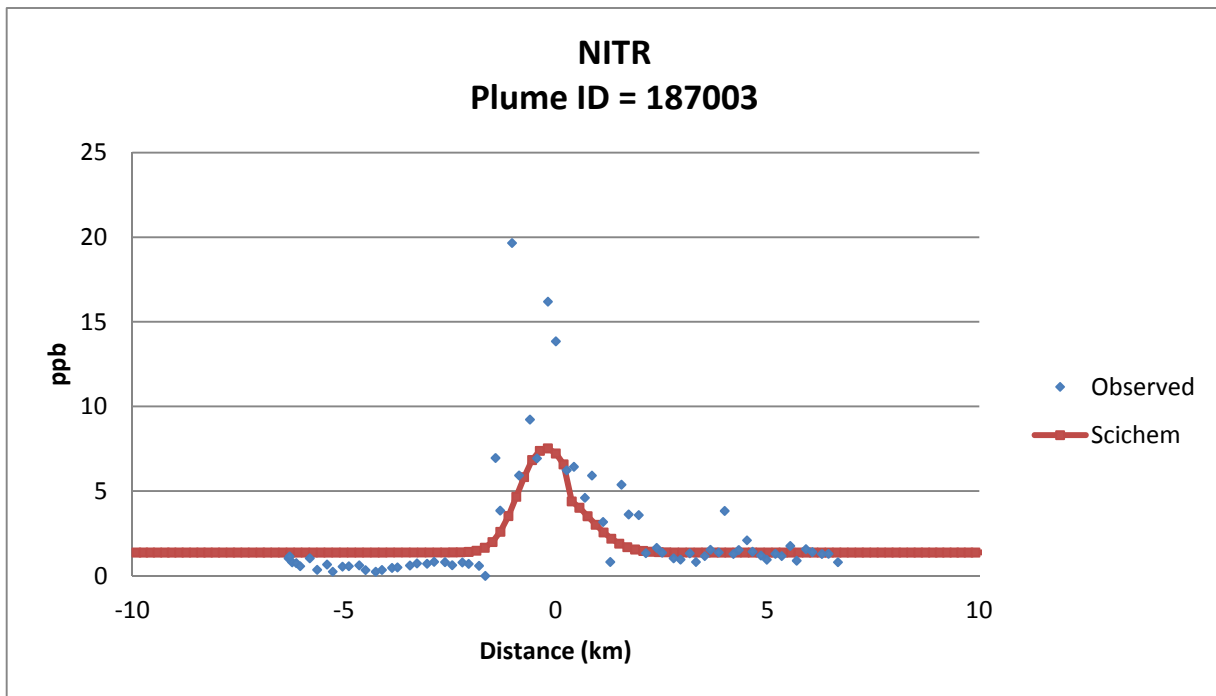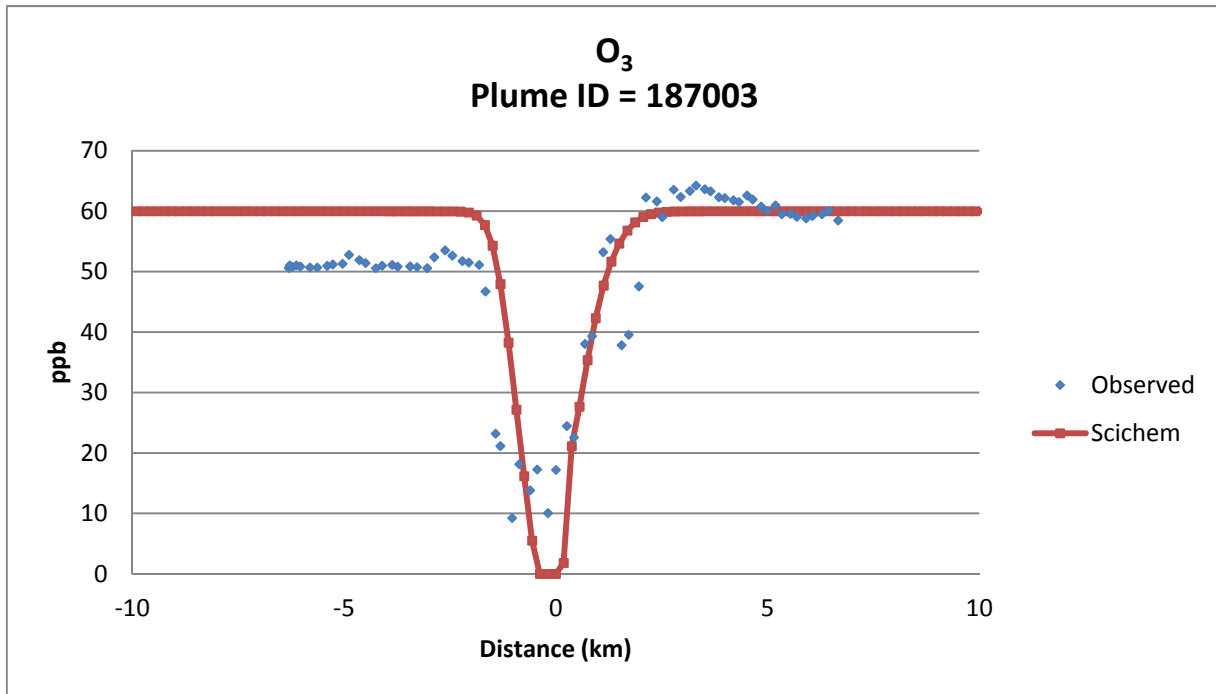
Figure 3-4c. **Observed and simulated (SCICHEM) cross-wind plume concentrations of O$_3$ and inorganic nitrate for Traverse 3 at 11 km downwind of the Cumberland power plant on July 6, 1999. SCICHEM results are based on WRF meteorology processed with MMIF.**

The SCICHEM results with observed meteorology for Traverse 8, at 31 km downwind of Cumberland, are compared with observations in Figure 3-5. As compared to the results for Traverse 3 (Figure 3-3), we note generally much better agreement between modeled and measured plume concentrations for all species. Both observations and model show ozone production over background at the plume edges (about 10 ppb production in the observations and 15 ppb production in the model). However, the model under-predicts the titration of ozone at the plume centerline. In contrast, the Traverse 8 SCICHEM results with WRF meteorology, shown in Figure 3-6, show significant discrepancies from the measured values.

Figure 3-7 show the SCICHEM results with observed meteorology versus measured plume concentrations for Traverse 10, at about 65 km downwind of Cumberland. The SCICHEM plume is wider than the observed plume, as shown in Table 3-1, and the peak predicted concentrations of SO_2 and NO_y are slightly lower than the observed values. But in general there is good agreement between simulated and measured concentrations, particularly in the conversion of NO to NO_2 and the formation of O_3 and inorganic nitrate. Peak ozone production of about 30 ppb above background is noted in both the observed and simulated plumes, but the observations show the peak ozone production away from the plume core , while the model predicts the peak ozone production at the plume centerline.

The corresponding comparisons with measurements for SCICHEM results with WRF meteorology for Traverse 10 are shown in Figures 3-8. As shown in Table 3-1, the measured and simulated plume widths for Traverse 10 are comparable, and we see from Figure 3-8a that the measured and simulated plume SO_2 and NO_y concentrations are also in good agreement. However, both NO and NO_2 concentrations are significantly over-predicted, as shown in Figure 3-8b. From Figure 3-8c, we see that this is due to insufficient conversion of NO_x to inorganic nitrate. We also note that SCICHEM shows a small production of about 6 ppb of O_3 at the plume edge, much lower than the 30 ppb production in the aircraft measurements and the SCICHEM results with observed meteorology. Furthermore, some titration of O_3 at the plume core of about 7 ppb below the background value is predicted, which is not seen in the measurements.

The results for Traverse 12, at a downwind distance of 90 km from Cumberland, are shown in Figure 3-9 for the SCICHEM simulation with observed meteorology. The agreement between simulated and observed NO_y concentrations is quite good, but there are some discrepancies in the NO and NO_2 concentrations, suggesting that more NO_x is converted to NO_z products in the SCICHEM simulation. At this downwind distance, there is significantly more production of ozone in the plume in both the measurements and model results, but the model predicts a peak ozone production within the plume over background of over 60 ppb, compared to the 40 ppb production noted in the observations. The peak inorganic nitrate production in the model is also about 20% higher than in the measurements.
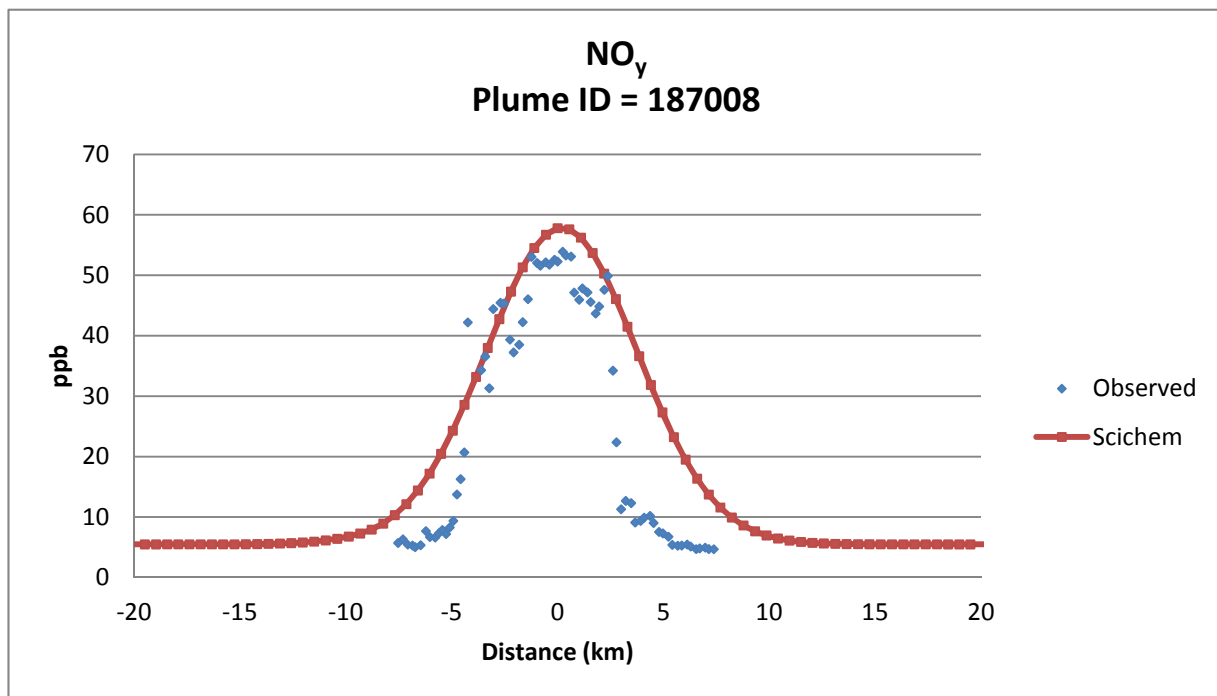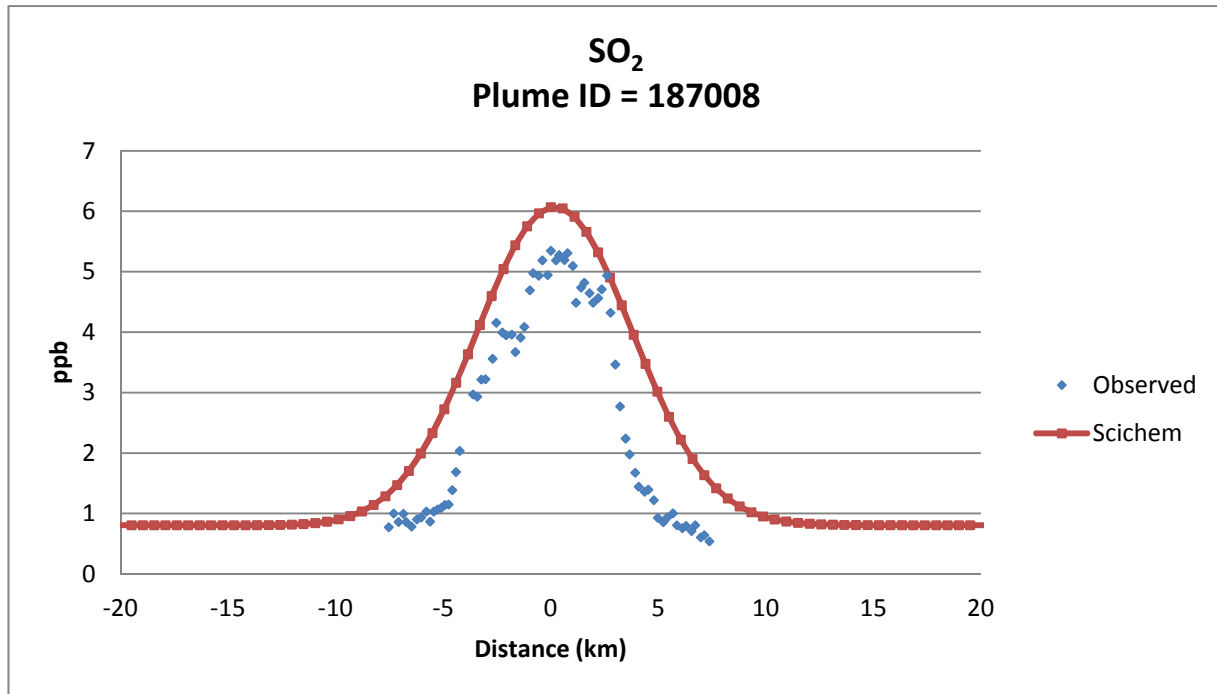
Figure 3-5a. **Observed and simulated (SCICHEM) cross-wind plume concentrations of SO₂ and NOᵧ for Traverse 8 at 31 km downwind of the Cumberland power plant on July 6, 1999. SCICHEM results are based on measured surface and upper air meteorology.**

NO
Plume ID = 187008

NO$_2$
Plume ID = 187008
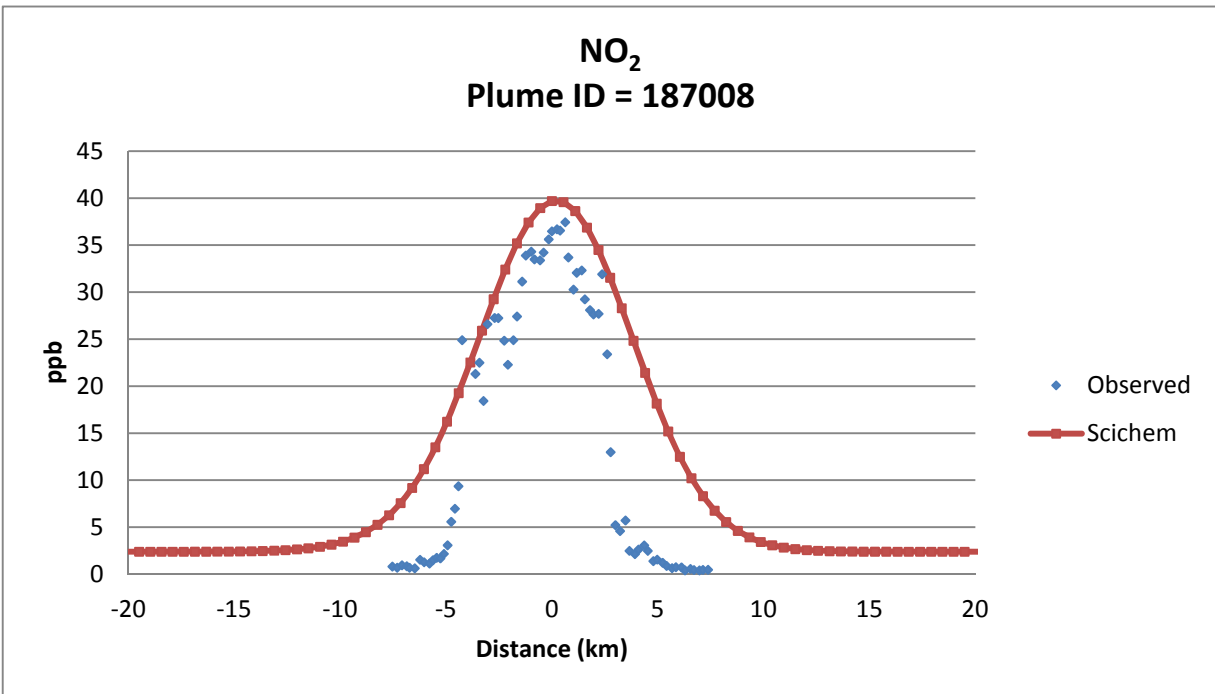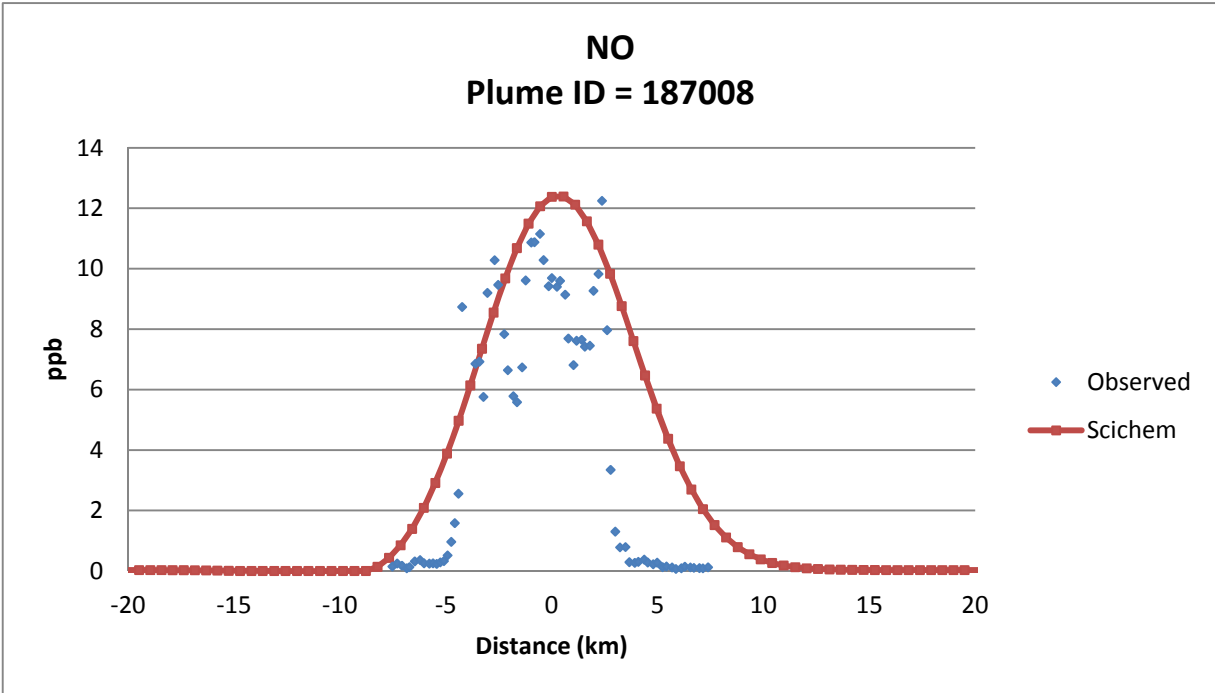
Figure 3-5b.   Observed and simulated (SCICHEM) cross-wind plume concentrations of NO and NO$_2$ for Traverse 8 at 31 km downwind of the Cumberland power plant on July 6, 1999. SCICHEM results are based on measured surface and upper air meteorology.
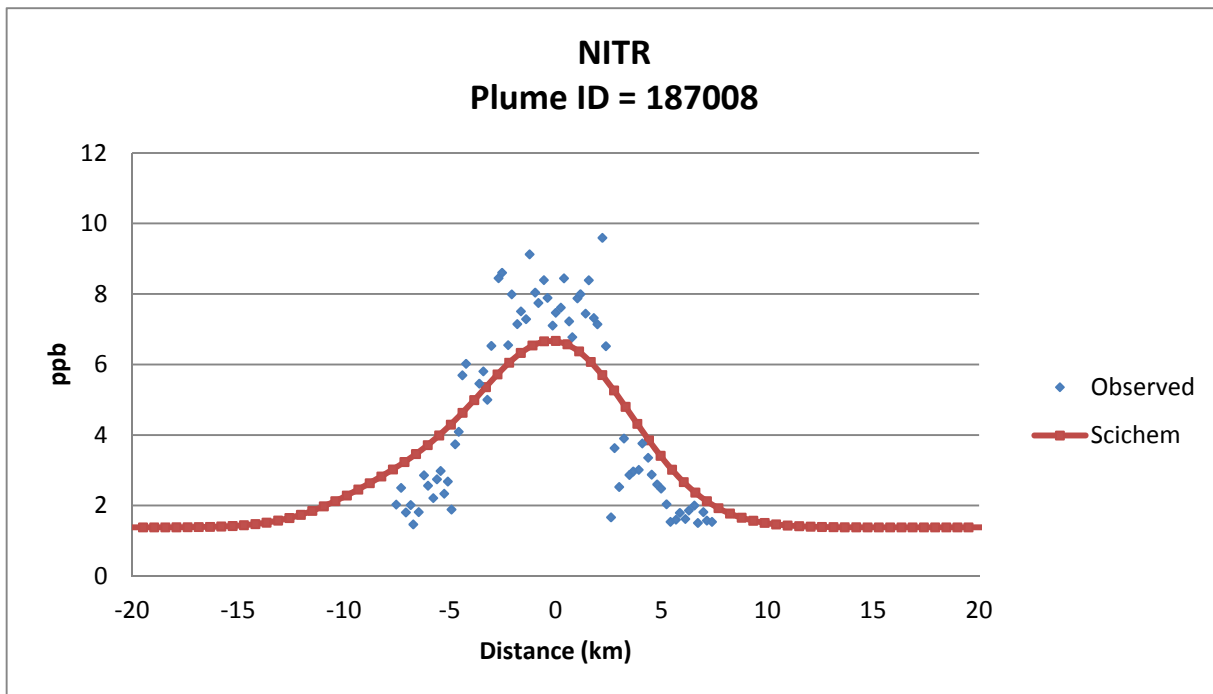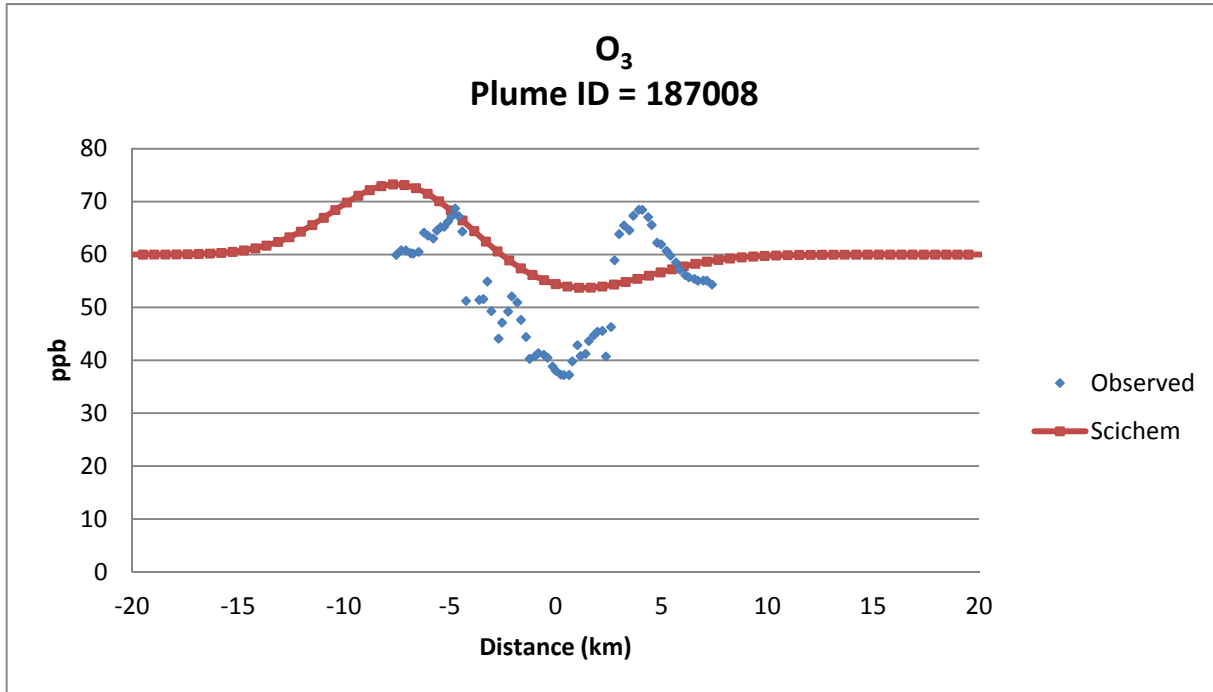
Figure 3-5c.   Observed and simulated (SCICHEM) cross-wind plume concentrations of O₃ and inorganic nitrate for Traverse 8 at 31 km downwind of the Cumberland power plant on July 6, 1999. SCICHEM results are based on measured surface and upper air meteorology.
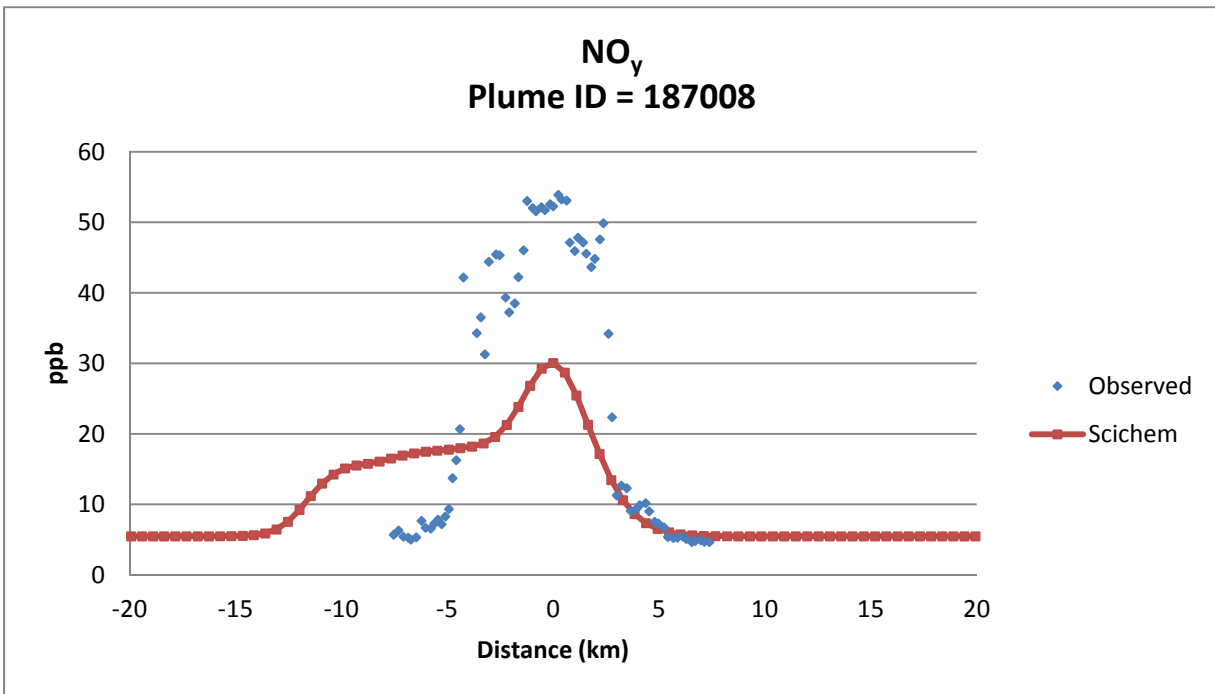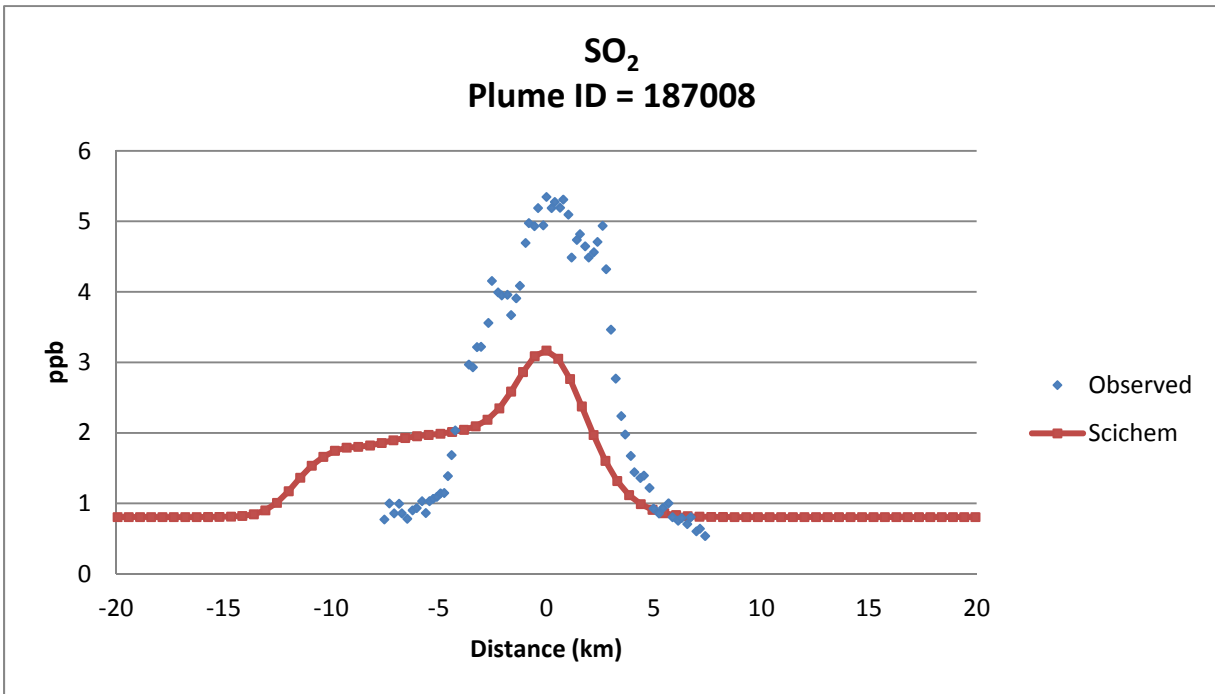
Figure 3-6a. **Observed and simulated (SCICHEM) cross-wind plume concentrations of SO$_2$ and NO$_y$ for Traverse 8 at 31 km downwind of the Cumberland power plant on July 6, 1999. SCICHEM results are based on WRF meteorology processed with MMIF.**
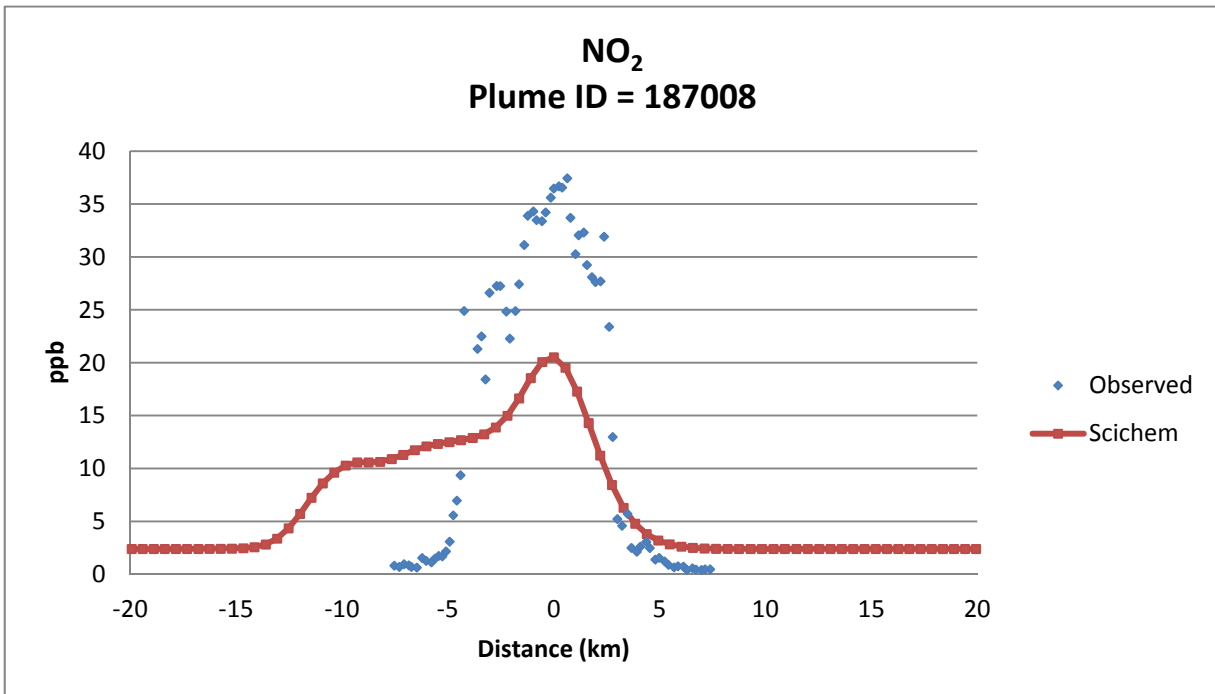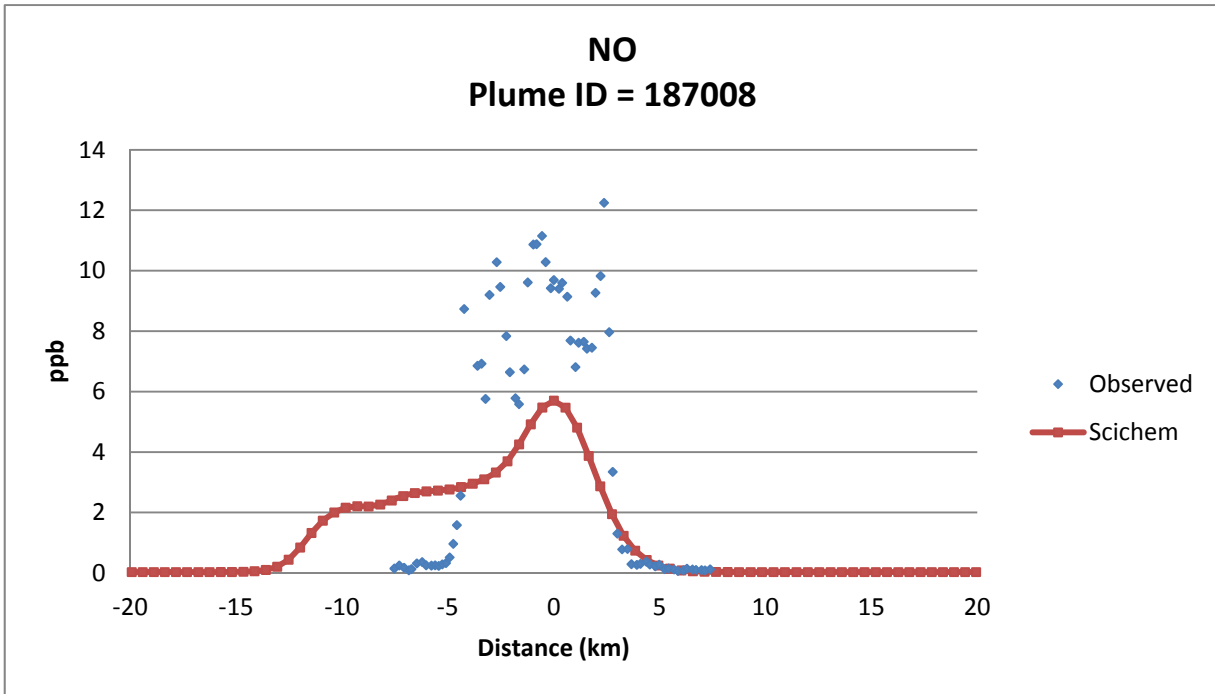
Figure 3-6b. **Observed and simulated (SCICHEM) cross-wind plume concentrations of NO and NO$_2$ for Traverse 8 at 31 km downwind of the Cumberland power plant on July 6, 1999. SCICHEM results are based on WRF meteorology processed with MMIF.**
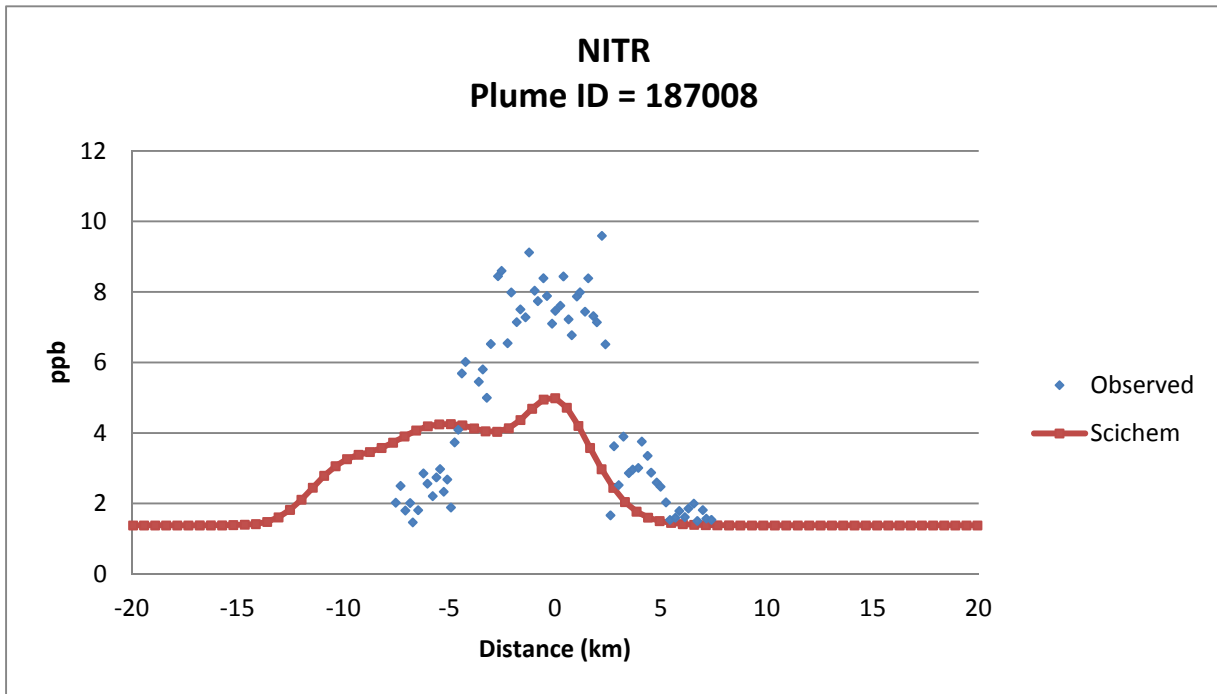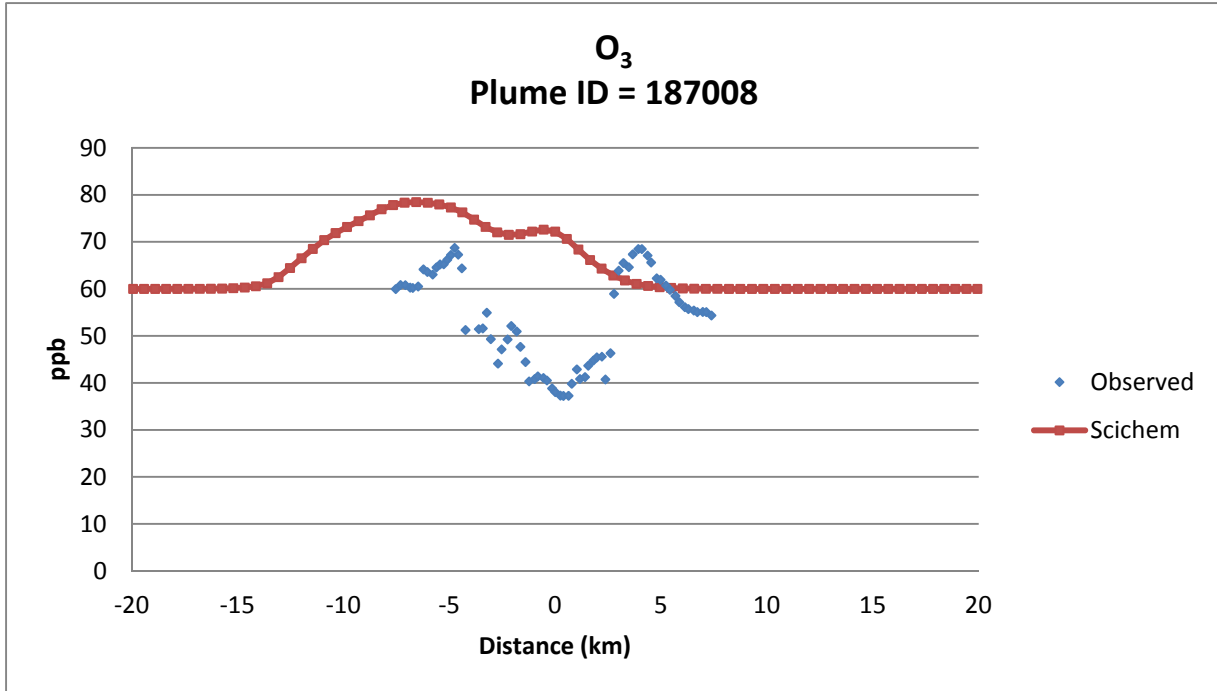
Figure 3-6c. Observed and simulated (SCICHEM) cross-wind plume concentrations of O_3 and inorganic nitrate for Traverse 8 at 31 km downwind of the Cumberland power plant on July 6, 1999. SCICHEM results are based on WRF meteorology processed with MMIF.
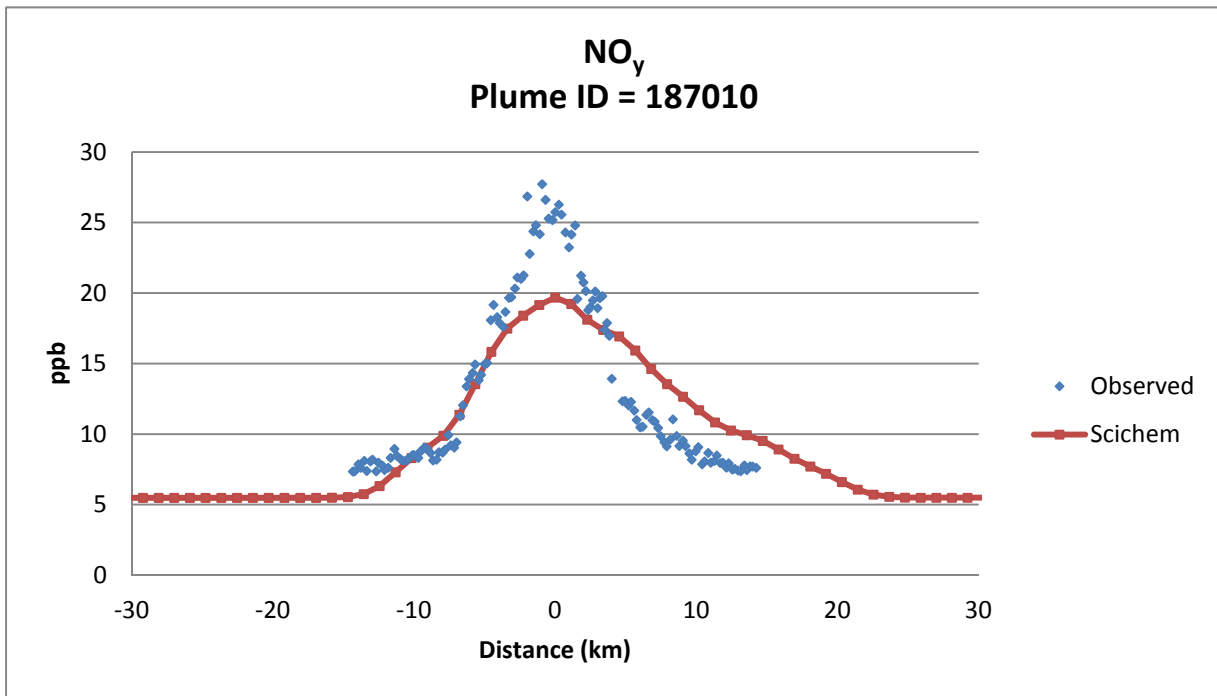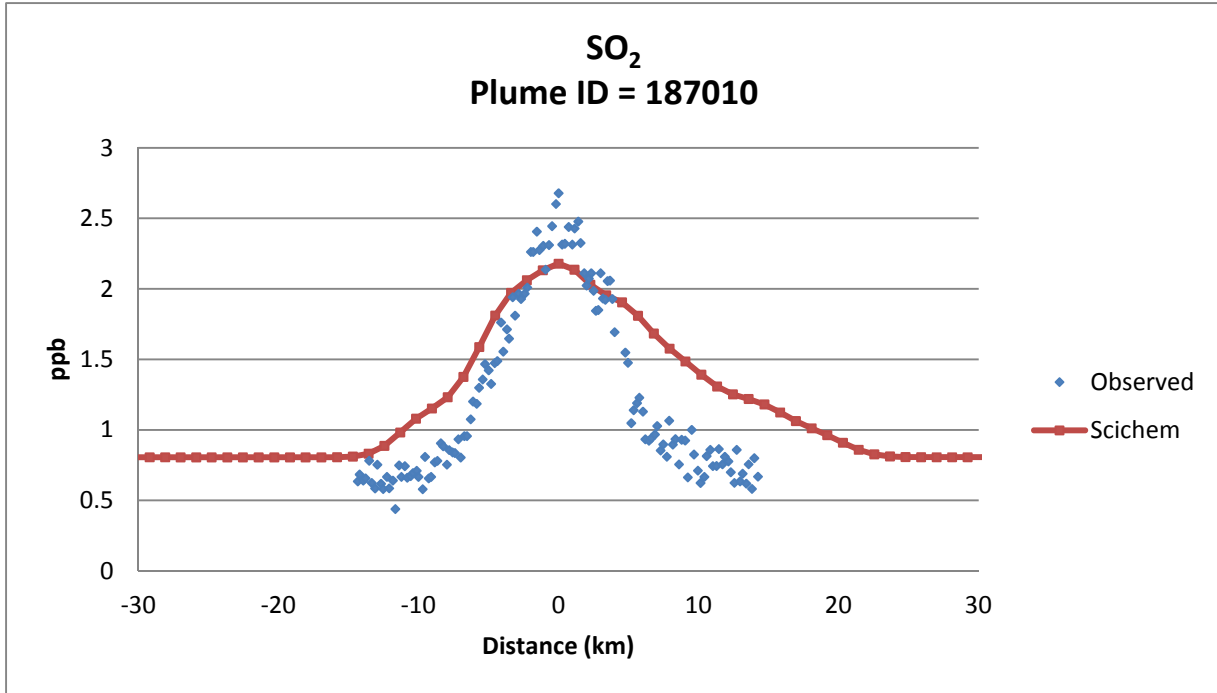
Figure 3-7a. **Observed and simulated (SCICHEM) cross-wind plume concentrations of SO₂ and NOᵧ for Traverse 10 at 65 km downwind of the Cumberland power plant on July 6, 1999. SCICHEM results are based on measured surface and upper air meteorology.**
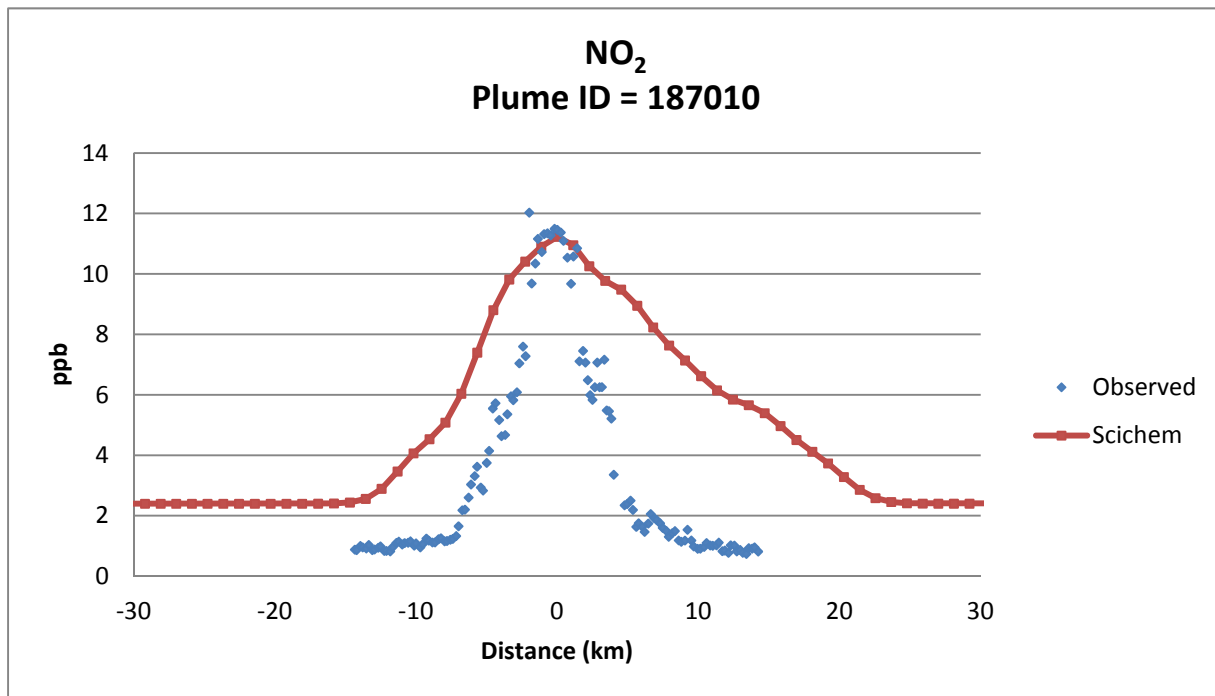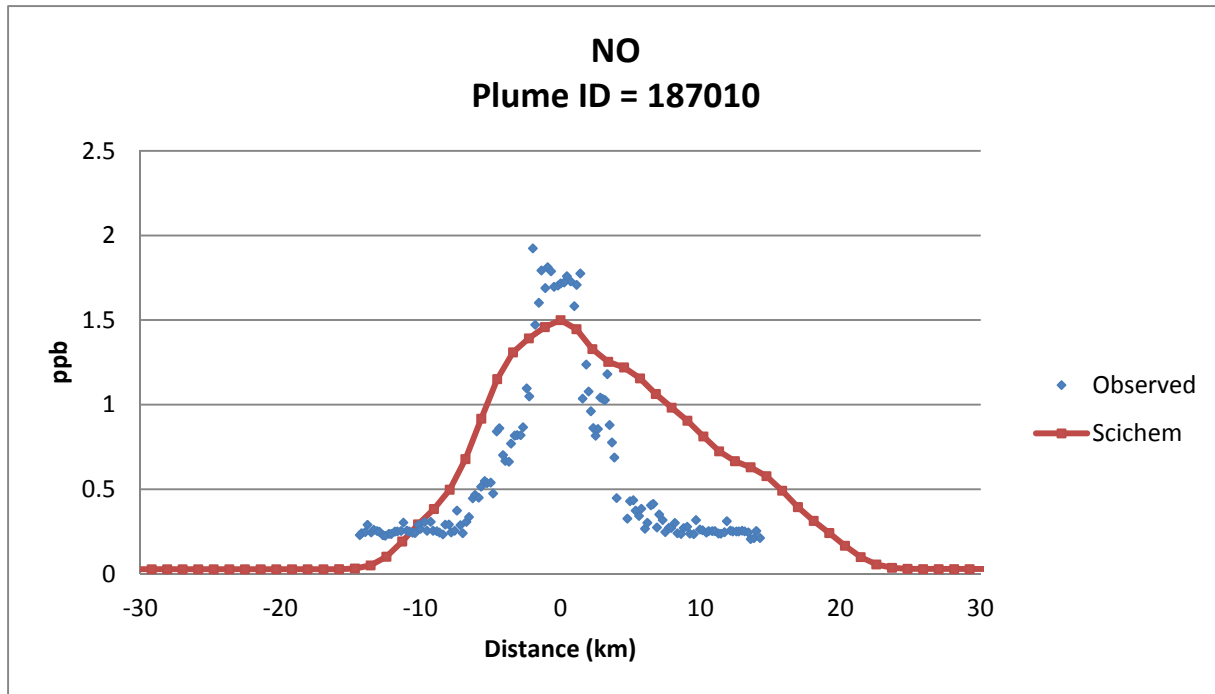
Figure 3-7b. **Observed and simulated (SCICHEM) cross-wind plume concentrations of NO and NO_2 for Traverse 10 at 65 km downwind of the Cumberland power plant on July 6, 1999. SCICHEM results are based on measured surface and upper air meteorology.**

O₃
Plume ID = 187010

NITR
Plume ID = 187010
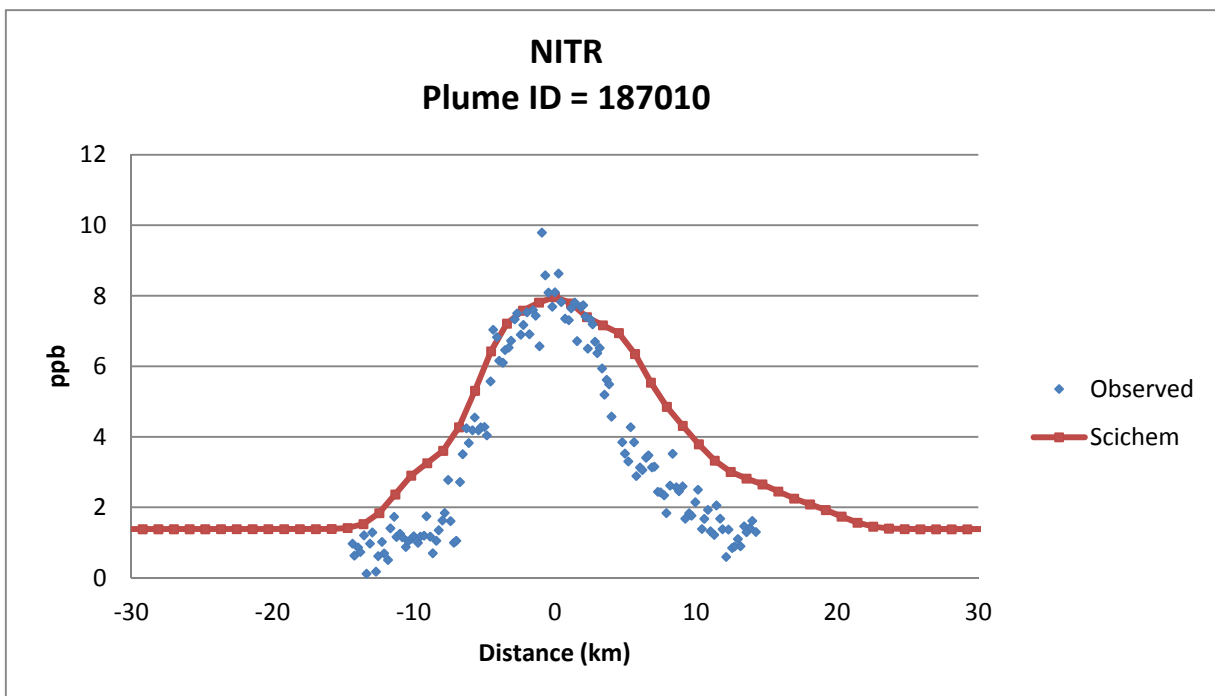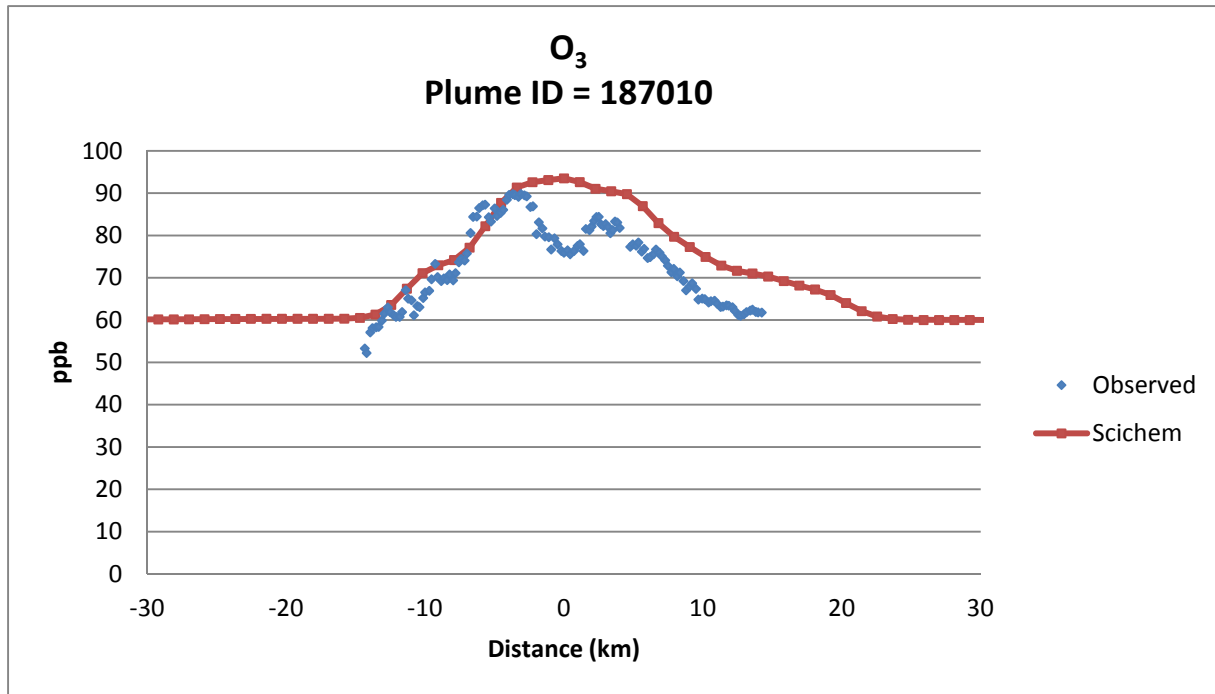
Figure 3-7c. **Observed and simulated (SCICHEM) cross-wind plume concentrations of O₃ and inorganic nitrate for Traverse 10 at 65 km downwind of the Cumberland power plant on July 6, 1999. SCICHEM results are based on measured surface and upper air meteorology.**
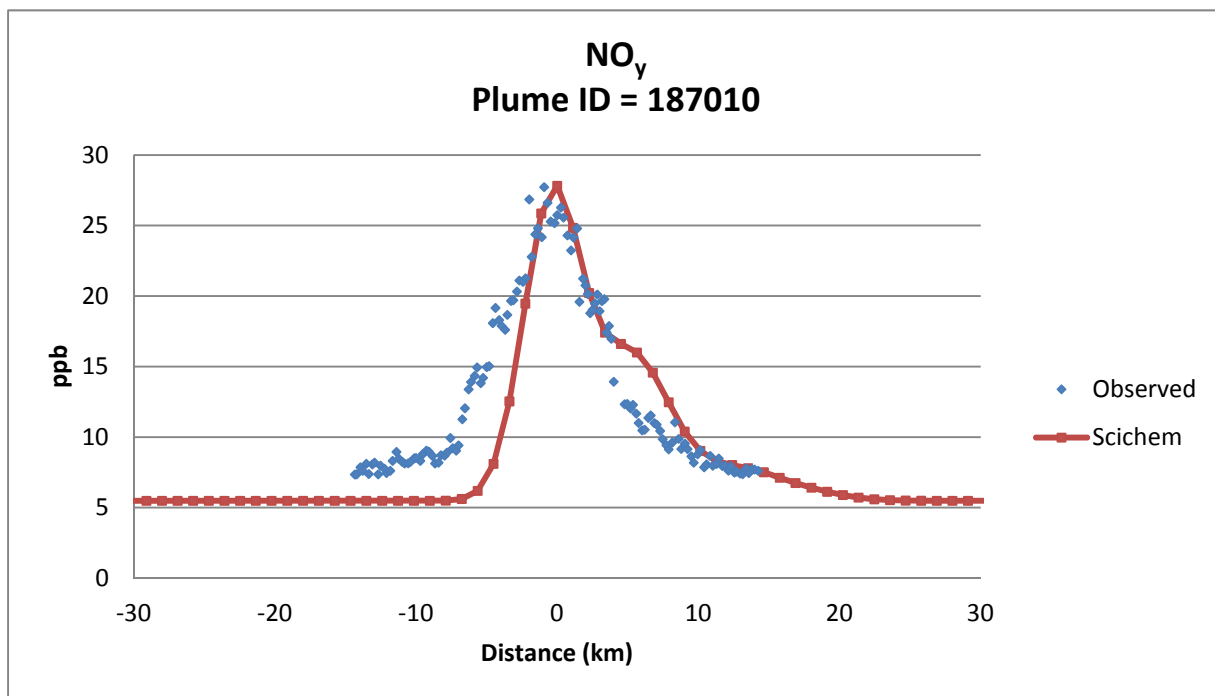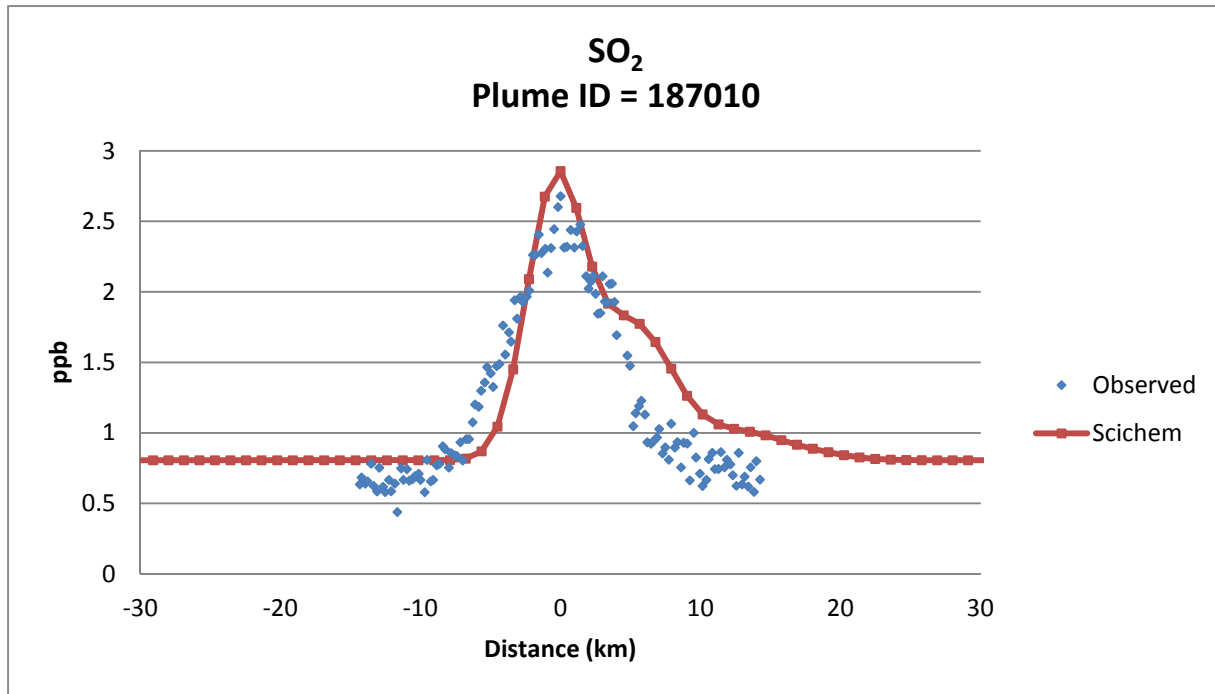
Figure 3-8a. **Observed and simulated (SCICHEM) cross-wind plume concentrations of SO_2 and NO_y for Traverse 10 at 65 km downwind of the Cumberland power plant on July 6, 1999. SCICHEM results are based on WRF meteorology processed with MMIF.**
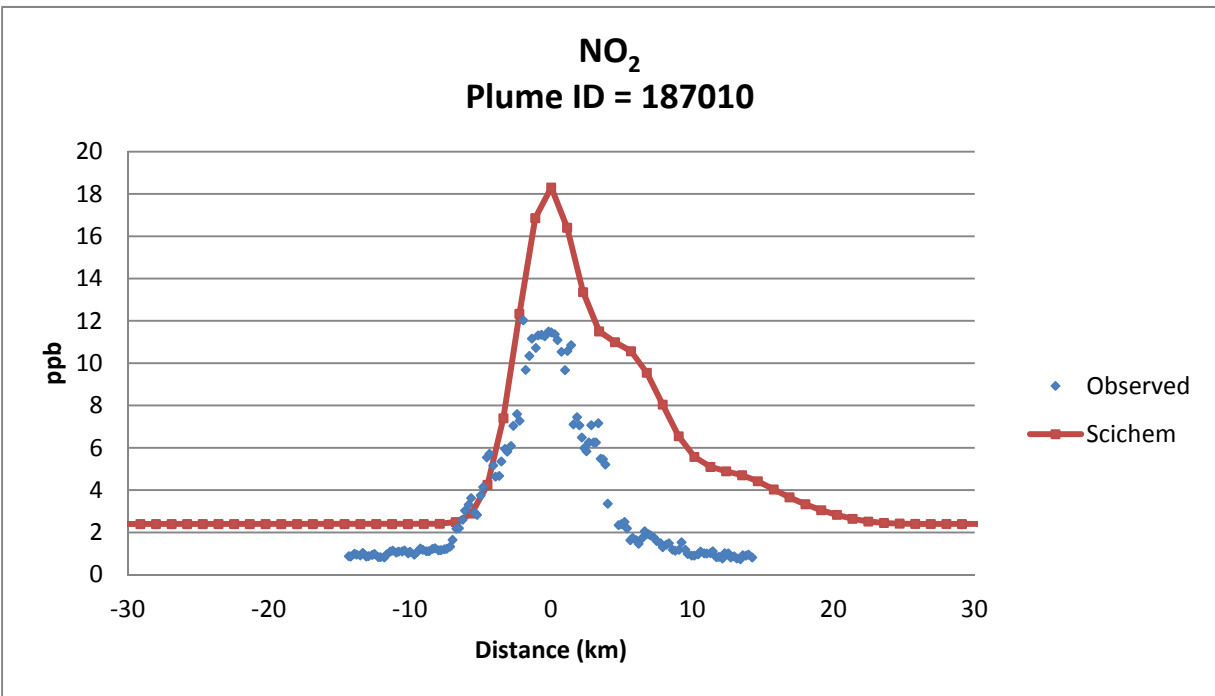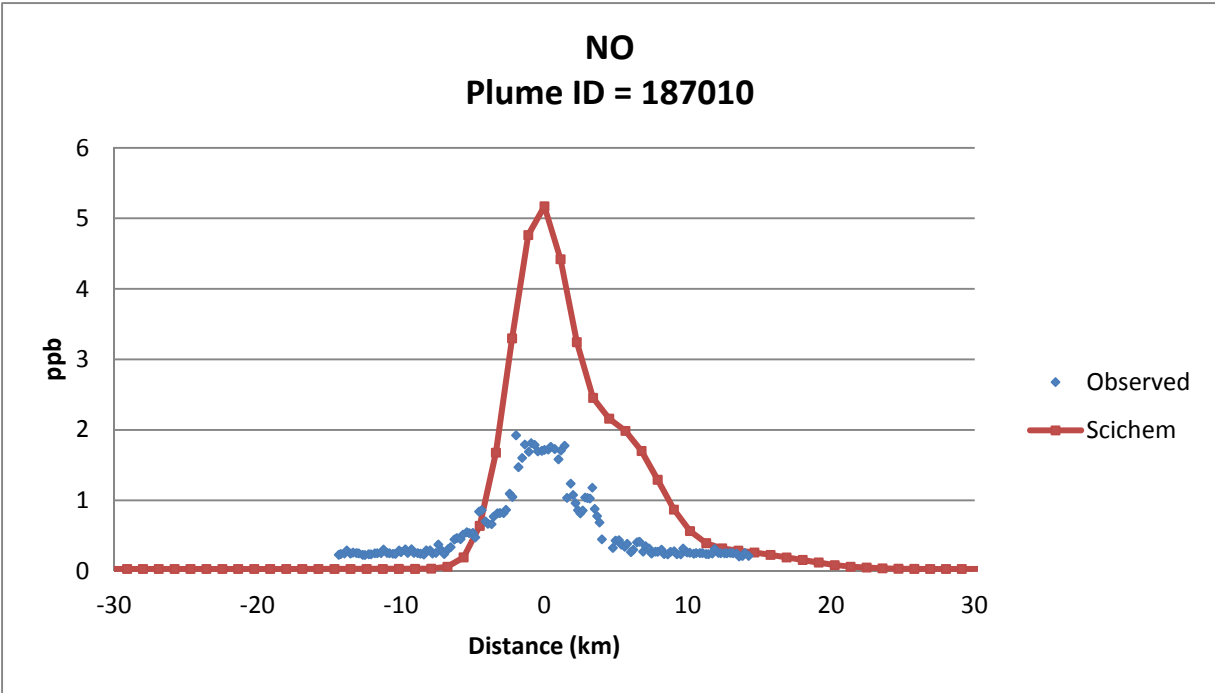
Figure 3-8b. **Observed and simulated (SCICHEM) cross-wind plume concentrations of NO and NO$_2$ for Traverse 10 at 65 km downwind of the Cumberland power plant on July 6, 1999. SCICHEM results are based on WRF meteorology processed with MMIF.**

O₃
Plume ID = 187010

NITR
Plume ID = 187010
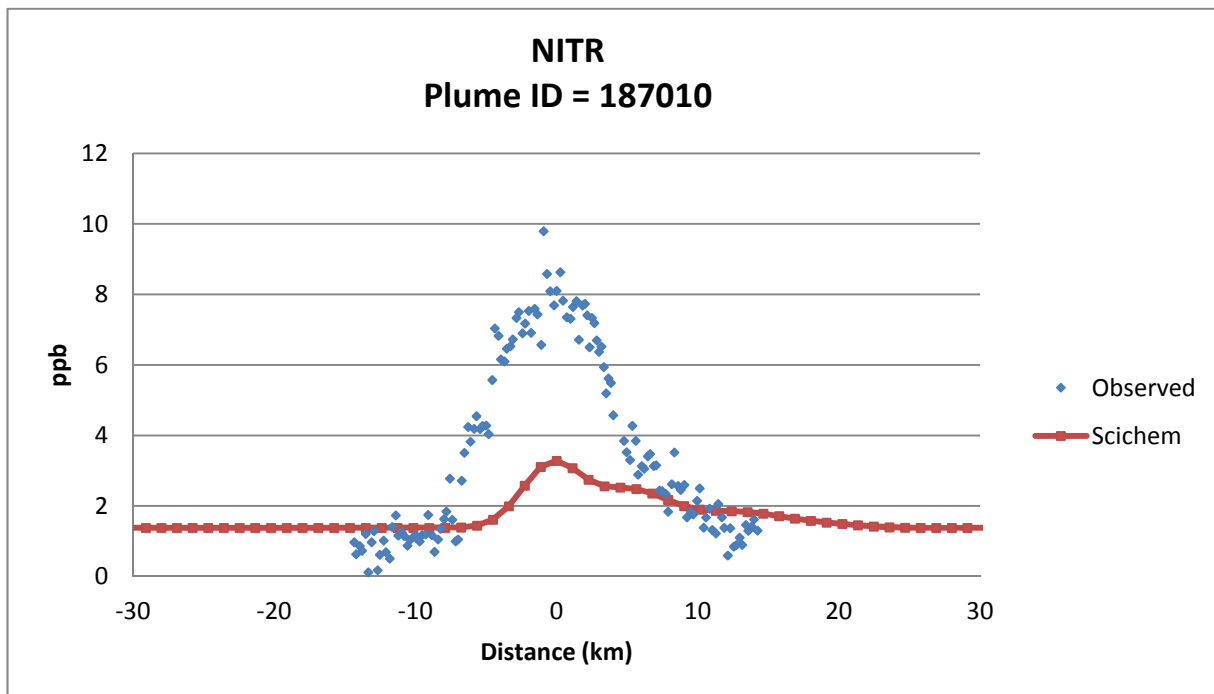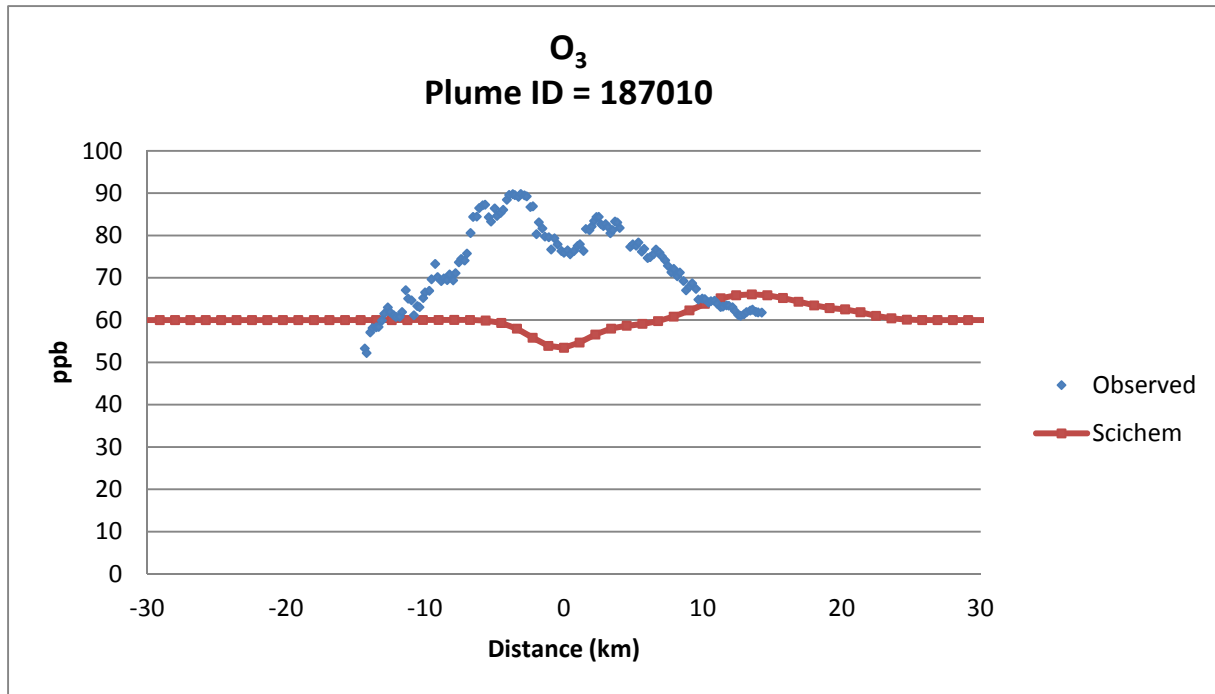
Figure 3-8c.   Observed and simulated (SCICHEM) cross-wind plume concentrations of O₃ and inorganic nitrate for Traverse 10 at 65 km downwind of the Cumberland power plant on July 6, 1999. SCICHEM results are based on WRF meteorology processed with MMIF.
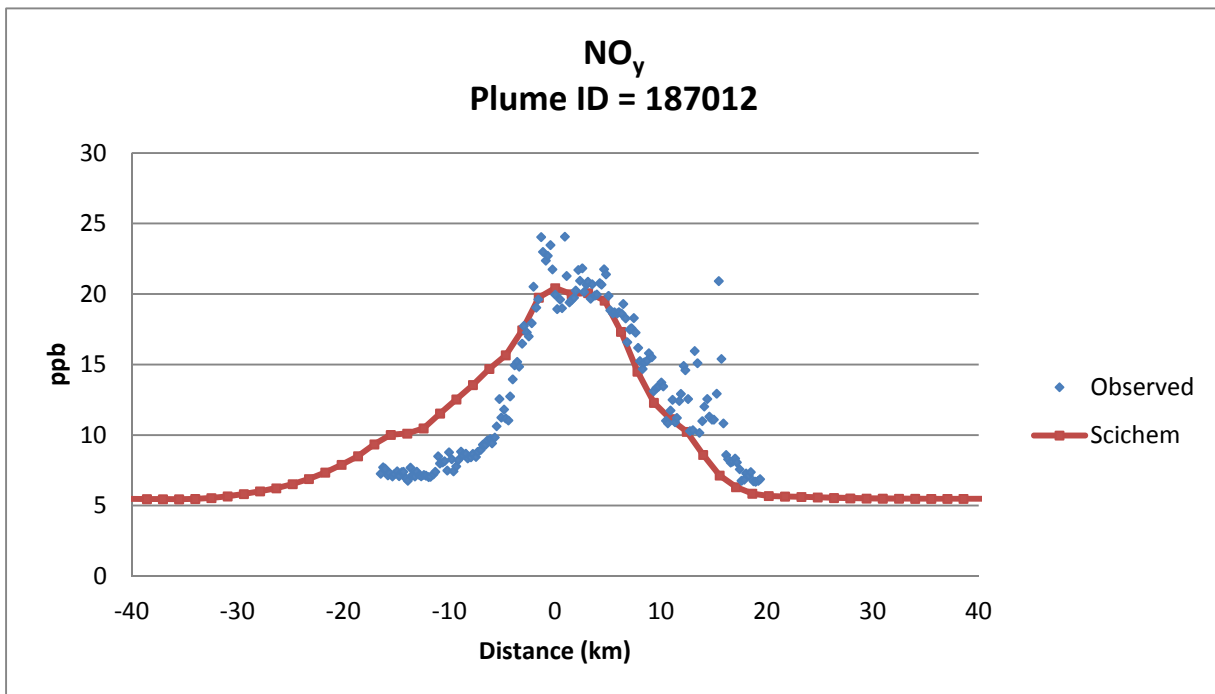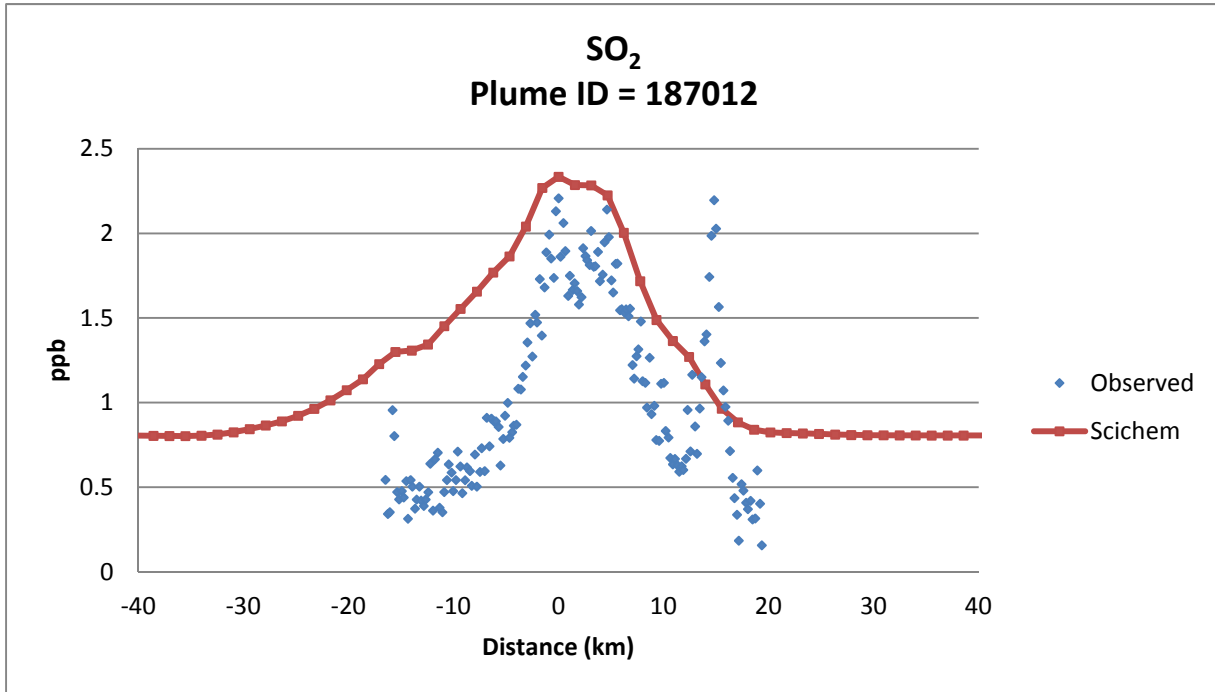
Figure 3-9a.   Observed and simulated (SCICHEM) cross-wind plume concentrations of SO$_2$ and NO$_y$ for Traverse 12 at 90 km downwind of the Cumberland power plant on July 6, 1999. SCICHEM results are based on measured surface and upper air meteorology.
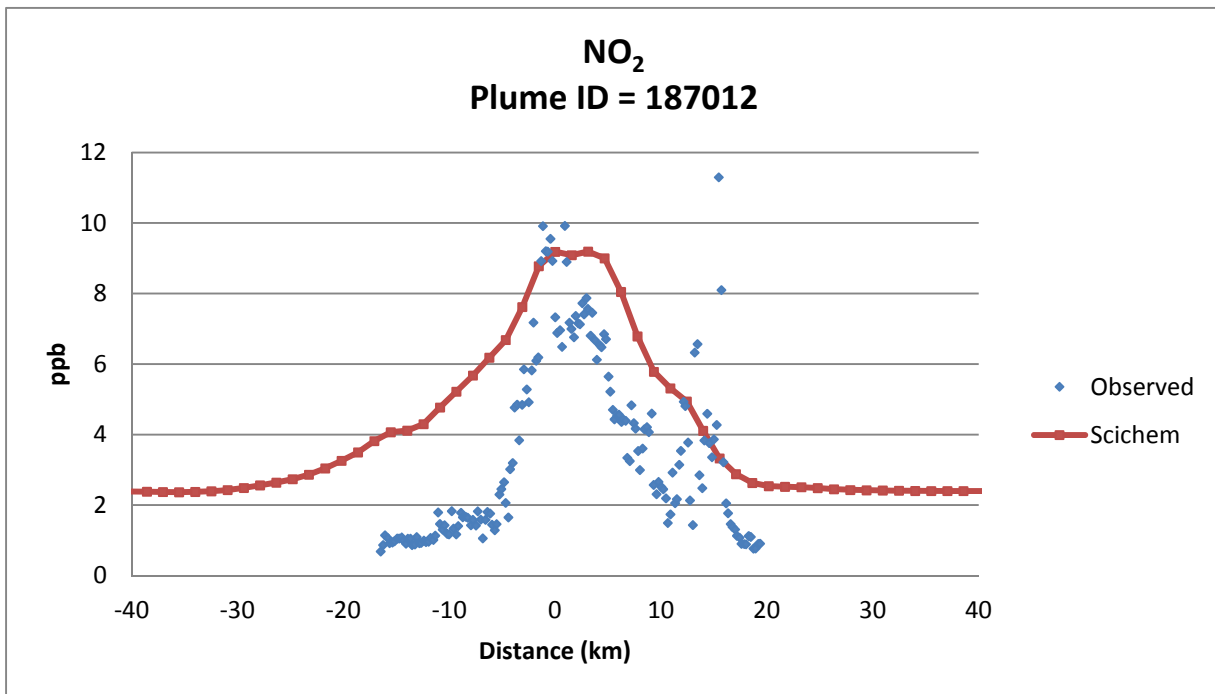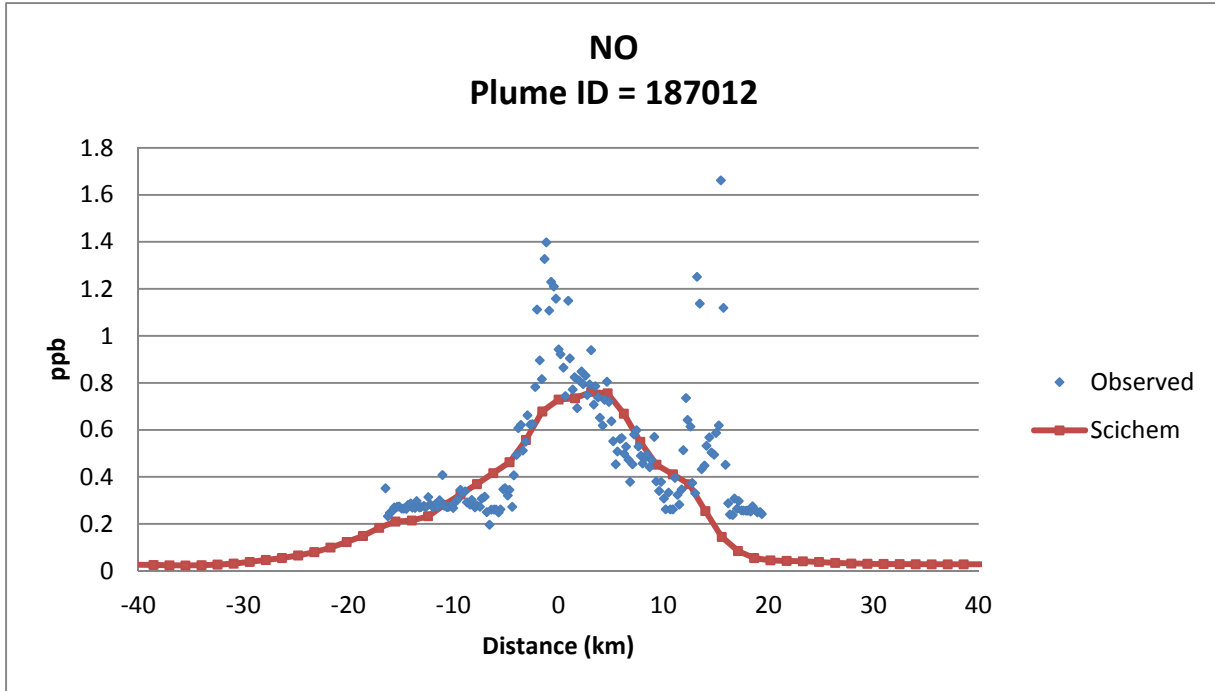
Figure 3-9b.   Observed and simulated (SCICHEM) cross-wind plume concentrations of NO and NO$_2$ for Traverse 12 at 90 km downwind of the Cumberland power plant on July 6, 1999. SCICHEM results are based on measured surface and upper air meteorology.
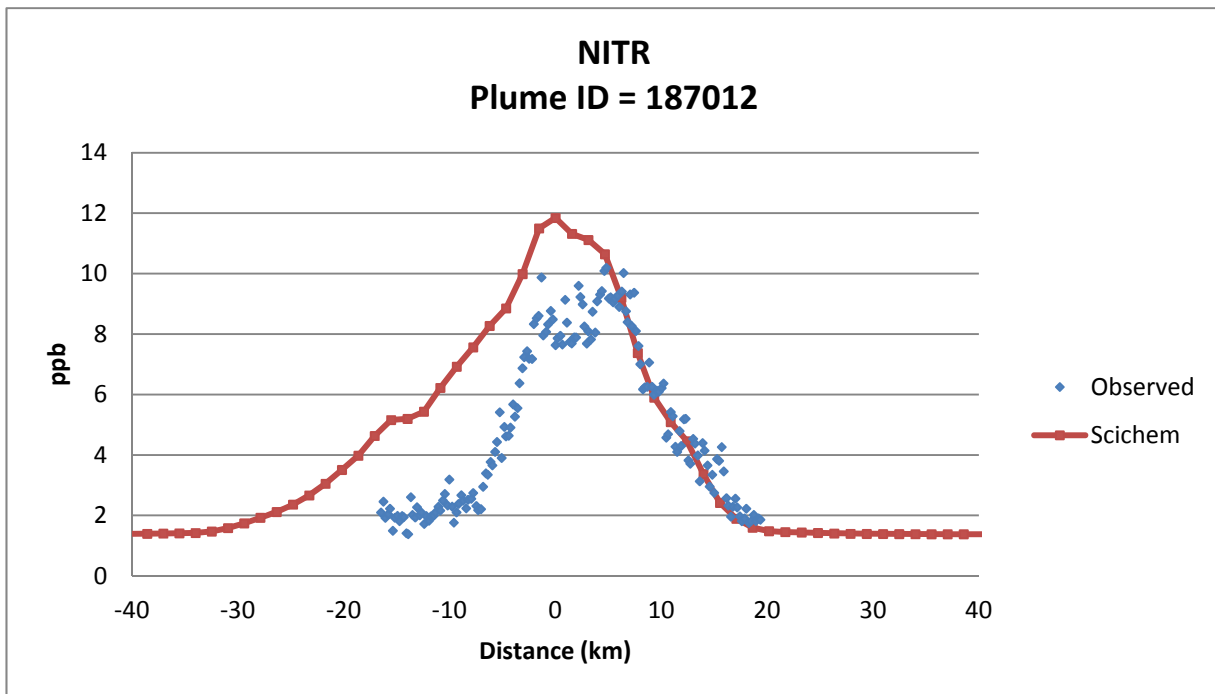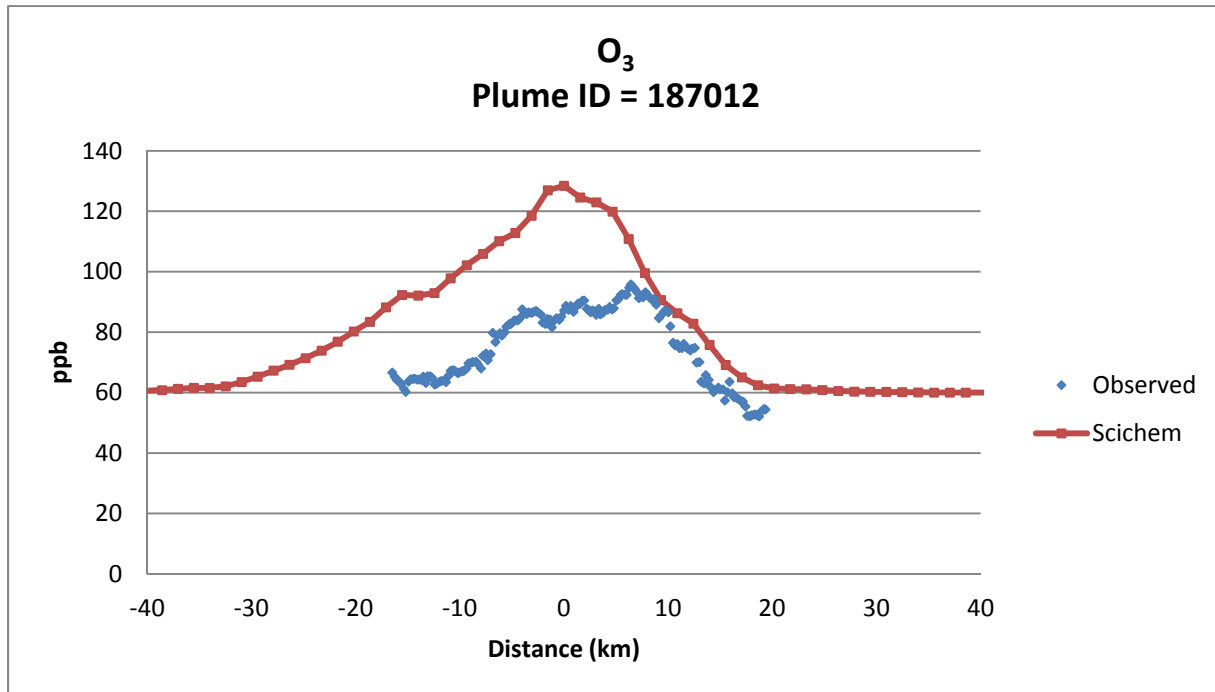
Figure 3-9c. Observed and simulated (SCICHEM) cross-wind plume concentrations of O_3 and inorganic nitrate for Traverse 12 at 90 km downwind of the Cumberland power plant on July 6, 1999. SCICHEM results are based on measured surface and upper air meteorology.

Finally, the Traverse 12 results for the SCICHEM simulation with WRF meteorology are compared with observed plume concentrations in Figure 3-10. We see from Figure 3-10a that both the predicted SO_2 and NO_y concentrations are in good agreement with the plume measurements. However, Figure 3-10b shows that both the NO and NO_2 concentrations are significantly over-predicted, although the peak NO_2 to NO ratios in the measurements and model results are comparable. In contrast to the results with observed meteorology (compare Figure 3-9c and Figure 3-10c), SCICHEM using WRF meteorology predicts very little formation of O_3 and inorganic nitrate in the plume at these transects.

The plume integrated concentrations of sulfate and nitrate measured by the helicopter at about 60 km downwind of the plant are about 6.5 and 3.65 µg/m^3, respectively (Tanner et al., 2002). The corresponding values from the SCICHEM simulation with observed meteorology are about 5 and 4 µg/m^3, respectively, which agree reasonably well with the observation. With WRF meteorology, the SCHICHEM plume integrated concentrations of sulfate and nitrate at this distance are 4.8 and 0 µg/m^3, respectively with the NO_3 value much lower than observed.

These results show that SCICHEM is quite sensitive to the meteorology used to drive the model. Except for Traverse 3, the SCICHEM results with observed meteorology are in generally better agreement with the measurements than the corresponding results with WRF meteorology, particularly with respect to the plume chemistry.

3.2 CAMX EVALUATION

We selected 4 plume transects, one each at downwind distances of 10.8 km, 11.0 km, 31.5 km, and 64.8 km for the CAMx plume evaluation using the SOS 99 Cumberland plume measurement database (see Table 3-2). Note that the time interval for CAMx simulation outputs is one hour, i.e., the model predictions are hourly-averaged values while the TVA helicopter measurements were conducted continuously with almost instantaneous time resolution. As described earlier (Section 2.3.4), the modeled concentrations at the 8th and 9th vertical layers are averaged and compared to the aircraft measurements. We first focus our analysis on the CAMx results using the MEGAN biogenic emissions and then discuss the differences when BEIS biogenic emissions are used.

Table 3-2. Cumberland power plant plume transects for CAMx comparisons.

Transect	Downwind distance (km)	Measurement start time (LST)	Measurement end time (LST)	Average aircraft ALT (m AGL)
3	10.8	11:19:06	11:24:51	495.7
5	11.0	11:33:21	11:36:41	500.6
8	31.5	12:22:31	12:28:21	510.6
11	64.8	15:19:06	15:29:06	511.5
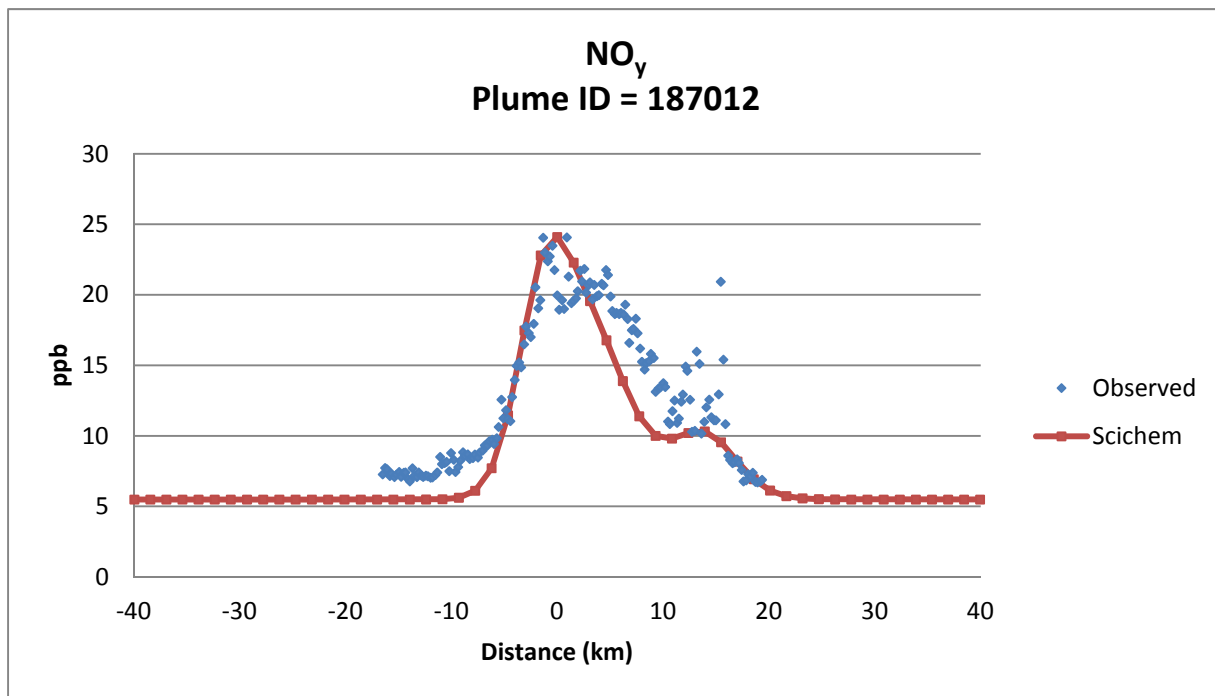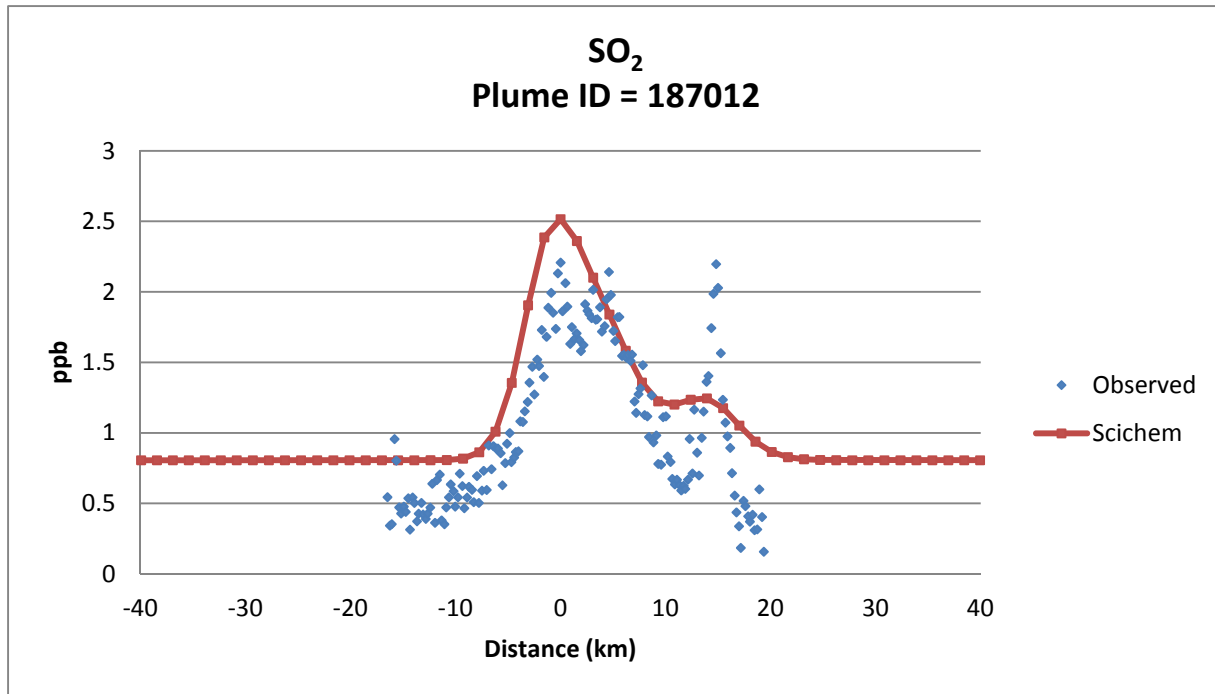
Figure 3-10a. Observed and simulated (SCICHEM) cross-wind plume concentrations of SO$_2$ and NO$_y$ for Traverse 12 at 90 km downwind of the Cumberland power plant on July 6, 1999. SCICHEM results are based on WRF meteorology processed with MMIF.
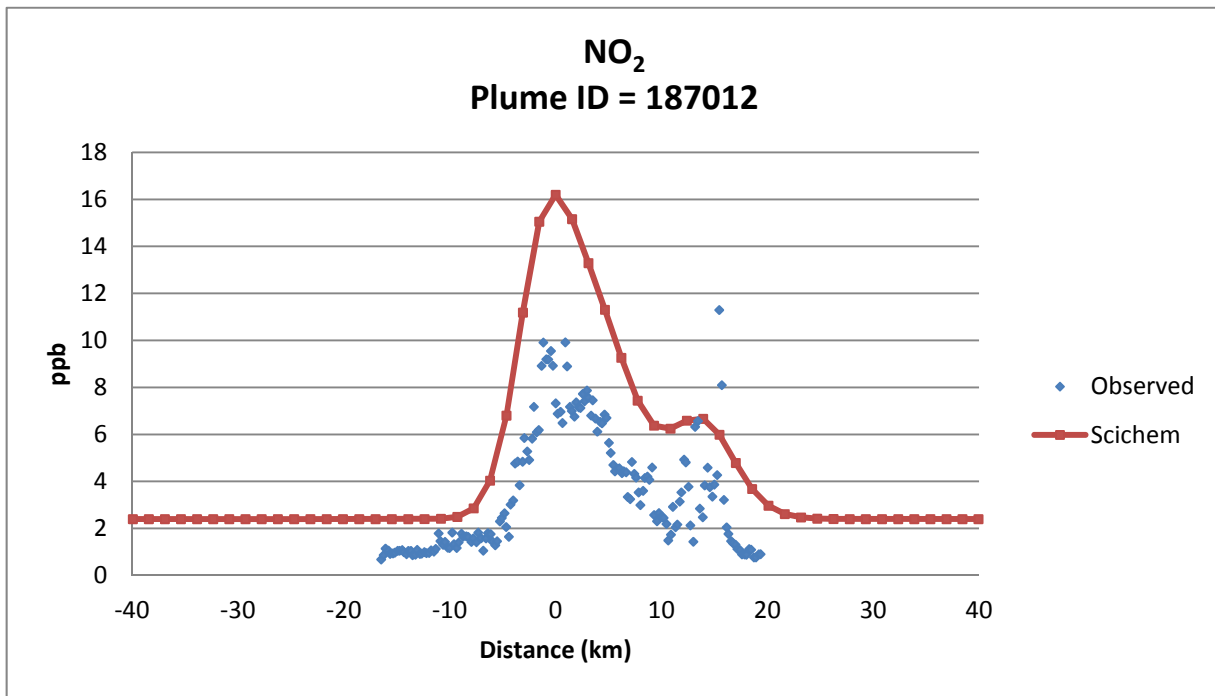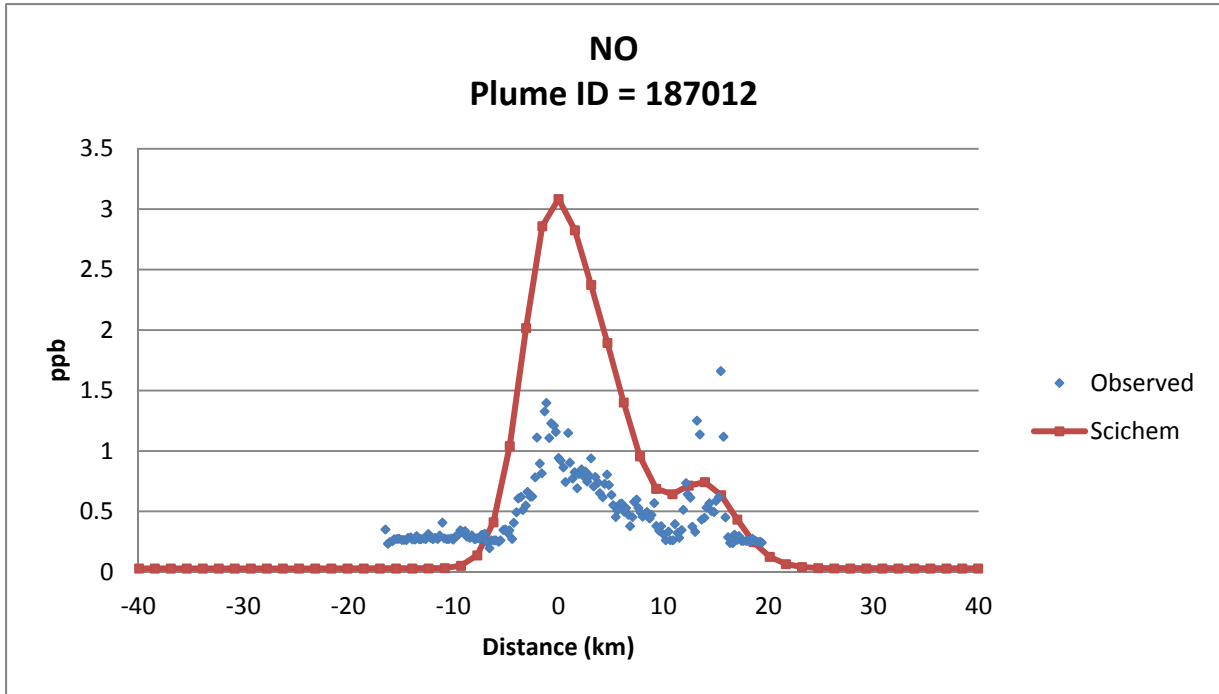
Figure 3-10b.   Observed and simulated (SCICHEM) cross-wind plume concentrations of NO and NO$_2$ for Traverse 12 at 90 km downwind of the Cumberland power plant on July 6, 1999. SCICHEM results are based on WRF meteorology processed with MMIF.
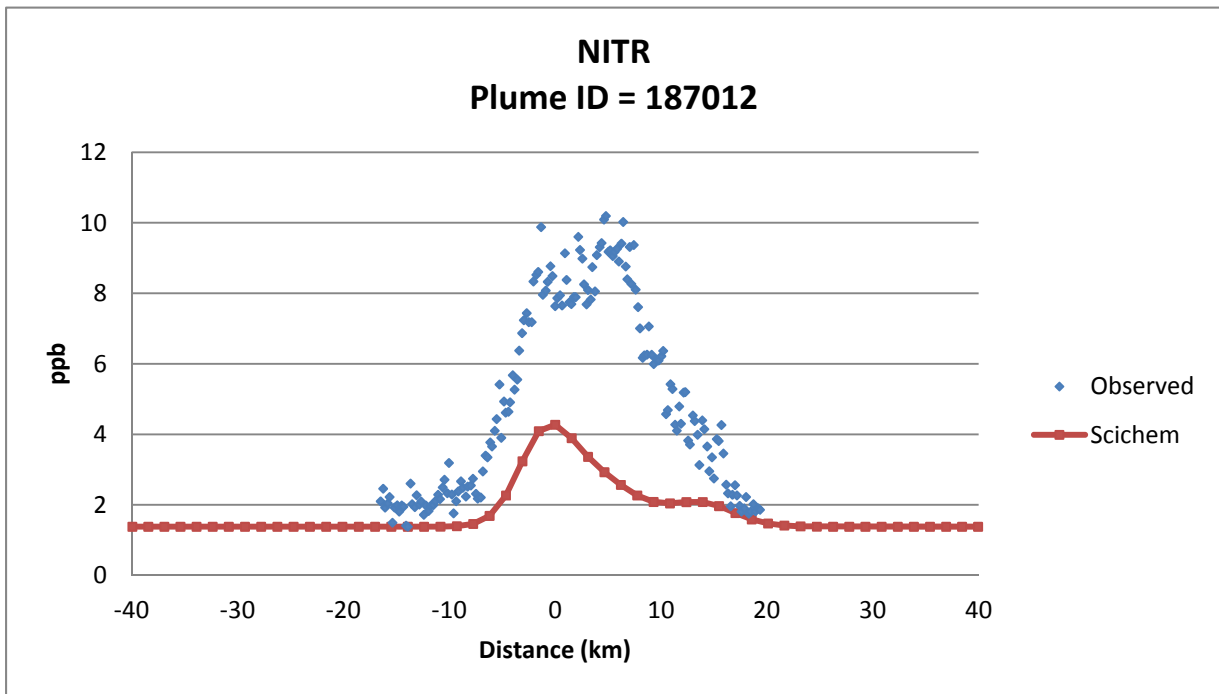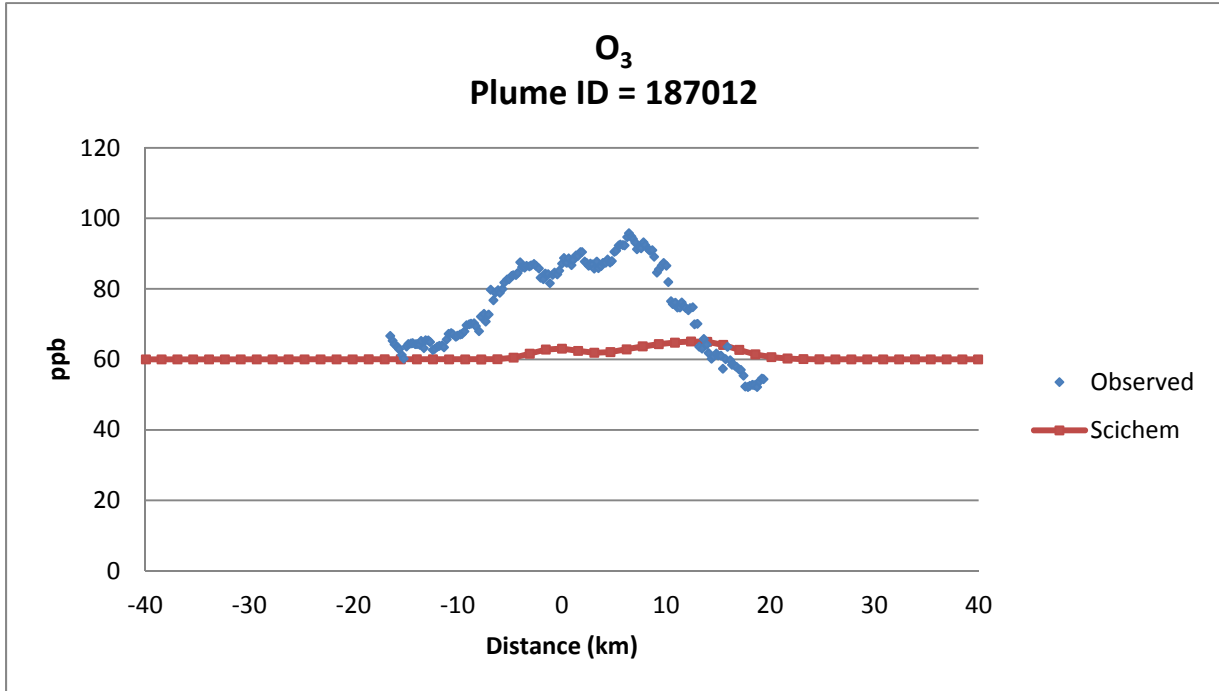
Figure 3-10c.   Observed and simulated (SCICHEM) cross-wind plume concentrations of O₃ and inorganic nitrate for Traverse 12 at 90 km downwind of the Cumberland power plant on July 6, 1999. SCICHEM results are based on WRF meteorology processed with MMIF.

Figure 3-11 shows the model-predicted NO$_X$ plumes from the Cumberland plant with the 500-m grid resolution, along with the plume transect at each downwind distance. The plume transects were determined so that the distances between the grid cells for the Cumberland plant and plume center at the transect match as close to those of aircraft traverses as possible.

Figure 3-12 compares the observed and modeled concentrations of SO$_2$, NO, NO$_2$, NOx, NO$_Y$ and O$_3$ for plume transect 3. The model under-predicts peak SO$_2$ concentration by 13% and peak NO$_Y$ concentration by 37% while the width of the modeled plume agrees relatively well with observations. The modeled NO$_2$/NO ratio is 0.97 at the plume center while the corresponding ratio in the observation is 0.65 indicating that the NO-to-NO$_2$ conversion is somewhat faster in the model than in the observations. Both the model and observation are showing decrease in ozone concentration in the plume due to NO$_X$ titration. The modeled decrease in ozone at the plume center is slightly less than in observation because the model under-predicted NO. Figure 3-13 shows the same plots as Figure 3-12, only slightly further downwind (by a few hundred meters), and agreement between the model and observation is similar to or slightly better than that for Transect 3. Figure 3-14 presents the modeled and observed plume concentrations for Transect 8, which is about 32 km downwind from the Cumberland plant. At this distance, the modeled plume is somewhat narrower than the observed one. Peak SO$_2$ concentration is slightly over-predicted and peak NO$_X$ (and NO$_2$) concentrations are slightly under-predicted. Peak concentrations of NO and NO$_Y$ are in good agreement with the observations. The ozone wing effect is more pronounced at this transect and the model is able to capture this phenomenon, but predicts much less NO$_X$ titration than observed. Figure 3-15 shows the comparison plots for Transect 11, which is about 65 km downwind from the Cumberland plant. The modeled plume width is again narrower than the observed width except for SO$_2$ for which the model agrees quite well with the observation. At this rather far downwind distance, the plume is quite diluted and NO$_X$ titration of ozone is not as significant.

With the SMOKE BEIS3 biogenic emissions, the model results are quite similar to those with the MEGAN biogenic emissions for the transects closer to the source (i.e., transects 3 and 5). For transects 8 and 11 that are further downwind (32 and 65 km, respectively), the model results with SMOKE BEIS3 show higher NO$_X$ than those with MEGAN; at these farther downwind distance the NO$_X$ in the plume due to the Cumberland emissions becomes more diluted so that the background NO$_X$ becomes more important and since SMOKE BEIS3 estimates higher biogenic NO than MEGAN (see Figure 2-3) then there is more NO$_X$ in the plume.

(a) Transect at 10.6 km

July 6,1999 17:00:00
Min= 0.00 at (1,1), Max=224.20 at (11,40)

(b) Transect at 11.1 km

July 6,1999 17:00:00
Min= 0.00 at (1,1), Max=224.20 at (11,40)
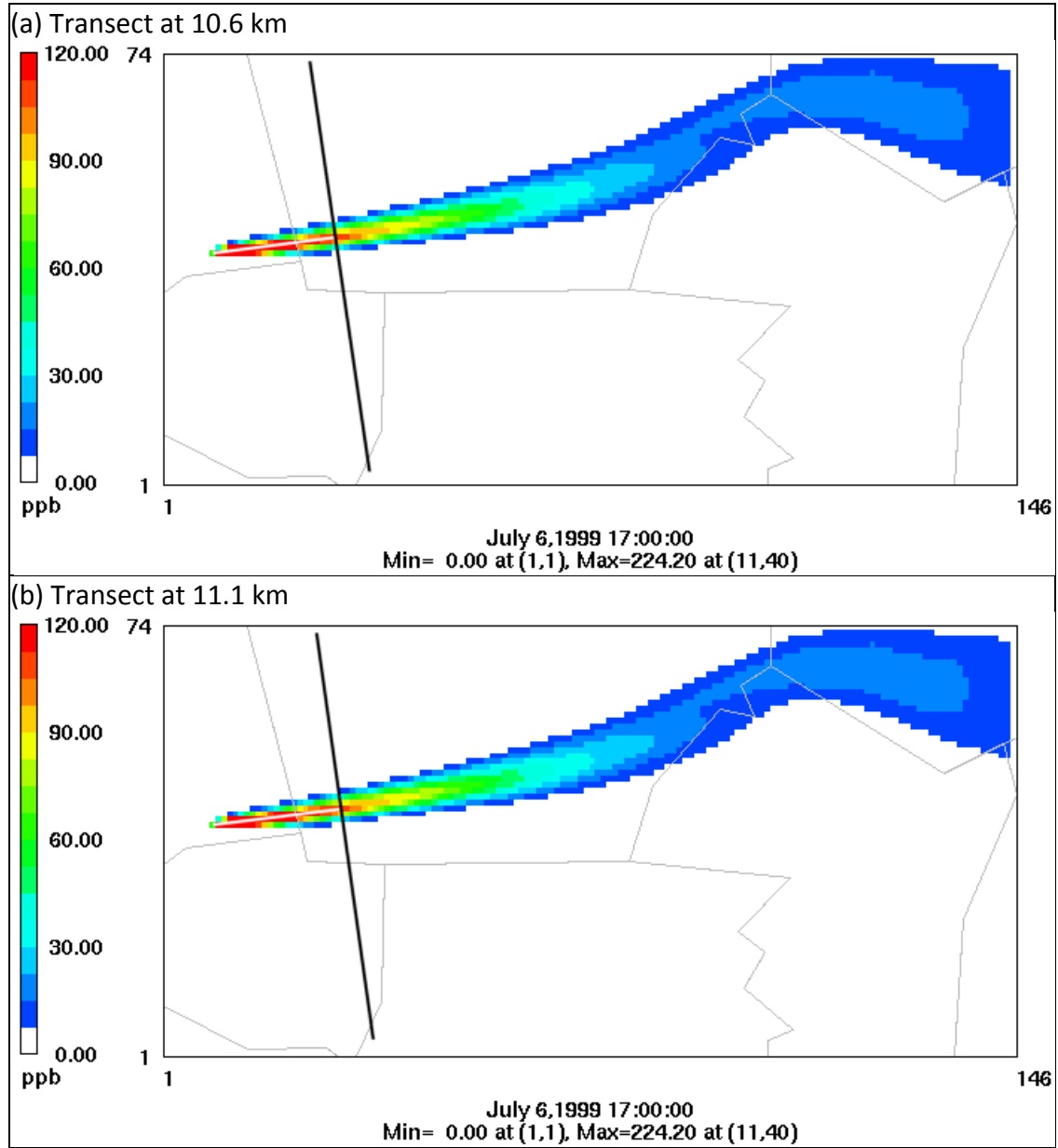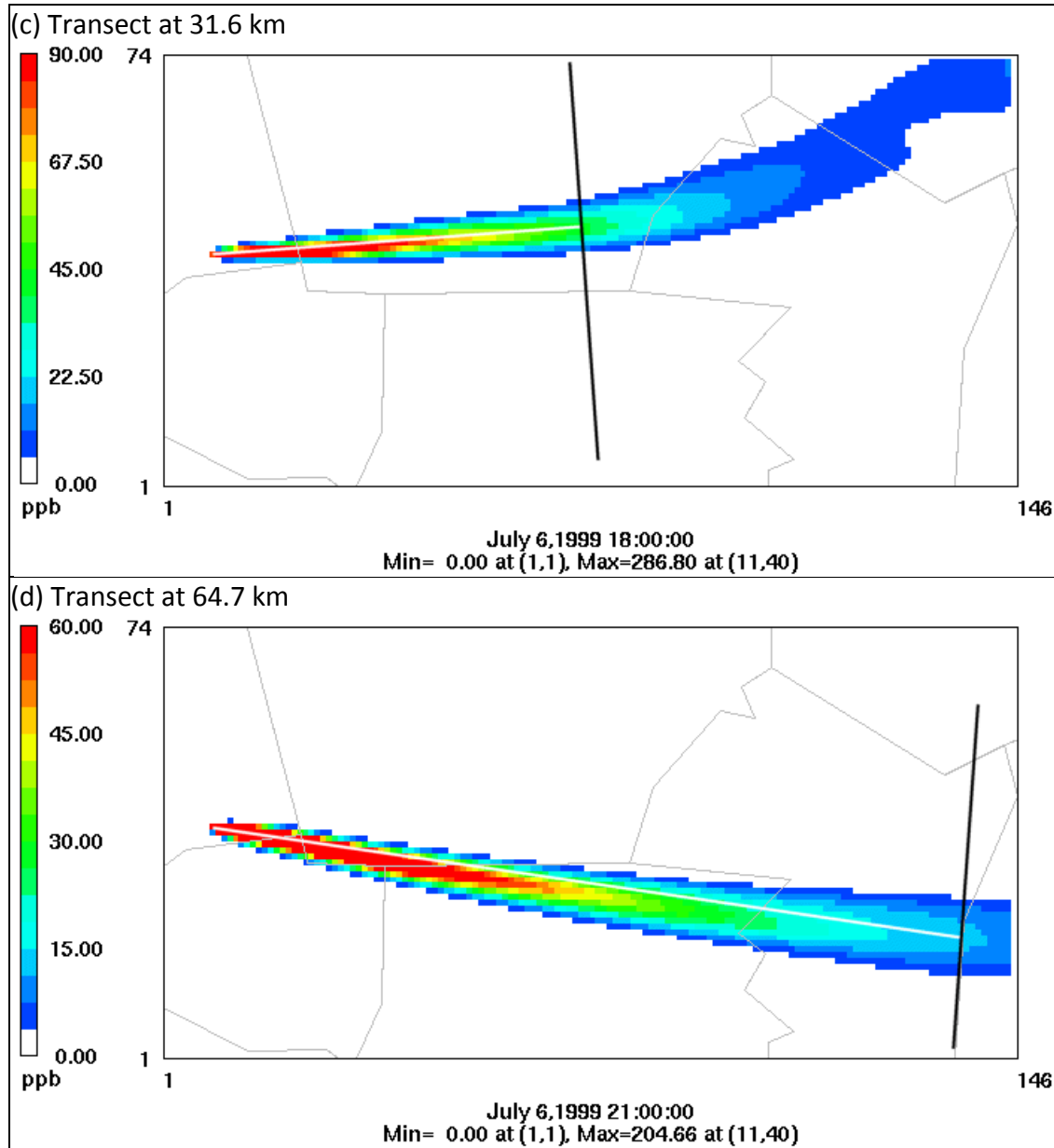
Figure 3-11. NOx plumes modeled with 500-m grid resolution (at the 8th layer). The black lines represent plume transects defined for model evaluation.
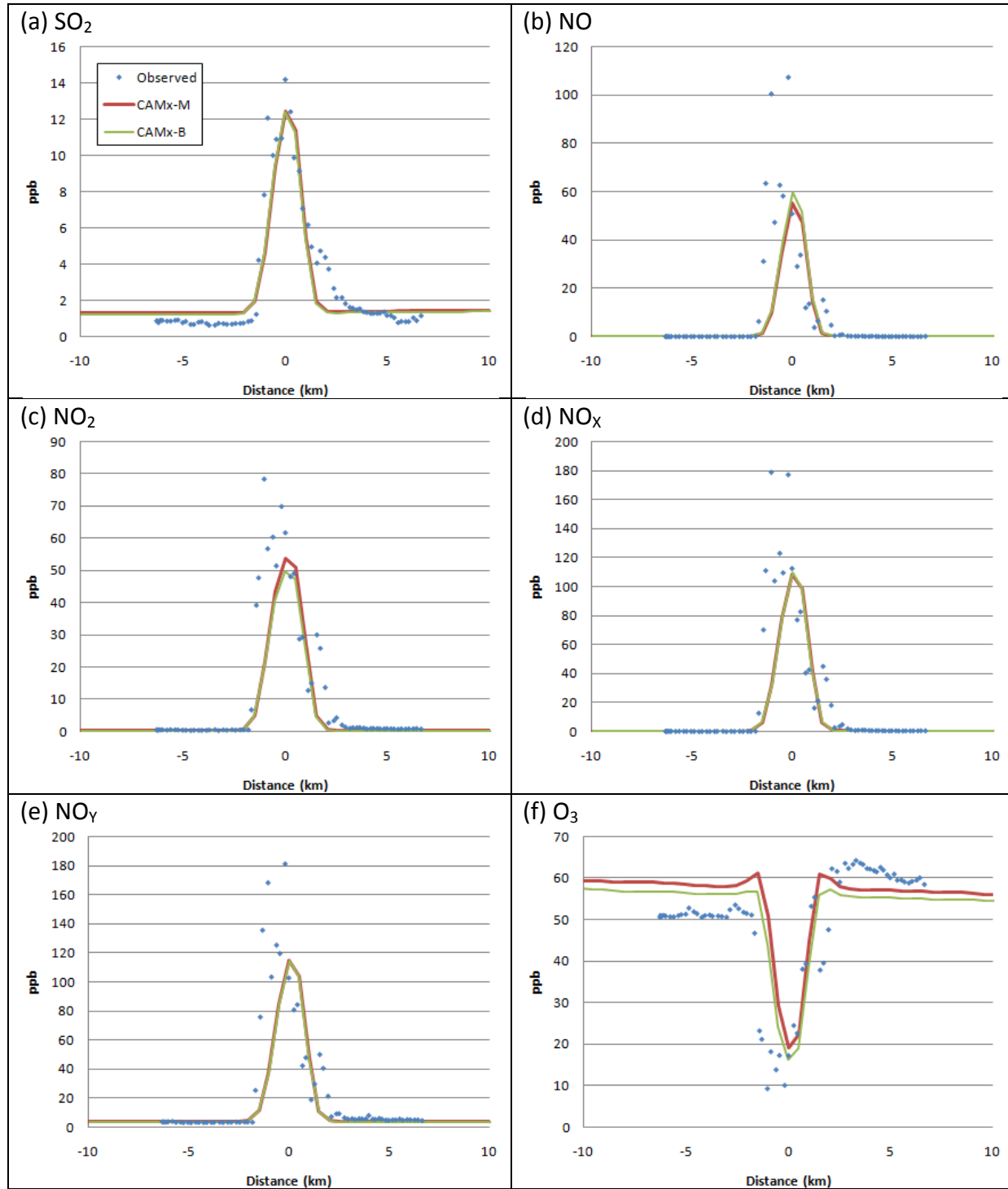
Figure 3-12. Comparison of CAMx simulations with MEGAN (CAMx-M) and SMOKE BEIS3 (CAMx-B) biogenic emissions with the TVA helicopter measurements for plume transect 3.
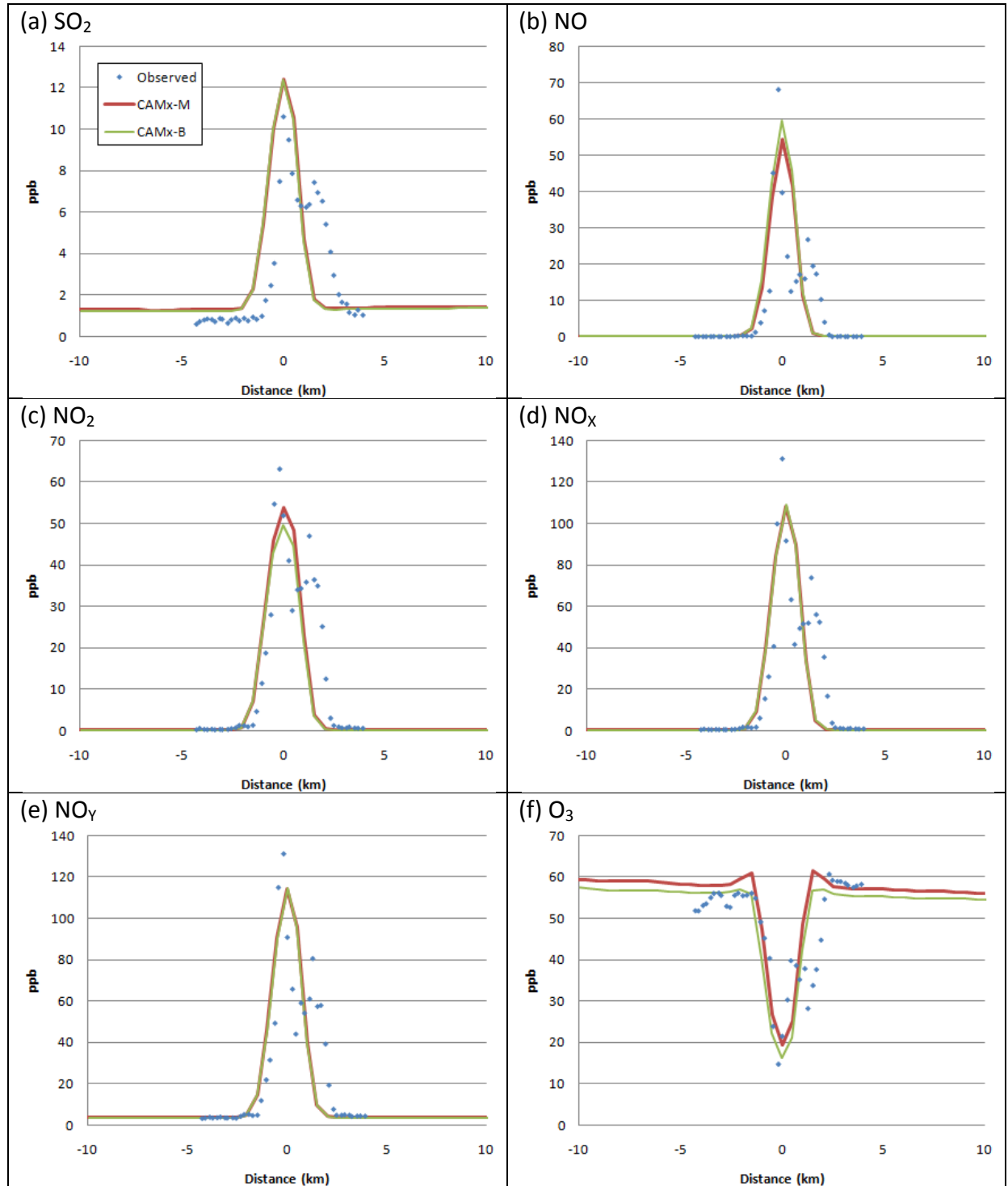
Figure 3-13. Comparison of CAMx simulations with MEGAN (CAMx-M) and SMOKE BEIS3 (CAMx-B) biogenic emissions with the TVA helicopter measurements for plume transect 5.
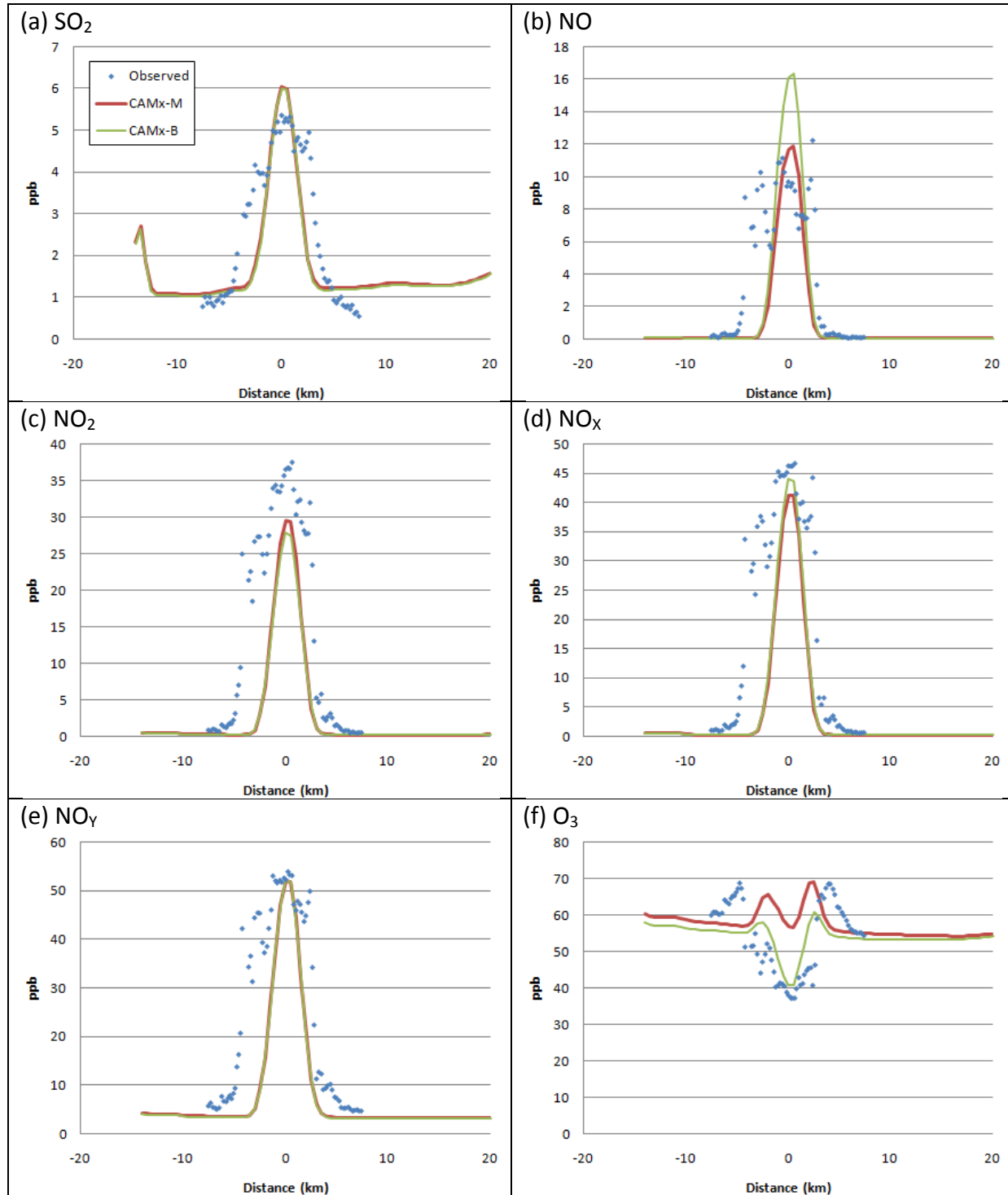
Figure 3-14. Comparison of CAMx simulations with MEGAN (CAMx-M) and SMOKE BEIS3 (CAMx-B) biogenic emissions with the TVA helicopter measurements for plume transect 8.
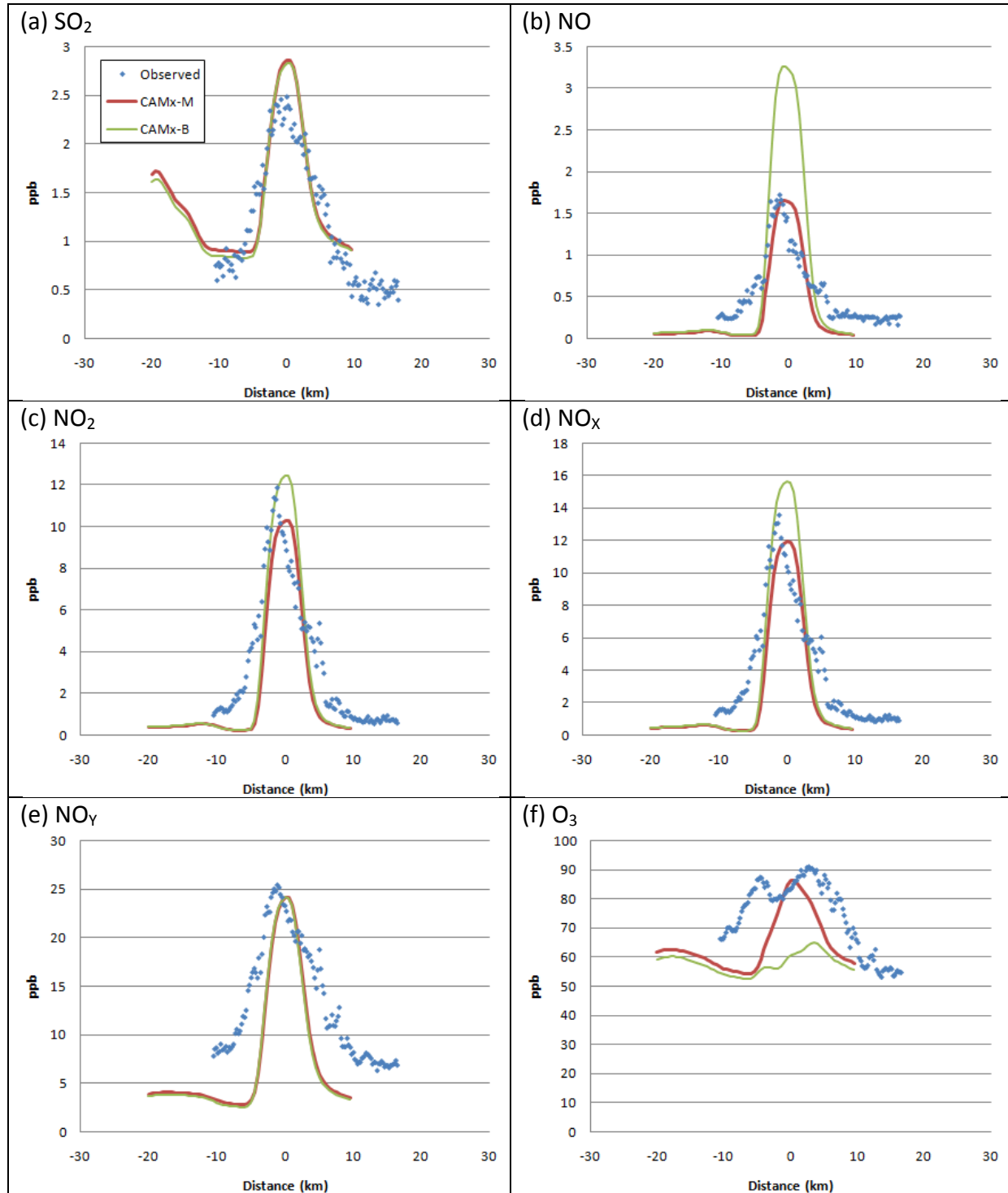
Figure 3-15. Comparison of CAMx simulations with MEGAN (CAMx-M) and SMOKE BEIS3 (CAMx-B) biogenic emissions with the TVA helicopter measurements for plume transect 11.

3.3 CALPUFF EVALUATION

The CALPUFF evaluation uses the same sampling locations as were selected for SCICHEM analysis. The helicopter transects that were selected are shown in Table 3-3, they are representative of 4 different downwind distances from the source.

Table 3-3. Selected TVA Bell 205 transects of the Cumberland power plant plume on July 6, 1999.

Transect	Plume ID Number	Downwind distance (km)	Measurement start time (LST)	Measurement end time (LST)
3	187003	10.8	11:19:06 a.m.	11:24:51 a.m.
8	187008	31.5	12:22:31 p.m.	12:28:21 p.m.
10	187010	64.9	3:05:11 p.m.	3:16:16 p.m.
12	187012	89.1	3:48:56 p.m.	4:02:46 p.m.

Figure 3-16 compares observed concentrations of SO_2, NO_x, and NITR, respectively, for Transects 3 and 8 of the Cumberland plume with CALPUFF v5.8/CALMET and CALPUFF v5.8/MMIF predictions. Figure 3-17 shows the same comparison for Transects 10 and 12. The predictions are extracted at the average sampling height of the helicopter measurements (500 m). NITR represents total inorganic nitrate (nitric acid + particulate nitrate, HNO3 + NO3 in CALPUFF terms).

3.3.1 CALPUFF Version 5.8 with CALMET Meteorology

SO_2 Analysis

For CALPUFFv5.8 with CALMET, the transect closest to the source at approximately 11 km downwind has the maximum modeled SO_2 value that closely matches the measured value (Figure 3-16a); the modeled plume width also matches the measured width reasonably well. Further downwind of the source, CALPUFFv5.8 with CALMET meteorological inputs underestimates the measured SO_2 plume values. At approximately 32 km downwind, the CALPUFF-estimated SO_2 maximum value is approximately half the observed value, but the plume width appears to be comparable to the observed width (Figure 3-16d). At approximately 65 km downwind, the CALPUFF-estimated SO_2 peak is again approximately half of the observed value and the plume width is wider than the observed width (Figure 3-17a). At approximately 90 km downwind, the CALPUFF SO_2 peak value is at least 7 times lower than observed. The SO_2 mass contained within the plume is significantly reduced at the 90 km downwind distance. The mechanism for this is unclear, possibly either by vertical dispersion or chemical transformation. Note that the observed values indicate that background SO_2 values of approximately 0.5 ppb and CALPUFF does not account for background SO_2. However, even accounting for background SO_2 by adding 0.5 ppb to the CALPUFF predictions would not increase CALPUFF plume SO_2 concentrations high enough to match the peak measured values.

NO_X Analysis

NO_X comparison of CALPUFFv5.8 with CALMET meteorology shows that CALPUFF underestimates NO_X for all transects. CALPUFF estimates are greater than a factor of 2 lower for the first transect (#3) and approximately a factor of 10 lower for next transect (#8) (Figures

3-16b and 3-16c); with CALPUFF NOX values even lower than observed for the two farthest most downwind transects. Since the background NO_X concentrations are near zero, then background does not play a role in CALPUFF/CALMET NO_X underestimation bias.

Nitrate Analysis

CALPUFF v5.8 with CALMET meteorology shows good agreement with the observed values for nitrate across the two transects closest to the source in terms of both plume peak concentrations and plume width (Figure 3-16 c and f). At the 65 km downwind transect (#10), the CALPUFF/CALMET-estimated nitrate concentrations are approximately half the measured values and the plume width is slightly wider than observed, possibly indicating excessive dispersion in CALPUFF (Figure 3-17c). Similar to the other pollutants, at approximately 90 km downwind of the source the CALPUFF/CALMET nitrate estimates greatly underestimate the measured values (Figure 3-17f). Note, the measured nitrate values for transects #8, #10, #12, have fairly uniform nitrate concentrations with a peak of approximately 10 ppb, whereas the modeled estimates show rapidly decreasing nitrate concentration downwind of the source.

3.3.2   CALPUFF Version 5.8 with MMIF/WRF Meteorology

SO_2 Analysis

CALPUFF v5.8/MMIF cross-wind plume distribution exhibits a bi-modal pattern with a double peak concentration for all pollutants at the ~ 11 km downwind distance. This bimodal pattern disappears further downwind (Figure 3-16, left panels). The observed peak SO_2 concentration is overestimated by almost a factor of 2 for the first transect (#3) and then underestimated for the other transects. For transects #8 and #10, it appears that accounting for background SO_2 would eliminate the CALPUFF/MMIF underestimation resulting in modeled SO_2 peak concentrations that match measured values reasonably well.

NO_X Analysis

For transect #3, CALPUFF v5.8/MMIF estimates the peak NO_X concentration very well (Figure 3-16b). The second transect (#8), at approximately 30 km downwind, the observed NO_X peak is underestimated by CALPUFF v5.8/MMIF that is due in part to a modeled plume width that is overestimated, indicative of excessive dispersion in the model (Figure 3-16e). Further downwind (~65 and ~90 km), the measured peak NO_X concentrations drop to approximately 13 ppb (at both distances) and the CALPUFF estimates decrease more slowly downwind resulting in CALPUFF v5.8/MMIF (~23 ppb) overestimating the observed peak NO_X concentration (~13 ppb) at ~65 km downwind (Figure 3-17b) with CALPUFF/MMIF NO_X peaks at 90 km downwind (~8 ppb) slightly lower than observed (~12 ppb; Figure 3-17e).

Nitrate Analysis

CALPUFF v5.8/MMIF estimates the observed nitrate concentrations reasonably well for the early transects #3 and #8 (Figure 3-16 c and f), but underestimate nitrate peaks for later transects by a factor of 5 or more. This underestimation of the CALPUFF/MMIF estimated nitrate peaks is partly due to not including background values in the CALPUFF-estimates, however even including background the CALPUFF/MMIF nitrate peaks at 90 km would be significantly smaller than observed.
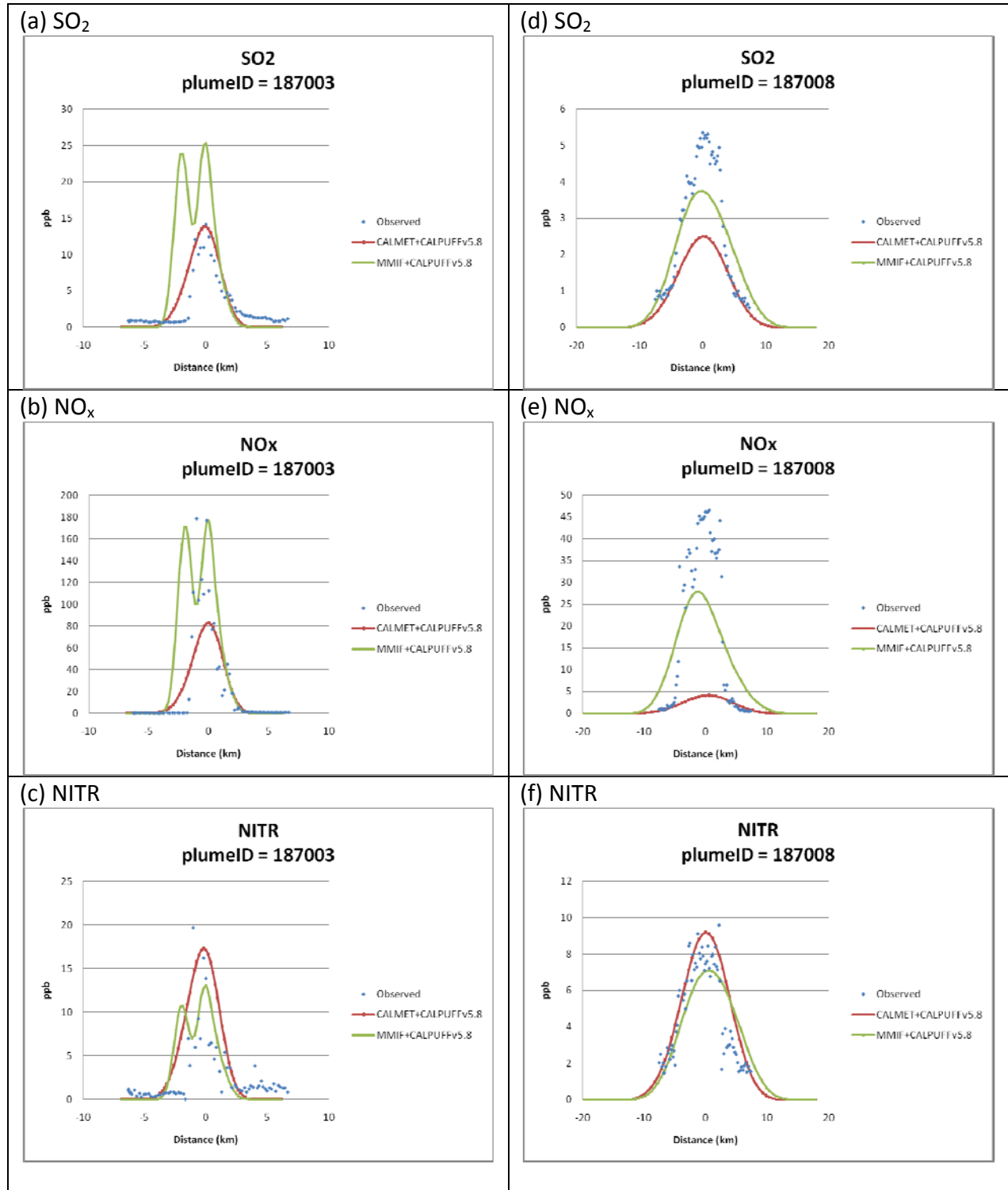
Figure 3-16. Comparison of CALPUFF v5.8 simulations using CALMET (red) and MMIF/WRF (green) meteorological inputs with the TVA helicopter measurements for plume Transect 3 (left) and Transect 8 (right) that are approximately 11 and 32 km downwind of the source.
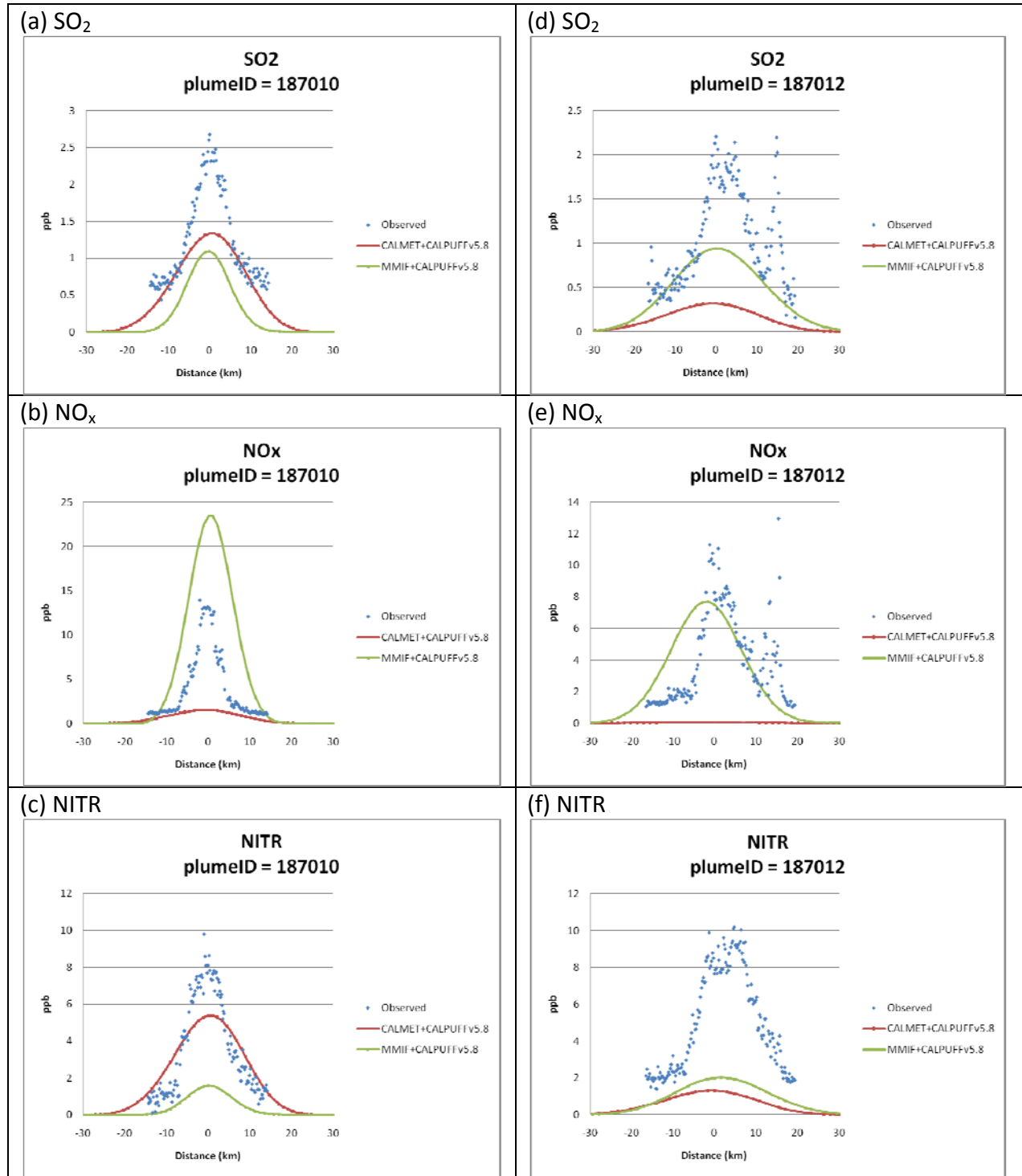
Figure 3-17. Comparison of CALPUFF v5.8 simulations using CALMET (red) and MMIF/WRF (green) meteorological inputs with the TVA helicopter measurements for plume Transect 10 (left) and Transect 12 (right) that are approximately 65 and 90 km downwind of the source.

3.3.5 Comparison of CALPUFF using CALMET and MIFF Meteorological Inputs

The different results using CALPUFF/CALMET and CALPUFF/MMIF are striking considering the CALPUFF emissions and options are identical and all differences arise from the meteorological inputs. This shows that the CALPUFF modeling results are highly sensitive to the meteorological inputs.

CALPUFFv5.8/MMIF has a bi-modal pattern for all pollutants in the first transect, this is not seen with CALPUFF v5.8/CALMET or for CALPUFF/MMIF for the further downwind transects. NO_X estimates using MMIF are closer to the observed values than using CALMET, but the CALPUFF/CALMET NO_X estimates are extremely low, and barely capture a plume at all in the later transects. For CALPUFF v5.8 there are only small differences between the SO_2 and NITR model performance using the two sets of meteorological inputs.

3.4   COMPARISON OF CHEMICAL DISPERSION MODELING

Results are presented for 6 different model/model configurations:

- SCICHEM with observed meteorology
- SCICHEM with WRF/MMIF meteorology
- CAMx with MEGAN biogenic emissions
- CAMx with BEIS biogenic emissions
- CALPUFF v5.8 with CALMET meteorology
- CALPUFF v5.8 with WRF/MMIF meteorology

For each of the models/model configurations, 4 cross-plume transects were compared with observed values, as shown in Table 3-4. The CALPUFF and SCICHEM selection is identical, CAMx selected transect #5, and #11 which were not selected for CALPUFF and SCICHEM, and CALPUFF and SCICHEM selected transects #10 and #12, which were not selected for CAMx. All three models selected transects #3 and #8, so the focus of the comparison discussion will be those 2 transects. Note that transects #10 and #11 are very similar, so for the ozone comparison of CAMx and SCICHEM, those transects are compared.

Table 3-4. Plume transects selected for multi-model observed/model comparisons.

Transect	Plume ID Number	Downwind distance, km	SCICHEM	CAMx	CALPUFF
3	187003	10.8	yes	yes	yes
5	187005	11.0	no	yes	no
8	187008	31.5	yes	yes	yes
10	187010	64.9	yes	no	yes
11	187011	64.8	no	yes	no
12	187012	89.1	yes	no	yes

There is a wide variation in results across models and there seems to be as much variation between a single model using different meteorology as there is between the different models. MMIF/WRF meteorology generally degrades the results for SCICHEM compared to the observed meteorology, this may be expected since at this local plume scale observed meteorology is likely to be more accurate than MMIF/WRF. The exception to this is for the SCICHEM model performance for Transect #3 and NO_Y results. The MMIF/WRF degradation effect compared to

observed meteorological inputs for SCICHEM was more pronounced for further downwind transects. In general, for SO_2 and NO_X or NO_Y, the CAMx results were consistently good, as were SCICHEM with observed meteorology. SCICHEM with MMIF/WRF and CALPUFF results for the first transect were reasonable, but deteriorated further downwind. It should be noted that the CALPUFF modeling was performed at the end of the study so further in-depth analysis was not possible.

<u>Ozone Comparison</u>

Comparison of ozone estimates for SCICHEM and CAMx show that for the earliest transect (#3) both CAMx configurations and SCICHEM with MMIF simulate the ozone titration by NO_X phenomenon quite well in terms of both maximum decrease in ozone in the center of the plume and the width of ozone dip. SCICHEM with observational data also exhibited the titration effect but did not match observed values as closely as the other cases.

Further downwind at transect #8, neither SCICHEM case matches the observed ozone very well, both cases do show a change from the titration regime of transect #3 to some ozone formation above base level, but they both show an asymmetry, whereas the observed ozone at this transect is fairly symmetrical about the plume centerline. Both CAMx cases for transect #8 exhibit symmetry about the plume centerline, the MEGAN biogenic emissions case (with higher VOCs), shows plume edge ozone formation peak that very closely matches the observed values, but since the plume width is narrower than the observed plume width, the cross-plume peak locations are narrower than the observed locations. Also the observed values for transect #8 show ozone titration still occurring in the plume centerline resulting in ozone about 15 ppb lower than background levels, whereas the CAMx/MEGAN case does not have such reduced ozone concentrations. CAMx with BEIS biogenic emissions (lower VOCs and higher NO_X than MEGAN), match the centerline ozone titrated concentrations very well, and shows a small ozone formation effect on the plume edge but not a large enough effect to match the observed values.

For transects #10 (SCICHEM) and #11 (CAMx) that are located approximately 65 km downwind from the source, SCICHEM with observed meteorology models the observed ozone formation within the peak fairly well, just slightly overestimating the peak concentration, however SCICHEM with MMIF meteorology does not show any ozone peak within the plume at all. CAMx/MEGAN shows ozone formation within plume that matches observed values quite well, just slightly underestimating the peak, whereas CAMx/BEIS showed barely any ozone formation within the plume.

Both CAMx and SCICHEM show skill in modeling ozone titration and formation effects within the Cumberland plume. Ozone formation at the larger downwind distances is quite sensitive to background VOCs in CAMx and to the different meteorology in SCICHEM.

4.0   EVALUATION USING THE 2006 TEXAQS II OKLAUNION PLUME MEASUREMENTS

The evaluation of the SCICHEM and CAMx models using the Oklaunion plume observations are presented in this section.

4.1   SCICHEM EVALUATION

Below, we present SCICHEM plume model performance evaluation results for two sets of two plume transects at varying downwind distances from the Oklaunion power plant using the TexAQS II P-3 measurements. The first set of plume transects (Transects 1 and 2 in Table 4-1) corresponds to measurements taken during the early part of the measurement period on the night of October, 10, 2006, between about 7:00 and 7:30 pm LST that occur approximately 20 km downwind of the source. The second set (Transects 14 and 15) corresponds to measurements taken about 2 hours later, between 9:00 and 10:00 pm LST, that occur approximately 30 and 60 km downwind of the source, respectively.

Table 4-1 lists the two sets of transects, with each transect numbered as in the P-3 data files provided by NOAA. As in the case of the Cumberland plume, the plume widths shown in Table 4-1 are inferred from the measured SO_2 concentration profile as 4σ, the extent of the plume containing about 95.5% of the plume mass (e.g., see Karamchandani et al., 2000). In contrast to the Cumberland results (Table 3-1), the SCICHEM plume widths with observed meteorology are narrower than those with MM5/MMIF meteorology, based on 12 km meteorological fields, and are generally in much better agreement with the observed plume widths.

Table 4-1. Selected NOAA P-3 transects of the Oklaunion power plant plume on October 10, 2006.

Transect	Downwind distance (km)	Measurement start time (LST)	Measurement end time (LST)	Plume width from measurements (km)	Plume width from SCICHEM (km)	
					Obs. Met.	MM5 Met.
1	18.4	7:17:36 p.m.	7:18:08 p.m.	0.94	1.21	2.57
2	24.5	7:21:21 p.m.	7:22:08 p.m.	2.14	1.28	3.21
14	29.8	9:33:26 p.m.	9:34:13 p.m.	1.07	1.56	3.59
15	57.7	9:39:14 p.m.	9:39:48 p.m.	1.32	3.12	6.65

As in the case of the Cumberland plume results discussed in Section 3, we compare the observed and simulated plume directions for selected Oklaunion plume intercepts (Intercepts 1 and 2 at 18 and 25 km downwind at about 7:00 p.m. LST, and Intercepts 14 and 15 at 30 and 58 km downwind at about 9:30 p.m. LST). The comparisons are shown for SCICHEM results with observed aircraft meteorology (Figure 4-1) and SCICHEM results with MM5 meteorology processed with MMIF (Figure 4-2). We see that there are more differences between the observed and simulated plume directions as compared to the Cumberland simulation, and the SCICHEM plume directions with observed meteorology again agree better with observed directions than the simulated plume directions with MMIF-processed 12 km MM5 meteorology.
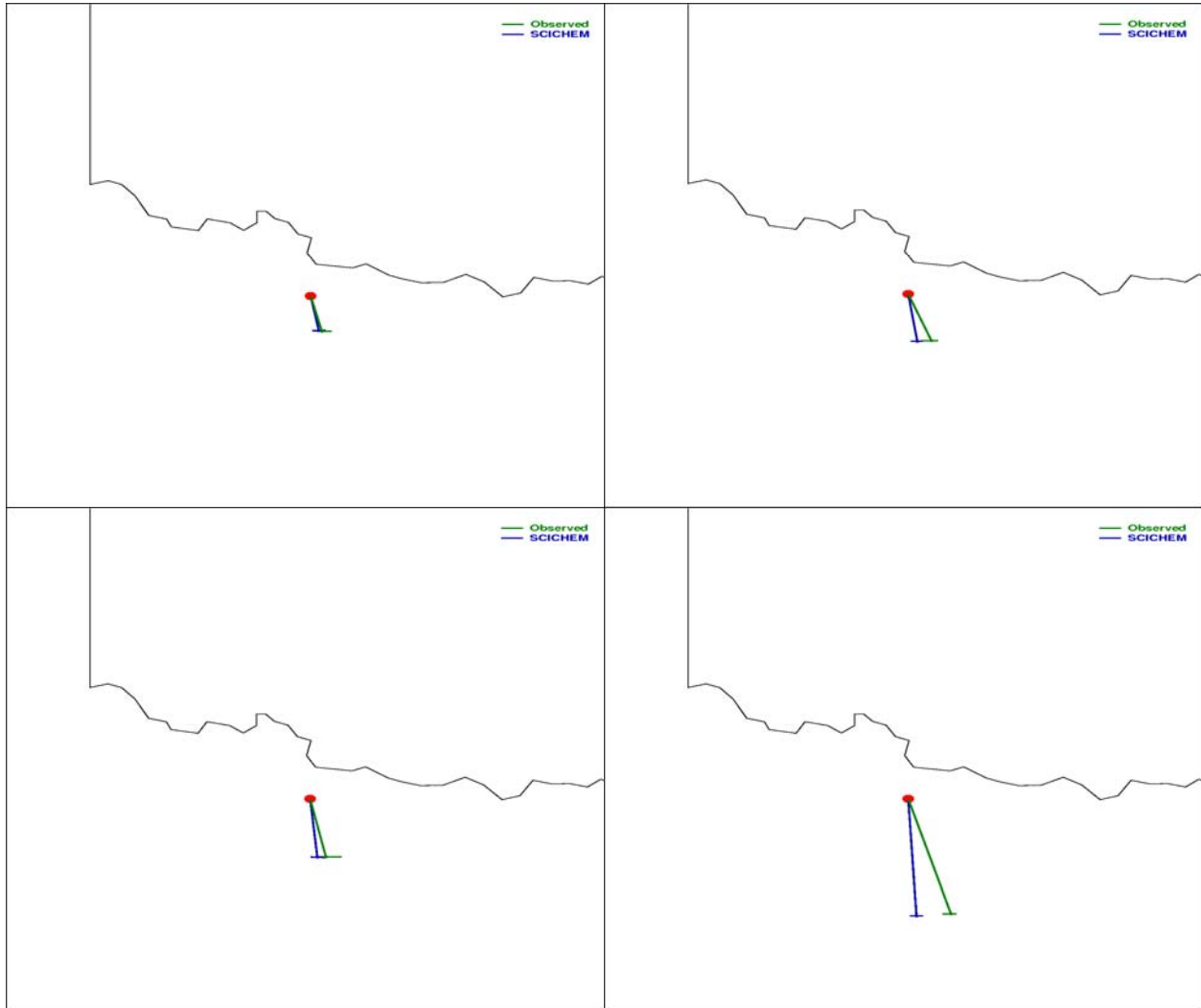
Figure 4-1. Observed and simulated (SCICHEM) plume transport directions and plume traverses at 18 km (top left), 25 km (top right), 30 km (bottom left) and 58 km (bottom right) downwind of the Oklaunion power plant on October 10, 2006. SCICHEM results are based on aircraft-observed meteorology.
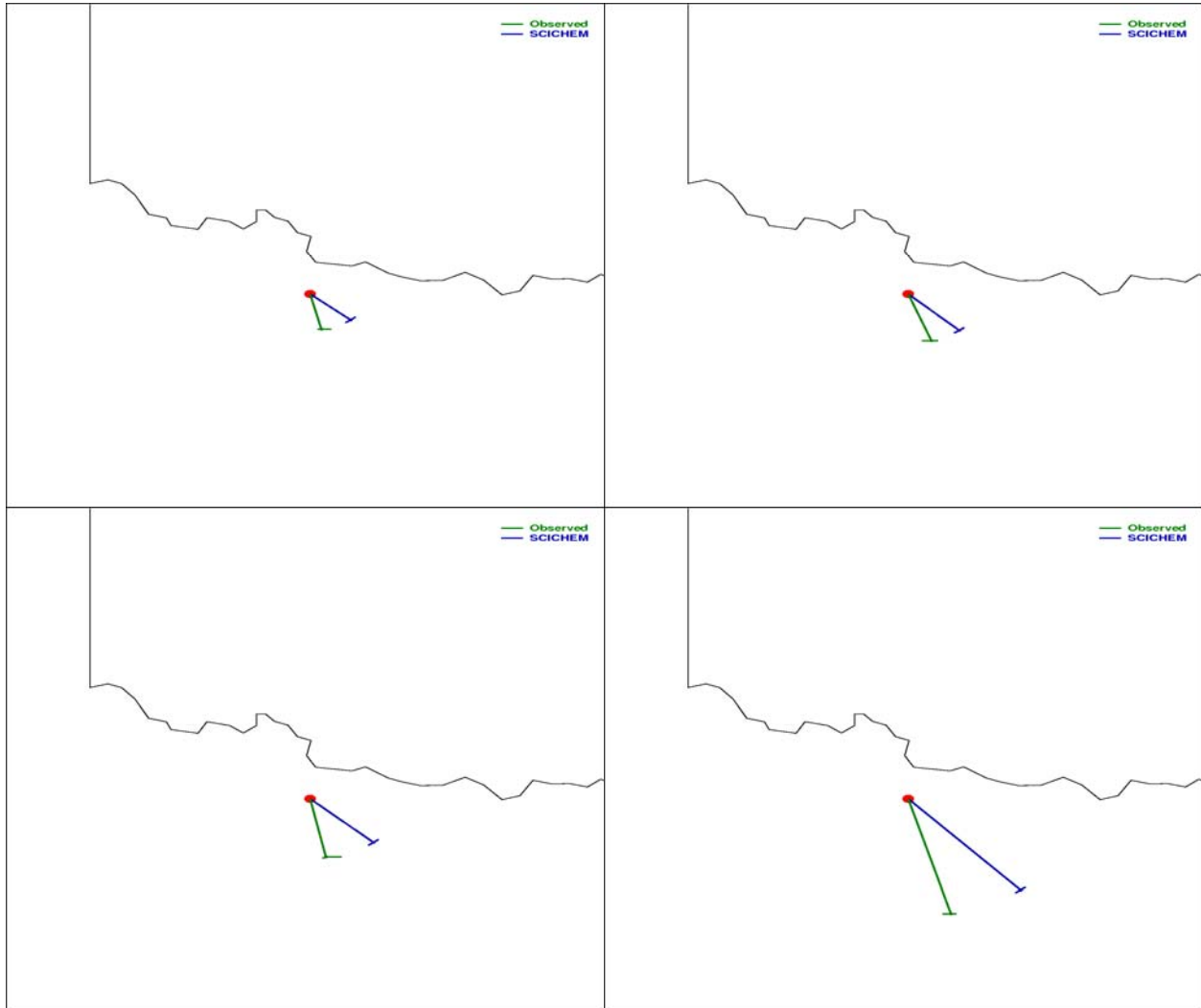
Figure 4-2. Observed and simulated (SCICHEM) plume transport directions and plume traverses at 18 km (top left), 25 km (top right), 30 km (bottom left) and 58 km (bottom right) downwind of the Oklaunion power plant on October 10, 2006. SCICHEM results are based on MM5 meteorology processed with MMIF.

Figure 4-3 shows observed and predicted SO_2, NO_y, NO, NO_2, O_3 and N_2O_5 concentrations for plume transect 1, when observed meteorology is used to drive SCICHEM. We see that the peak measured and predicted SO_2 concentrations at plume centerline are in excellent agreement (within 9%), while the peak NO_y concentrations differ by about 14%, with the model predicting a lower peak than observed. The model over-predicts the NO to NO_2 conversion in the plume, but not as much as in the Cumberland plume simulation. Both measurements and model results show complete titration of background ozone by plume NO_x at the plume centerline. The observed reduction in N_2O_5 concentrations at the plume centerline is also predicted by the model, as is the production of N_2O_5 at the plume edges. The peak N_2O_5 concentration at the plume edge is about 120 ppt, about 75 ppt above the background value. Note that SCICHEM simulations using the default splitting and merging criteria produced zero N_2O_5 at the plume edges, so it is clear that increasing puff resolution plays a vital role in capturing this nighttime observed plume behavior. As discussed later in the description of the CAMx results, the same conclusion is obtained with the CAMx simulations of the Oklaunion plume, with the high grid resolution (200 m) simulation capturing some of the behavior observed in the aircraft measurements.

The corresponding results for plume transect 1 with MMIF-processed MM5 meteorology is shown in Figure 4-4. As compared to the results with aircraft meteorology, we see that the agreement between observed and simulated plume concentrations is not as good. The modeled plume is considerably wider, consistent with the plume widths reported in Table 4-1, and the peak concentrations of SO_2 and NO_y (Figure 4-4a) are lower than those observed. The NO to NO_2 conversion is significantly over-predicted when the MMIF meteorology is used, as shown in Figure 4-4b. We also note that N_2O_5 production at the plume edges is significantly over-predicted (Figure 4-4c).

The SCICHEM results (with observed aircraft meteorology) for plume transect 2 are shown in Figure 4-5. For this plume intercept, the modeled plume is about 40% narrower than the measured plume (plume widths of 1.3 km and 2.1 km, respectively). As in the case of transect 1, the predicted peak centerline SO_2 concentration is in very good agreement with the observed peak concentration (within 10%). The peak predicted and measured NO_y and NO_2 concentrations are also in good agreement. The peak NO concentration is under-predicted by about 40%. Background ozone is fully titrated by the plume NO_x at the plume centerline in both the model results and observations. The N_2O_5 results show that the fine-resolution plume model allows the production of N_2O_5 at the plume edges that is seen in the observations as well as the reduction at the plume centerline, but the maximum N_2O_5 in the simulation is about 130 ppt, substantially lower than the observed value of 350 ppt.

When MMIF-processed MM5 meteorology is used to drive SCICHEM, we see from Figure 4-6 that that the agreement between predicted and measured plume concentrations is generally poorer than the case using the aircraft meteorology. However, the N_2O_5 produced at the plume edges in this simulation is much higher than with observed meteorology and the peak N_2O_5 is closer to the observed value (compare Figure 4-6c with Figure 4-5c).
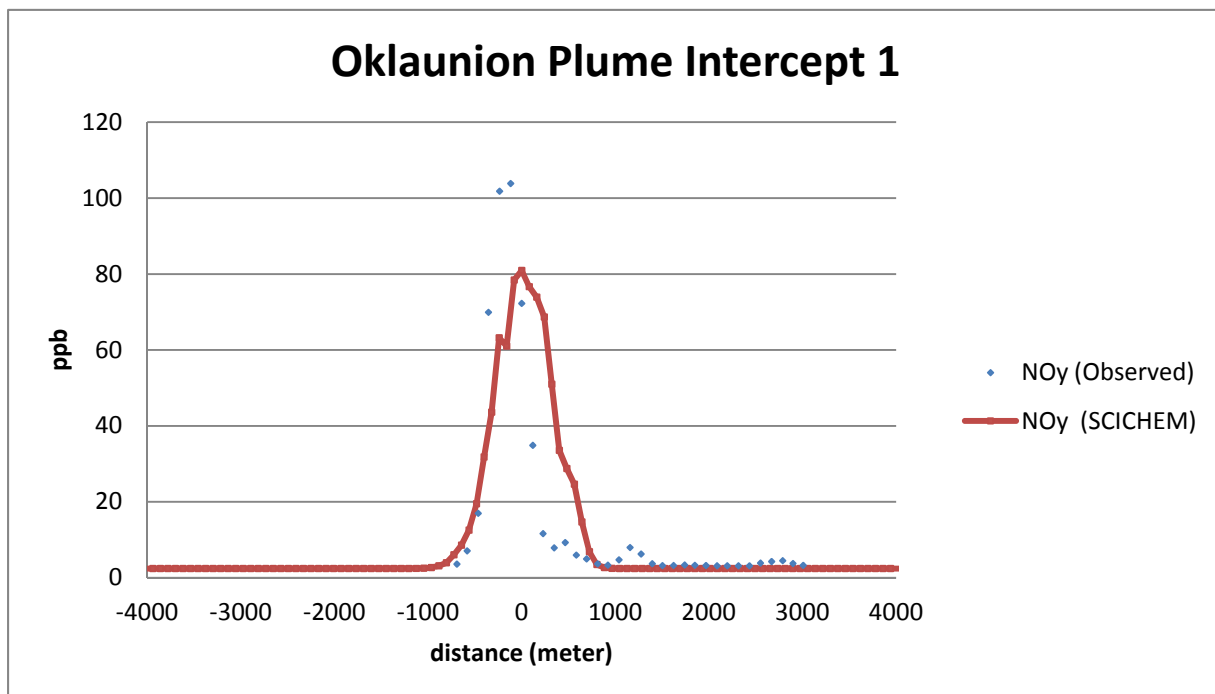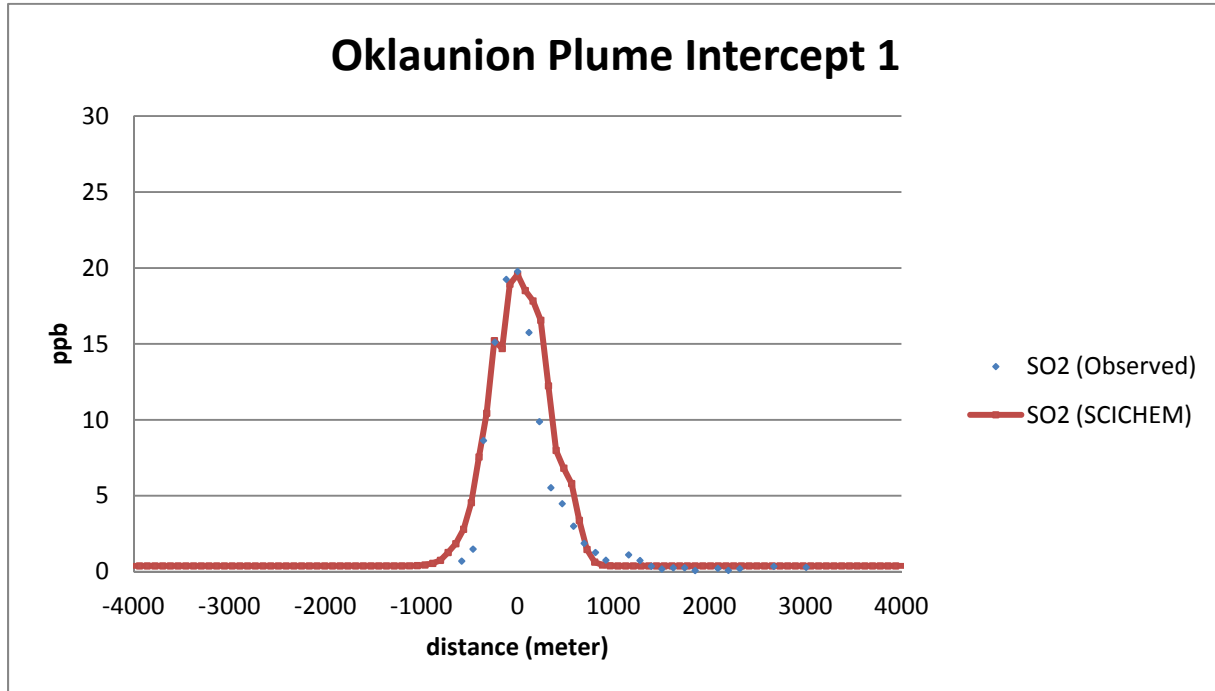
Figure 4-3a.   Observed and simulated (SCICHEM) cross-wind plume concentrations of SO$_2$ and NO$_y$ for plume intercept 1 at 18 km downwind of the Oklaunion power plant on October 10, 2006. SCICHEM results are based on aircraft-observed meteorology.
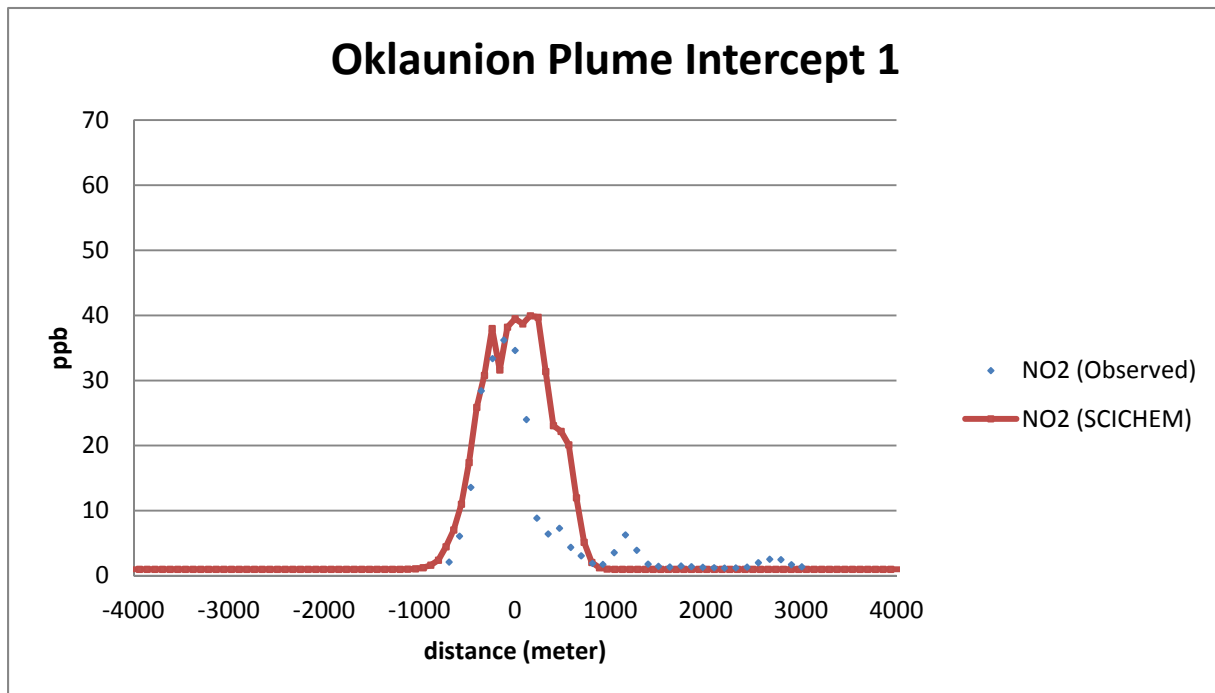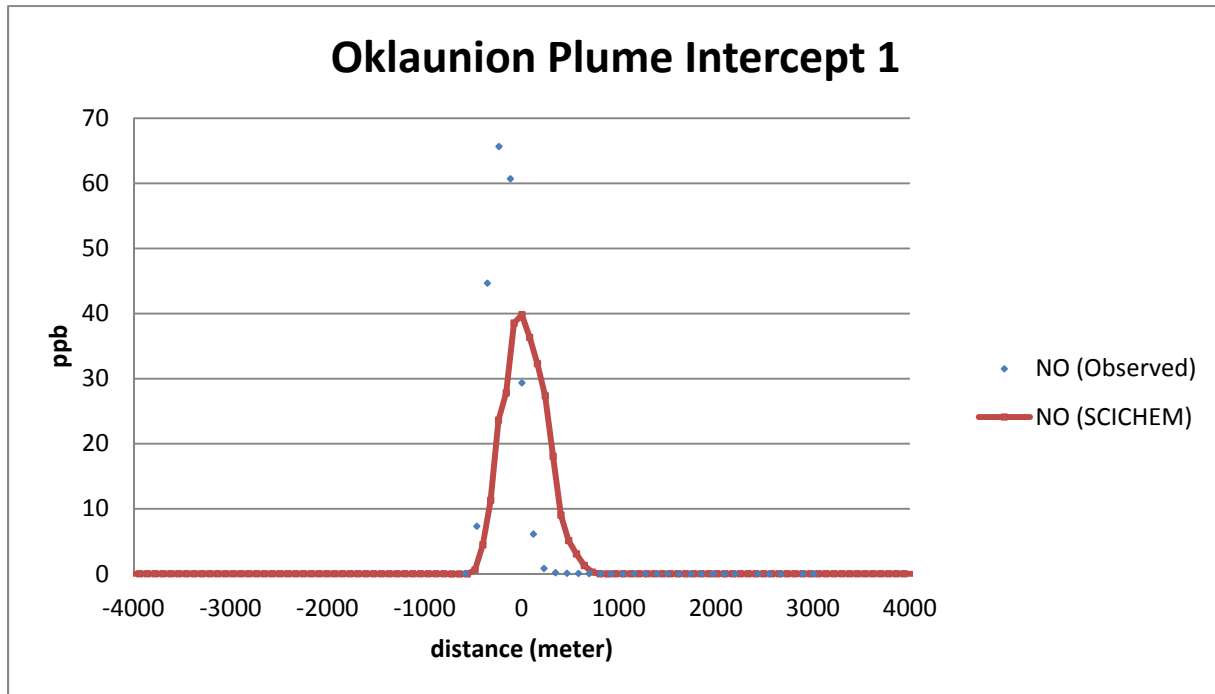
Figure 4-3b. **Observed and simulated (SCICHEM) cross-wind plume concentrations of NO and NO$_2$ for plume intercept 1 at 18 km downwind of the Oklaunion power plant on October 10, 2006. SCICHEM results are based on aircraft-observed meteorology.**
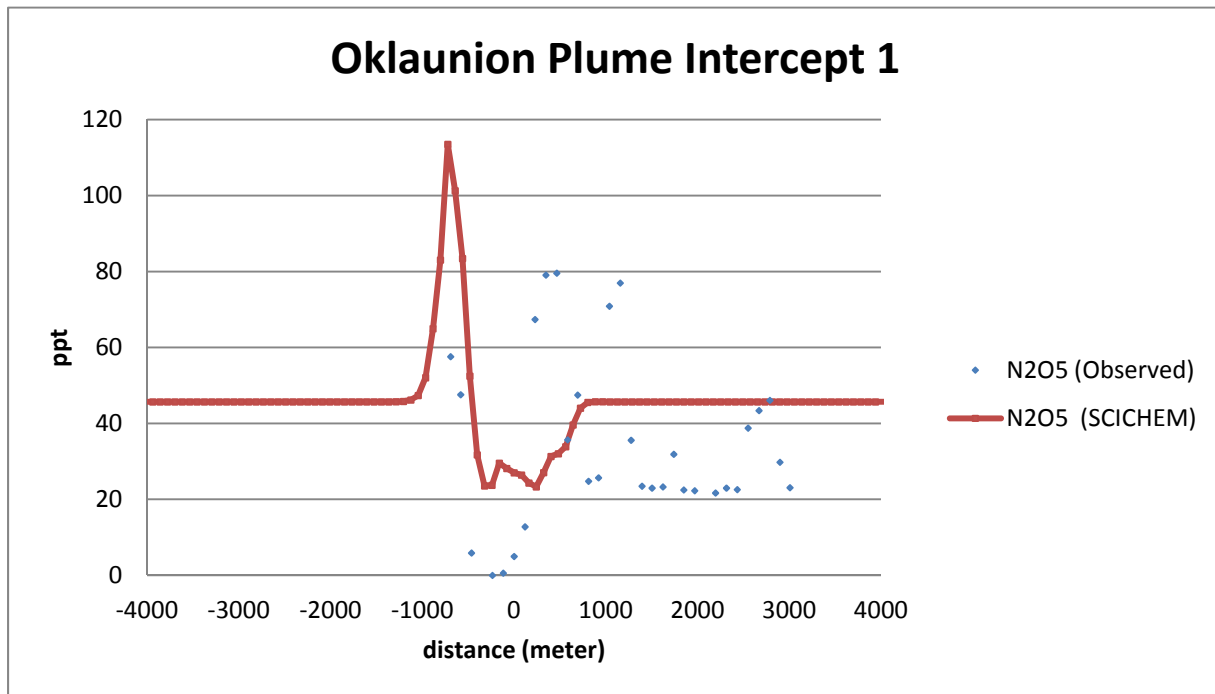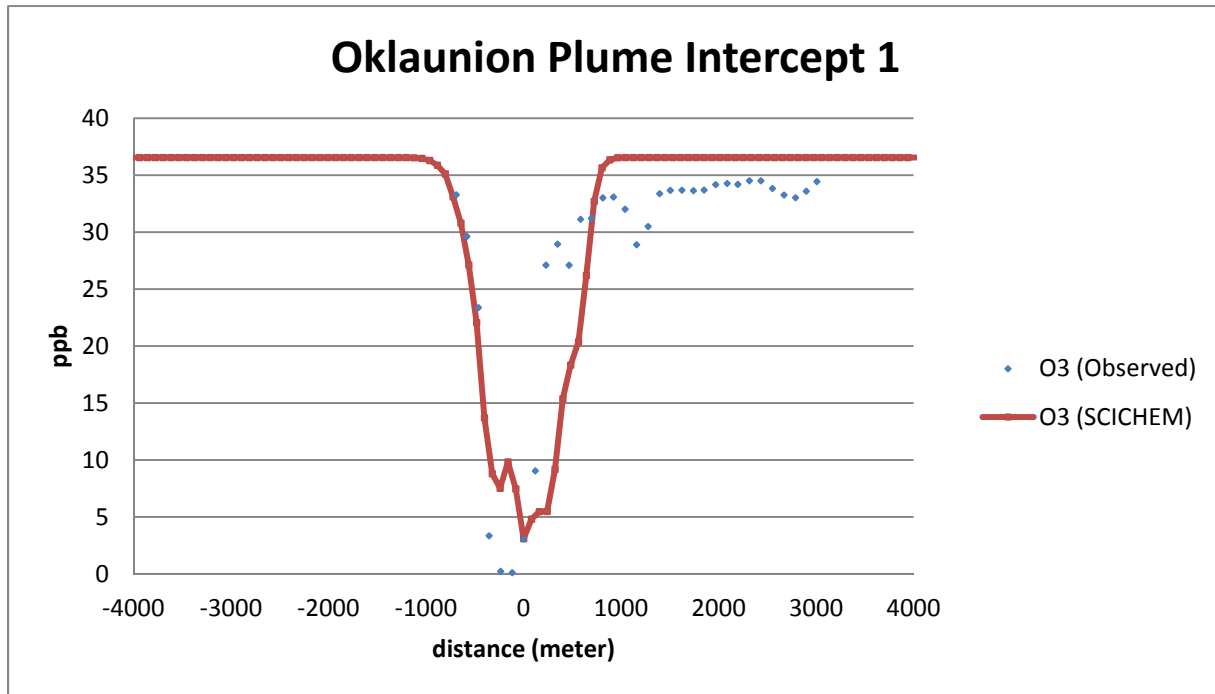
Figure 4-3c.   Observed and simulated (SCICHEM) cross-wind plume concentrations of O_3 and N_2O_5 for plume intercept 1 at 18 km downwind of the Oklaunion power plant on October 10, 2006. SCICHEM results are based on aircraft-observed meteorology.
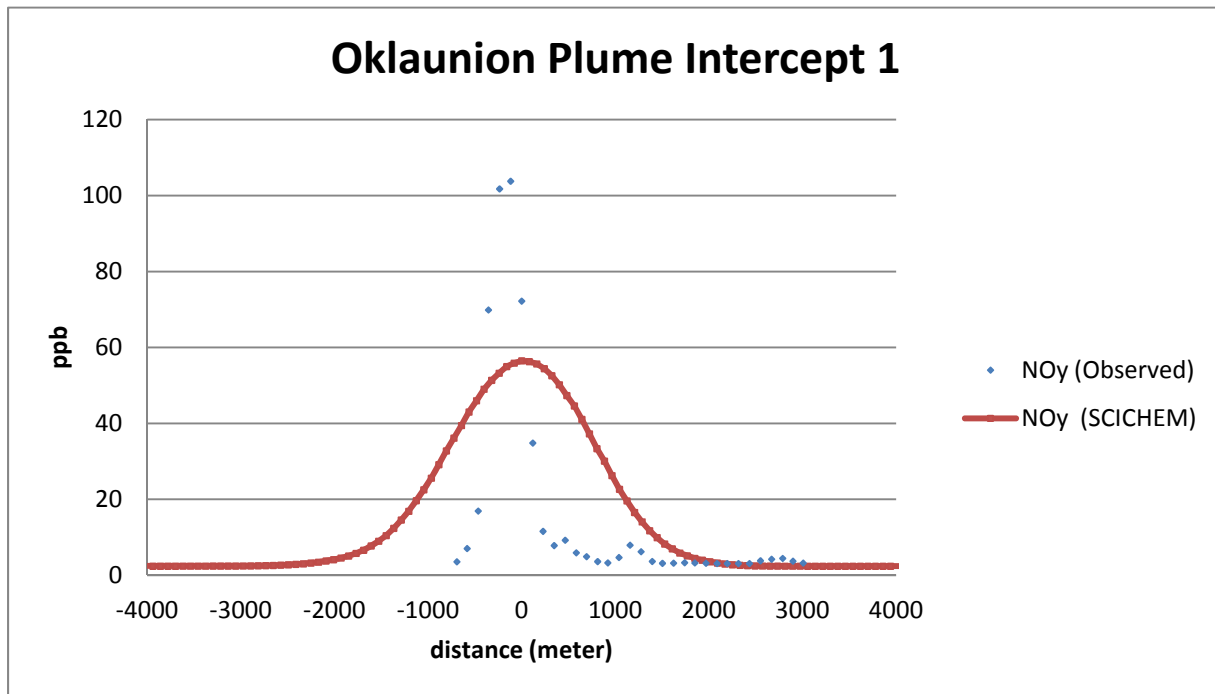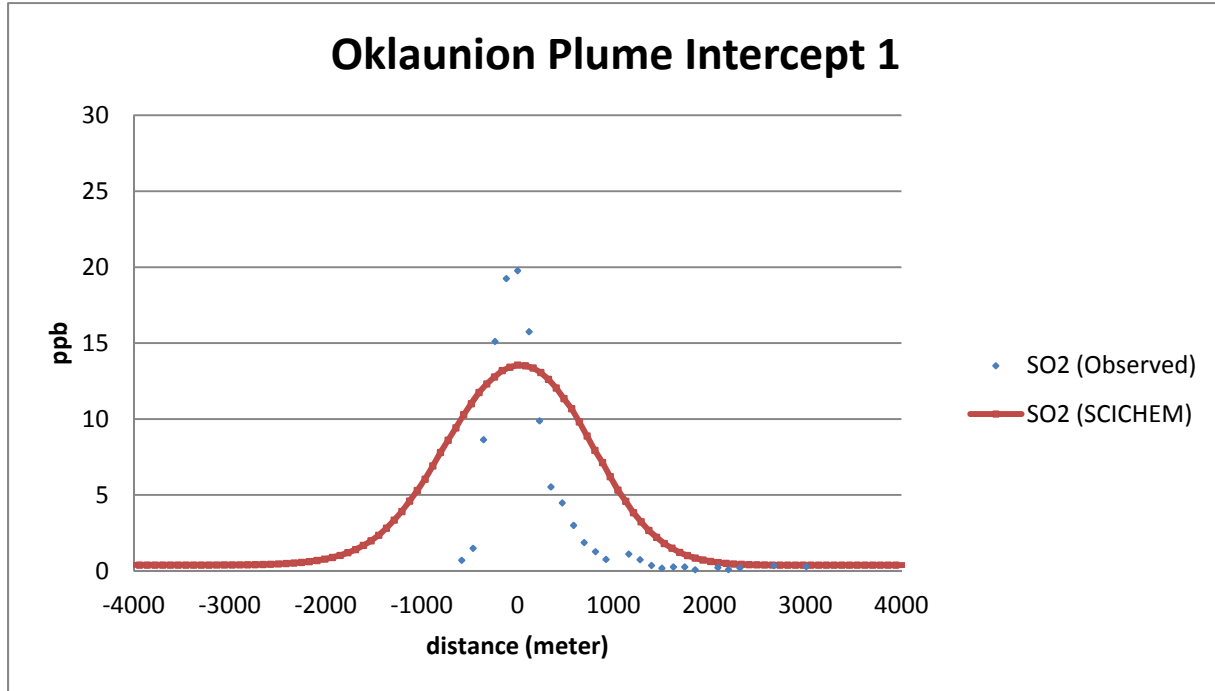
Figure 4-4a.   **Observed and simulated (SCICHEM) cross-wind plume concentrations of SO$_2$ and NO$_y$ for plume intercept 1 at 18 km downwind of the Oklaunion power plant on October 10, 2006. SCICHEM results are based on MM5 meteorology processed with MMIF.**
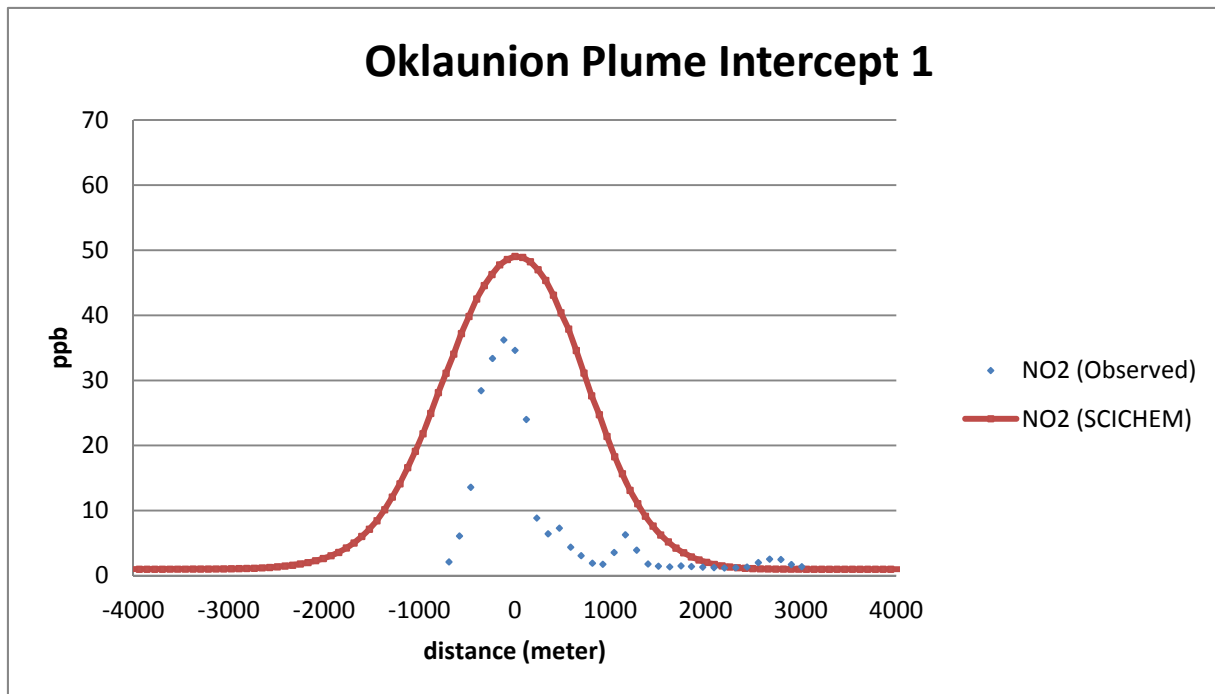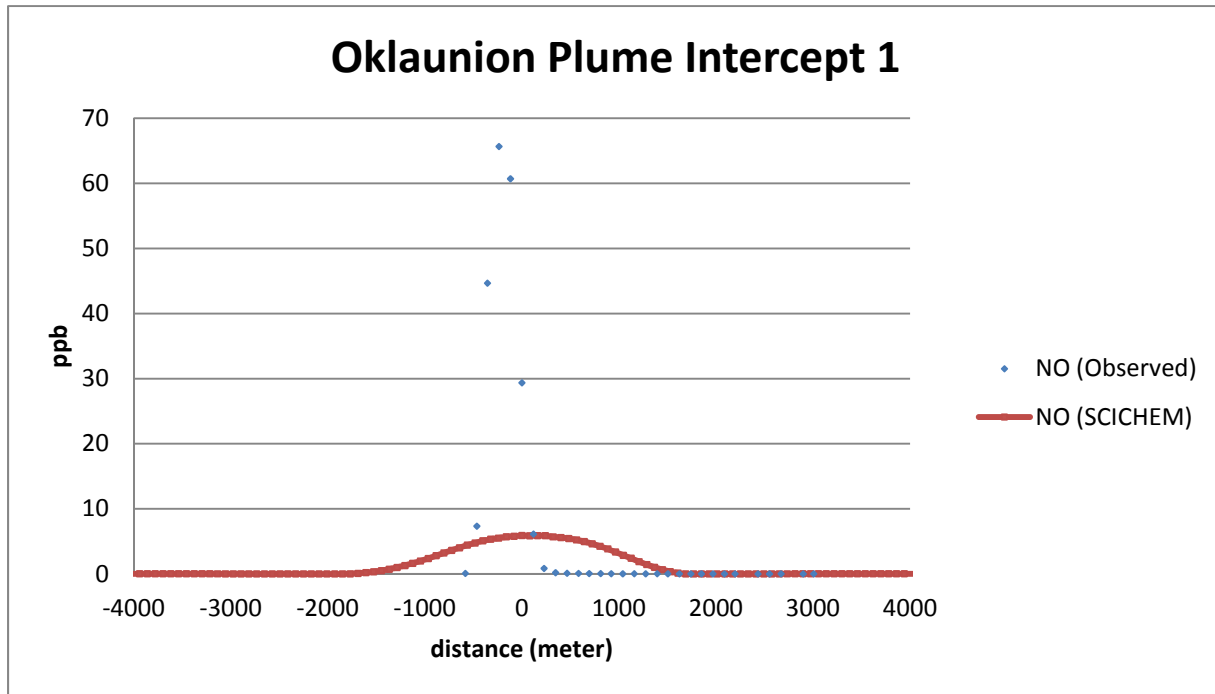
Figure 4-4b.   Observed and simulated (SCICHEM) cross-wind plume concentrations of NO and NO$_2$ for plume intercept 1 at 18 km downwind of the Oklaunion power plant on October 10, 2006. SCICHEM results are based on MM5 meteorology processed with MMIF.
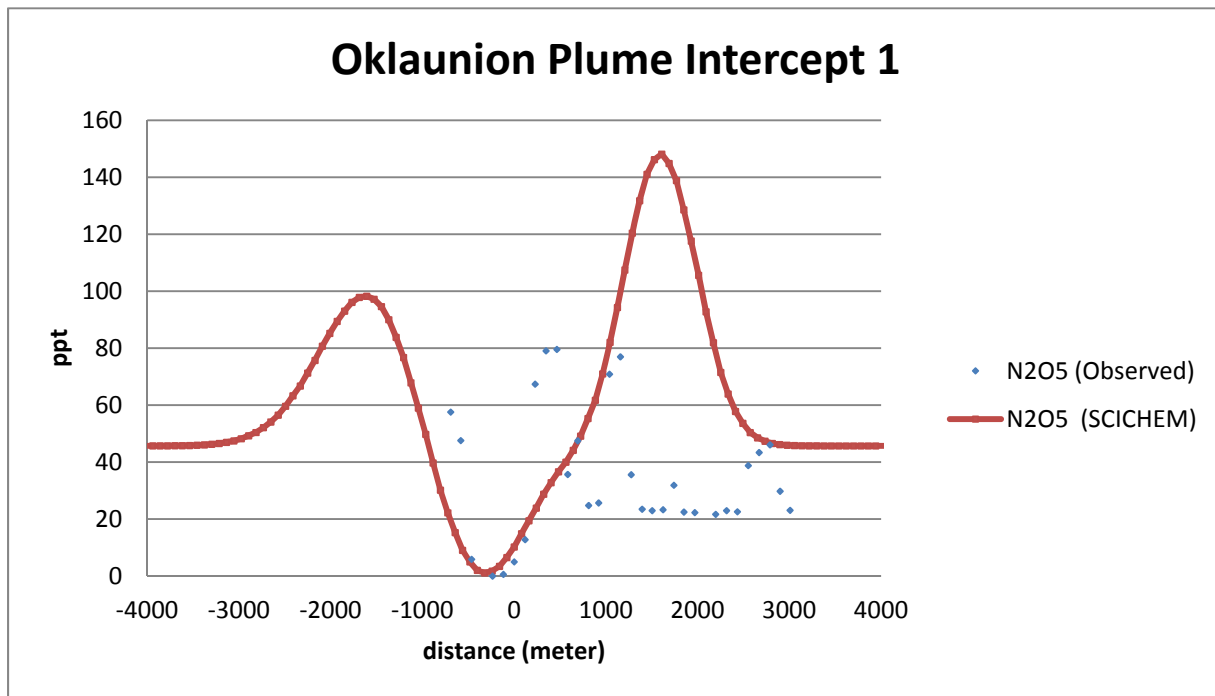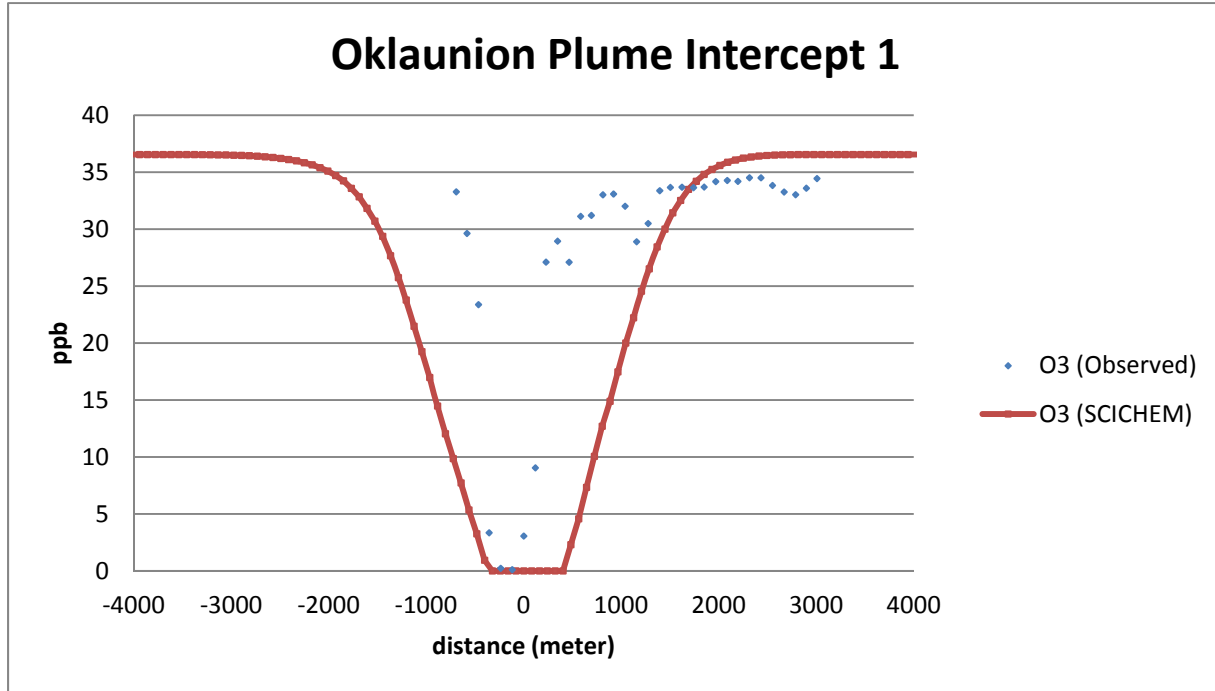
Figure 4-4c. Observed and simulated (SCICHEM) cross-wind plume concentrations of O_3 and N_2O_5 for plume intercept 1 at 18 km downwind of the Oklaunion power plant on October 10, 2006. SCICHEM results are based on MM5 meteorology processed with MMIF.
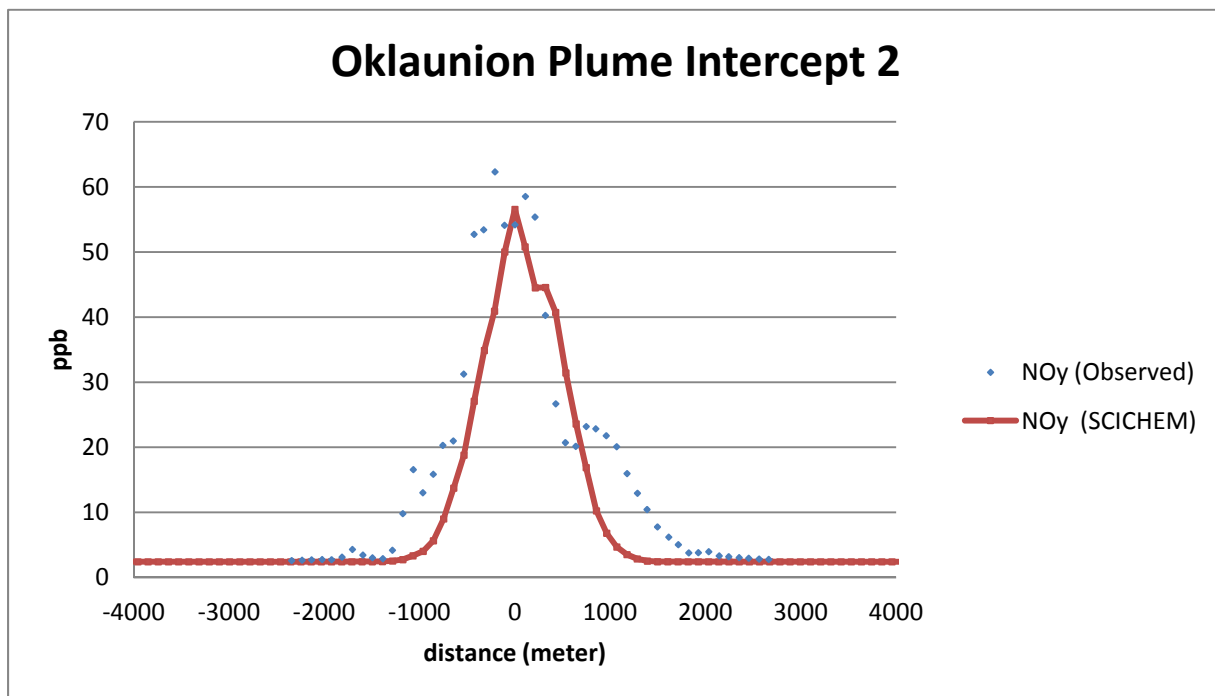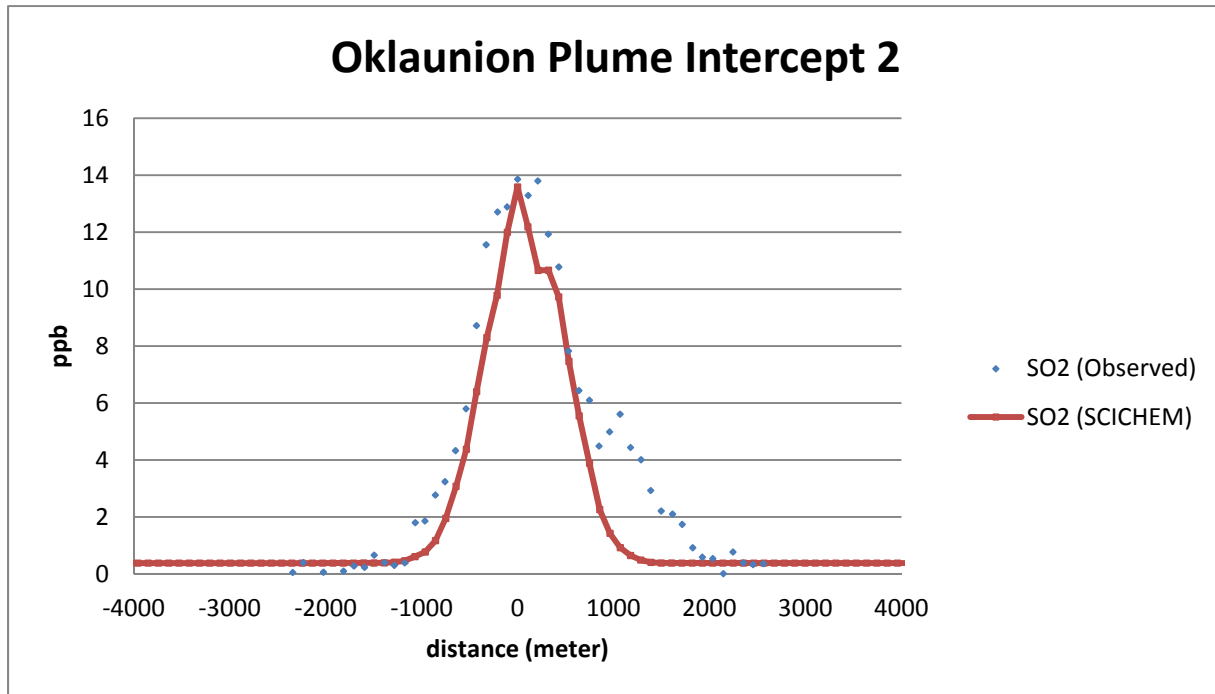
Figure 4-5a. Observed and simulated (SCICHEM) cross-wind plume concentrations of SO$_2$ and NO$_y$ for plume intercept 2 at 25 km downwind of the Oklaunion power plant on October 10, 2006. SCICHEM results are based on aircraft-observed meteorology.
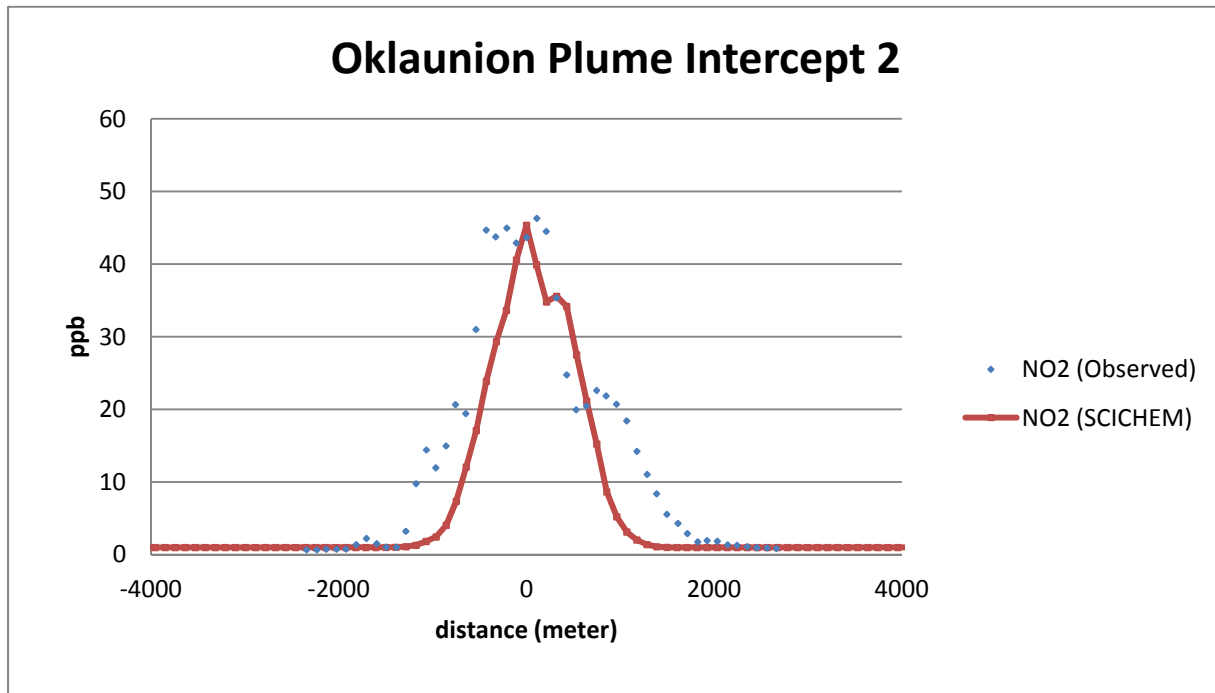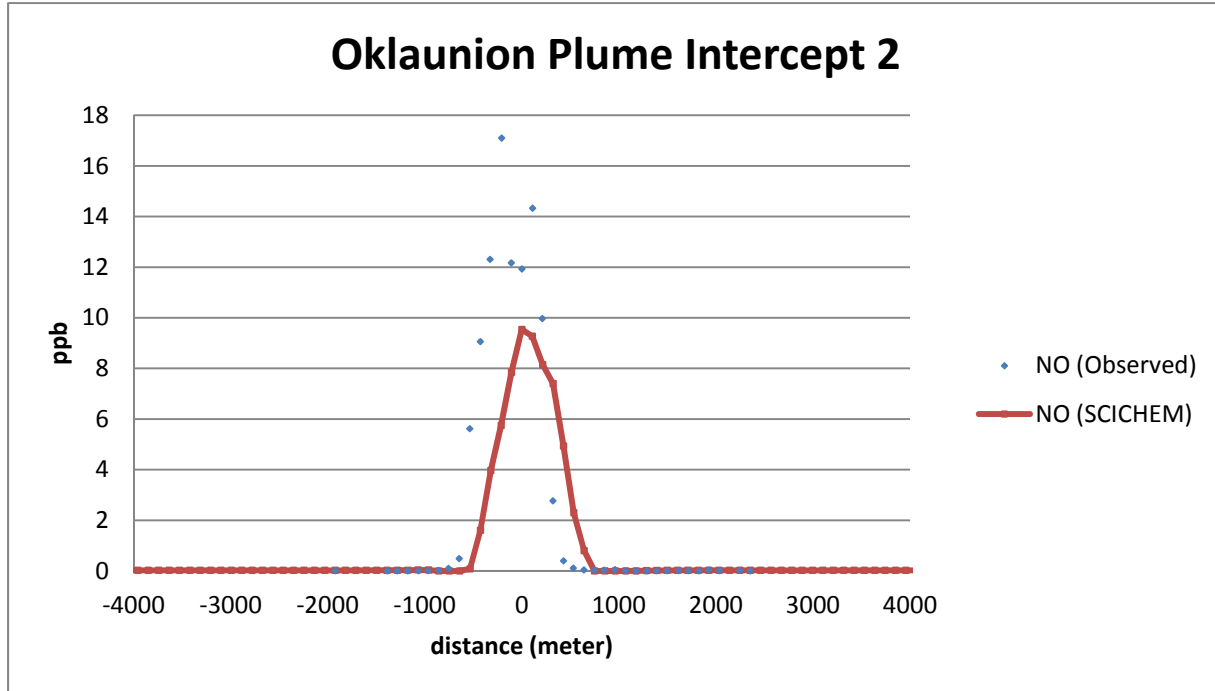
Figure 4-5b.   Observed and simulated (SCICHEM) cross-wind plume concentrations of NO and NO$_2$ for plume intercept 2 at 25 km downwind of the Oklaunion power plant on October 10, 2006. SCICHEM results are based on aircraft-observed meteorology.
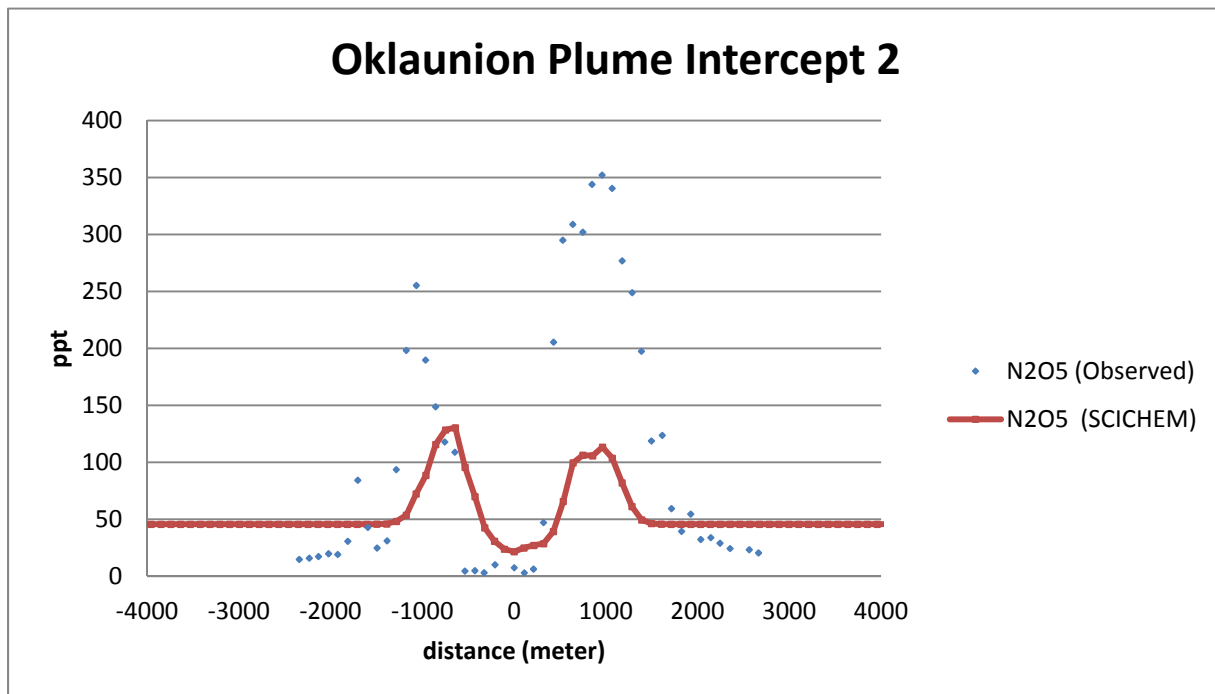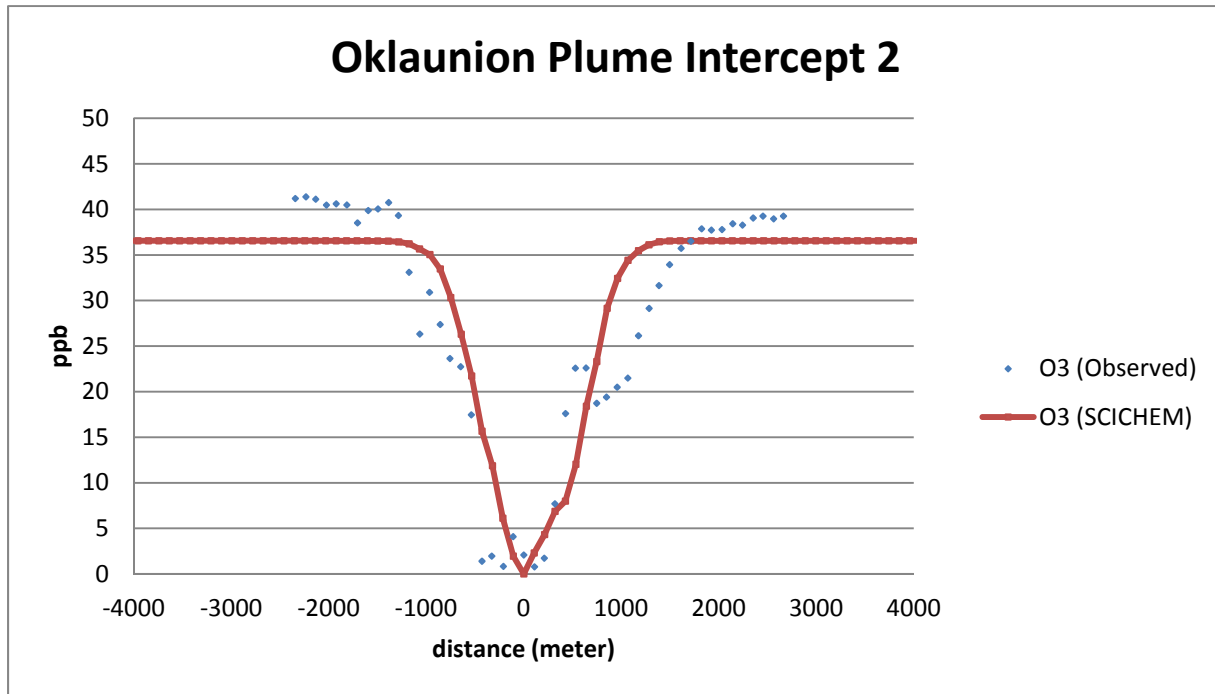
Figure 4-5c. Observed and simulated (SCICHEM) cross-wind plume concentrations of O_3 and N_2O_5 for plume intercept 2 at 25 km downwind of the Oklaunion power plant on October 10, 2006. SCICHEM results are based on aircraft-observed meteorology.
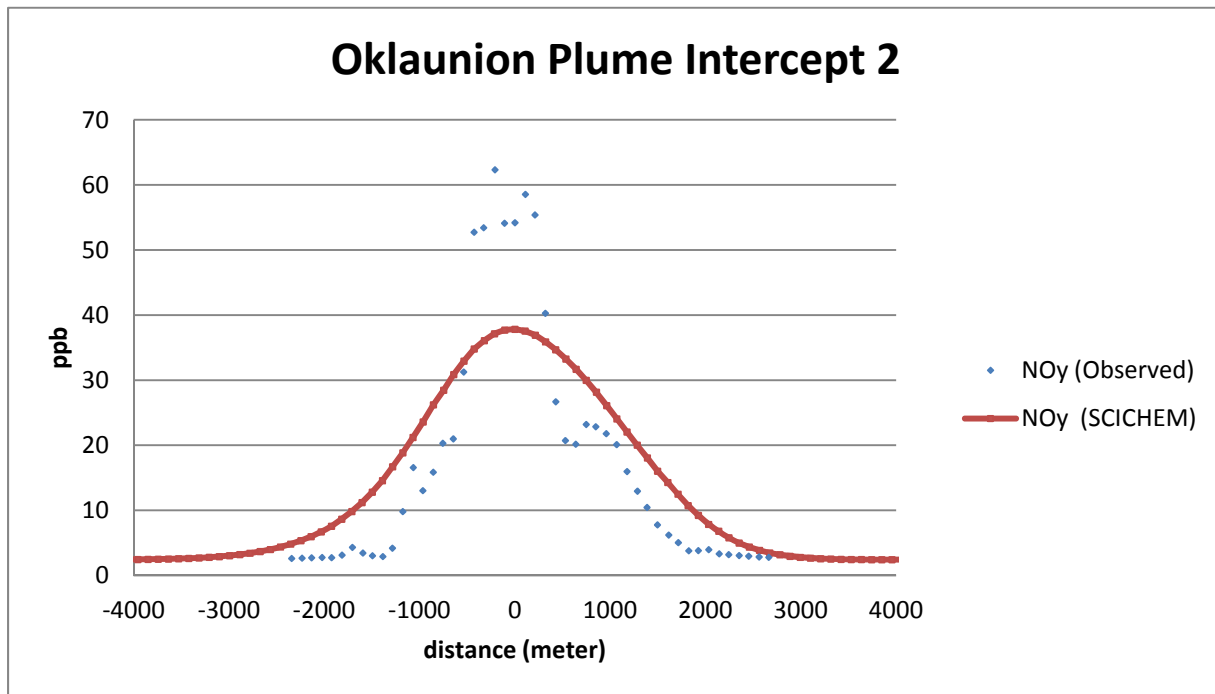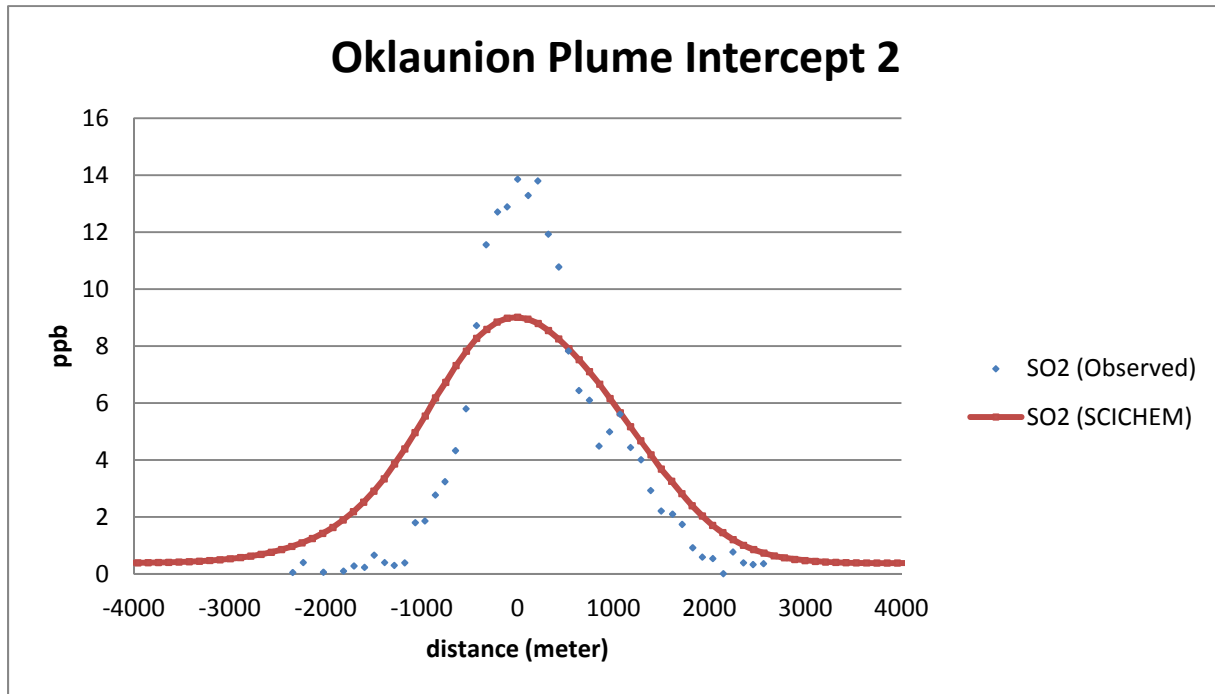
Figure 4-6a.   Observed and simulated (SCICHEM) cross-wind plume concentrations of SO₂ and NOᵧ for plume intercept 2 at 25 km downwind of the Oklaunion power plant on October 10, 2006. SCICHEM results are based on MM5 meteorology processed with MMIF.
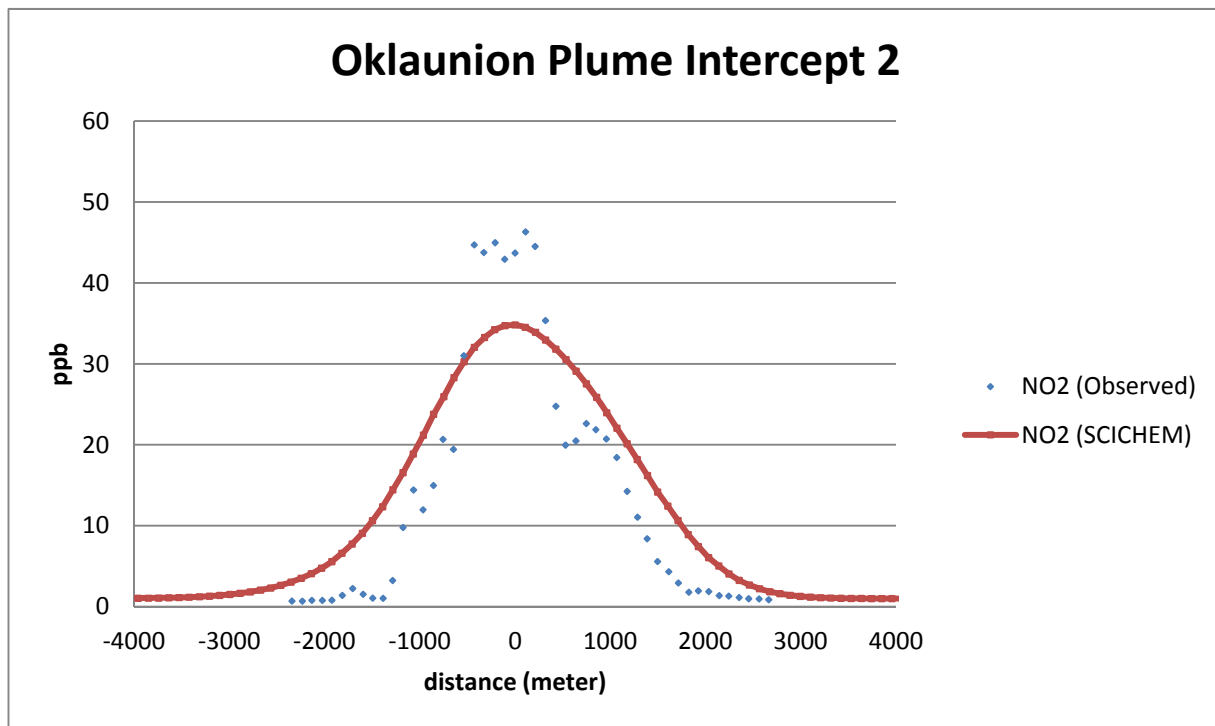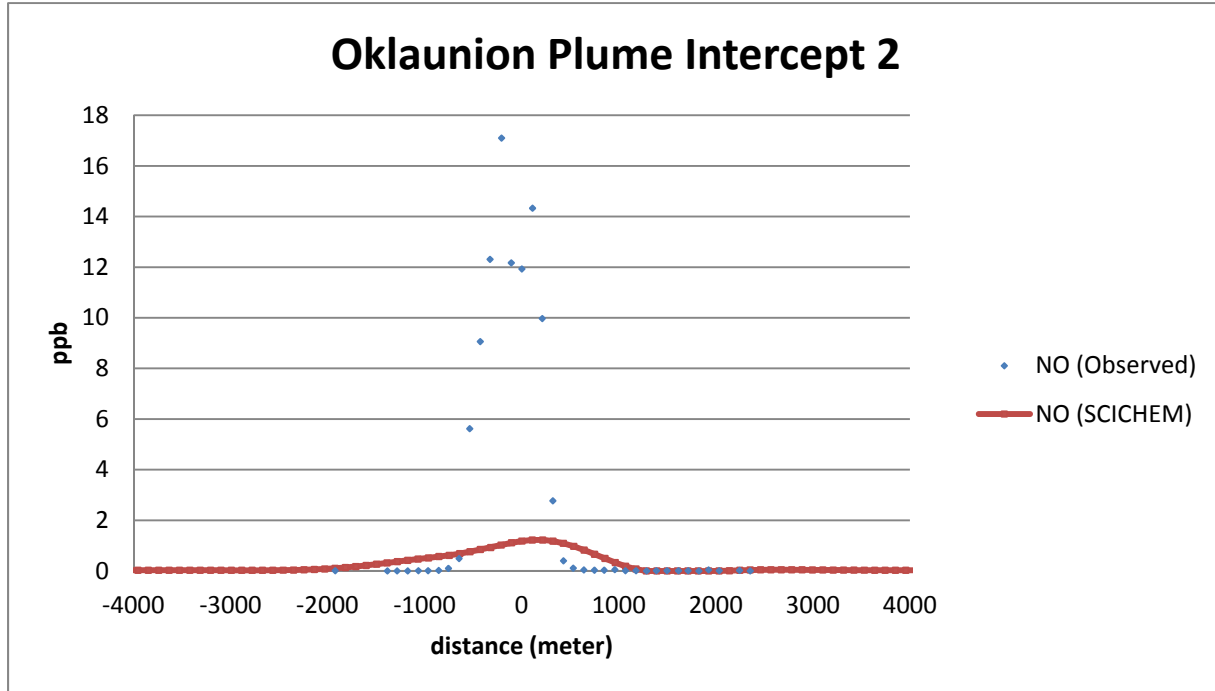
Figure 4-6b.   Observed and simulated (SCICHEM) cross-wind plume concentrations of NO and NO$_2$ for plume intercept 2 at 25 km downwind of the Oklaunion power plant on October 10, 2006. SCICHEM results are based on MM5 meteorology processed with MMIF.
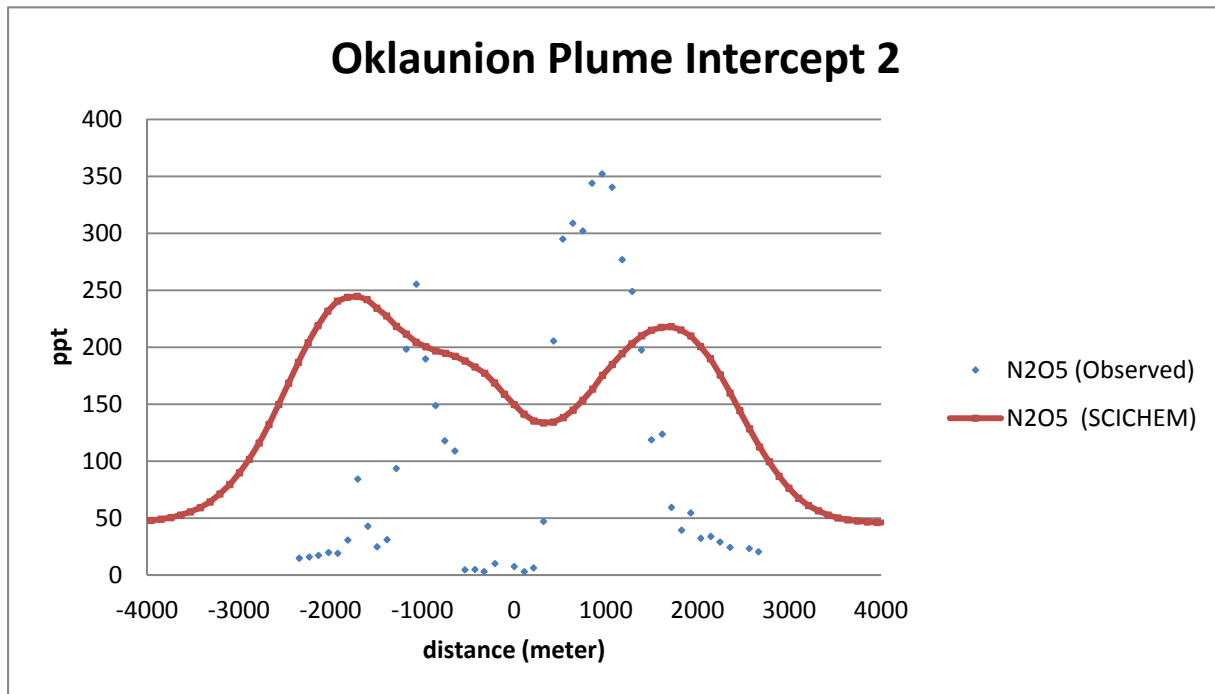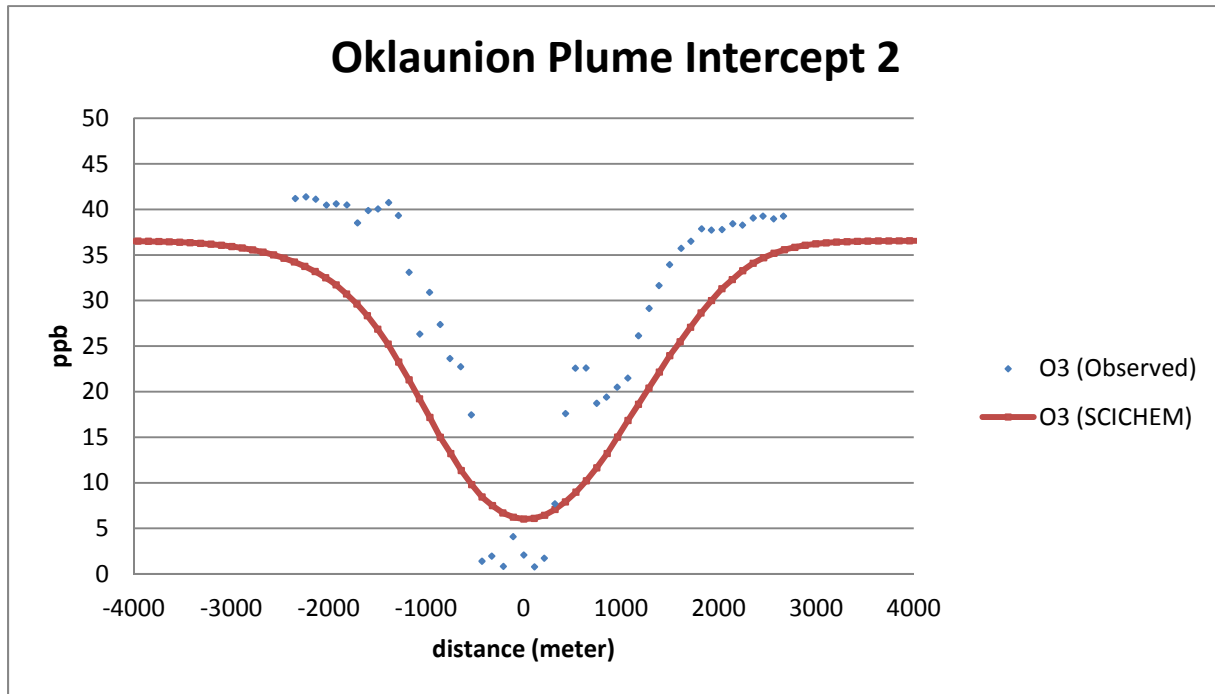
Figure 4-6c. Observed and simulated (SCICHEM) cross-wind plume concentrations of O_3 and N_2O_5 for plume intercept 2 at 25 km downwind of the Oklaunion power plant on October 10, 2006. SCICHEM results are based on MM5 meteorology processed with MMIF.

The results for plume intercept 14 (downwind distance of 30 km) are shown in Figure 4-7 for the case when SCICHEM is run with observed aircraft meteorology. While the measured and modeled SO_2, NO_y and O_3 concentrations along the plume traverse are in fairly good agreement, we note that the model significantly over-predicts the conversion of NO to NO_2 in the plume. Some of this over-prediction appears to be due to the lower observed background O_3 concentration for transect 14 (about 25 ppb) as compared to the fixed average value used in the simulation (about 36 ppb). Peak measured and modeled N_2O_5 production rates at the plume edges are similar, with the model producing 80 ppt of total N_2O_5, versus 65 ppt in the measurements. The corresponding results when SCICHEM is run with MM5 meteorology, shown in Figure 4-8, deviate significantly from the plume measurements.

Figure 4-9 shows the SCICHEM results with aircraft meteorology for plume intercept 15, at a very large downwind distance (nearly 58 km) from Oklaunion, compared to the other intercepts discussed above. The measurements show a fairly narrow and concentrated plume (a little more than 1 km wide), even at this large downwind distance. The model, however, predicts a plume that is over 3 km wide and quite dilute. Thus, there are large differences in the observed and modeled concentrations for all species, with lower modeled peak concentrations of conserved or nearly conserved species (SO_2 and NO_y). The most dramatic differences are for the NO and the N_2O_5 concentrations: in the modeled dilute plume, the modeled peak N_2O_5 concentration is about 500 ppt at plume centerline, and tapers down to background values at the plume edges; in the measured plume, there is a reduction in N_2O_5 concentrations at the plume centerline, and N_2O_5 peaks at the plume edges of about 250 ppt. This difference is consistent with the differences in NO concentrations, with negligible NO concentrations throughout the modeled plume, but peak measured NO concentrations of 40 ppb at the plume centerline. When MMIF-processed 12 km MM5 meteorology is used as input to SCICHEM, the results degrade further, as shown in Figure 4-10.
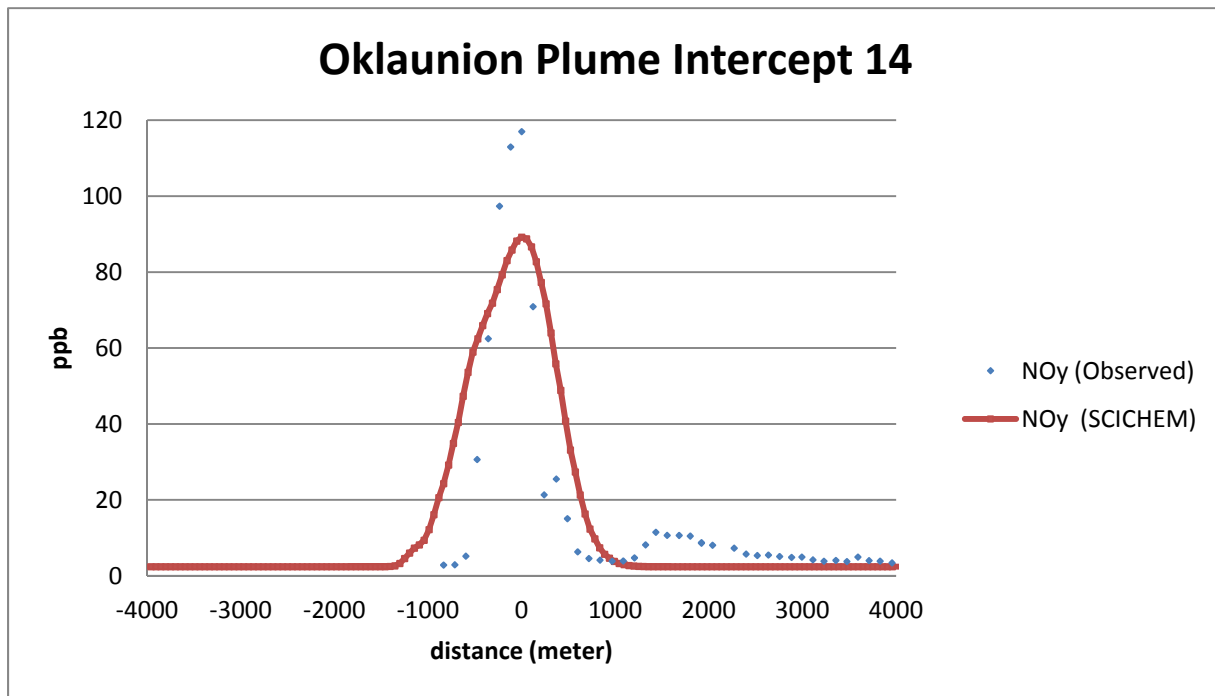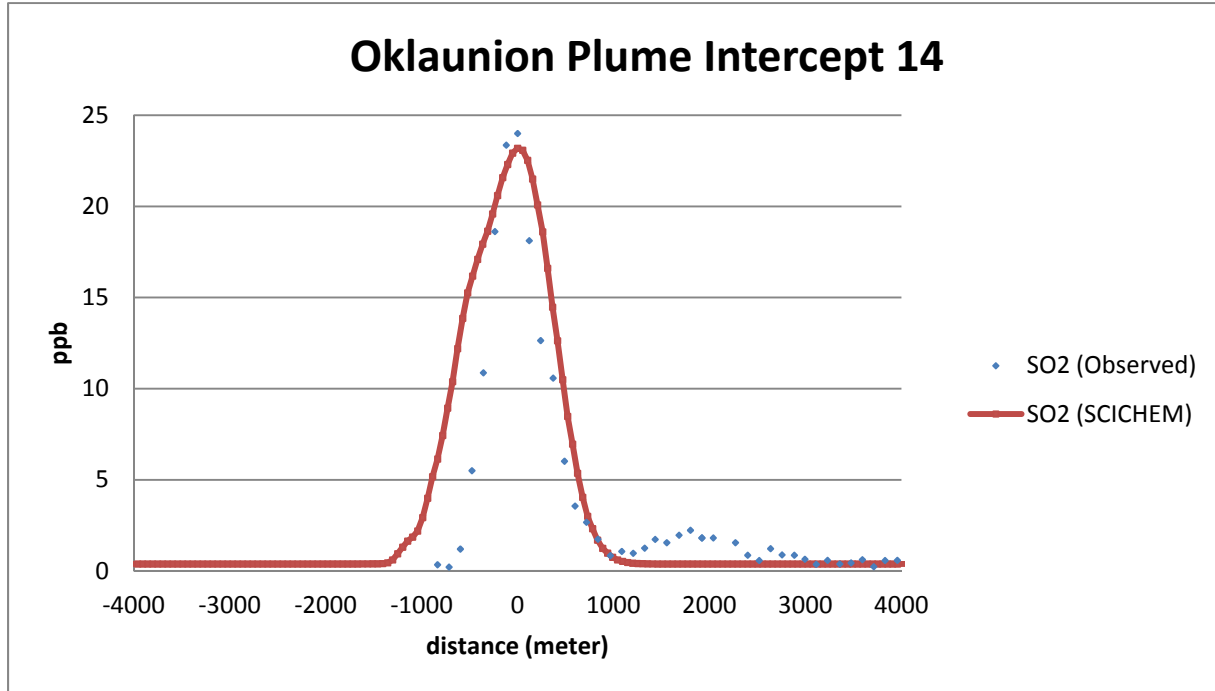
Figure 4-7a.   Observed and simulated (SCICHEM) cross-wind plume concentrations of SO_2 and NO_y for plume intercept 14 at 30 km downwind of the Oklaunion power plant on October 10, 2006. SCICHEM results are based on aircraft-observed meteorology.

Oklaunion Plume Intercept 14

Oklaunion Plume Intercept 14
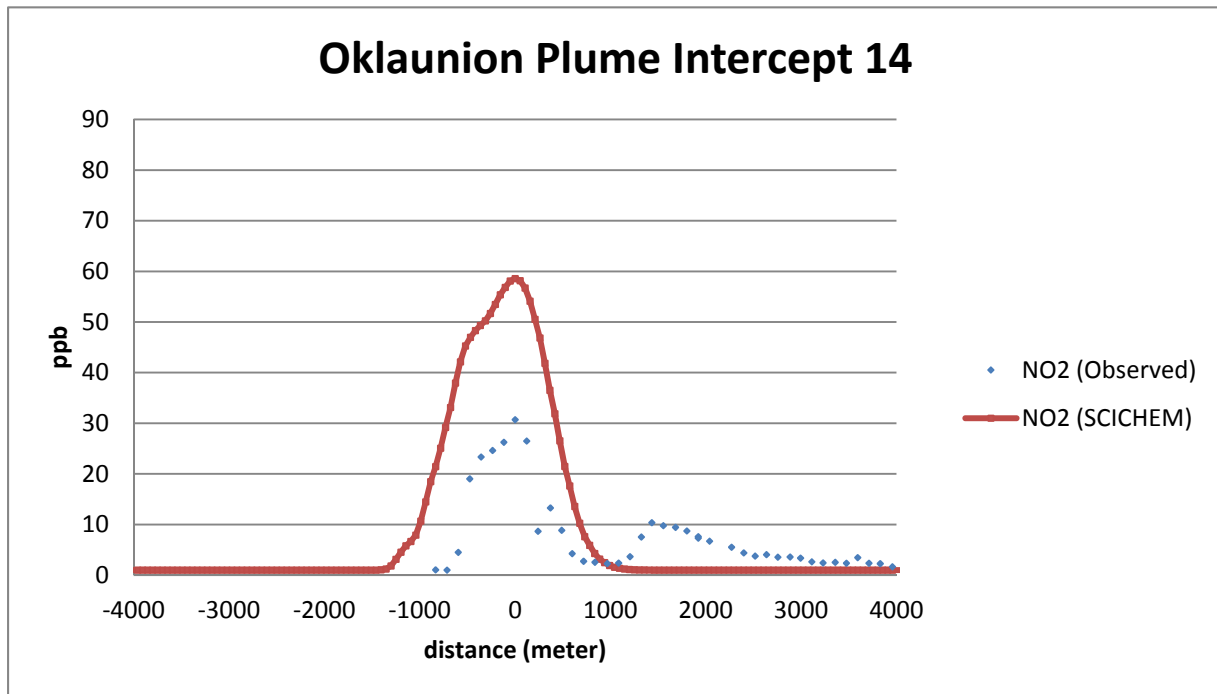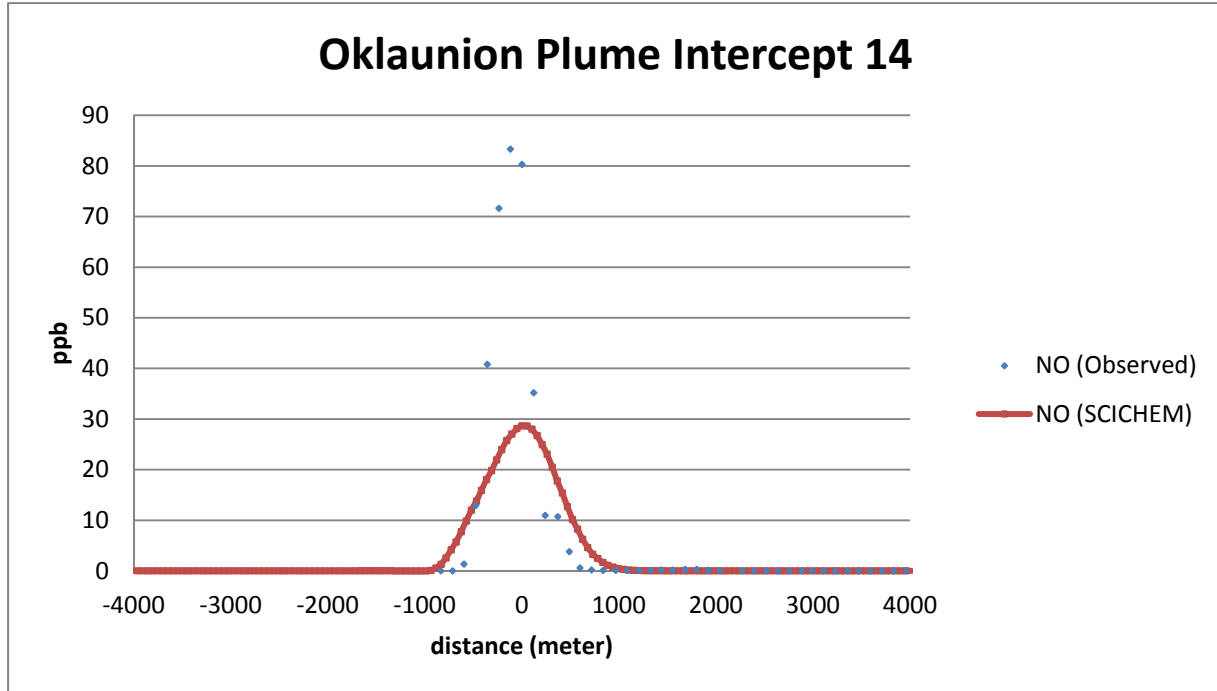
Figure 4-7b.   Observed and simulated (SCICHEM) cross-wind plume concentrations of NO and NO$_2$ for plume intercept 14 at 30 km downwind of the Oklaunion power plant on October 10, 2006. SCICHEM results are based on aircraft-observed meteorology.
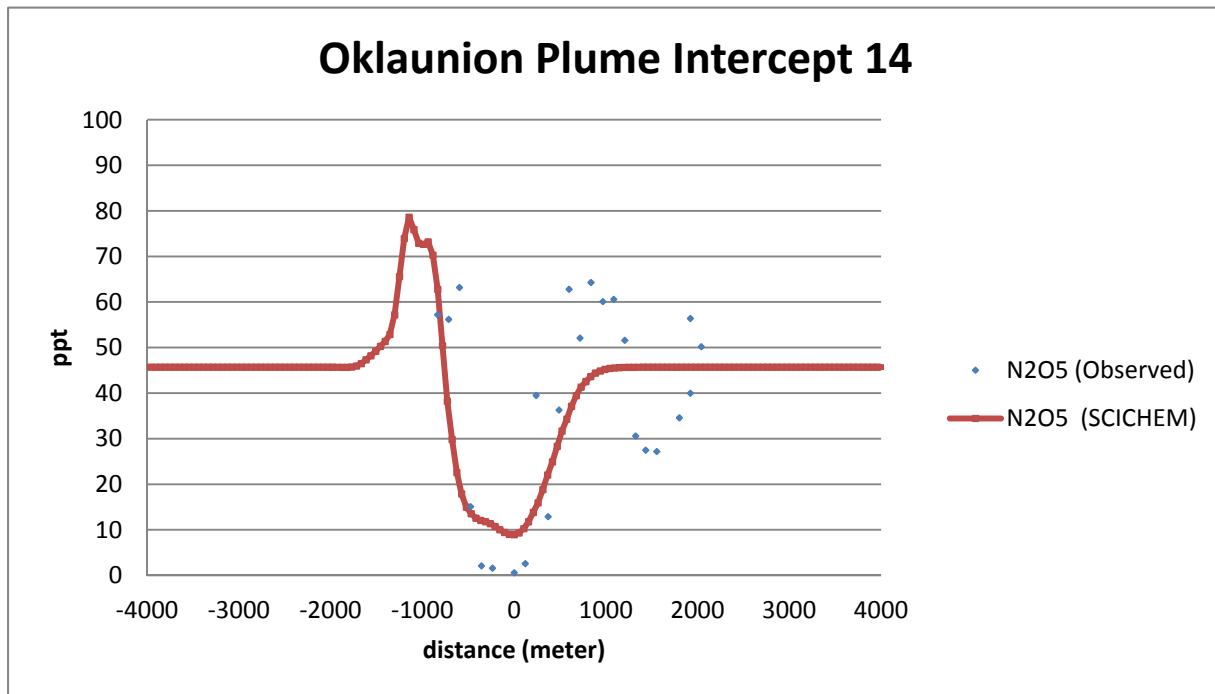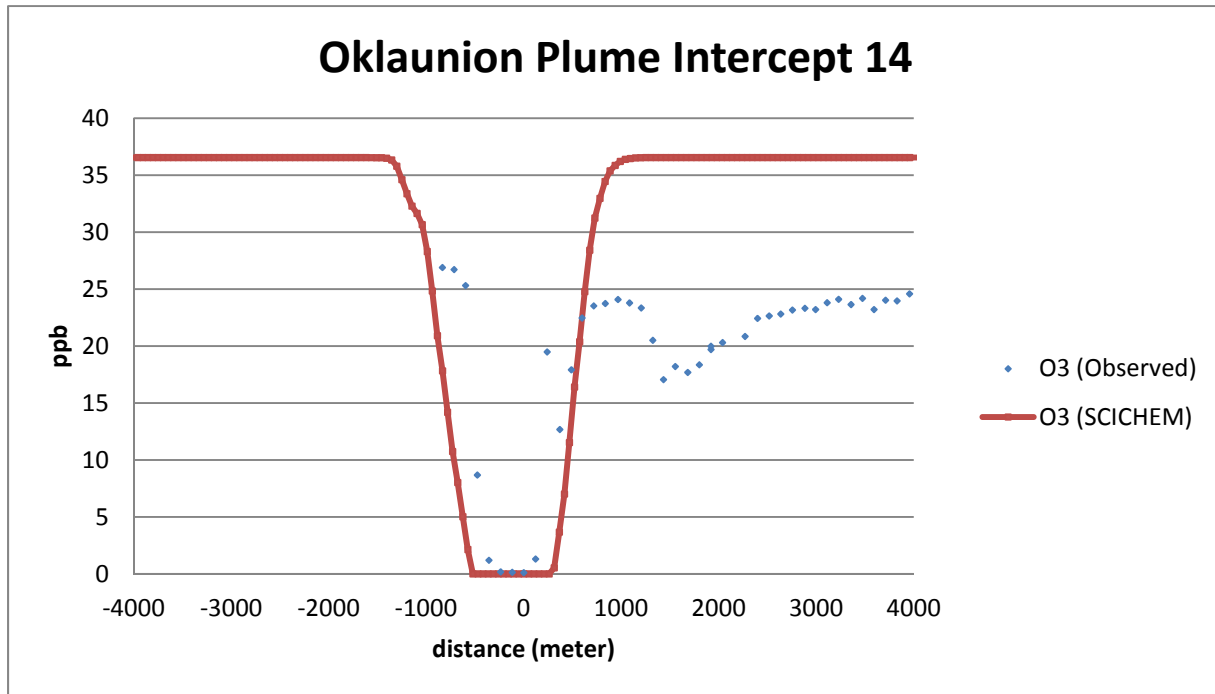
Figure 4-7c.   **Observed and simulated (SCICHEM) cross-wind plume concentrations of O_3 and N_2O_5 for plume intercept 14 at 30 km downwind of the Oklaunion power plant on October 10, 2006. SCICHEM results are based on aircraft-observed meteorology.**
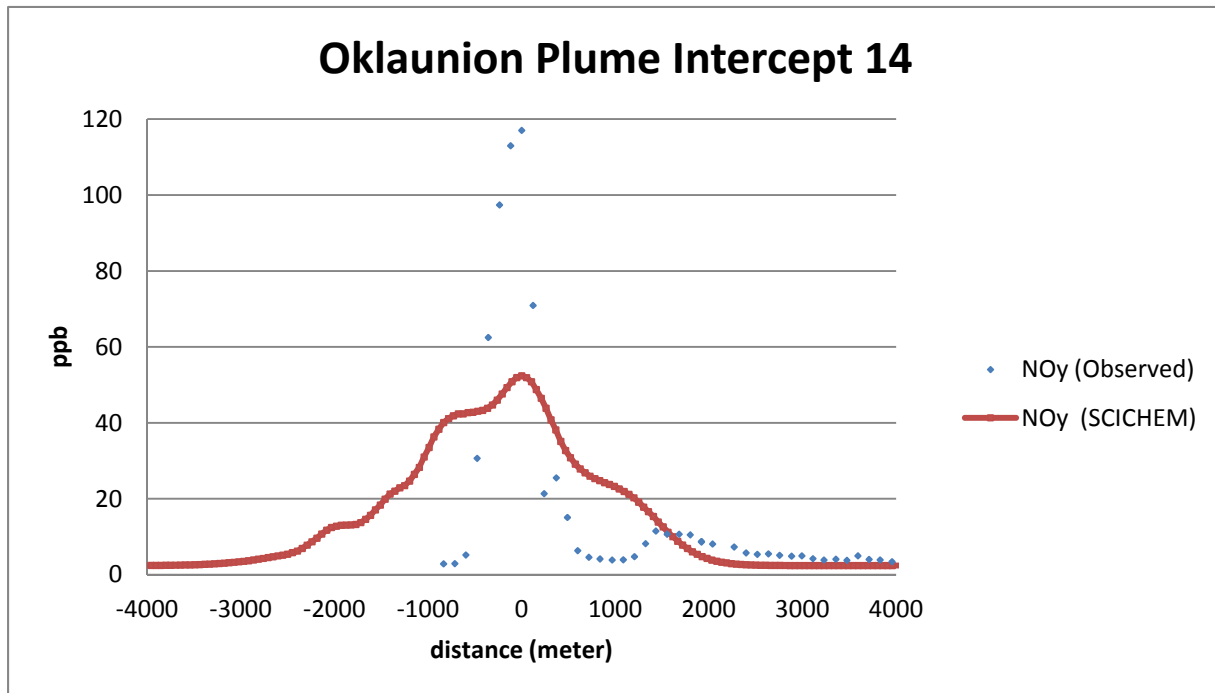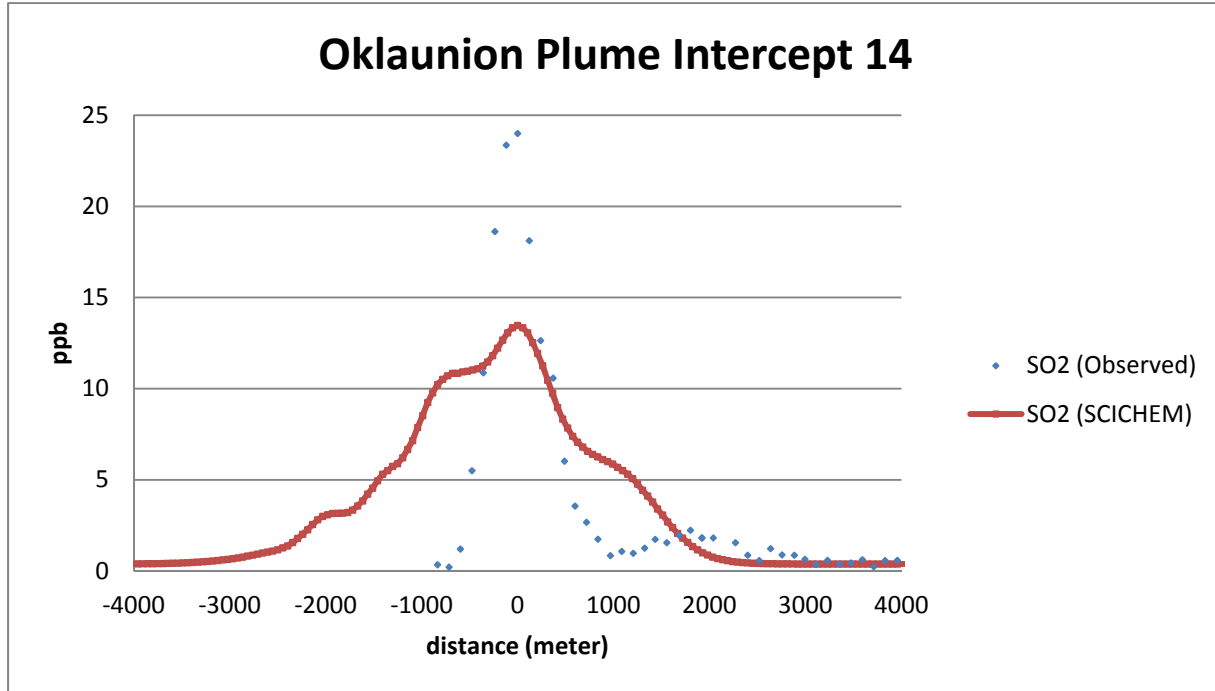
Figure 4-8a. **Observed and simulated (SCICHEM) cross-wind plume concentrations of SO$_2$ and NO$_y$ for plume intercept 14 at 30 km downwind of the Oklaunion power plant on October 10, 2006. SCICHEM results are based on MM5 meteorology processed with MMIF.**
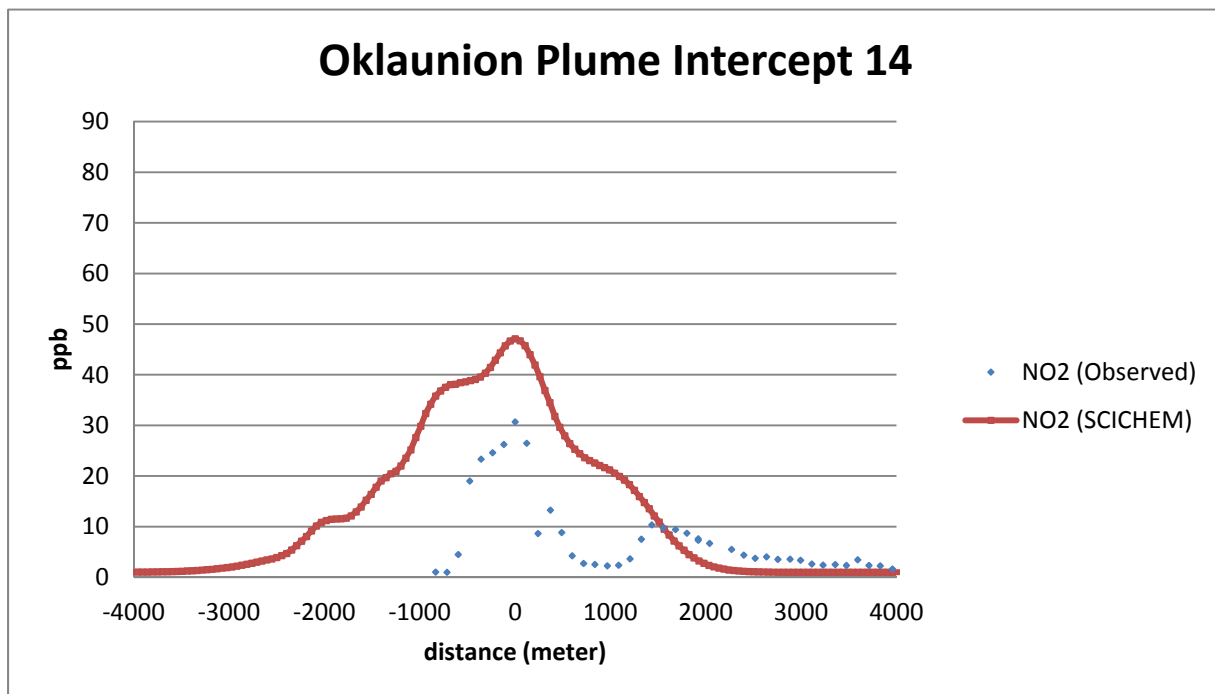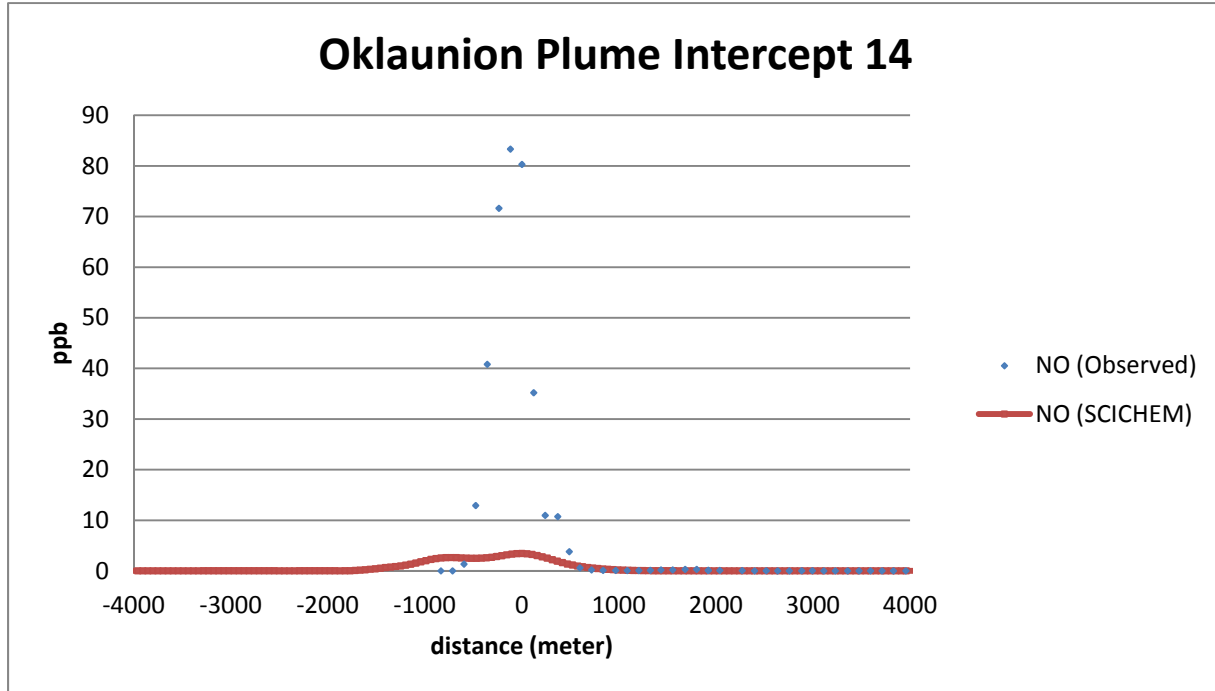
Figure 4-8b. **Observed and simulated (SCICHEM) cross-wind plume concentrations of NO and NO$_2$ for plume intercept 14 at 30 km downwind of the Oklaunion power plant on October 10, 2006. SCICHEM results are based on MM5 meteorology processed with MMIF.**

Oklaunion Plume Intercept 14

Oklaunion Plume Intercept 14
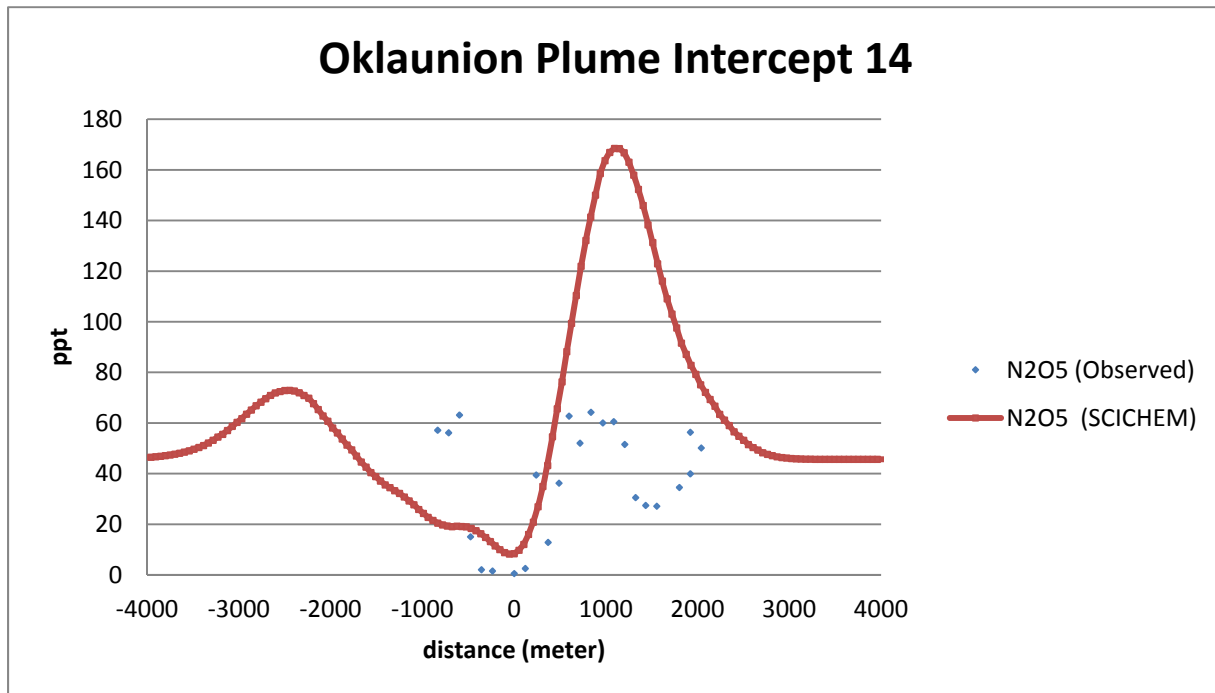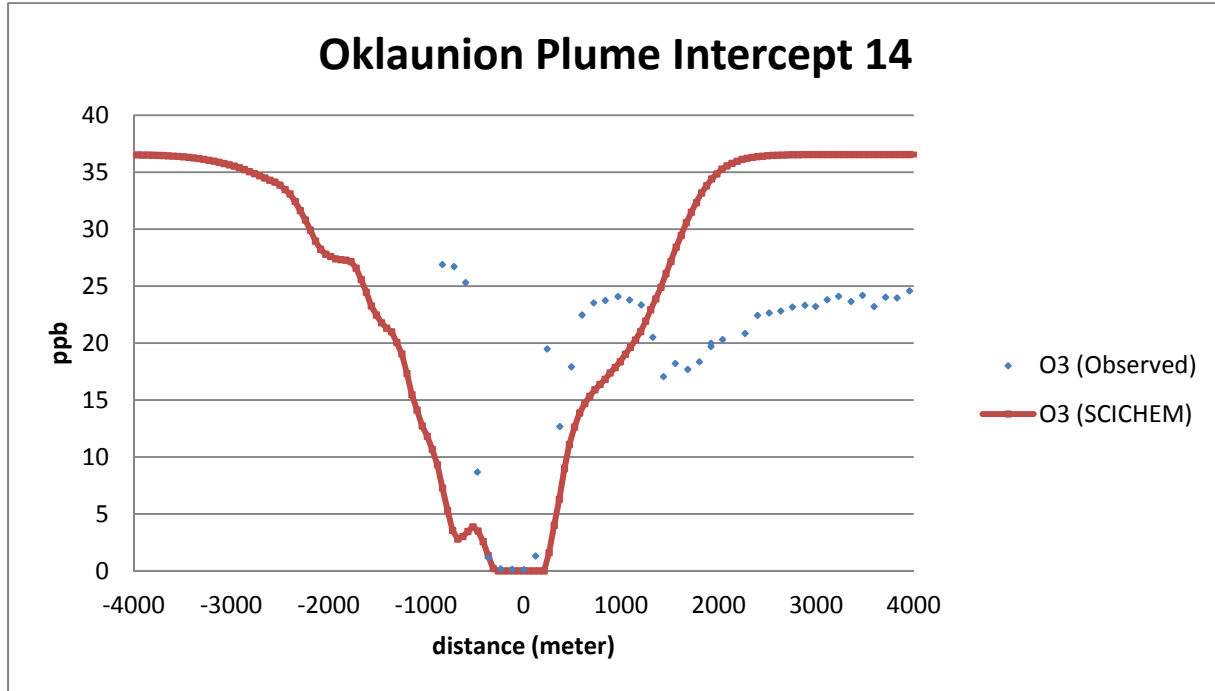
Figure 4-8c.   Observed and simulated (SCICHEM) cross-wind plume concentrations of O_3 and N_2O_5 for plume intercept 14 at 30 km downwind of the Oklaunion power plant on October 10, 2006. SCICHEM results are based on MM5 meteorology processed with MMIF.
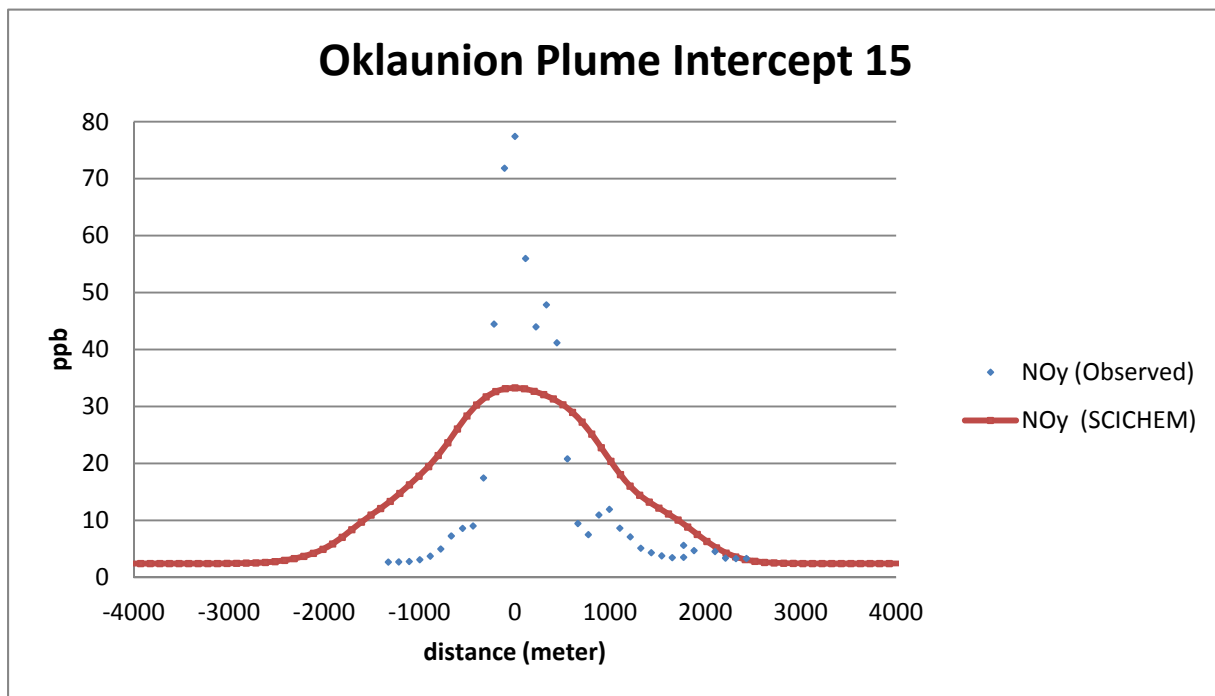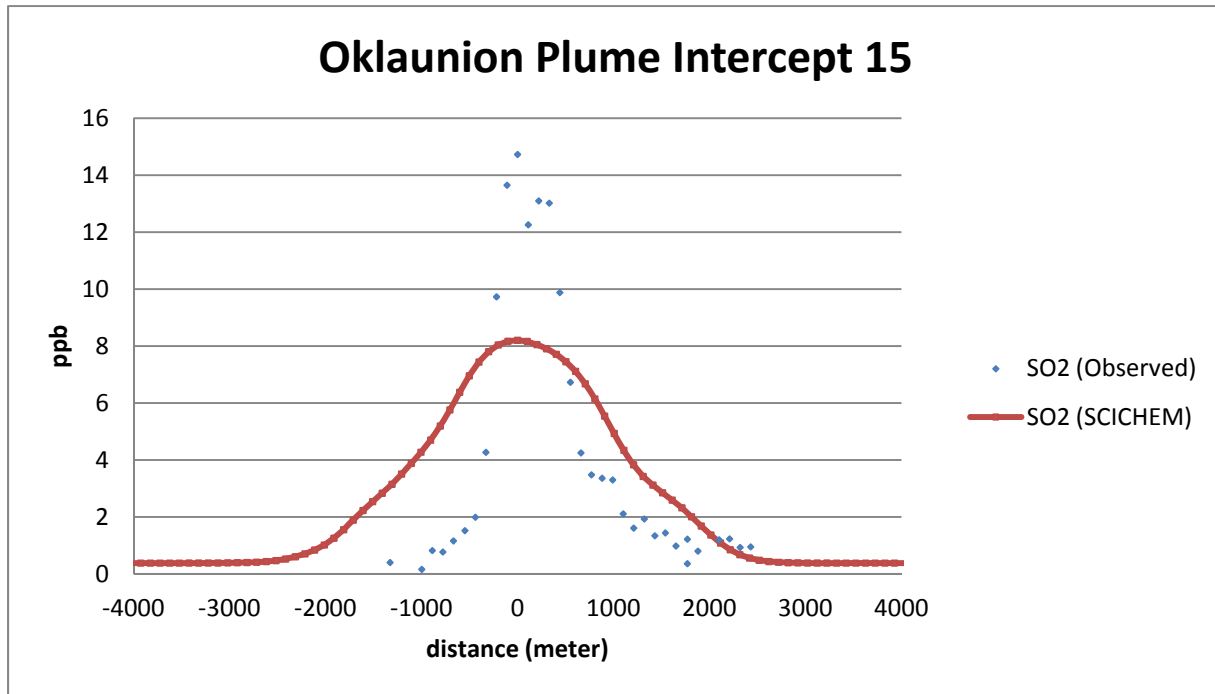
Figure 4-9a. **Observed and simulated (SCICHEM) cross-wind plume concentrations of SO$_2$ and NO$_y$ for plume intercept 15 at 58 km downwind of the Oklaunion power plant on October 10, 2006. SCICHEM results are based on aircraft-observed meteorology.**
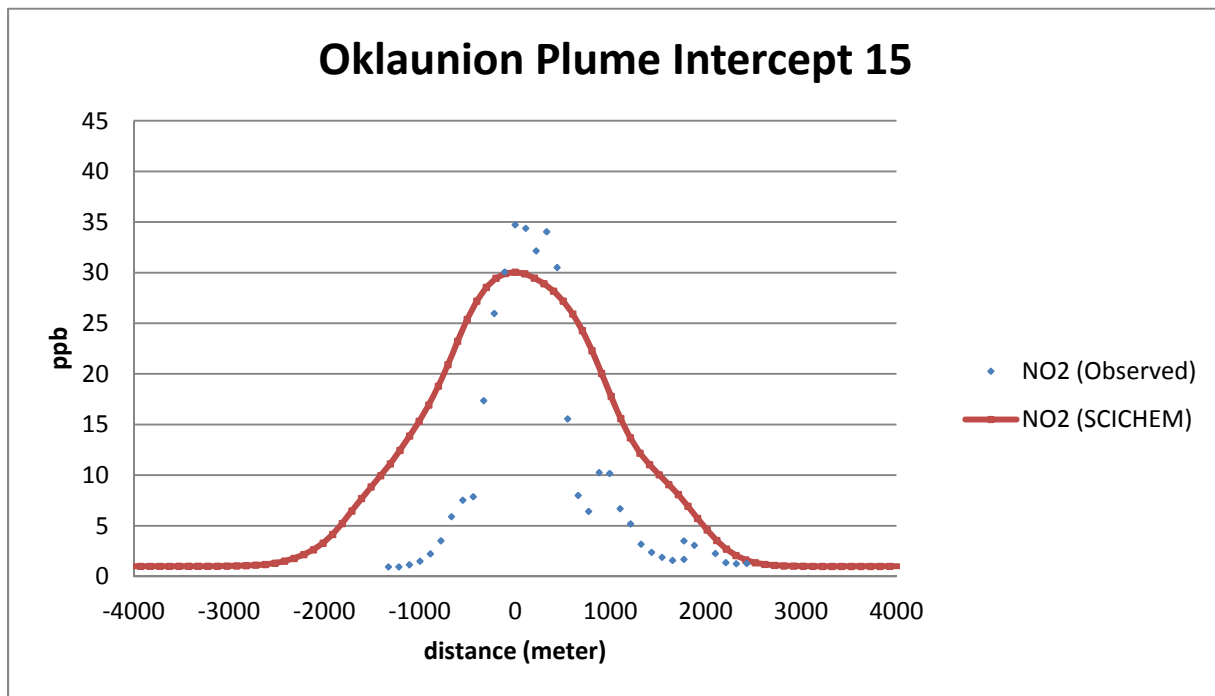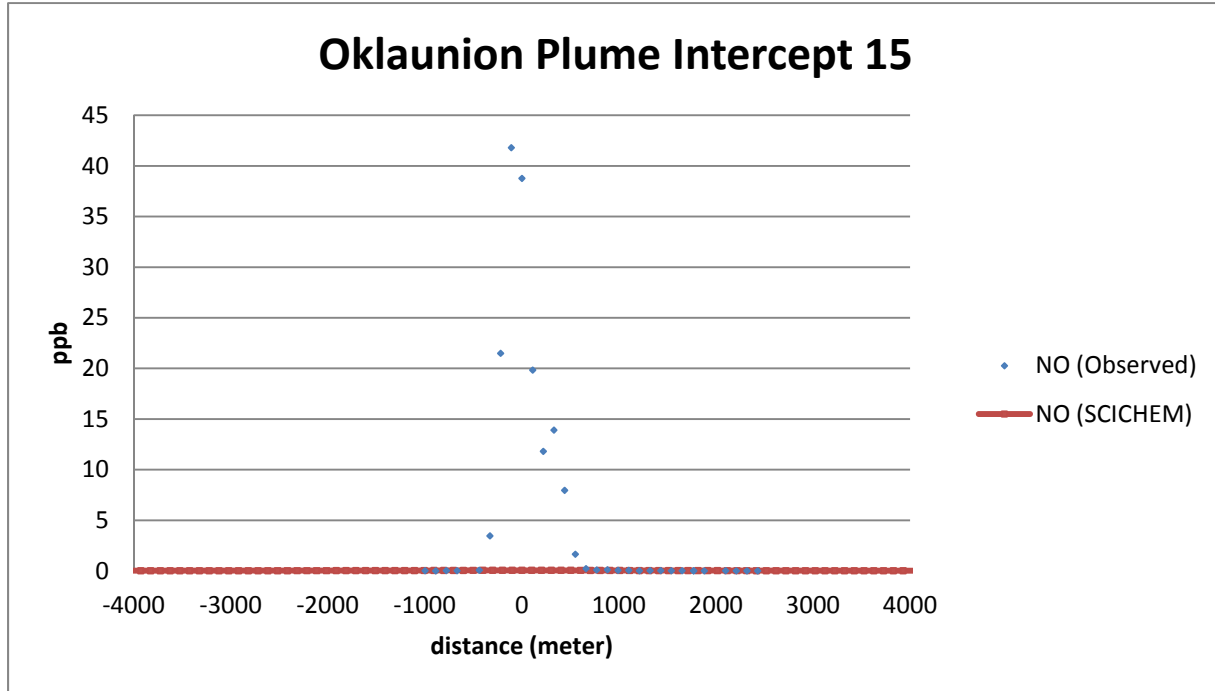
Figure 4-9b. **Observed and simulated (SCICHEM) cross-wind plume concentrations of NO and NO₂ for plume intercept 15 at 58 km downwind of the Oklaunion power plant on October 10, 2006. SCICHEM results are based on aircraft-observed meteorology.**
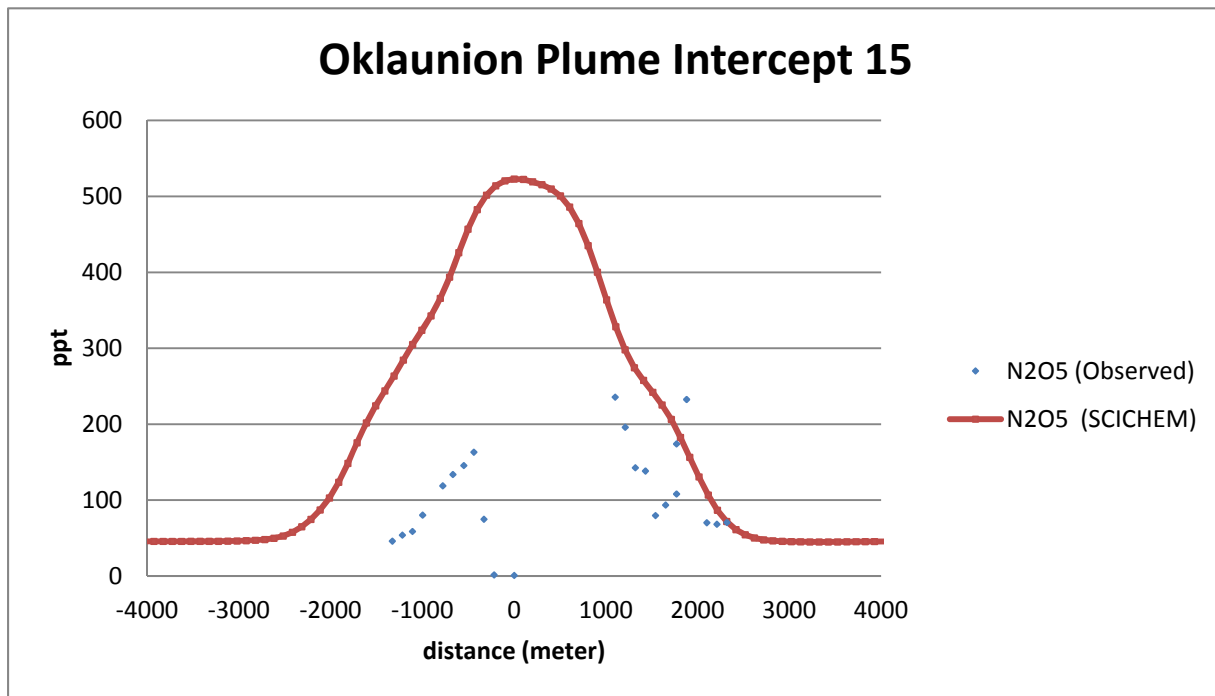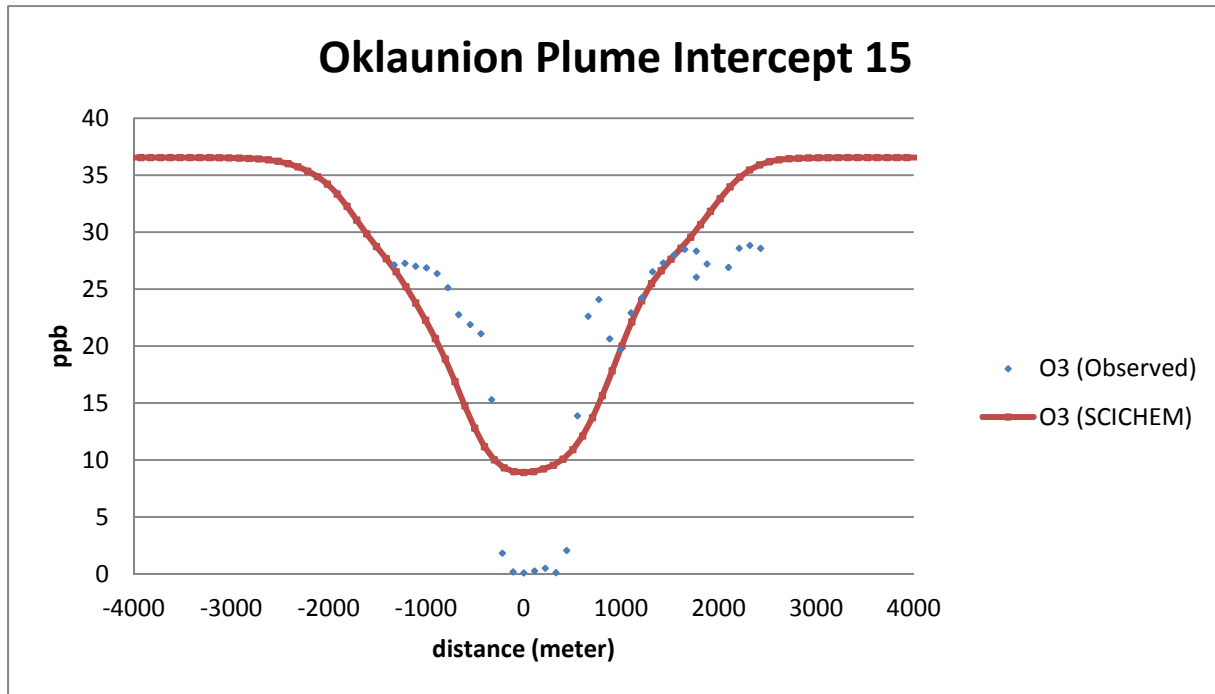
Figure 4-9c. Observed and simulated (SCICHEM) cross-wind plume concentrations of O_3 and N_2O_5 for plume intercept 15 at 58 km downwind of the Oklaunion power plant on October 10, 2006. SCICHEM results are based on aircraft-observed meteorology.
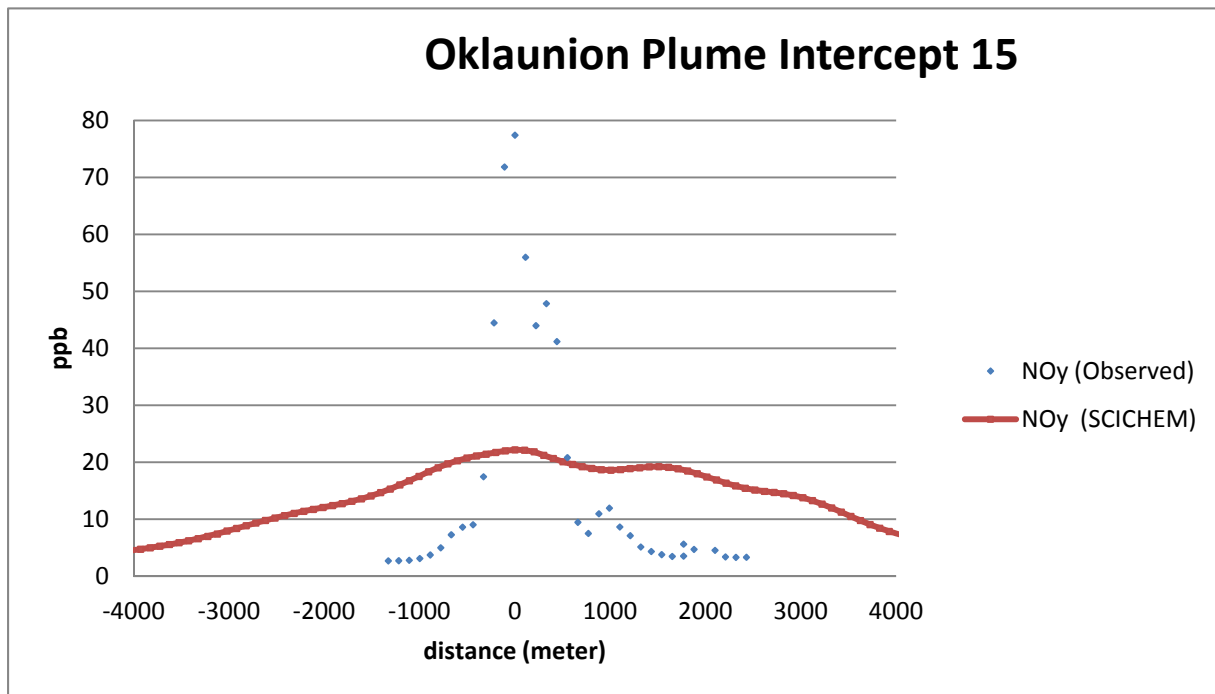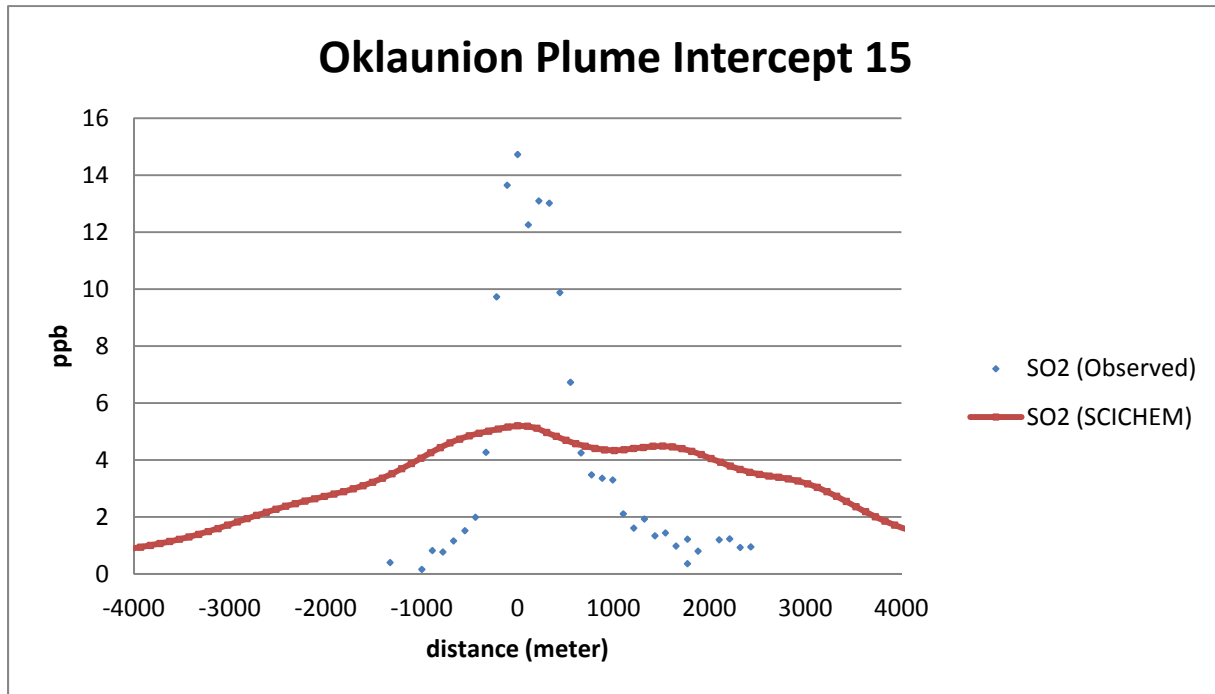
Figure 4-10a. Observed and simulated (SCICHEM) cross-wind plume concentrations of SO$_2$ and NO$_y$ for plume intercept 15 at 58 km downwind of the Oklaunion power plant on October 10, 2006. SCICHEM results are based on MM5 meteorology processed with MMIF.
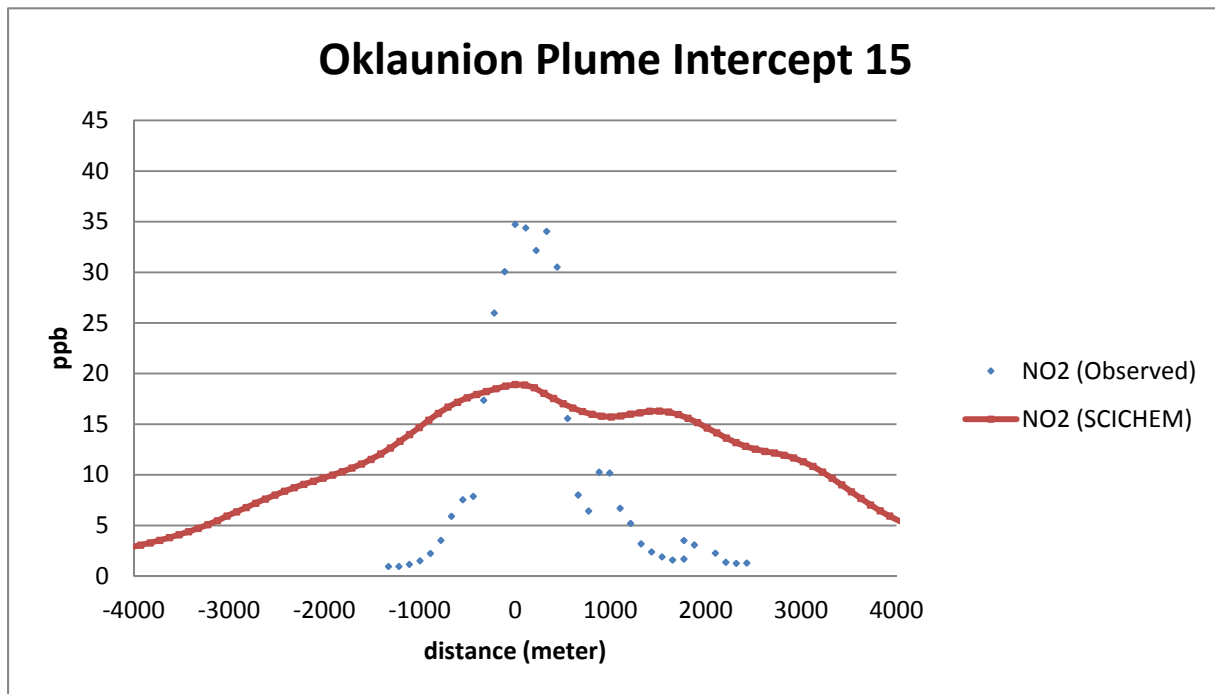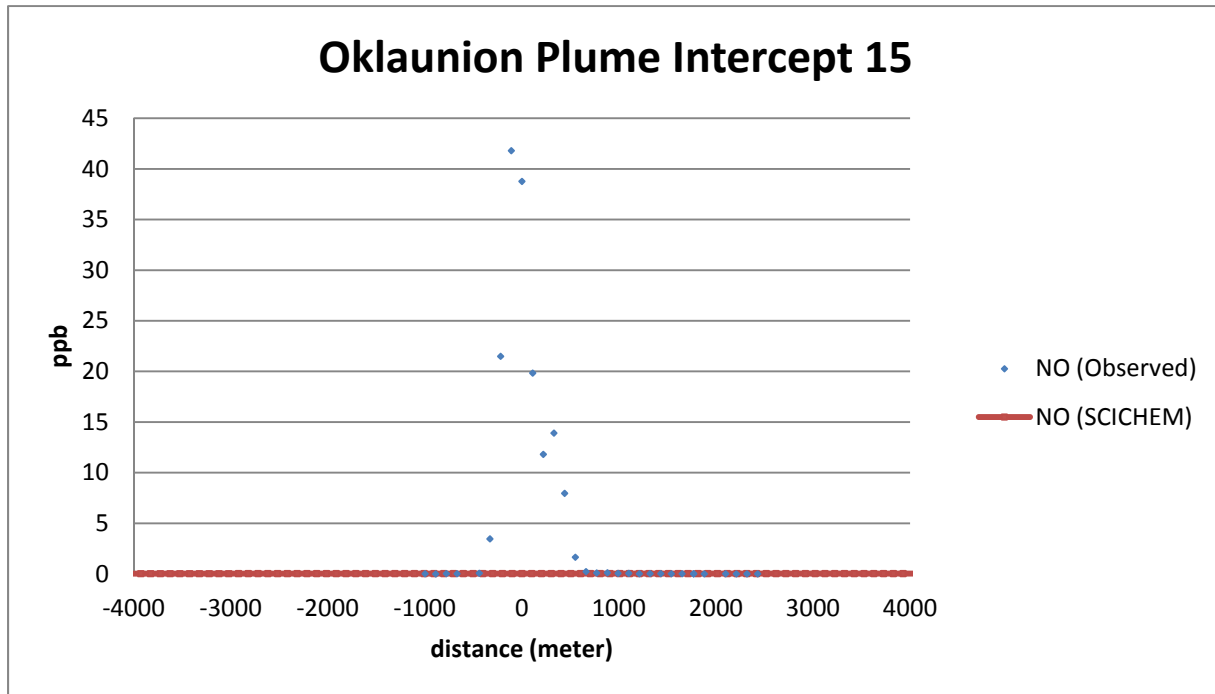
Figure 4-10b. Observed and simulated (SCICHEM) cross-wind plume concentrations of NO and NO$_2$ for plume intercept 15 at 58 km downwind of the Oklaunion power plant on October 10, 2006. SCICHEM results are based on MM5 meteorology processed with MMIF.
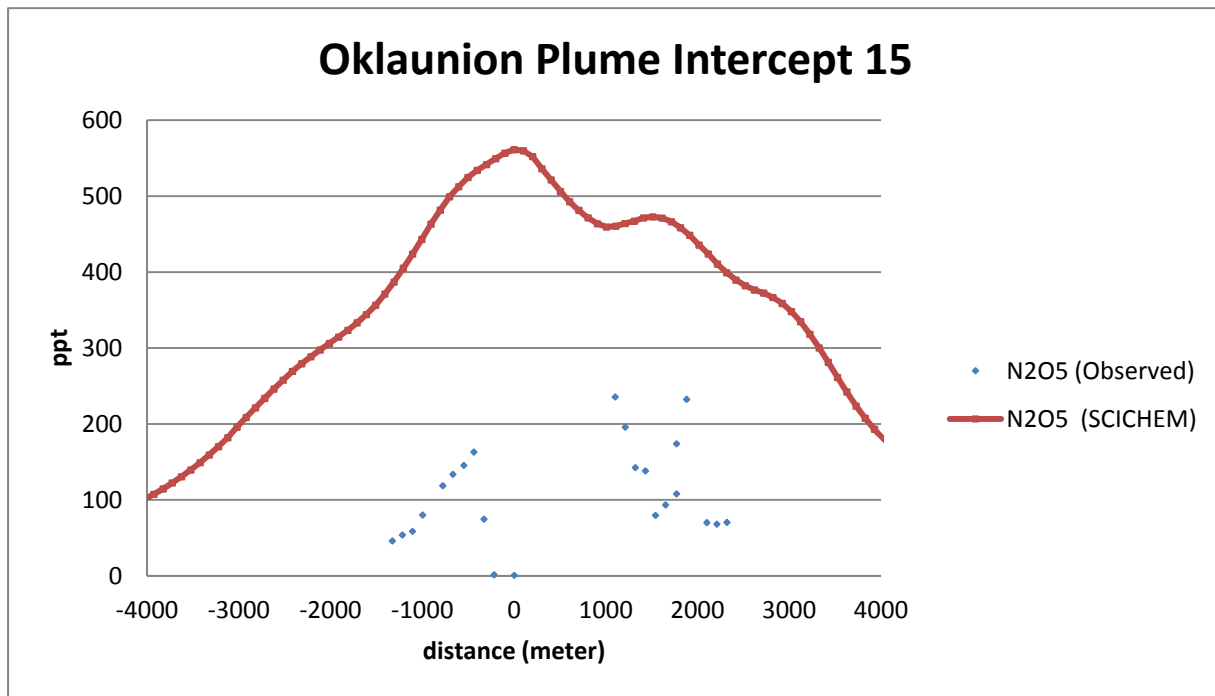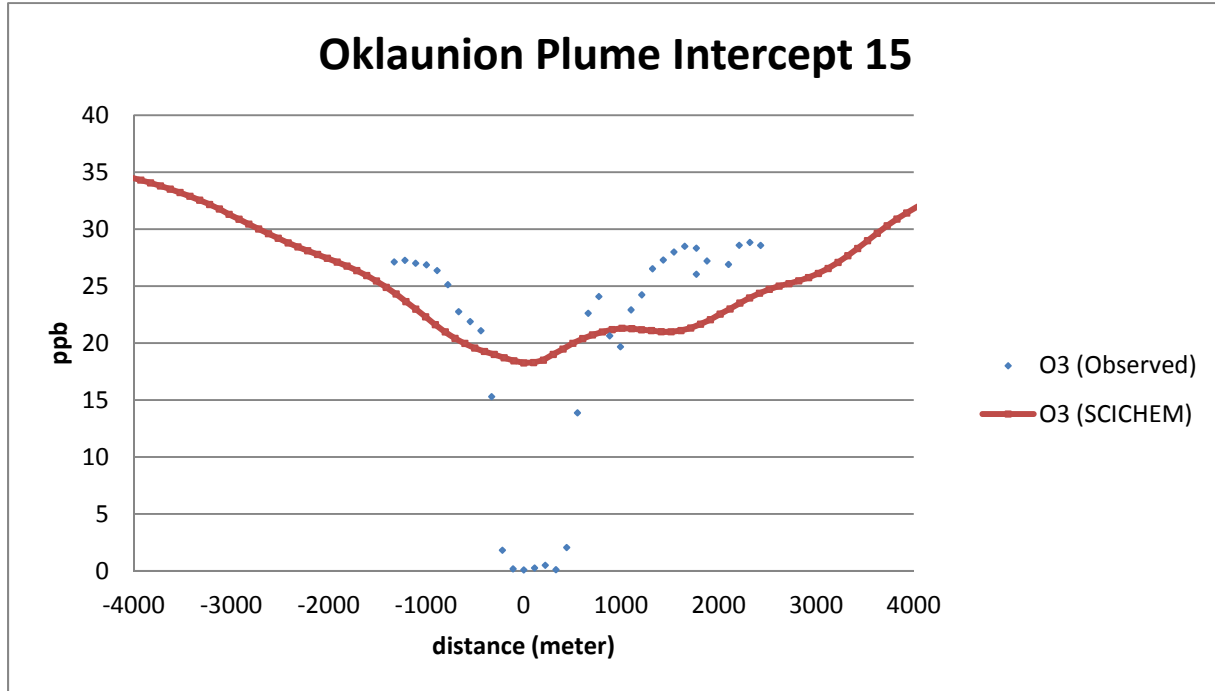
Figure 4-10c. **Observed and simulated (SCICHEM) cross-wind plume concentrations of O_3 and N_2O_5 for plume intercept 15 at 58 km downwind of the Oklaunion power plant on October 10, 2006. SCICHEM results are based on MM5 meteorology processed with MMIF.**

4.2   CAMX EVALUATION

The CAMx photochemical grid model simulation of the Oklaunion power plant plume was evaluated two ways: (1) using the subgrid-scale Plume-in-Grid module with a 12 km resolution grid; and (2) using a 200 m high-resolution grid. Both simulations were based on 12 km MM5 meteorological data processed by MMIF.

4.2.1   PiG Results

We evaluated the CAMx Plume-in-Grid (PiG) results for the evening of October 10 measurements with respect to plume dimensions and chemical evolution. Figure 4-11 shows a snapshot at 2200 LST of the entire train of puffs emanating from Oklaunion and heading southward consistent with aircraft observations. Puff widths are symmetrically defined as ±1.5σ about the puff centerline (3σ total width), where σ is one standard deviation of a Gaussian distribution. The plume extends just under 2 hours downwind, quickly exceeding 5 km wide within an hour of release and expanding to roughly 20 km wide when it is terminated and all mass is transferred to the host 12 km grid. This is significantly wider than observed in aircraft transects at similar distances downwind that suggest plumes no wider than about 1 km according to a full width half maximum (FWHM) metric. FWHM is roughly equivalent to a 2σ (±1σ) plume width, but reducing the PiG puff widths by a factor of 2/3 to account for this difference is clearly insufficient to match the measured widths.

The PiG simulation was re-run with reduced puff growth rates by removing the contribution from wind shear. The evolution of puff size is defined by σ growth equations that include a turbulent component, which affects lateral (σ_y) and longitudinal (σ_x) dimensions equivalently, and a shear component, which leads to asymmetric horizontal growth from resolved three-dimensional wind shear defined by the meteorological input fields. Vertical growth contains only the turbulent component, so shear plays no role in puff depth. Cross-plume shear causes the puffs in Figure 4-11 to translate from ellipses oriented along the plume path just after release to much larger ellipses oriented across the plume path as they approach termination. Figure 4-12 shows a comparison of the standard and "no-shear" puff trains at 2200 LST. Plume growth in the latter case is quickest just after release, and slows dramatically after 30 minutes. The plume is consistently between 5 and 10 km wide out to 2 hours, and because puffs remain smaller they extend farther downwind before being terminated due to size. Nevertheless, the PiG plume continues to be far wider than measurements suggest.

The differences between the standard and "no-shear" PiG runs implicate the gridded meteorological fields as the source of excessive PiG plume spread via horizontal and vertical shears. Plots of PiG puff trains and animations of the high resolution plume between 1800 and 2400 LST reveal that model winds shifted steadily from northwest to north behind an eastward propagating frontal system. Furthermore, this shift occurred at different rates in the vertical, with the lower layers (1-4) shifting more rapidly than upper layers (5-6).

Figure 4-13 shows the centerline heights and puff depths for the train of puffs in the "no-shear" case at the same time as Figures 4-11 and 4-12. Puff height ranges between 250-300 m AGL, which is consistent with aircraft measurements, and is clearly a function of puff age as the stabilizing boundary layer steadily reduces plume rise. Plume depth grows steadily to over 300

m at 2 hours downwind, which is deeper than the ~100-200 m depth estimated by in situ evidence.

22:00 on October 10, 2006
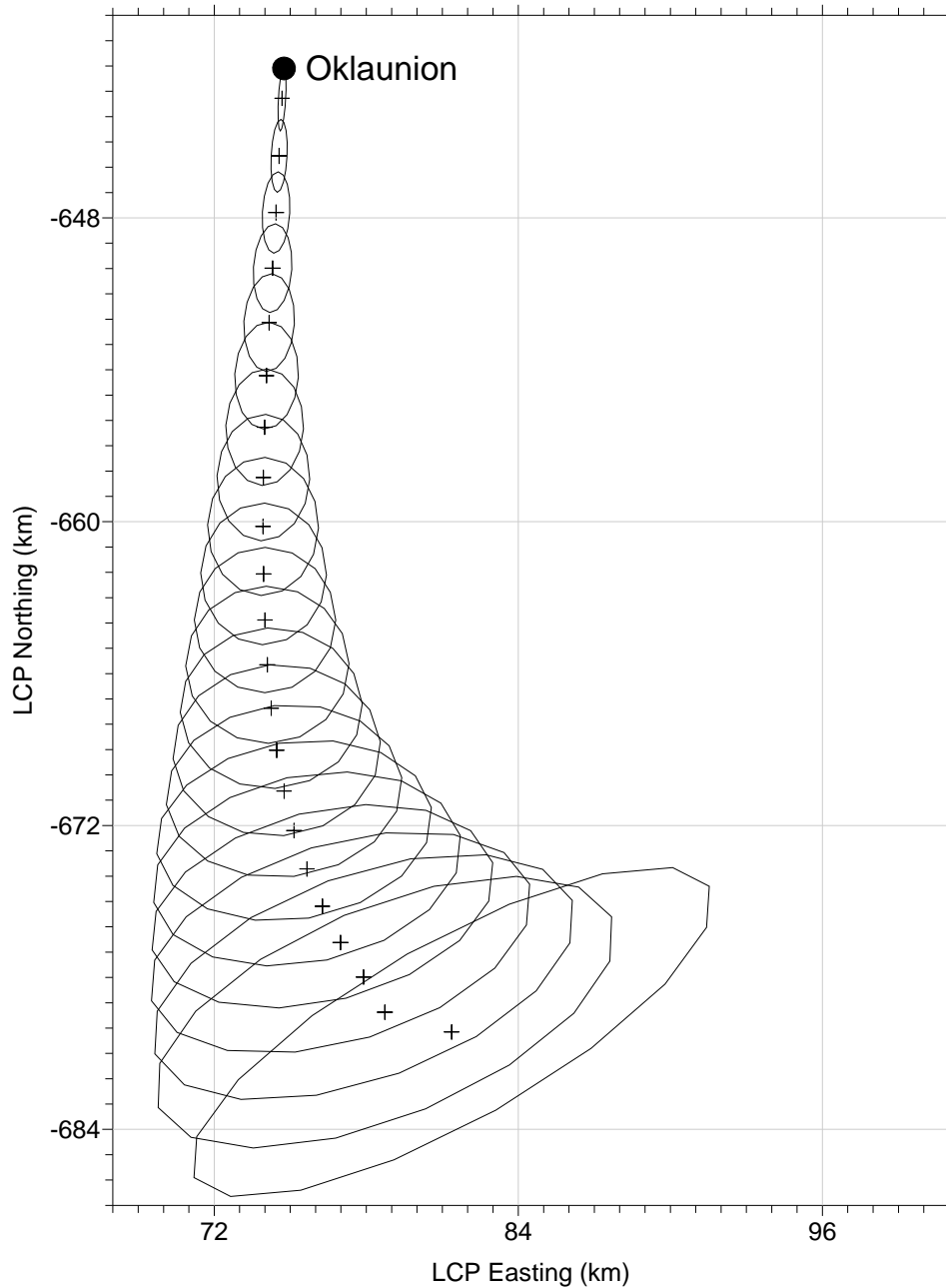
Figure 4-11. Depiction of the train of CAMx PiG puff dimensions (ellipses) and puff center points (crosses) at 2200 LST October 10. Axis tick marks are 1 km apart, and the 12 km grid is denoted by the grey lines.

22:00 on October 10, 2006
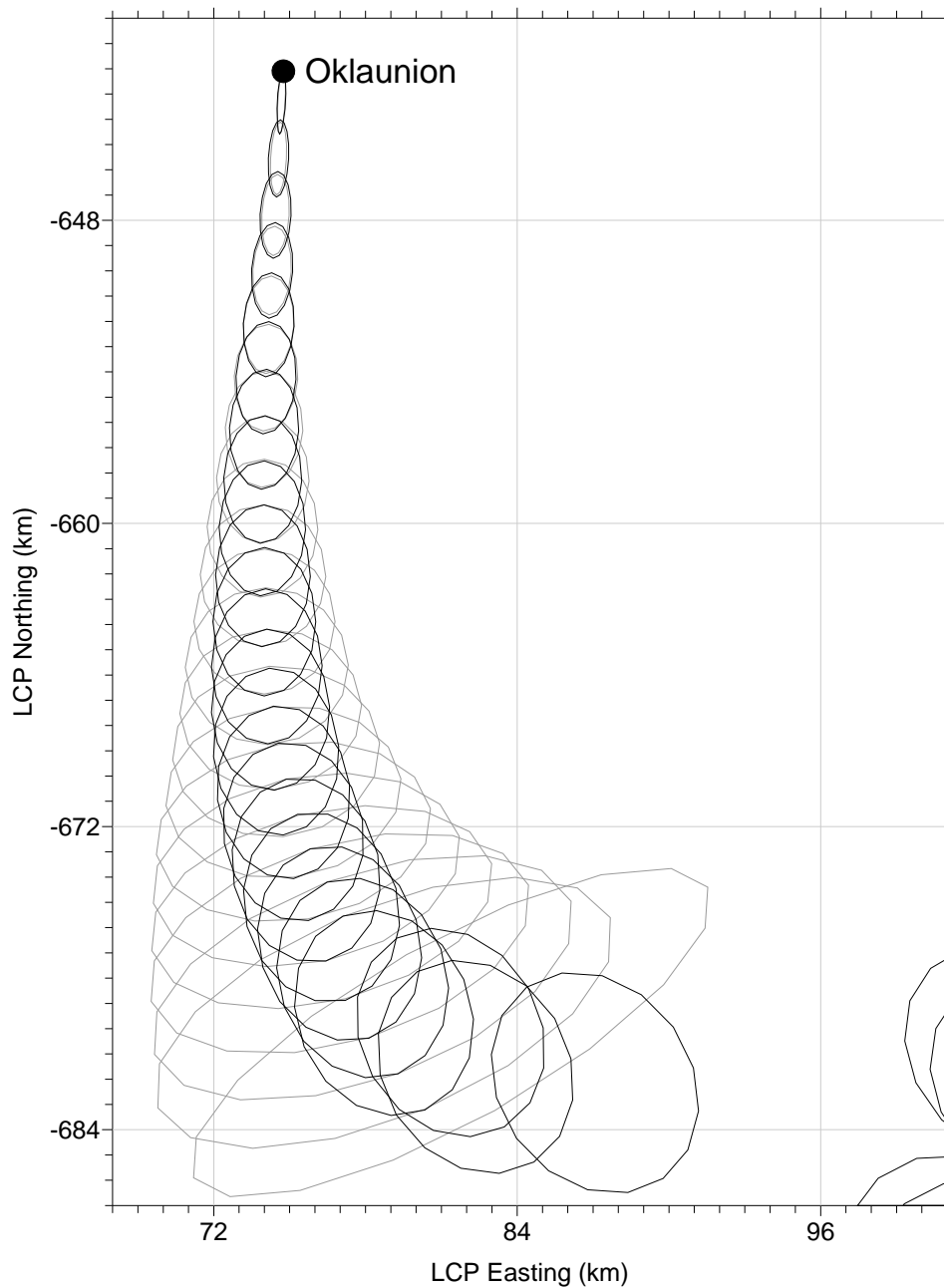
Figure 4-12. Depiction of the train of CAMx PiG puff dimensions (ellipses) at 2200 LST October 10. Grey puffs are those from the standard PiG application shown in Figure 4-11, and the smaller black puffs are the result of removing wind shear contributions from the puff growth equations.
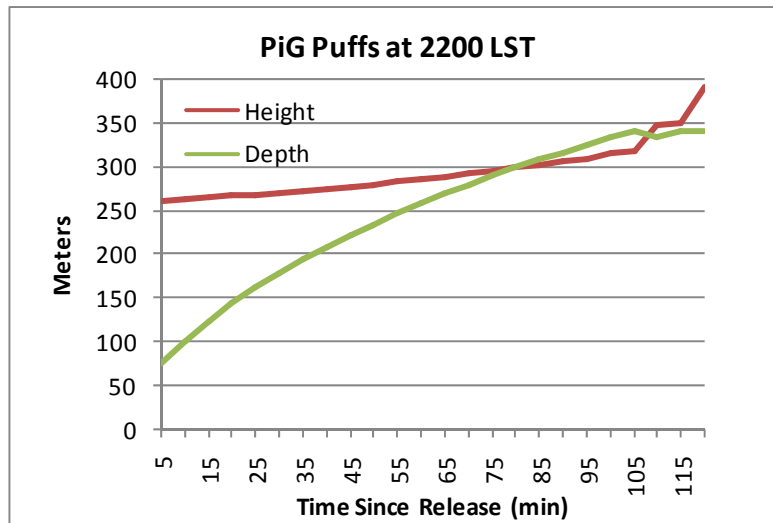
Figure 4-13. Timeline of PiG puff height and depth at 2200 LST October 10. Total PiG plume lifetime shown is 2 hours.

Figure 4-14 displays the cross-sectional chemical evolution of the "no-shear" plume at 2200 LST; plots are shown for puff ages of 5, 30, 60, 90, and 120 minutes. Puff concentrations are increments above (+) or below (-) the background defined on the 12 km grid. Fresh NO is exhausted within an hour, replaced with NO_2 that is further reduced by puff dilution and oxidation to NO_z products. Core NO_2 remains several ppb above background until puff termination, while NO_2 is practically all removed in the outer reactor by then. N_2O_5 is initially all background, and is depleted early when NO_x is high, but then it starts to build in the outer reactor first, around 60 minutes downwind, due to dilute NO_x and available oxidants. The core generates N_2O_5 rapidly after 1 hour. N_2O_5 production reaches maxima of several hundred ppt, which is in general agreement with aircraft measurements, but this peak occurs two hours downwind, which is too fast. HNO_3 production begins in the outer reactors at 90 minutes and reaches almost 100 ppt by 2 hours. Overestimates of both plume width and depth result in an improper characterization of NO_x concentrations and chemistry in the nighttime plume.

4.2.2 High Resolution Flexi-Nest Results

A high resolution simulation of the Oklaunion plume was performed to compare against the PiG results and the aircraft measurement data. Figure 4-15 shows contours of the NO_2 plume from layer 5 at 2200 LST using the 200 m high-resolution grid, together with the previous PiG puff plots from Figure 4-12. The high resolution plume is consistently about 1 km wide within an hour of release (as defined by NO_x FWHM) and slowly grows to several km wide well downstream. While the standard PiG run tracks the centerline well, it is about six times wider than the high resolution plume. The PiG puff width with all shear-induced growth removed matches the high resolution results better. Another high resolution test was conducted in which all explicit horizontal diffusion was set to zero. The resulting NO_x plume was not significantly altered by this change, suggesting that plume spread is dictated by grid resolution

and numerical diffusion associated with the advection solver (PPM in this case) under these nocturnal stable conditions.

Vertical west-east cross sections through the high resolution grid between 2000-2200 LST (e.g., Figure 4-16 shows a cross section at about 25 km south of Oklaunion) indicate that the plume ranged between layers 4 – 6 (170-430 m AGL, 260 m deep), with the highest core concentrations maintained in layer 5 (255-345 m AGL, 90 m deep). This is similar to PiG and in excellent agreement with aircraft data. The peak concentrations across layers 4 – 6 were separated by 5 – 10 km, even though plume spread in each individual layer was only 1 – 3 km. Viewed in its entirety, the plume takes on a diagonally-oriented cross section, where the entire plume cross section width is similar to the PiG spread with shear included. Whereas it is possible that the gridded meteorological fields may possess too much shear, the PiG and high resolution plume results are actually more similar than they first appear, and it raises the possibility that lowest aircraft transects at 300 m sampled a small portion of a diagonally-oriented plume cross section (i.e., a tilted plume).
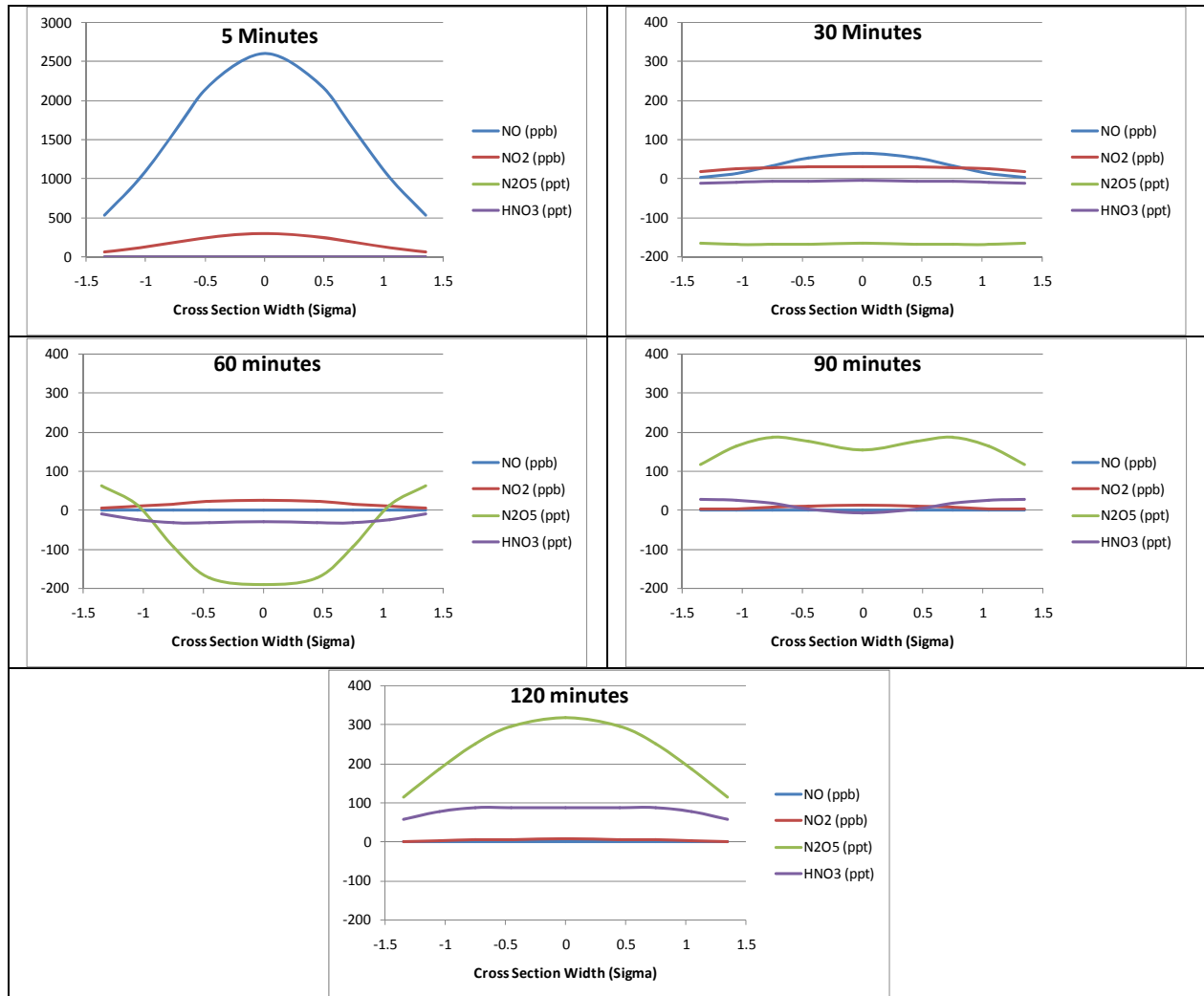
Figure 4-14. Cross-sectional depiction of PiG puff NOy component concentrations at 2200 LST for puffs ages of 5, 30, 60, 90, and 120 minutes. Puff width is given by multiples of the Gaussian sigma.

22:00 on October 10, 2006
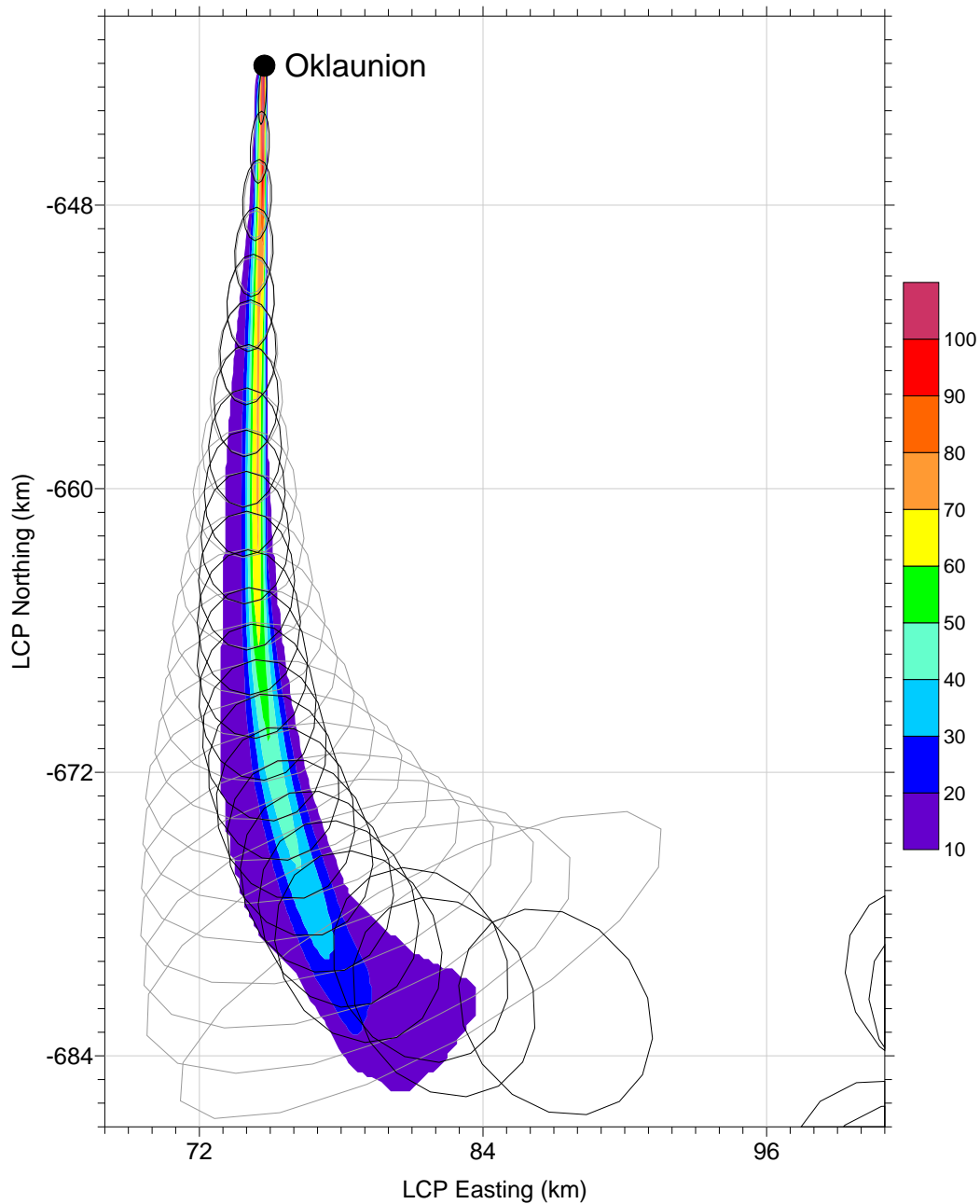
Figure 4-15. Comparison of the train of CAMx PiG puff dimensions (ellipses) against the high resolution NO$_2$ plume (colored contours in ppb) in CAMx layer 5 at 2200 LST October 10. Puffs are the same as shown in Figure 4-12.
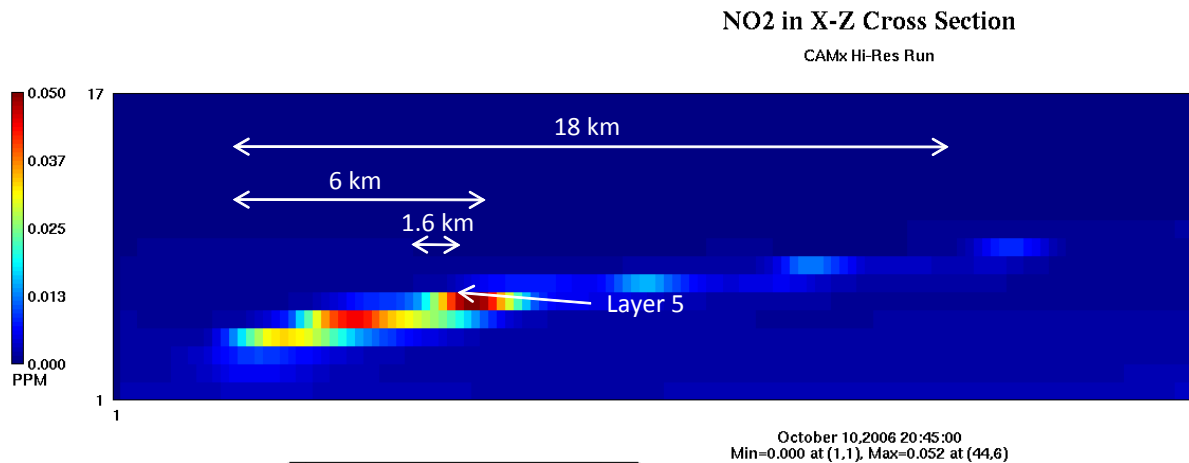
Figure 4-16. X-Z cross section of the high resolution NO$_2$ plume at roughly 25 km south of the Oklaunion source at 2045 LST October 10.

Figure 4-17 displays the high resolution Oklaunion plume in layer 5 for NO, NO$_2$ and ozone at 2130 LST. Aircraft measurements along the flight path are overlaid, showing plume transects 13 (north) and 14 (south); measured concentrations are denoted with the same color scale as the simulated plume to facilitate the comparison. Relative to transect 13, the simulated plume is located very near the measured plume, and the NO plume width agrees well (note that there are missing NO$_2$ aircraft data as the plume was encountered). However, the ozone impact from NO$_X$ appears to be too wide. According to transect 14, aircraft data suggest little plume growth 16 km south from transect 13, but the high resolution plume is too wide by about a factor of 2. Note that at 2130 LST the plume in layer 5 has not yet fully extended to the position of transect 14. From a chemical processing standpoint, too much NO is converted to NO$_2$, caused by overly rapid dilution and mixing with ambient ozone. Aircraft data also suggest that simulated background ozone is too high ~10 ppb.

4.2.3 Cross-Plume Comparisons with Aircraft Measurements

Measured and simulated plume concentrations were compared in more detail by aligning the plumes and overlaying their cross-sectional profiles. Figure 4-18 displays these comparisons for the high-resolution run. At transect 13, the plume widths agree quite well for all species, except that NO is under predicted. While there is zero ozone and N$_2$O$_5$ in the plume core, these plots show that simulated background values for these species are much higher than measured. At transect 14, the simulated plumes are far too wide and diffuse. A very confined core of measured NO remains at this downwind distance but nearly all simulated NO has diffused and converted to NO$_2$. While the peak NO$_2$ is well replicated, the simulated plume FWHM is ~5 km while the measured plume width is only ~1 km. As expected, the ozone profiles are inverses of the NO$_2$ profiles. Excessive dilution and NO$_x$ oxidation has generated substantial concentrations of simulated N$_2$O$_5$ at transect 14, reaching 350-400 ppt on the plume edge (100-150 ppb above background), while measured N$_2$O$_5$ remains near zero in the highly concentrated NO core.

Figure 4-19 displays similar comparisons for the 5-reactor PiG run with shear-induced puff growth removed. Similarly to the high-resolution results, the PiG plume width agrees generally well with measurements from transect 13, roughly 1 km. However, there is far too much NO_x dilution and associated conversion of NO to NO_2. While ozone titration occurs, ozone is not reduced to zero in the plume core even though there is more NO in the core (~50 ppb) than ambient ozone (30-40 ppb). We tracked this to the operator splitting procedure in PiG, where puff chemistry is performed prior to puff growth. While chemistry does reduce ozone to zero in the plume core, subsequent growth dilutes the negative ozone mass increment (making it less negative), thereby artificially increasing puff ozone when background is added back in. The same effect is seen for the N_2O_5 deficit at transect 13, which should be closer to zero in the core. Beyond the obvious chemistry implications derived from excessive puff growth rates, we expect that this operator splitting issue has no significant impact on net chemistry over the life of the PiG plume, and would likely be visually alleviated by re-ordering puff growth to occur before chemistry (so that on output puffs reflect the last chemistry effect rather than the last dilution effect). Puffs grow up to three times too wide by the time they reach transect 14 resulting in an underestimation of the NO concentrations and resultant titration of background ozone in the plume (Figure 4-19b).
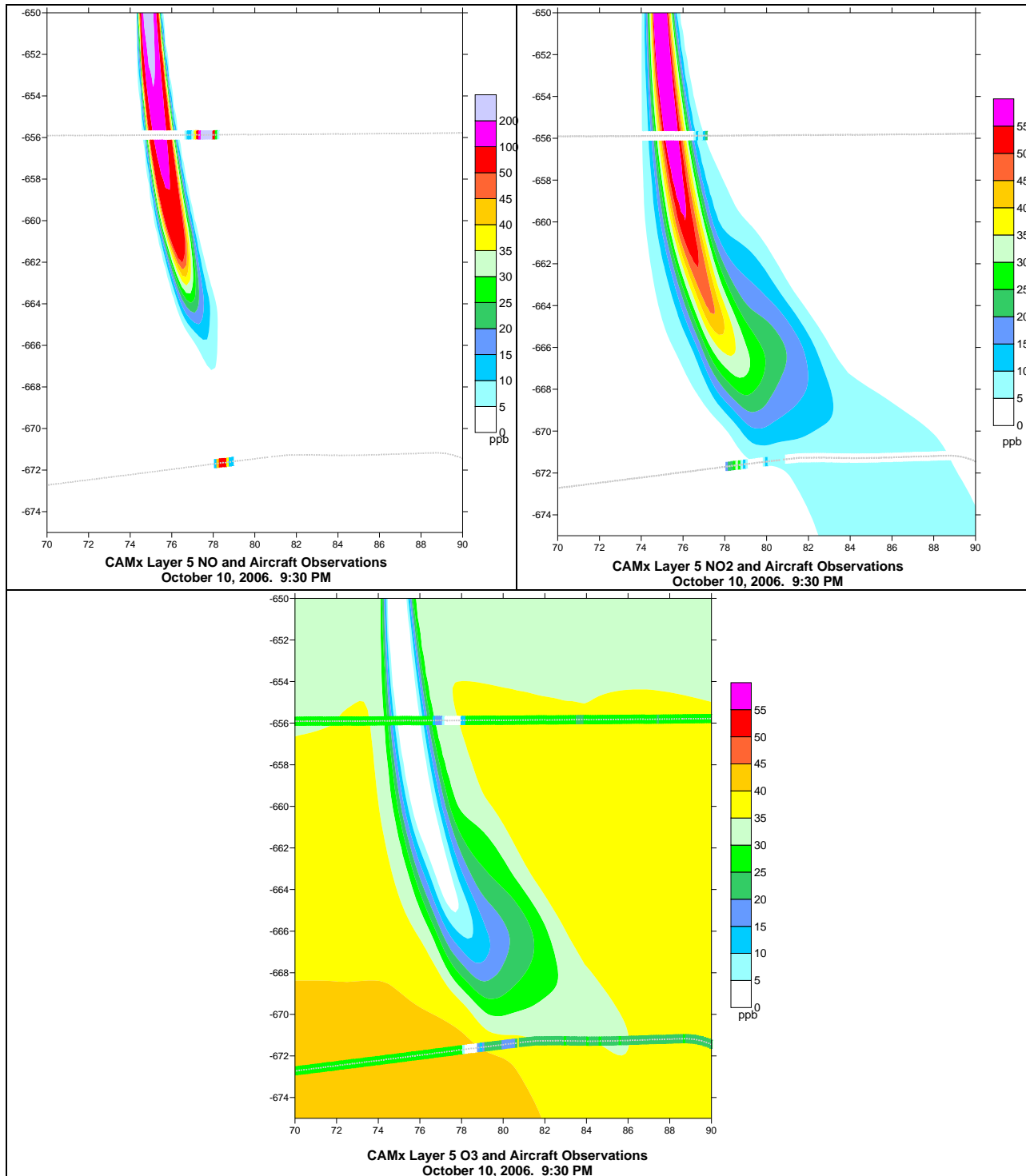
Figure 4-17. Simulated and measured NO (top left), NO₂ (top right) and ozone (bottom) at 2130 LST October 10. Simulated concentrations are from layer 5 in the high resolution run. Aircraft measurements are shown along flight paths for transects 13 and 14.
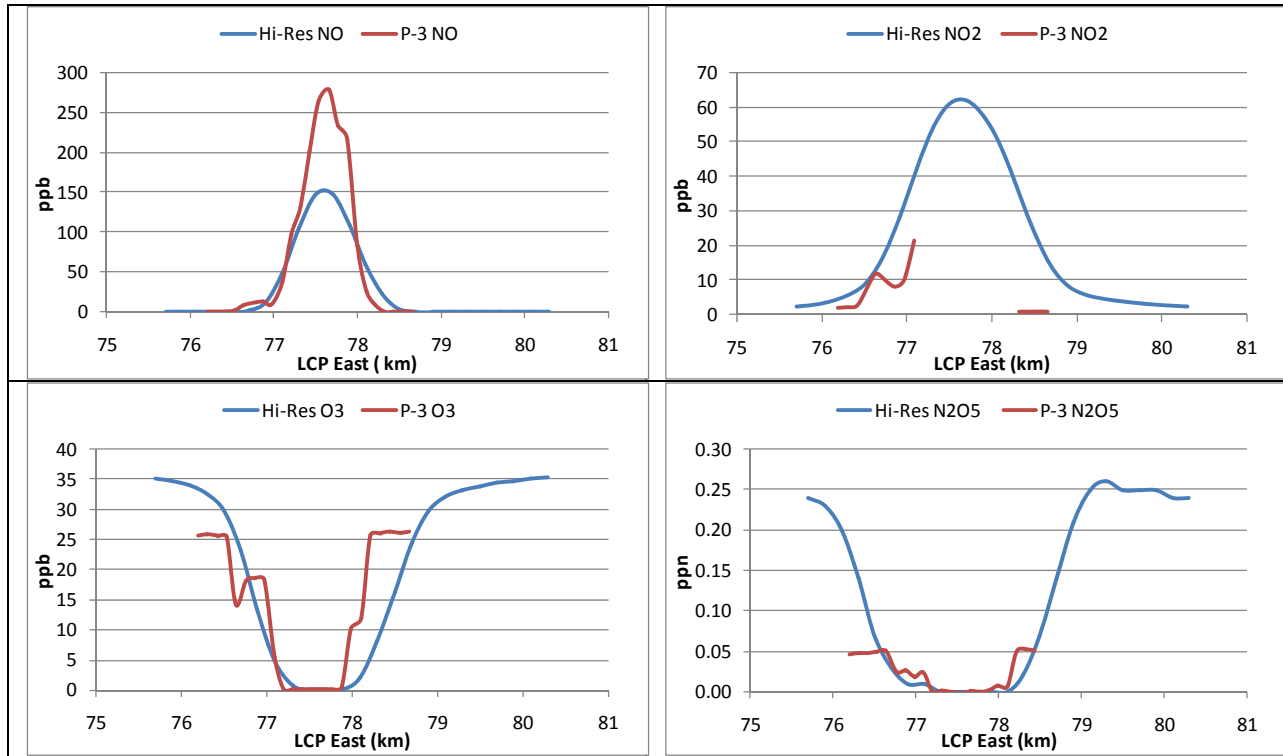
Figure 4-18a. Aligned simulated and measured plume cross sections of NO (upper left), NO$_2$ (upper right), ozone (lower left) and N$_2$O$_5$ (lower right) at transect 13 shown in Figure 4-17. Simulated concentrations are taken from layer 5 of the high resolution run at 2130 LST October 10.
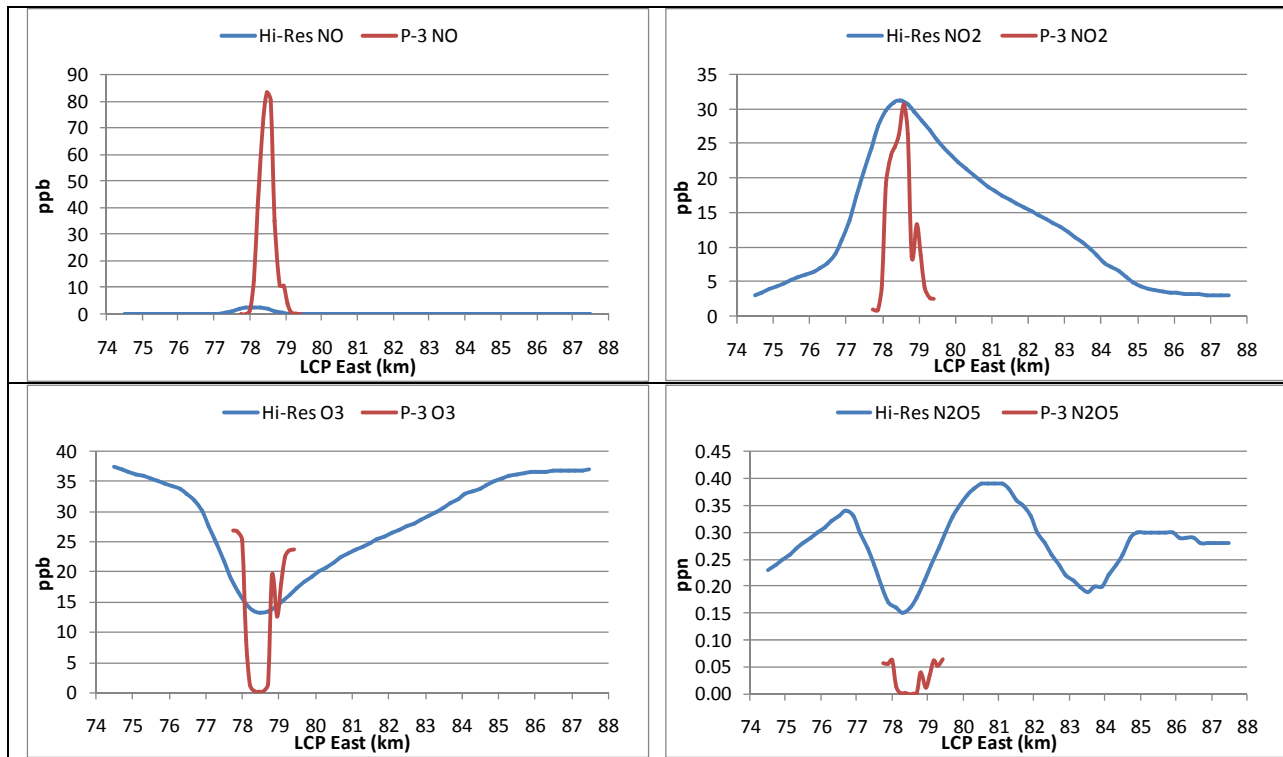
Figure 4-18b. Aligned simulated and measured plume cross sections of NO (upper left), NO$_2$ (upper right), ozone (lower left) and N$_2$O$_5$ (lower right) at transect 14 shown in Figure 4-17. Simulated concentrations are taken from layer 5 of the high resolution run at 2130 LST October 10.
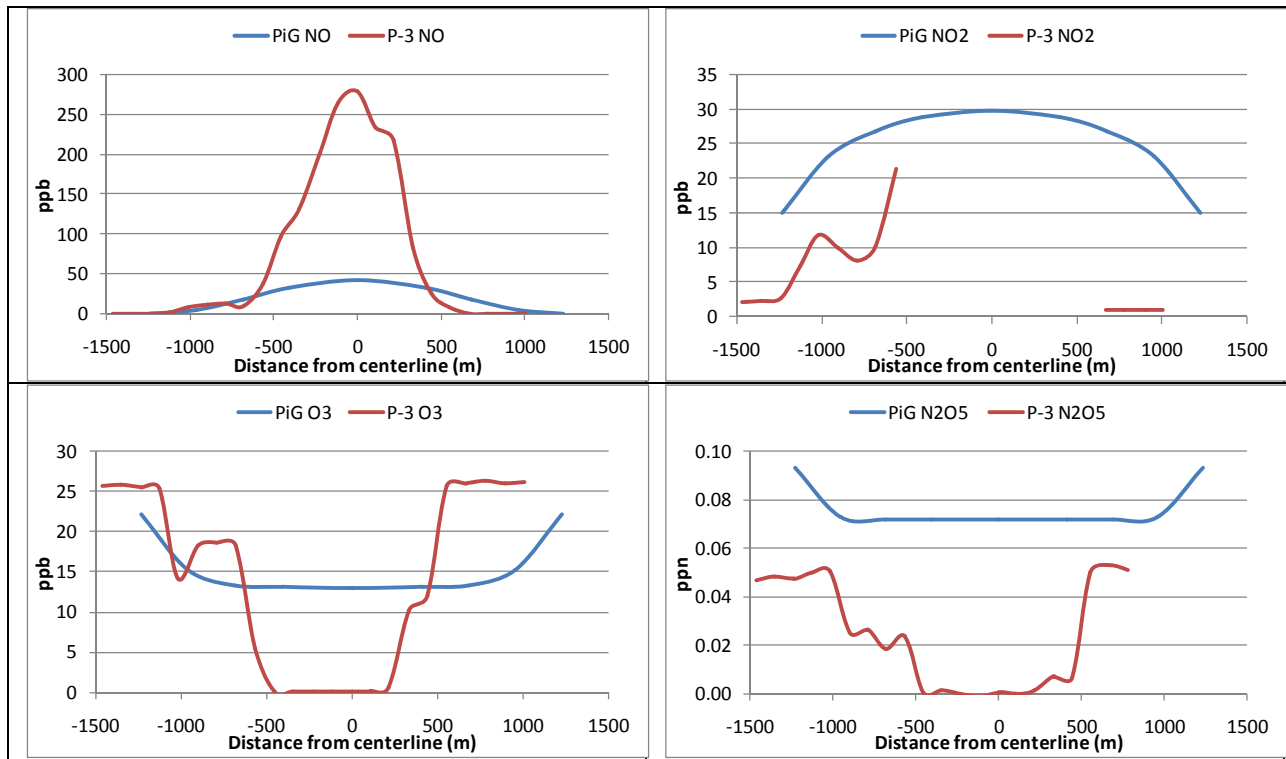
Figure 4-19a. Aligned simulated and measured plume cross sections of NO (upper left), NO₂ (upper right), ozone (lower left) and N₂O₅ (lower right) at transect 13. Simulated concentrations are taken from the 5-reactor PiG run at 2200 LST October 10.
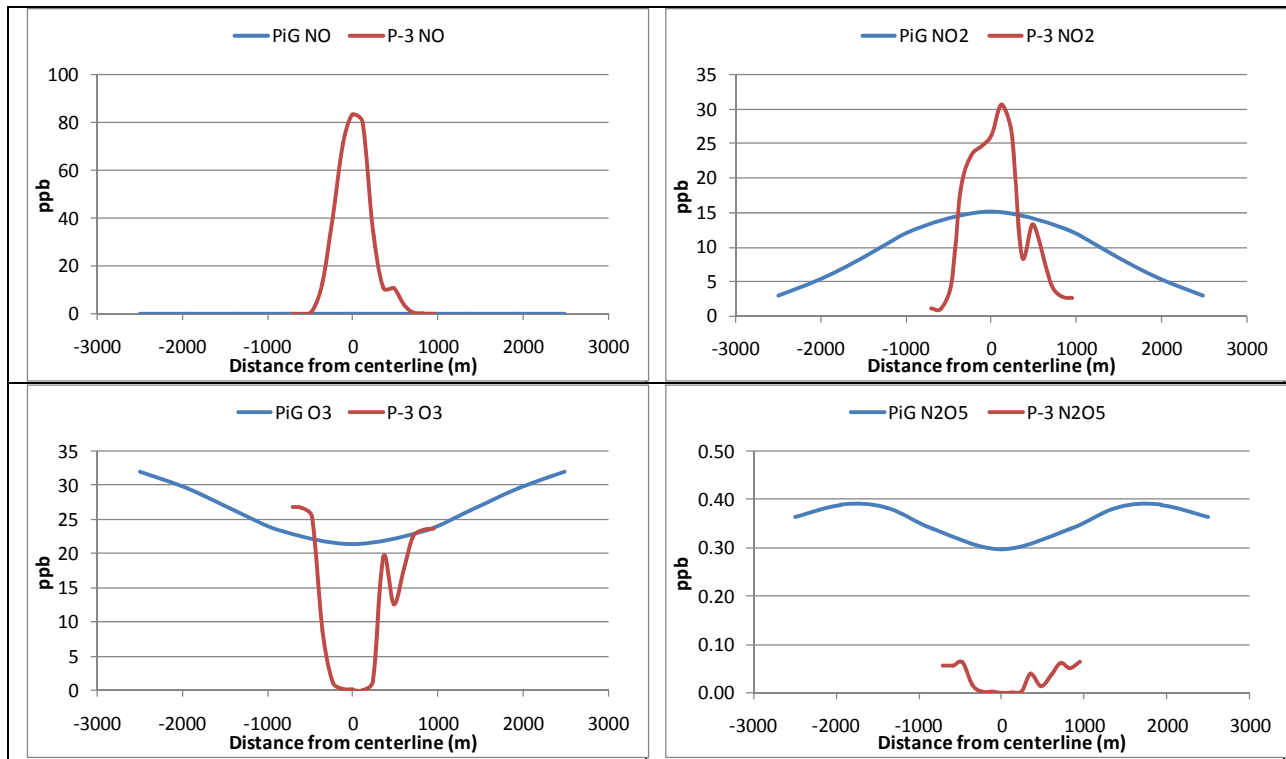
Figure 4-19b. Aligned simulated and measured plume cross sections of NO (upper left), NO₂ (upper right), ozone (lower left) and N₂O₅ (lower right) at transect 14. Simulated concentrations are taken from the 5-reactor PiG run at 2200 LST October 10.

4.2.4   Summary and Conclusion for the CAMx Oklaunion Evaluation Simulations

We note the following characteristics of the CAMx-simulated Oklaunion plume relative to aircraft measurements on the evening of October 10. First, the CAMx-simulated plume rise agreed well with the altitudes of aircraft intercepts. However, PiG plume spread was too wide within 1 hour of transport, while plume spread on the high resolution (200 m)-flexi-nest was too wide after about 2 hours. Second, restricting PiG horizontal growth by removing effects of wind shear resulted in better agreement with the high resolution plume, while removing all explicit horizontal diffusion in the latter case had only a minor effect on simulated plume width. Third, while both PiG and high-resolution techniques can produce observed NO_z structures (e.g., enhanced NO_z on plume edges well before the core converts NO_x to NO_z), over-dilution speeds and spreads NO_x chemistry. Removing all vertical growth in PiG (not shown) resulted in much better agreement with NO_x measurements by significantly reducing dilution, extending the life of PiG puffs, and improving the characterization of NO_x chemistry well downstream. Finally, the plume exhibited a complicated structure: aircraft data suggested a scattered and disjointed plume, while modeling suggests that the transport environment involved a high degree of shear and post-frontal wind shifts. The CAMx high resolution case resulted in a tilted plume with a top around 300-400 m (coincident with the lowest allowed aircraft altitude). These features can explain patterns in the measurements.

Whereas the high resolution simulation resulted in less plume dilution and better agreement with aircraft measurements in general, it required an infeasible amount of computing time for a longer-term (e.g., seasonal or annual) simulation while addressing only the first 2-3 hours of downwind transport and chemistry. PiG simplifies plume modeling and is much more computational efficient. Some simple adjustments to the PiG plume expansion rates will allows us to focus on characterizing plume dimensions correctly, which transfers to proper dilution rates and NO_x chemistry within the plume. We have demonstrated through the use of PiG that NO_x controls can lead to more efficient nocturnal NO_x processing with commensurate impacts on next day ozone.

This research has led us to consider several modifications to the CAMx PiG algorithm, including setting limits on horizontal and vertical growth in nighttime/stable environments, reviewing/revising minimum values for certain internal puff growth parameters, and re-ordering the puff operator splitting methodology.

4.3   COMPARISON OF CHEMICAL DISPERSION MODELING

As in the case of the Cumberland plume modeling, SCICHEM was run with 2 different sets of meteorology (observed and MMIF/WRF), CAMx was run two different ways (PiG and higher-resolution gridded) and CALPUFF was not fully evaluated due to time and resource constraints. The initial CALPUFF simulations placed the plume height higher than the aircraft sampling height so that the receptors failed to fully capture the predicted plume. There were insufficient resources to optimize the receptor heights to capture the CALPUFF plume or force the CALPUFF plume height to match the aircraft sampling height for this report. Model performance evaluation results varied greatly for each of the models run with their different configurations, as well as for the different models. For the early plume transects, SCICHEM estimated SO_2 and NO_2 peaks and plume widths match the observed values very well using observed meteorology, but the comparisons of SCICHEM plume peaks and widths using MMIF/MM5 meteorology is not as good due in part to an overly dispersed plume. CAMx typically produced overly dispersed plumes, likely due to the meteorology. This was especially true in the first applications of the PiG subgrid-scale plume model whose shear enhanced plume dispersion resulted in far too much plume dispersion in the nighttime stable environment. Modifications to the PiG dispersion algorithms were able to improve the PiG plume representation. The CAMx high-resolution (200 m) grid model produced much better performance including reproducing the tilted plume, albeit with higher computational requirements.

5.0   CONCLUSIONS

The TVA Cumberland power plant plume modeling experiment and TexAQS II Oklaunion power plant plume modeling experiment represent two very different scenarios in terms of meteorology and source strengths, with the Cumberland experiment taking place in the day with photochemical production and higher plume dispersions rates and the Oklaunion experiment occurring in the evening/night with very little plume dispersion and no photochemistry.

The Cumberland experiment provides a database to test model chemical mechanisms - in particular ozone titration and formation - within the plume for CAMx and SCICHEM and both models showed skill with specific sets of inputs in modeling this phenomenon.

Oklaunion was a greater challenge to model and compare with the observations due to the stable nocturnal environment, a highly stratified atmosphere and a vertically confined plume. Flight data indicate a vertical plume depth of no more than 300 m and suggest that the plume was located at the lowest operational limit of the aircraft (about 300 m AGL). There is uncertainty associated with the measurements and the CAMx modeling suggests it is possible that not all aircraft transects were perpendicular to the plume direction, but may have been diagonal slices in some cases. SCICHEM and CAMx optimized model configurations to replicate observed values but lack of resources did not enable CALPUFF modelers to perform the same type of optimization. Given that the models can be optimized to estimate dispersion characteristics reasonably well, an assessment of dispersion is not valid. However, an assessment of chemical transformations within the plume over time is valid provided the modeled and observed dispersions are forced to match.

Model-to-model comparison is challenging due to the number of model configurations, transects, and model species. The model performance results are very sensitive to different meteorology, inputs based on observed meteorology near the plume (e.g., aircraft observations) versus regional WRF/MM5 meteorological modeling processed with MMIF. In general, using the local observations produced better model performance than using the regional WRF/MM5 meteorological modeling. However, it is reasonable to expect that WRF or MM5 could be reconfigured and applied with a different set of options to get better model performance and better representation of plume placement in downstream air quality models.

For future work, to facilitate model comparisons, it would be helpful to use the same meteorology for all models as much as possible, to isolate difference due to the models instead of the meteorology. Also, to enable more quantitative and less qualitative comparisons, and to incorporate all results, a system should be devised including metrics and/or statistics that can incorporate and summarize all the results, integrating observed vs. modeled comparisons for peak values/plume widths/total mass etc. For the CALPUFF modeling, a vertical array of receptors should be used to locate the plume in the vertical direction for the Oklaunion experiment. Careful attention should be paid to the time period averaging of results, since measurements were at arbitrary time intervals and the models typically work on hourly results, to see if time resolution can be changed for CALPUFF and CAMx. A distinction should be made as to whether the focus is on evaluation of model dispersion characteristics or model chemistry or both. For a chemistry evaluation, the modelers could perform tests to force the dispersion parameters to match observed dispersion and then the evaluation of the chemistry within a

plume will be independent from the dispersion. For a dispersion evaluation, model default parameters should be used.

6.0   REFERENCES

Bott, A. 1989. A positive definite advection scheme obtained by nonlinear renormalization of the advective fluxes, *Mon. Wea. Rev.*, **117**, 1006-1015.

Brashers, B. and C. Emery. 2009. *Draft User's Guide – The Mesoscale Model Interface Program (MMIF) – Version 1.0,* ENVIRON International Corporation, Novato, CA. June 11.

Brashers, B. and C. Emery. 2011. *Draft User's Guide – The Mesoscale Model Interface Program (MMIF) – Version 2.0*, ENVIRON International Corporation, Novato, CA. September 30.

Brown, S.S., W.P. Dubé, H. Fuchs, T.B. Ryerson, A.G. Wollny, C.A. Brock, R. Bahreini, A.M. Middlebrook, J.A. Neuman, E. Atlas, et al. 2009. Reactive uptake coefficients for N_2O_5 determined from aircraft measurements during the Second Texas Air Quality Study: Comparison to current model parameterizations, *J. Geophys. Res.*, **114**, D00F10.

Brown, S.S., W.P. Dubé, P. Karamchandani, G. Yarwood, J. Peischl, T.B. Ryerson, J.A. Neuman, J.B. Nowak, J.S. Holloway, R.A. Washenfelder, et al. 2011. The effects of NO_x control and plume mixing on nighttime chemical processing of plumes from coal-fired power plants, *J. Geophys. Res.*, submitted.

Colella, P. and P.R. Woodwar. 1984. The Piecewise Parabolic Method (PPM) for gas-dynamical simulations, *J. Comp. Phys.*, **54**, 174-201.

Donaldson, C. du P. 1973. Atmospheric turbulence and the dispersal of atmospheric pollutants, In: *AMS Workshop on Micrometeorology*, D.A. Haugen (Ed.), Science Press, Boston, pp. 313-390.

ENVIRON. 2010. *Users Guide: Comprehensive Air Quality model with extensions (CAMx)*. Prepared by ENVIRON International Corporation, Novato, CA (www.camx.com).

EPA. 1995. *User's Guide for the Industrial Source Complex (ISC) Dispersion Model – Volume I User Instructions,* U.S. Environmental Protection Agency, Office of Air Quality, Planning and Standards, Research Triangle Park, NC. September. (http://www.epa.gov/ttn/scram/userg/regmod/isc3v1.pdf).

EPA. 1998. *Interagency Workgroup on Air Quality Modeling (IWAQM) Phase 2 Summary Report and Recommendations for Modeling Long-Range Transport Impacts*, U.S. Environmental Protection Agency EPA-454/R-98-019, Research Triangle Park, NC.

EPA. 2003. *Revisions to the Guideline on Air Quality Models: Adoption of a Preferred Long Range Transport Model and Other Revisions, Final Rule. 40 CFR Part 51*, Federal Register, Vol. 68, 72, Tuesday April 15, 2003. (http://frwebgate3.access.gpo.gov/cgi-bin/PDFgate.cgi?WAISdocID=xoakAq/0/2/0&WAISaction=retrieve).

EPA. 2004. *AERMOD: Description of Model Formulation*, Tech Rep., EPA-454/R- 03-004, Research Triangle Park, NC, 91 pp. (http://www.epa.gov/scram001/7thconf/aermod/aermod_mfd.pdf).

EPA. 2008. Clarification of Regulatory Status of CALPUFF for Near-Field Applications. Memorandum from Richard A. Wayland, Director Air Quality Assessment Division, Office of Air Quality Planning and Standards, U.S. Enviromental Protection Agency to EPA

Regional Air Directors. August 13. (http://www.epa.gov/ttn/scram/guidance/clarification/clarification%20of%20regulatory%20status%20of%20calpuff.pdf).

EPA. 2009a. *Reassessment of the Interagency Workgroup on Air Quality Modeling (IWAQM) Phase 2 Summary Report: Revisions to Phase 2 Recommendations*. Draft. U.S. Environmental Protection Agency, Office of Air Quality, Planning and Standards, Air Quality Analysis Division, Air Quality Modeling Group, Research Triangle Park, NC. May 27. (http://www.epa.gov/scram001/guidance/reports/Draft_IWAQM_Reassessment_052709.pdf).

EPA. 2009b. *Clarification on EPA-FLM Recommended Settings for CALMET*, Memorandum from Tyler J. Fox, Group Leader, Air Quality Modeling Group, Office of Air Quality, Planning and Standards, U.S. Environmental Protection Agency to Regional Modeling Contacts. August 31. (http://www.epa.gov/ttn/scram/CALMET%20CLARIFICATION.pdf).

EPA. 2009c. *AERMOD Implementation Guide*, AERMOD Implementation Workgroup, U.S. Environmental Protection Agency, Office of Air Quality, Planning and Standards, Air Quality Assessment Division. Last Revised March 19, 2009. (http://www.epa.gov/scram001/7thconf/aermod/aermod_implmtn_guide_19March2009.pdf).

EPA. 2012. Documentation of the Evaluation of CALPUFF and Other Long Range Transport Models Using Tracer Field Experiment Data. U.S. Environmental Protection Agency, Office of Air Quality Planning and Standards, RTP, NC. EPA-45/R-12-003. May. (http://www.epa.gov/ttn/scram/reports/EPA-454_R-12-003.pdf).

EPRI. 1988. *A Hierarchy of Dynamic Plume Models Incorporating Uncertainty, Volume 4: Second-order Closure Integrated Puff*, EPRI EA-6095 Volume 4, Project 1616-28, Palo Alto, CA.

EPRI. 2000. *SCICHEM Version 1.2: Technical Documentation*, EPRI Report 1000713, Palo Alto, CA.

Gabruk, R.S., R.I. Sykes, C. Seigneur, P. Pai, P. Gillespie, R.W. Bergstrom, and P. Saxena. 1999. Evaluation of the Reactive and Optics Model of Emissions (ROME). *Atmos. Environ.*, **33**, 383-399.

Gery, M.W., G.Z. Whitten, J.P. Killus, and M.C. Dodge. 1989. A photochemical kinetics mechanism for urban and regional scale computer modeling. *J. Geophys. Res.*, **94** , 12,925–12,956.

Hindmarsh, A.C. 1983. ODEPACK: a systematized collection of ODE solvers, In: *Numerical Methods for Scientific Computing*, Stepleman, R.S. et al., Eds.; North-Holland, New York, pp. 55–64

Imhoff, R.E., R.L. Tanner, R.J. Valente, and M. Luria. 2000. The evolution of particles in the plume from a large coal-fired boiler with flue gas desulfurization, *J. Air Waste Manag. Assoc.*, **50**, 1207-1214.

Karamchandani, P., L. Santos, I. Sykes, Y. Zhang, C. Tonne, and C. Seigneur. 2000. Development and evaluation of a state-of-the-science reactive plume model, *Environ. Sci. Technol.*, **34**, 870-880.

Karamchandani, P., S.-Y. Chen and C. Seigneur. 2008. *CALPUFF Chemistry Upgrade, AER Final Report CP277-07-01*, prepared for API, Washington, DC, February.

Lewellen, W.S. 1977. Use of invariant modeling, In: *Handbook of Turbulence*, W. Frost and T.H. Moulden (Eds.), Plenum Press, New York, pp. 237-280.

Luria, M., R.L. Tanner, R.E. Imhoff, R.J. Valente, E.M. Bailey and S.F. Mueller. 2000. Influence of natural hydrocarbons on ozone formation in an isolated power plant plume, *J. Geophys. Res.*, **105**, 9177-9188.

Martinez, M., H. Harder, T.A. Kovacs, J.B. Simpas, J. Bassis, R. Lesher, W.H. Brune, G.J. Frost, E.J. Williams, et al. 2003. OH and HO_2 concentrations, sources, and loss rates during the Southern Oxidants Study in Nashville, Tennessee, summer 1999, *J. Geophys. Res.*, **108**, 4617.

Morris, R.E., C. Tana, G. Yarwood. 2003. Evaluation of the Sulfate and Nitrate Formation Mechanism in the CALPUFF Modeling System. Presented at *AWMA Specialty Conference Guideline on Air Quality Models: The Path Forward,* Mystic, CT. October.

Morris, R.E., S. Lau, B. Koo. 2005. Evaluation of the CALPUFF Chemistry Algorithms. Presented at the *98th Annual Air and Waste Management Conference*, Minneapolis, MN. June.

Morris, R., S. Lau, B. Koo, A. Hoats and G. Yarwood. 2006. Further Evaluation of the Chemistry Algorithms used in the CALPUFF Modeling System. Presented at the *AWMA Guidelines on Air Quality Models Conference*, Denver, Colorado. April 26-28.

NCAR. 2011. *The Tropospheric Visible and Ultraviolet (TUV) Radiation Model* web page. National Center for Atmospheric Research, Atmospheric Chemistry Division, Boulder, Colorado, http://cprm.acd.ucar.edu/Models/TUV/index.shtml.

Nenes A., S.N. Pandis, and C. Pilinis, 1998. ISORROPIA: A new thermodynamic model for inorganic multicomponent atmospheric aerosols, *Aquat.Geoch.*, **4**, 123-152.

Parrish, D.D., D.T. Allen, T.S. Bates, M. Estes, F.C. Fehsenfeld, G. Feingold, R. Ferrare, R.M. Hardesty, J.F. Meagher, J.W. Nielsen-Gammon, et al. 2009. Overview of the Second Texas Air Quality Study (TexAQS II) and the Gulf of Mexico Atmospheric Composition and Climate Study (GoMACCS), *J. Geophys. Res.*, **114**, D00F13.

Pleim, J. 2007. "A combined local and nonlocal closure model for the atmospheric boundary layer. Part I: Model description and testing." *J. Appl. Met. and Clim.*, **46**, 1383-1395.

Schulman, L.L., D.G. Strimaitis, and J.S. Scire. 2000. Development and evaluation of the PRIME plume rise and building downwash model, *J. Air Waste Manag. Assoc.*, 50, 378-390.

Scire, J.S., F.W. Lurmann, A. Bass, and S.R. Hanna. 1983. *Development of the MESOPUFF-II Dispersion Model.* EPA, ESRC, RTP, NC. Contract No. 68-02-3733. September.

Scire, J.S., D.G. Strimaitis, and R.J. Yamartino. 2000a. *A User's Guide for the CALPUFF Dispersion Model (Version 5)*, Earth Tech, Inc. Report, Concord, MA, January 2000.

Scire, J.S., F.R. Robe, M.E. Fernau, and R.J. Yamartino. 2000b. *A User's Guide for the CALMET Dispersion Model (Version 5)*, Earth Tech, Inc. Report, Concord, MA, January 2000.

Slinn, S.A. and W.G.N. Slinn. 1980. Predictions for particle deposition on natural waters. *Atmos. Environ.*, **24**, 1013-1016.

Stroud, C.A., J.M. Roberts, E.J. Williams, D. Hereid, W.M. Angevine, F.C. Fehsenfeld, A. Wisthaler, A. Hansel, M. Martinez-Harder, H. Harder, et al. 2002. Nighttime isoprene trends at an urban forested site during the 1999 Southern Oxidant Study, *J. Geophys. Res.*, **107**, 4291.

Sykes, R.I., S.F. Parker, D.S. Henn, and W.S. Lewellen. 1993. Numerical simulation of ANATEX tracer data using a turbulence closure model for long-range dispersion, *J. Appl. Met.*, **32**, 929-947.

Sykes, R.I. and D.S. Henn. 1995. Representation of velocity gradient effects in a Gaussian puff model, *J. Appl. Met.*, **34**, 2715-2723.

Sykes, R.I. and R.S. Gabru. , 1997. A second-order closure model for the effect of averaging time on turbulent plume dispersion, *J. Appl. Met.*, **36**, 165-184.

Tanner, R.L., R.J. Valente, R.E. Imhoff, and M. Luria. 2002. *Plume Study to Characterize Fine Particulate Emissions and Secondary Particle Formation at a Large Coal-Fired Power Plant (Cumberland Visible Emissions Study Phase II)*, Final Report prepared for EPRI and DOE's Federal Energy Technology Center, Tennessee Valley Authority, Muscle Shoals, AL, available at http://www.netl.doe.gov/technologies/coalpower/ewr/air_quality_research/docs/Final%20report%204%20CUF%20TC%20project%20rev2Fi.pdf.

Wesely, M.L. 1989. Parameterization of Surface Resistances to Gaseous Dry Deposition in Regional-Scale Numerical Models. *Atmos. Environ.*, **23**, 1293-1304.

Young, T.R. and J.P. Boris. 1977. A numerical technique for solving stiff ordinary differential equations associated with the chemical kinetics of reactive-flow problems, *J. Phys. Chem.*, **81**, 2424-2427.

Zhang, L., S. Gong, J. Padro, and L. Barrie. 2001. A size-segregated particle dry deposition scheme for an atmospheric aerosol module. *Atmos. Environ.*, **35**, 549-560.

Zhang, L., J. R. Brook, and R. Vet. 2003. A revised parameterization for gaseous dry deposition in air-quality models. *Atmos. Chem. Phys.*, **3**, 2067–2082.

Zhang, Y., B. Pun, K. Vijayaraghavan, S.-Y. Wu, C. Seigneur, S.N. Pandis, M.Z. Jacobson, A. Nenes, and J.H. Seinfeld. 2004. Development and application of the Model of Aerosol Dynamics, Reaction, Ionization, and Dissolution (MADRID), *J. Geophys. Res.*, **109**, D01202.